Master Thesis, Department of Geosciences

Reconstructing volcanism, deformation and sedimentation in the Dugurdsknappen area, south Trøndelag

From marginal basin formation to Caledonian collapse

Ella Stokke

UNIVERSITY OF OSLO

FACULTY OF MATHEMATICS AND NATURAL SCIENCES

Reconstructing volcanism, deformation and sedimentation in the Dugurdsknappen area, south Trøndelag

From marginal basin formation to Caledonian collapse

Ella Stokke

Master Thesis in Geosciences

Discipline: Structural geology and tectonics
Department of Geosciences
Faculty of Mathematics and Natural Sciences

University of Oslo

June 2016

Supervisors: Dr. Deta Gasser and Prof. Fernando Corfu

This work is published digitally through DUO – Digitale Utgivelser ved UiO
http://www.duo.uio.no
It is also catalogued in BIBSYS (http://www.bibsys.no/english)

Front page: Photo of ribbon-chert in the southern end of Dugurdsknappen, in the early morning on a cold day.

Acknowledgement

This thesis is written in collaboration with the Institute of Geoscience at the University of Oslo and the Norwegian Geological Survey. I firstly like to thank my supervisors Deta Gasser and Fernando Corfu for giving me the opportunity to write this thesis and for all help and advice during field- and lab-work and for good feedback during later writing. I especially want to thank Deta Gasser for the enormous amount of advice, help, patience and inspiration you've given me throughout this year. You are always happy to spear a moment for a discussion with a lost student and have inspired me to always do my outmost. I am forever grateful that you agreed to be my supervisor!

A big thank you to Bjørgunn Dalslåen for our many good discussions and helping me all along the way. I also want to thank the people of NGU and especially everyone at Bedrock geology for accommodating me with an office and for including me in seminars, lunches and good discussions, you have all inspired me. Also a special thank you to Espen Torgersen for helping me through a rough start in ArcGIS and Move, and to Tor Grenne for all your help and advice with geochemistry. Thanks to the lab at NGU for doing the geochemical analyses, and for helping me with preparation of samples and geochronological analyses, particularly Øyvind Skår, who patiently taught me how to work with the LA-ICP-MS. Also thank you to Gunnborg Bye Fjeld at UiO for your patience when teaching me all about mineral separation, and to Salahalldin Akhavan at UiO for preparing all my thin sections.

I also want to thank all my fellow students at NTNU, UNIS and UiO, who have been great company and support through these last five years, and especially for coping with me this last year. Good colleagues make all the difference. Last but not least I want to thank my friends and family who supported me throughout, especially my mother who joined me for fieldwork. Thanks to my flatmates and all our cats and kittens. And a very special thanks to my lovely Gauti, who have helped me with everything from fieldwork to late night dinners, and put up with me talking all about greenstone and chert. Thank you for all your love and support, you are amazing.

Abstract

The Dugurdsknappen area is part of the Tronget unit, which has traditionally been placed in the Støren Nappe of the Trondheim Nappe Complex, thought to be part of the Upper Allochthon of the Scandinavian Caledonides. Several studies have been conducted in the northern and northwestern parts of the Støren Nappe, which is thought to comprise mainly ocean floor to island-arc volcanic and sedimentary successions derived from the Laurentian side of the Iapetus Ocean. They were later thrust onto the Baltic continent through several stages of accretion and nappe translation, though much of this evolution is still heavily disputed. Far less have been done in the Tronget unit, including Dugurdsknappen, thus the tectonic evolution of this area and correlation northward is still unclear.

In order to better constrain the tectonic evolution of Dugurdsknappen, and to understand the genesis of the unconformity and the structural difference between units above and below it, four weeks of lithological and structural mapping have been conducted, with subsequent petrographic, geochemical and geochronological analyses of samples. Possible correlation to surrounding related geology, particularly northwards in the Støren Nappe, have been discussed on the basis of these collected observations and analyses.

The oldest part of the area comprises a succession of rift-related pillow-basaltic greenstones, possibly formed in a marginal basin, with local agglomerates and jaspers. It is covered by a thick succession of ribbon-chert, with interbedded conglomerates and sandstone layers, followed by silty chert and green siltstones. This sedimentary succession is thought to have been deposited relatively continuous after the basaltic volcanism, in a marine basin close to a terrestrial source, with gradually increasing terrestrial input upward in the succession. The whole succession is isoclinally folded in syn- and antiforms, seen as a large S-SE trending synform in the mapped area, with abundant tight and isoclinal internal folding, particularly within the ribbon-chert. Folding occurred prior to deposition of the overlying units and is possibly related to accretion of the succession, rather than eastward nappe translation during the main Scandian phase of the orogeny. An erosional unconformity, signified by a basal conglomerate, parts these heavily deformed lower units from an overlying less deformed, cross-laminated, green sandstone. A tonalitic clast in the sandstone is dated to 485.0 ± 3.7 Ma, and a detrital zircon spectrum from the sandstone defines a maximum depositional age of 427 ± 3 Ma. A younger subduction-related volcanic episode intrudes the sandstone, and possibly also the underlying greenstone. This magmatic episode is likely younger than 430 Ma, and has not been previously described in the Trondheim region. A second deformation phase folds and refolds all mapped units in SW trending open to tight folds, which leads to development of a regional axial-plane foliation. These folds are generally NW verging, indicating relation to the post-orogenic extensional phase of the Caldonian orogeny.

Table of Contents

Chapter 1 – Introduction **1**

Chapter 2 – Geological background **3**

2.1 – The geology of Norway 3

2.2 – Plate-tectonic framework 4

2.3 – The Caledonide orogeny 5

2.3.1 – The Wilson Cycle 5

2.3.2 – The Scandinavian Caledonides 6

2.4 –Geology of the study area 9

2.4.1 – The Trondheim Nappe Complex 9

2.4.2 – Dugurdsknappen and the Tronget unit 11

Chapter 3 – Methods **13**

3.1 – Fieldwork 13

3.2 – Software 13

3.3 – Petrographic observations 14

3.4 – Geochemical analysis 14

3.5 – Geochronological analysis 15

Chapter 4 – Description of mapped units **17**

4.1 – Topographic overview 17

4.2 – Description of the map 18

4.3 – Mapped lithologies 19

4.3.1 – Greenstone-related rocks 19

4.3.2 – Chert-related rocks 24

4.3.3 – Green siltstone 27

4.3.4 – Rocks above the unconformity 28

Chapter 5 – Structural description **32**

5.1 – Mapped structures below the unconformity 33

5.1.1 – Greenstone-related rocks 33

5.1.2 – Chert-related rocks 35

5.1.3 – Green siltstone 43

5.2 – Mapped structures above the unconformity 45

5.2.1 – Green sandstone 45

5.2.2 – Intermediate volcanic and intrusion 46

5.3 – Main features 48
5.4 – Mapped boundaries 50
5.4.1 – Boundary between green sandstone and greenstone/ribbon-chert 50
5.4.2 – Boundary between greenstone and ribbon-chert 52
5.5 – Brittle deformation 53
Chapter 6 – Petrographic and geochemical description 55
6.1 – Petrography 56
6.1.1 – Greenstone-related rocks 56
6.1.2 – Chert-related rocks 59
6.1.3 – Green siltstone 61
6.1.4 – Rocks above the unconformity 62
6.2 – Geochemistry 65
6.2.1 – Igneous rocks - Major element geochemistry 65
6.2.2 – Igneous rocks - Trace element and rare earth element (REE) geochemistry 67
6.2.3 – Sedimentary rocks 71
Chapter 7 – Geochronology 75
7.1 – Samples EST_3 and EST_96 75
7.2 – Sample EST_12 76
7.3 – Sample EST_112 77
Chapter 8 – Discussion 80
8.1 – Tectonic setting and depositional environment 80
8.1.1 – Magmatism and deposition in a rift-related basin 80
8.1.2 – Deposition in a shallow marine basin 84
8.1.3 – Extent and setting of the younger intermediate volcanic/intrusion: subduction-related shallow magmatism 85
8.2 – Structural evolution 86
8.2.1 – First folding phase 86
8.2.2 – Genesis of the unconformity 88
8.2.3 – Second folding phase and related foliation 89
8.3 – Palaeotectonic interpretation 90
8.4 – Relation to the Scandinavian Caledonides 93
8.4.1 – Early Cambrian to Ordovician greenstone units 93
8.4.2 – Mid-Silurian sandstone basins 94
8.4.3 – Post-mid-Silurian volcanics 96

8.4.4 – Structural evolution in a wider context 96
Chapter 9 – Conclusion 98
References 100
Appendix
Appendix 1 – Maps of Dugurdsknappen I
Appendix 2 – Geochemical analyses, tables VIII
Appendix 3 – Geochronological analyses, tables XIII
Appendix 4 – Main geological map of Dugurdsknappen XVII

Chapter 1 – Introduction

This master project was initiated by Deta Gasser and Tor Grenne, when they during preliminary fieldwork related to Bjørgunn Dalslåens PhD project recognized the existence of an unconformity between folded greenstone, ribbon-chert and siltstones overlain by less deformed sandstones at Dugurdsknappen, within the northwestern part of the Tronget unit (Fig. 1.1; Fig. 2.5; Map, appendix 4). It is part of a larger project under the direction of the Norwegian Geological Survey to map the county of Sør-Trøndelag, and eventually all of Norway, in 1:50 000 scale. This master thesis is one small piece in a very large puzzle.

Figure 1.1: Picture of the small mountain-top Dugurdsknappen 1063 m.a.s.l, as seen from the northwest. The area extends from the north side of the mountain and southward about 1.5 km. The top itself comprises mainly ribbon-chert and green siltstone, with bounding greenstone both to the east and west.

The aim of the thesis is to produce a detailed lithological and structural map of a key area around the small mountain Dugurdsknappen, in Nerskogen, Rennebu County in Norway (Fig. 1.2); an area extending about 1.5x1.5 km. Understanding the genesis of the unconformity and whether the difference in structural style between the greenstone, ribbon-chert and siltstones below the unconformity and the overlying sandstones is the result of different rheological behaviour, or due to difference in structural history, has also been an important focus during fieldwork and later interpretations. Several samples for petrography, geochemistry and geochronology have been taken throughout the area to help answer these questions, and to hopefully give key information to link this area to adjacent areas in the Trondheim region and

better constrain the tectonic evolution of these little investigated units. Through working with these questions by means of several weeks of fieldwork and extensive structural, petrographic, geochemical and geochronologic investigations, an evolutionary model for the structural and tectonic history of the area should be produced, and a 3D model of the geometry of the area developed.

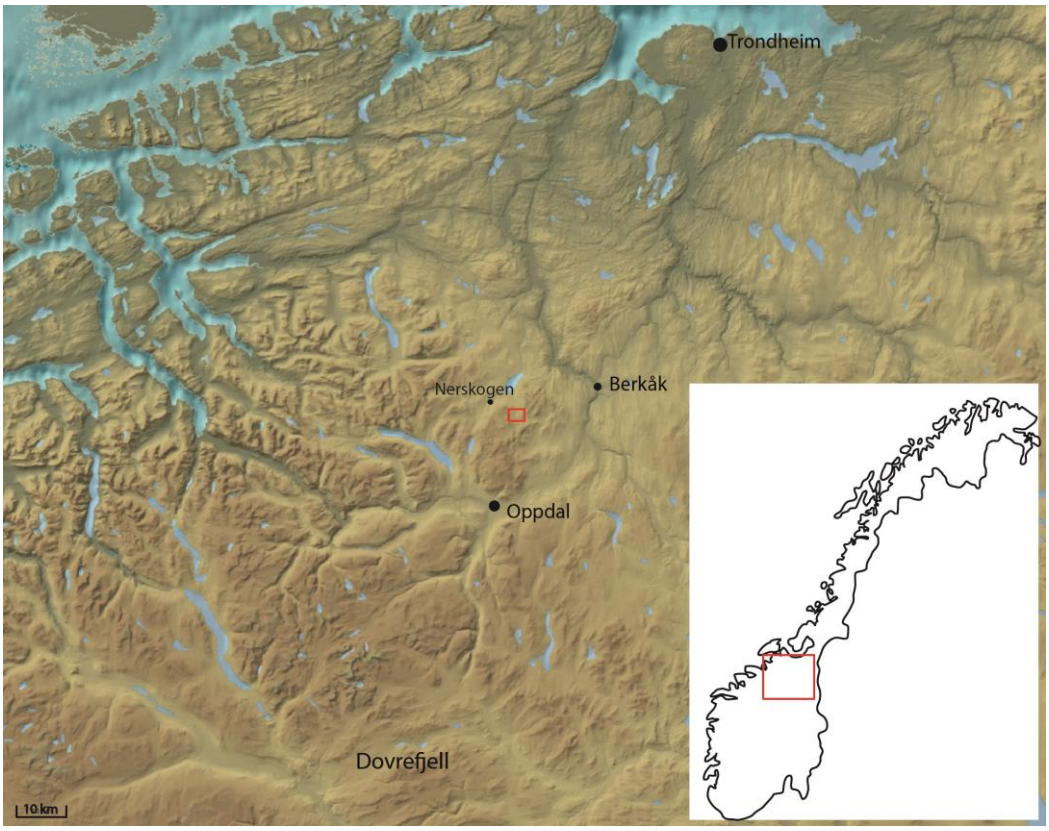

Figure 1.2: Map of parts of Sør-Trøndelag. Red rectangle indicates position of Dugurdsknappen. Small map indicate location of Sør-Trøndelag in Norway. Map modified from norgeskart.no

The area of interest is part of the debated Tronget unit in the Støren Nappe of the Trondheim Nappe Complex, which is thought to be part of the Upper Allochthon of the Scandinavian Caledonides, typically containing exotic oceanic terrains probably derived from the Iapetus Ocean. This thesis will initiate with a presentation of the general geological background, both of the Scandinavian Caledonides as a whole and tectonic processes in general, and of the more local geology of the Tronget unit and the surrounding Trondheim Nappe Complex. A short chapter will present methods used to collect and produce observations and results, and very shortly on some theory related to these methods. The result section will start with presenting lithological observations of the units, and follow up with detailed structural descriptions of units and boundaries. Succeeding this are descriptions of the petrographic and geochemical results, and geochronology will be presented in the end. The discussion starts with presenting interpretations of depositional environment and tectonic regimes during formation of the different units and an interpretation of the structural history, before an evolutionary model summarizing the history is presented and discussed related to the known geology of the Scandinavian Caledonides. An appendix in the end presents several different maps, as well as the geochemical and geochronological data collected.

Chapter 2 – Geological background

2.1 – The geology of Norway

The geology of Norway today can roughly be subdivided into three main units (Fig. 2.1). (1) Precambrian basement with a thin cover of Upper Proterozoic to Lower Palaeozoic rocks dominates in the south, southeast and west, with variable Caledonian overprint in the western part. (2) Caledonian thrust sheets cover large parts of Norway, stretching from north to south. (3) Post-Caledonian rocks including Devonian basins in western Norway and igneous and volcanic rocks related to the Permian Oslo rift.

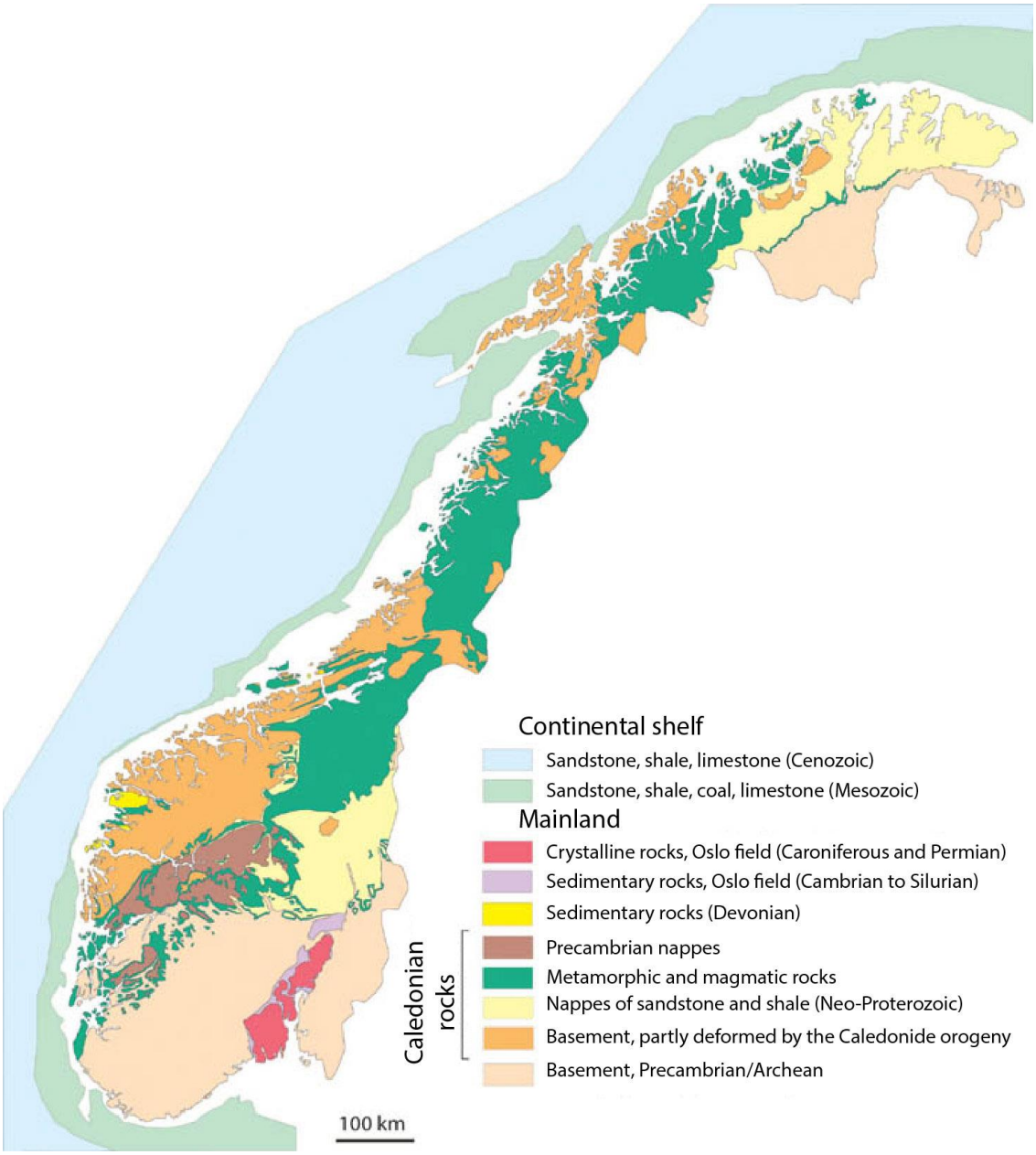

Figure 2.1: Generalized geological map of Norway and the surrounding continental shelf (Ramberg et al., 2008)

2.2 – Plate-tectonic framework

Present-day Norway lies on the Eurasian plate, with a complex plate tectonic history. It was previously part of the continent Laurussia, and before that the Precambrian basement was part of the continent Baltica, while other parts are derived from the Iapetus Ocean and even the Laurentian plate. The continent of Baltica lies as the base of what is today most of northern Europe, with a core (called protobaltica) dating back to over 3 Ga (Cocks and Torsvik, 2005). In the Meso- to Neoproterozoic, Baltica was a part of the supercontinent Rodinia and attached to the continent Laurentia, until they separated, thus opening the Iapetus Ocean between 570 and 550 Ma (Torsvik and Cocks, 2005). During the Cambrian and Ordovician, Baltica probably rotated counter-clockwise into the present day orientation, subsequently colliding first with the continent of Avalonia before the main collision with the continent Laurentia (Fig. 2.2). This led to the closing of the Iapetus Ocean, followed by an oblique collision causing the Caledonian Orogen during Ordovician and Silurian times (Torsvik and Cocks, 2005).

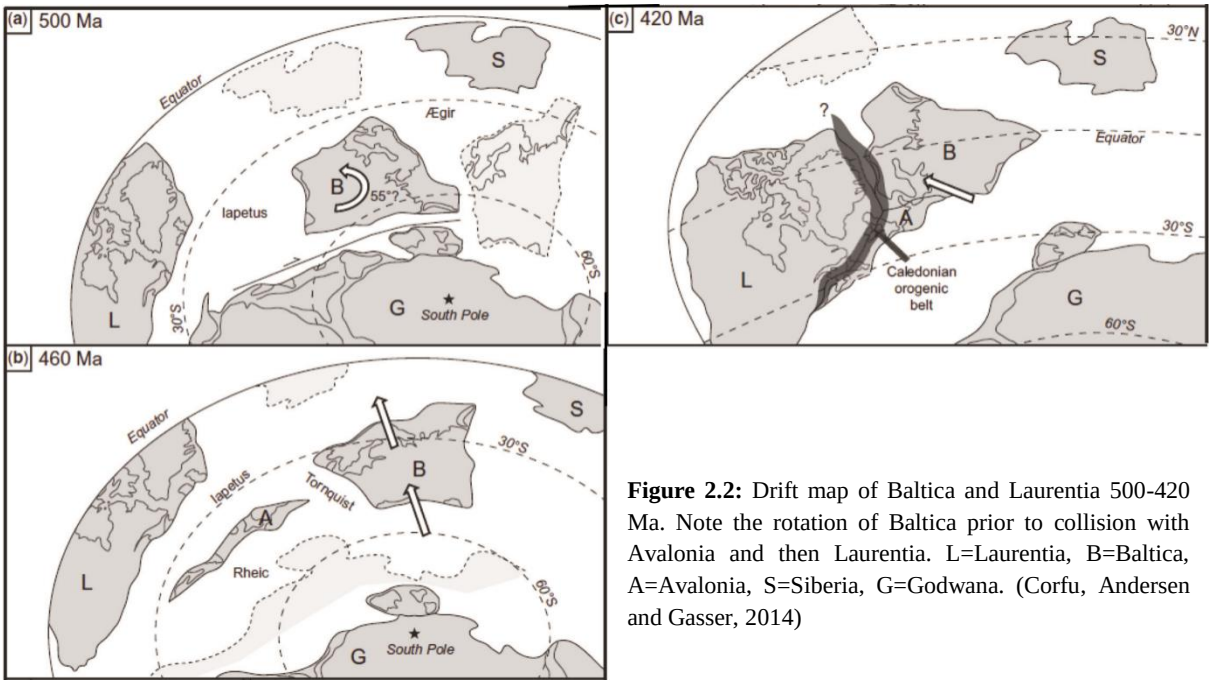

Figure 2.2: Drift map of Baltica and Laurentia 500-420 Ma. Note the rotation of Baltica prior to collision with Avalonia and then Laurentia. L=Laurentia, B=Baltica, A=Avalonia, S=Siberia, G=Godwana. (Corfu, Andersen and Gasser, 2014)

Post-orogenic Devonian extension and later Carboniferous and Permian rifting succeeded the collision. This was followed by the assembling of the supercontinent Pangea, caused by the collision of Godwana in the south and Laurussia in the north. Baltica did not split up from Laurentia until the opening of the North Atlantic in the Neogene, at about 53 Ma, during the last stages of the dismembering of Pangea (Torsvik and Cocks, 2005). So from the late Proterozoic until today, Norway as part of Baltica has gradually moved from high southern latitudes to high northern latitudes in a relatively steady northwards direction, with only short episodes of southern drifting (Torsvik and Cocks, 2005).

2.3 – The Caledonide orogeny

2.3.1 – The Wilson Cycle

To help understand the Caledonian orogeny, it can be useful to first investigate the general principles of plate tectonics and the process of orogenesis. Though already suggested by Alfred Wegener in 1912, it was not until the 1960's that the concept of plate tectonics was first proposed (Buiter and Torsvik, 2014). This was led by J. T. Wilson, who recognized three basic principles of geodynamics: plate tectonics, mantle plumes with a deep source and the Wilson Cycle, named after Wilson later by K. Burke (Burke, 2011). The process of the Wilson Cycle was described in Wilson's famous 1966 paper: Did the Atlantic close and then re-open? It describes the possibility of a proto-Atlantic ocean existing prior to the Caledonides, based on the recognition that this was the best explanation for the diverse marine palaeo-faunas found on each side of the present Atlantic Ocean (Wilson, 1966). He postulated a hypothesis saying that the building of mountains is closely related to the opening and closing of oceans with oceanic lithosphere (Wilson, 1966). The Wilson cycle describes the unavoidable consequence of subduction, explicitly that when the entire ocean is consumed, the two continental plates will collide. Fig. 2.3 shows the general structure of the cycle.

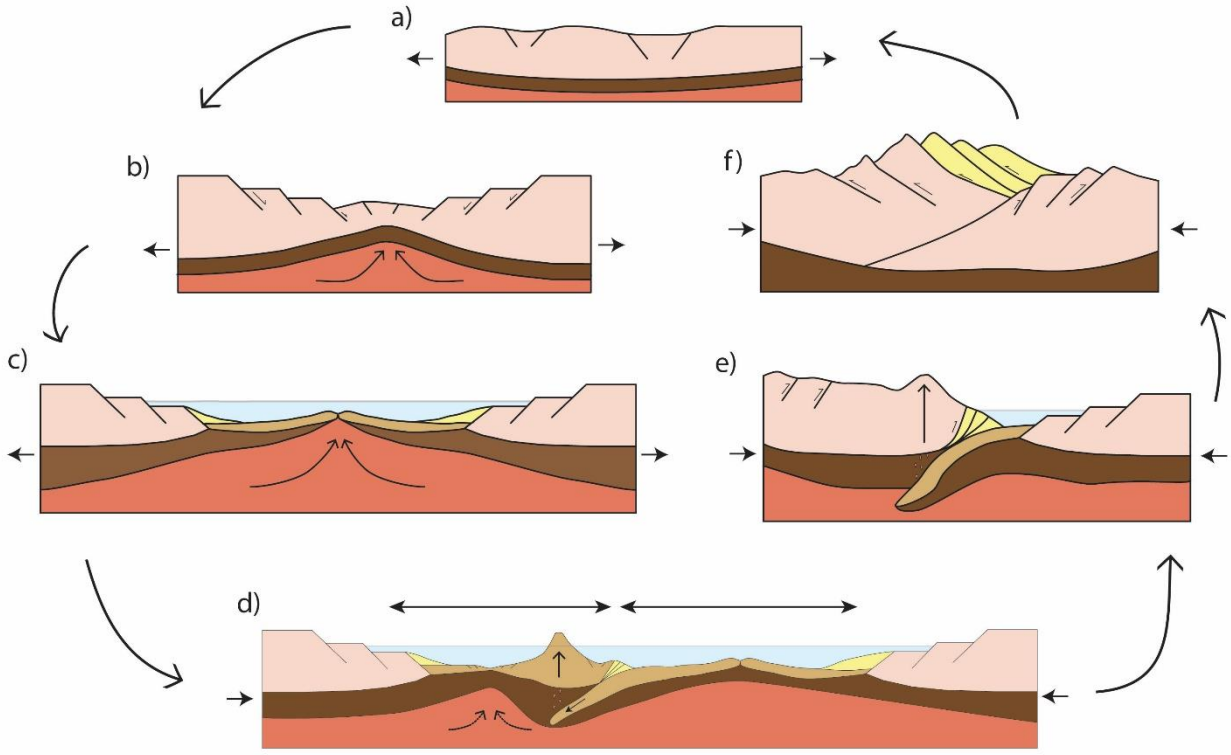

Figure 2.3: Illustration of the Wilson Cycle. a) An eroded craton resulting from extensional collapse of a mountain chain and subsequent erosion will b) experience extension and start rifting. c) These rifts gradually develop into a sea-floor spreading scenario and become a mid-ocean rift. d) Compressional tectonics takes over and subduction is initiated producing trenches and volcanic arcs, with fore arc and back arc basin systems. e) Subduction progresses and Andean-type subduction develops, as well as accretion of microcontinents and volcanic arcs and ophiolite obduction. f) Subduction is complete and the two continents collide resulting in thrusting of tectonic nappes. This is followed by post-orogenic extension and collapse, leading back to stage a).

Wilson described a two dimensional scenario where the two continents would collide and then rift along the old suture, opening the "same" ocean, but the reality is far more complex.

Continental margins are not simple straight lines, but highly complex areas with irregular geometry both inherited from the initial rifting and later reformed by incision and hyperextension (Dewey and Burke, 1974). This results in protrusions in the margin colliding before embayments, giving a diachronous development of the suture with increased deformation in the areas of initial collision and declining deformation towards the embayments (Dewey and Burke, 1974). Wilson also assumed an orthogonal pattern of rifting and collision, but as with the oblique polyphasal collision of the Caledonides, this is usually not the case. There are several other factors complicating the understanding of orogenesis, diverging from the general principles of the Wilson cycle. Yet, it is still a useful framework to base further analyses of orogenic evolution.

2.3.2 – The Scandinavian Caledonides

The Scandinavian Caledonides are exposed in Norway and Sweden and extend for about 1500 km from south in the Stavanger region to the north into the Barents Sea (Fig. 2.1). The orogen is characterized by nappes of different origin thrust eastward into Sweden and generally thinning westward, as well as large N-S along-length thickness variations (Roberts and Gee, 1985). The Caledonian nappe stack is thrust onto a basement of Archean to Neoproterozoic mainly crystalline rocks of the Fennoscandian shield, and is cut by post-orogenic Devonian extensional basins (Corfu, Andersen and Gasser, 2014). The Caledonian nappes dip under younger Palaeozoic to Cenozoic sedimentary rocks to the north and west in the marine basins on the Norwegian shelf (Corfu, Andersen and Gasser, 2014). The presently most widely accepted, yet heavily debated model of the tectonostratigraphy of the Scandinavian Caledonides, parts it up into an autochthonous and parautochthonous basement followed by the Lower-, Middle-, Upper- and Uppermost Allochthon (Fig. 2.4; Roberts and Gee, 1985; Slagstad et al., 2013).

At the base of the orogen is the autochthonous to parautochthonous basement, consisting of Archean to Neo-Proterozoic crystalline rocks covered by a Cambro-Silurian sedimentary succession. This sedimentary cover has been partly affected by Caledonian compressional structures, and has been incorporated in the overlying fold-and-thrust belt, becoming parautochthonous in places (Roberts and Stephens, 2000). The basement also appears in windows in several areas within the orogen (Fig. 2.4; Grenne, Ihlen and Vokes, 1999). The Lower and Middle Allochthons are thrust on top of the autochthonous basement, making up the lowermost levels of the tectonostratigraphy. They comprise sedimentary and magmatic rocks of the shortened Late Neoproterozoic to Early Palaeozoic Baltoscandian margin (Roberts and Stephens, 2000), as well as some older Precambrian crystalline rocks (Gee et al., 1985). There is a transition in the Middle Allochthon with increasing metamorphic grade from greenschist facies, to eclogite and granulite facies at the base of Upper Allochthon, while the Upper Allochthon is dominated by low-to medium-grade greenschist facies, as well as occurrences of ocean floor metamorphism (Bryhni and Andréasson, 1985; Gee et al., 1985). The Upper Allochthon contains mainly Early Palaeozoic sheets of volcanosedimentary successions originating from different terrains outboard Baltica and Laurentia, including oceanic crust derived from the margins of the Iapetus Ocean (Gee et al., 1985; Roberts and Stephens, 2000). These volcanosedimentary complexes are associated with the closing of

Iapetus Ocean, and include ophiolites and island-arc volcanic rocks with related sedimentary successions (Gee et al., 1985). The highest tectonostratigraphic sheets are found in the Uppermost Allochthon, which comprises Neoproterozoic to Silurian sedimentary and magmatic rocks, characterised by large carbonate rock units, metasedimentary iron ore formations and large Ordovician arc-type granitoid plutons and batholiths (Roberts, Nordgulen and Melezhik, 2007). The allochthon is interpreted to be derived from continental crust of exotic terrains, possibly of Laurentian origin (Roberts and Stephens, 2000; Roberts, Nordgulen and Melezhik, 2007).

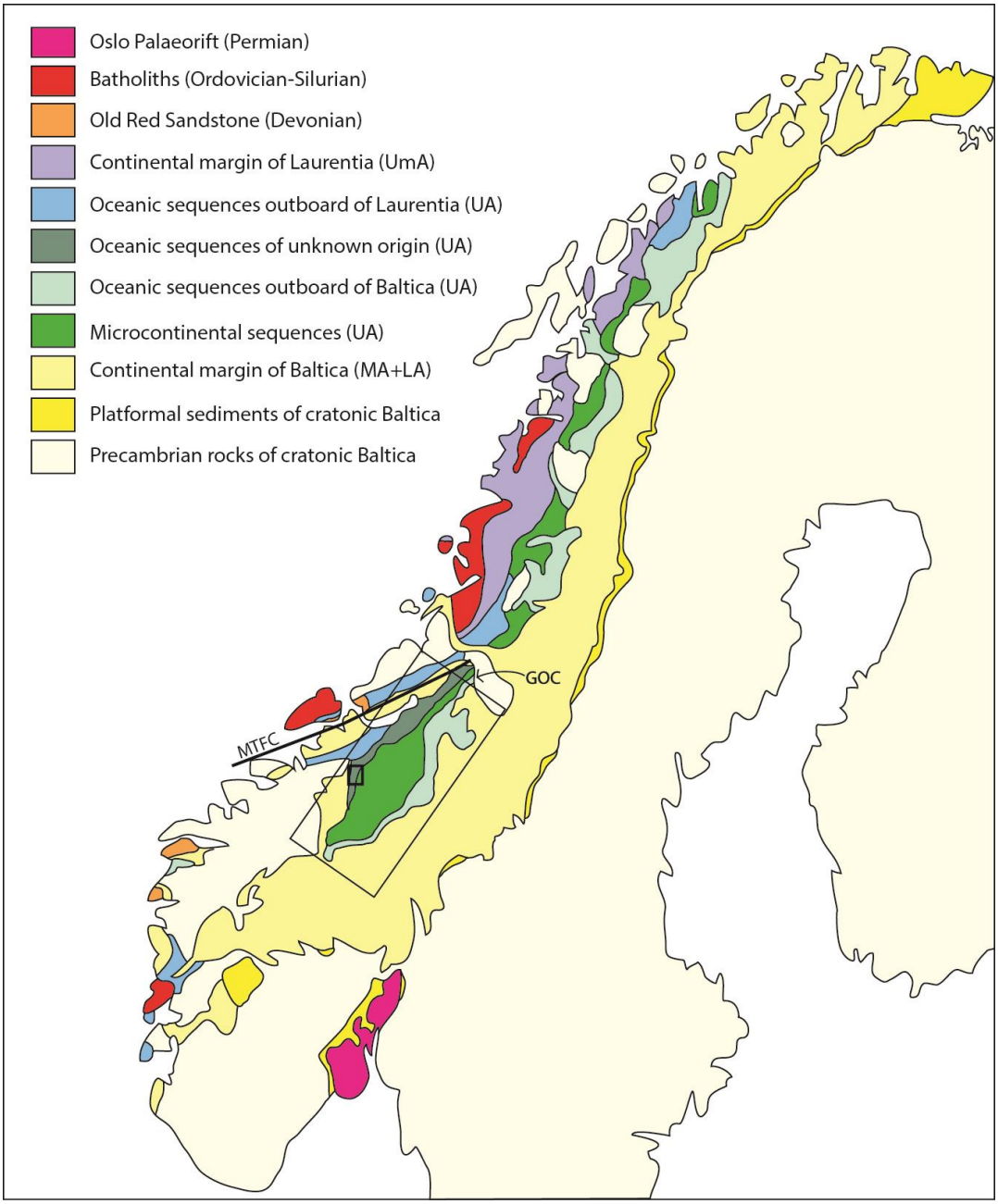

Figure 2.4: Map showing the different components of the Scandinavian Caledonides, and their proposed palaeotectonic origin. Large rectangle shows approximate extent of the Trondheim Nappe Complex, small rectangle shows the study area. MTFC=Møre Trøndelag Fault complex, GOC=Grong-Olden Culmination, LA=Lower Allochthon, MA=Middle Allochthon, UA=Upper Allochthon, UmA=Uppermost Allochthon. (Modified from Grenne, Ihlen and Vokes, 1999)

Recently, there has been some discussion of whether this present understanding with a simple layer-cake model of the Scandinavian Caledonides is too strict and simplistic (Corfu, Andersen and Gasser, 2014). It was developed to a large degree in the Swedish part of the Caledonides, where the nappes lie more or less in a tidy tectonostratigraphic order. When moving into Norway however, the picture becomes much more complicated, and there are large along-strike differences from south to north. Corfu, Andersen and Gasser (2014) suggest that the Caledonian nappes should rather be described as separate units, characterized by their different origin and structures, and tectonically placed on top of each other. They part the Norwegian Caledonides in three areas, the Southern, Central and Northern sectors, rather than tectonostratigraphic levels, and describe the different units of each sector. Corfu, Andersen and Gasser (2014) also point out that the old model does not take in account several aspects of the complexity of the different units and the tectonic processes themselves, such as the architecture of hyperextended margins, polyphase and out-of-sequence thrusting, and post-orogenic extension. In addition, more recent and detailed plate reconstructions have age limitations which show that Baltica might have been rotating prior to the Caledonian Orogeny (Torsvik et al., 1996; Torsvik and Cocks, 2005). That would indicate that it has faced other terrains, like Siberia and Peri-Godwana, which means the exotic terrains found in present day Caledonides might in fact be derived from other sources than just Laurentia (Corfu, Andersen and Gasser, 2014). Though it is important to keep in mind these limitations of the four-allochthon model, it still gives a good first-order approach when studying the Scandinavian Caledonides.

The Caledonian Orogeny was a result of plate movements starting with the rifting and opening of the supercontinent Rodinia about 700 Ma and ending with the main continent-continent collision of Laurentia and Baltica about 300 million years later in the Early Devonian (Grenne, Ihlen and Vokes, 1999; Cocks and Torsvik, 2005). The orogen was assembled in several stages during the Ordovician and Silurian, starting with closing of the ancient Iapetus Ocean in the Ordovician followed by continent-continent collision between Baltica and Laurentia in the Silurian and ending with subsequent Devonian extensional tectonics. Though it follows the typical Wilson cycle in very broad terms, there are many intermediate stages and a general along-strike polyphase sequence of events that makes it significantly different. The first signs of compressional tectonics occurred in the Taconian phase, which represent a period lasting from Late Cambrian to Middle-Late Ordovician dominated by subduction-related immature island-arc development and arc-accretion along the Laurentian margin and the Laurentian side of Iapetus (Van Staal et al., 2009). This phase included several stages of subduction polarities, obduction and collisions between arcs and microcontinents, but no attempt to discuss the details of this complex and much debated process are made in this thesis. The Taconian orogenic event is mainly seen in the Upper- and Uppermost Allochthons, which comprise rocks located along the Laurentian margin during the Taconian orogeny (Roberts, 2003). An early Late Cambrian to Early Ordovician (Finnmarkian) event on the Baltic side have been described (Sturt, Pringle and Ramsay, 1978), but more recent dating suggests this was the result of much earlier tectonic events, perhaps the Timanian orogeny (Corfu, Andersen and Gasser, 2014), though other studies still supports the presence of the event, but links it to the Taconian phase on the Laurentian side

rather than the Baltic (Yoshinobu et al., 2002). The presence of high-pressure Ordovician eclogites in the Baltoscandian margin-derived Seve Nappe Complex has been interpreted to indicate some tectonic event on the Baltic side as well during the Ordovician, but this is still fairly cryptic (Root and Corfu, 2012). The last signals of subduction-related magmatism and the youngest marine sediments along the suture are dated to c. 430 Ma, which together with the appearance of high pressure rocks in the Western Gneiss Region (WGR) indicates the initiation of the main collisional phase, the Scandian phase, dominated by continent-continent collision (Tucker et al., 2004; Corfu, Andersen and Gasser, 2014). This led to the rapid subduction of the Baltic margin under the Laurentian plate, as seen in the high pressure and temperature rocks of WGR, and thrusting of nappes eastward on the Baltic continent (Grenne, Ihlen and Vokes, 1999; Roberts, 2003). The collision continued throughout the Silurian and ended in the Early Devonian, when it was followed by late- to post-orogenic extension leading to rapid exhumation of subducted lithosphere and strike-slip deformation, as well as deposition in localized fault controlled extensional basins (Roberts and Stephens, 2000).

2.4 –Geology of the study area

2.4.1 – The Trondheim Nappe Complex

The study area lies in the Trondheim Nappe Complex, which includes the western parts of the Upper Allochthon in central Norway (Fig. 2.4; Dunning and Grenne, 2000). It is limited to the north by the Grong-Olden Culmination and is generally restricted to a NE-SW trending depression in central Norway (Gee et al., 1985). The nappe complex is part of the Central Scandinavian Caledonides, an area which is structurally marked by a basal fold-and-thrust belt and a general stepping up of thrust sheets from east to west, as well as the structurally controlling Møre Trøndelag Fault Complex (MTFC) to the north-west, and a north-south undulation exposing several basement windows (Fig. 2.4; Corfu, Andersen and Gasser, 2014). The nappe complex consists of the low-grade metamorphic Støren Nappe in the west, the high-grade metamorphic Gula Nappe in central parts and the variably metamorphic Meråker Nappe in the east (Fig. 2.5; Nilsen and Wolff, 1989). The three units are typically intruded by smaller plutons and dykes of trondhjemites, diorites and plagiogranites, as well as gabbros and more mafic type intrusions from different magmatic episodes, with older Early to Middle Ordovician plutons mainly in the Western Støren Nappe, while Early Silurian activity dominates in the Gula and Meråker Nappes (Nilsen et al., 2003; Nilsen, Corfu and Roberts, 2007; Slagstad et al., 2013).

The Støren Nappe is dominated by Early Ordovician meta-volcanic sequences (e.g. pillow-basaltic greenstones, cherts, tuffites) of typically ophiolitic MORB and island-arc affinities, including the Vassfjell-Løkken ophiolites and the Støren Group meta-basalts (Roberts and Wolff, 1981; Dunning and Grenne, 2000; Corfu, Andersen and Gasser, 2014). These rocks are overlain by the Late Ordovician to Early Siluran metasedimentary successions of the Lower and Upper Hovin Groups and the Horg Group (Roberts and Wolff, 1981; Nilsen and Wolff, 1989; Dunning and Grenne, 2000; Corfu, Andersen and Gasser, 2014). The southern part of these sedimentary successions, in the Oppdal area (Fig. 2.5), have by Nilsen and Wolff (1989) been correlated with the Hovin Groups, though more recent studies suggests that this could be

debated (Dunning and Grenne, 2000; T. Grenne, personal communication; B. H. Dalslåen, work in progress).

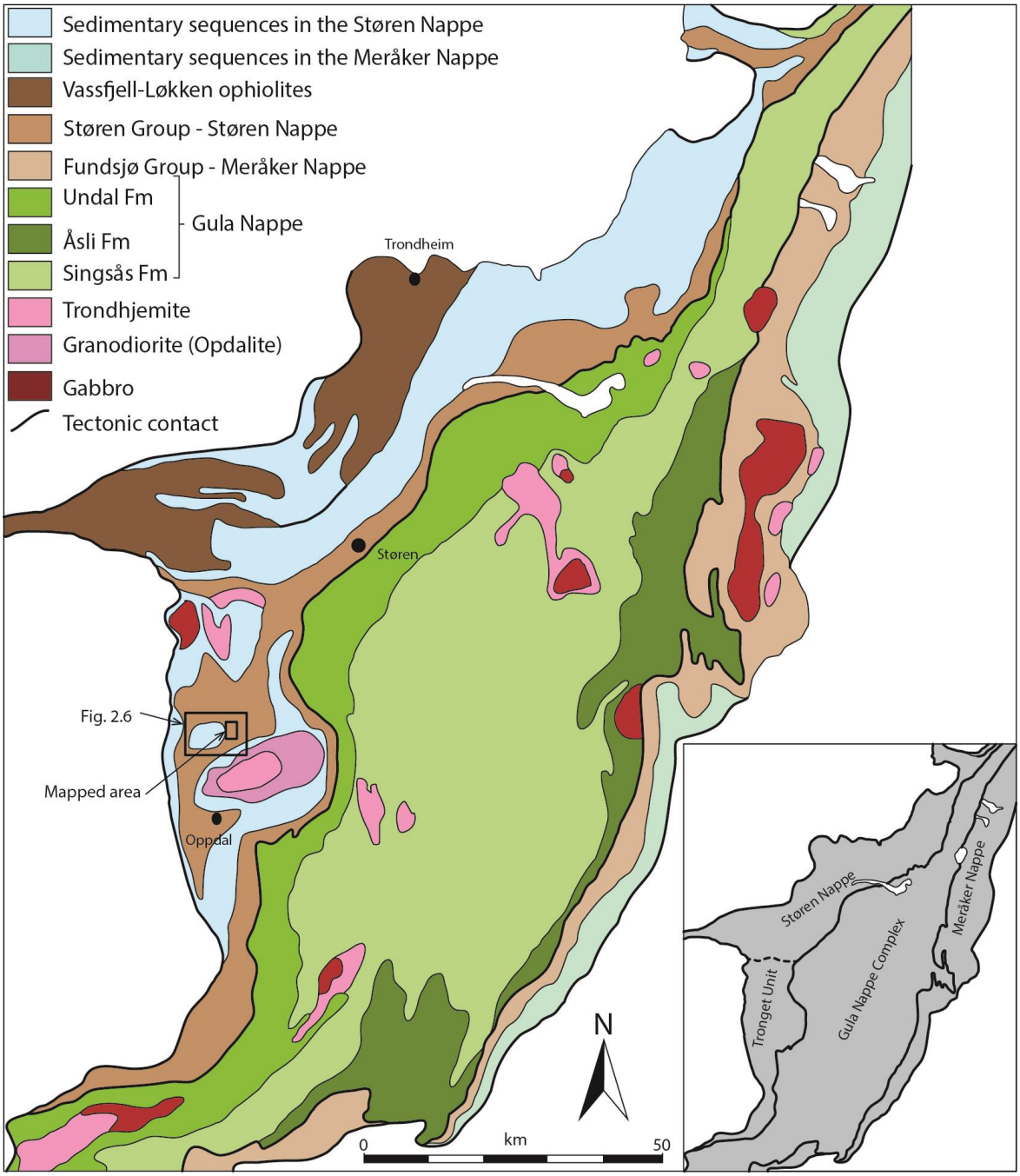

Figure 2.5: Generalized map of the Trondheim Nappe Complex with small inserted map of Trondheim Nappe Complex tectonostratigraphy. Large rectangle indicates position of the map in figure 2.6, small rectangle indicates position of the study area. Modified from Dunning and Grenne, 2000, modifications based on Wolff, 1976; Grenne, 1987; Nilsen and Wolff, 1989.

The eastern Meråker Nappe consists of the lower metavolcanic Fundsjø Group and the higher metasedimentary Sulåmo Group and younger units of up to Early Silurian age (Grenne and Lagerblad, 1985; Dunning and Grenne, 2000; Roberts and Stephens, 2000). The volcanic sequences of the Fundsjø Group have often been correlated with the Støren Group, yet petrologic evidence indicates a MORB-type to island-arc basaltic geochemistry for the Støren Group and a bimodal volcanic geochemistry of the Fundsjø Group, typical for more

subduction related island arc settings (Grenne and Lagerblad, 1985, Roberts and Stephens, 2000). Faunal evidence also suggests that the Støren Nappe originates from the Laurentian side, while black shales in the Meråker Nappe are similar to those in the Oslo area, indicating a more Baltic affinity for this nappe (Corfu, Andersen and Gasser, 2014).

The central Gula Nappe is one of the most heterogeneous rock sequences in the Scandinavian Caledonides, generally consisting of metasedimentary and metavolcanic rocks, including gneisses, medium- to high-grade schists, amphibolites and minor metasandstones, phyllites, quartzites, conglomerates, marbles and ribbon-cherts (Roberts and Wolff, 1981; Dunning and Grenne, 2000; Roberts and Stephens, 2000). It has been subdivided into three formations with the low-grade metamorphic Undal Fm to the west and the medium- to high-grade Singsås Fm in the centre and the Åsli Fm to the east (Dunning and Grenne, 2000). It is one of the least understood complexes in the Scandinavian Caledonides, with neither depositional age nor source area known (Corfu, Andersen and Gasser, 2014). Though previously believed to be of Laurentian origin, it might very well be a former microcontinent, or simply derived from a completely different continent, as suggested by Corfu, Andersen and Gasser (2014). The structure of the Gula Nappe and its tectonic contact to neighbouring nappes is also poorly understood, and it is debated whether it is an antiform, a synform, a klippe or a thrust between the Støren and Meråker nappes (Gee et al., 1985; Corfu, Andersen and Gasser, 2014).

Due to complex and varying lithologies and metamorphic grade together with poor age limitation, the understanding of internal contacts and timing of nappe displacement in the Trondheim Nappe Complex is still poorly understood. It is suggested that some internal structures and associated metamorphism in the complex is related to ophiolite obduction of the Støren and Fundsjø nappes onto the Laurentian and Baltoscandian miogeocline respectively, during the Early Ordovician, predating the main Scandian deformation (Gee et al., 1985; McClellan, 1994; Roberts et al., 2002). This episode is associated with regional low-grade metamorphism, isoclinal folding and a regional schistosity, as well as subsequent erosion and later Early Ordovician deposition (Roberts and Wolff, 1981; Gee et al., 1985; Roberts and Stephens, 2000). The subsequent Scandian phase included general ESE-ward nappe-displacement, imbrication and diachronous metamorphism, which to a large extent overprinted the pre-Scandian deformation (Roberts and Wolff, 1981; McClellan, 1994). Roberts and Wolff (1981) suggest a Mid-Silurian age for the start of the Scandian phase in the region, while Tucker et al. (2004) suggest emplacement of the Støren Nappe onto the Baltoscandian margin in Late Silurian based on recent U-Pb zircon data, though the structural relationship between the three nappes are still not properly understood. Later deformation included major upright syn- and anti-forms and extensional collapse, possibly starting in the Late Silurian/Early Devonian (Roberts and Wolff, 1981; Tucker et al., 2004).

2.4.2 – Dugurdsknappen and the Tronget unit

According to the geological map by Nilsen and Wolff (1989), the Dugurdsknappen area comprises greenstone and banded quartzite continuing towards the north and south, with a small quartz keratophyre. These units are overlain by a sandstone which continuous westward into a small restricted basin (Fig. 2.6). The area lies just north of Oppdal in what was described by Krill (1980) as the Tronget unit. He described this as the unit comprising

everything above and east of the Blåhø Nappe, characterized by a similar lithology, but lower-grade metamorphism than the underlying Blåhø Nappe. Gee et al. (1985) used the term to define the southwestern part of the Trondheim area, which were similar to the Støren Nappe, but lacking fossils. They speculated in whether it was an underlying unit or possibly related to the Støren Nappe, and suggested that it could be followed northwards as the sedimentary sequence parting the Støren Group greenstones and the Gula mica schists, possibly correlated with the northern Lower Hovin Group (Gee et al., 1985). Rohr-Torp (1972) describes the Oppdal-Innset area and draws a profile through Dugurdsknappen, depicting several lava horizons interbedded with alternating green lithic greywackes, sandstones, siltstones and tuffs. He also describes way up structures in pillows, cross-lamination and graded bedding, as well as the presence of banded quartzites in the upper and lower sides of all lava horizons, and uses this as an indication that the whole succession is tightly folded (Rohr-Torp, 1972). The unit has later been generally incorporated in the Støren Group (Nilsen and Wolff, 1989), though there is some debate as to whether it is in fact a separate unit (T. Grenne and D. Gasser, personal conversation, B. H. Dalslåen, work in progress).

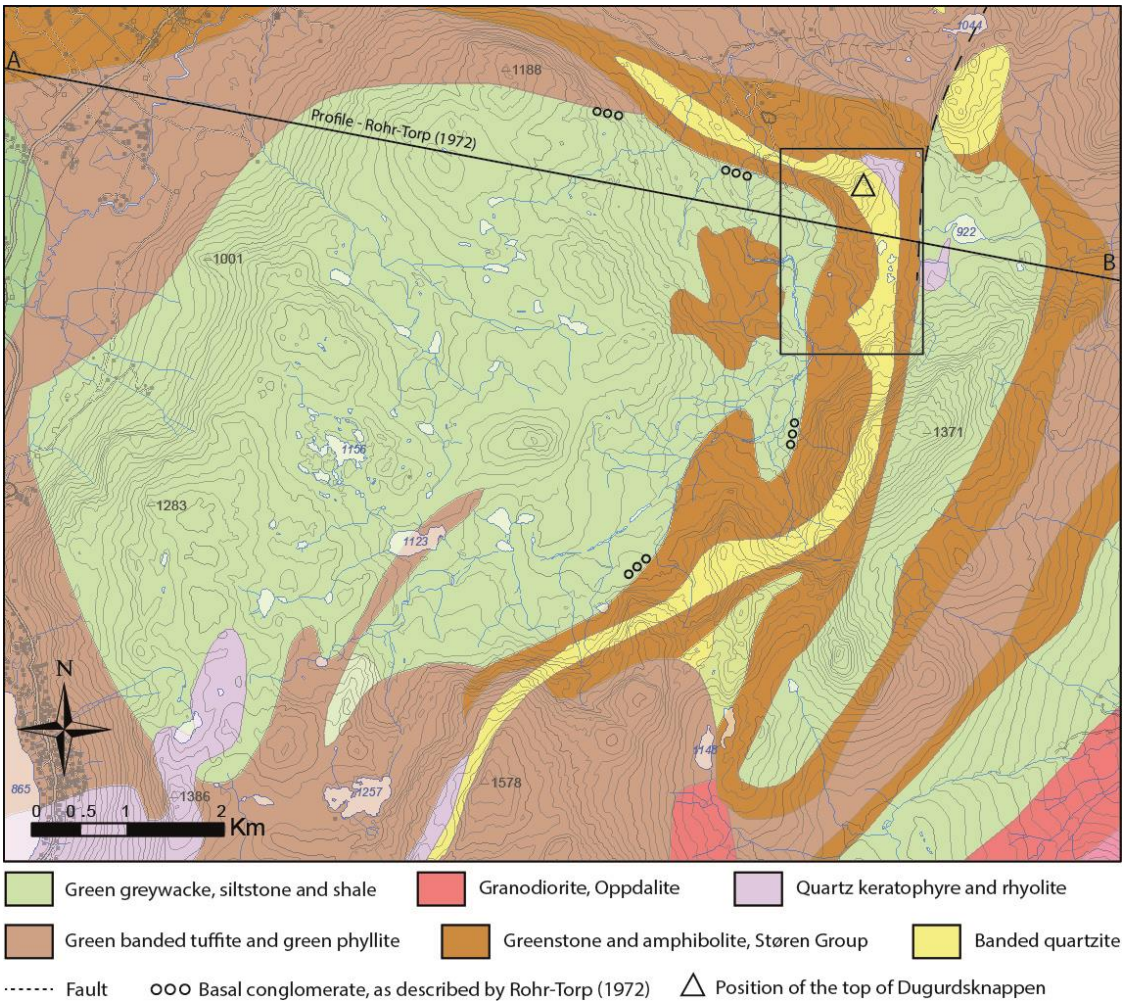

Figure 2.6: Geological map taken from the digital 1:250 000 bedrock database of NGU of the area mainly west and south of Dugurdsknappen. Rectangle shows the extent of the mapped area, which can be viewed in detail in appendix 4. Granodiorite in lower right corner is a small piece of the larger Innset Massif. Note that it is quartz keratophyre and not rhyolite that has been mapped within the working area. Map modified from Nilsen and Wolff (1989). Basal conglomerates and the profile described by Rohr-Torp (1972) are inserted. The profile and map by Rohr-Torp (1972) can be viewed in detail in figure 8.3.

Chapter 3 – Methods

3.1 – Fieldwork

About four weeks of fieldwork were conducted during July and August 2015, as well as a short field visit in October 2015. The field area is relatively easily accessible, starting a short walk from the car and stretching a few kilometres inwards into a mountainous area. The weather during the four weeks was varied with continuous rain the two first weeks and dry weather for the remaining time. This leads to some complications regarding the different appearance of the rocks when they are wet and dry, as well as generally worse accessibility during very wet conditions.

During these weeks 1000 GPS points with observations including photos, sketches, structural measurements and rock samples were collected.

Navigation and collection of GPS points was achieved using a Motion MC F5t field computer with integrated GPS and ArcGIS software. The digital field-data capture system BGS-SIGMAmobile was used together with ArcMAP to connect the observations directly to the GPS points while collecting them. By giving colour codes to the observed lithologies, a preliminary map was produced while in the field (Fig. 4.2).

A Canon compact digital camera was used for photographing and a Krantz-version – Geologist's compass for structural measurements. For the latter, the dip and dip direction method was applied, rather than using strike and dip. In addition to this a hand lens, a magnetic pen, ~5 % hydrochloric acid (HCL) and a hammer was used to examine the rocks closely.

45 samples were collected during the field work, with the intension to get a good representation of all units. Sampling was done for petrographic studies in thin sections, geochemical analysis and geochronology.

3.2 – Software

The software ArcGIS 10.2 (ESRI, 2011), and the BGS-SIGMAmobile system (British Geological Survey) were used during fieldwork, in subsequent treating of the data and in production of the final map. The BGS-SIGMAmobile database, which actually consists of a Microscoft Access database, was used separately to organise and look through the structural data together with Microsoft Excel.

The structural data was plotted using the software Stereonet 8 (Allmendinger, Cardozo and Fisher, 2013; Cardozo and Allmendinger, 2013). The software Move (Midland Valley Exploration: Move Suite) was applied to create profiles and a 3D surface, and in attempting to make a 3D model of the area, by importing the map and structural data exported from ArcMAP, together with a digital elevation model from NGU.

Profiles and figures were altered and produced using Adobe Illustrator CS6 and Incscape 0.91. Thin section photographs were taken with an Axiocam MRc5 camera and manipulated in Adobe Photoshop CS6, which was also used for editing field photographs and other

figures. Geochemical data was investigated using Michrosoft Excel and the geochemical software IgPet 2007, from RockWare. Geochronological data was analysed in Isoplot (Ludwig, 2001) and visualized with DensityPlotter (Vermeesch, 2012).

3.3 – Petrographic observations

Petrographic observations were done on forty ~30µm thick polished thin sections. These were produced at the thin section workshop at the Department of Geosciences at UiO by Salahalldin Akhavan, after being cut on a diamond saw at NGU. They were then studied and described using an Axioscope 40 optical microscope.

3.4 – Geochemical analysis

Geochemical analysis was done on 32 samples using XRF for main (>~0.5%) and trace (<~0.5%) element analysis. XRF is best suited on elements with atom number 9 or higher, and has low precision on Rare Earth Elements (REE). LA-ICP-MS was therefore also used for trace element analysis. Four sandstone samples were only analysed for major elements on XRF, thus only 28 samples were analysed on LA-ICP-MS.

The samples were both prepared and analysed by the laboratory at the Norwegian Geological Survey (NGU). Preparation for main element analysis is done by melting of 0.6 g sample material (crushed to a fine powder) mixed with 4.2 g lithium borate ($Li_2B_4O_7$) into homogenous glass beads. For trace element analysis the samples are prepared by compacting 9.6 g sample material (fine powder) mixed with 2.4 g wax into tablets. The XRF-instrument used at the NGU-lab is a PANaluthical Axios 4kW XRF Rh-X-ray tubes. In the following, a short description of the XRF-method follows.

X-Ray Fluorescence (XRF)

X-ray fluorescence is a non-destructive method to determine the bulk chemical composition of major, minor and trace elements in a sample by the use of x-rays.

X-rays are produced by heating up a filament in a tube (e.g. wolfram filament), producing electrons which are then accelerated towards an anode. The deceleration when the electrons reach the anode causes brehmsstrahlung, or emission of x-rays. The x-rays are directed towards the sample, where they are either absorbed or scattered. If the absorbed x-rays have higher energy than the bonding energy of the atom, an electron will be pushed out, forcing an electron from an outer shell to move inwards. This causes the electron to lose energy which will be emitted as fluorescence and transferred to a detector.

Each element emits fluorescence with a characteristic wavelength, which can be detected by reflecting them at known angles through crystals with known spacing. The wavelengths get reflected according to Braggs law (equation 3.1), where n = an integer representing the order, λ = the wavelength, d = crystal spacing (d-spacing) and θ = angle of incoming radiation. Because all other variables are known, the wavelength can be calculated.

$$n\lambda = 2d * sin\theta \qquad \text{(Eq. 3.1)}$$

Laser-Ablation Inductively Coupled Plasma Mass Spectrometry (LA-ICP-MS)

In this instrument a laser beam is directed to the sample and evaporates parts of it, creating aerosols that are transferred with helium gas into plasma of argon gas. This plasma heats up the aerosols causing them to ionize, and the ions are transported further into the mass spectrometer. Here they are separated according to their mass/charge (m/e) ratio, before they are counted by a detector. Both trace elements and isotope ratios for radiometric dating can be detected with this method, making it a versatile instrument.

3.5 – Geochronological analysis

Four samples were collected for U-Pb zircon geochronology. Mineral separation was conducted at the Department of Geosciences at the University of Oslo. Preparations of the samples included crushing with jaw crusher followed by Retch crusher. Conventional magnetic and heavy liquid techniques were used to separate zircons from four samples. Individual zircon crystals were hand-picked under a binocular microscope, mounted in epoxy and polished down to expose the grain centers. Backscatter (BSE) and cathodoluminescence (CL) images of the zircons were obtained prior to analysis using a Scanning Electron Microscope (SEM). The laser ablation inductively coupled plasma mass spectrometry (LA-ICP-MS) was performed using a New Wave UP193FX Excimer laser coupled to a Thermo Element XR single collector high resolution ICP-MS at the Geological Survey of Norway. A 15μm wide line scan at a speed of 2μm/sec was used at energies of 4.0 J/cm^2 and a repetition rate of 10 Hz. ca 0.4 l/min. He gas was used as a carrier gas flushing through the sample chamber, mixed with ca 0.9 l/min Ar gas and transported to the ICP-MS. The measurement time was first 30 s of gas blank acquisition and thereafter up to 30 s data acquisition. Masses ^{202}Hg, ^{204}Hg + ^{204}Pb, ^{206}Pb, ^{207}Pb, ^{208}Pb, ^{232}Th and ^{238}U were acquired in a time-resolved counting scanning mode. ^{235}U was recalculated from the natural abundance for ^{238}U/^{235}U (Steiger and Jäger, 1977). The measured isotope ratios were corrected for element- and mass-bias effects using the zircon standard GJ (607 ± 0.4 Ma; Jackson et al., 2004). The zircon standards 91500 (1065 ± 0.3 Ma; Wiedenbeck et al., 1995) and Temora II (416.5 ± 0.22 Ma; Black et al., 2004) were used as control standards, and reference zircons ØS-99-14 (1797 ± 3 Ma; Skår, 2002), Z6412 (1160 ± 1.6 Ma; unpublished, GSC Ottawa) and the in-house standard T33187 (2674 ± 8; unpublished, NGU) were used for standardization. The data were not corrected for common Pb, but the signal from ^{204}Pb is used to exclude analysis containing common Pb. The data reduction was done with the GLITTER® software version 4.4.4 (Van Achterberg et al., 2001). U-Pb ages of the zircons are calculated using the ISOPLOT software for Microsoft Excel version 2.49 (Ludwig, 2001).

Scanning Electron Microscope (SEM)

SEM works somewhat similar to XRF, but instead of transferring the produced electrons into x-rays, they are transported directly to the sample where they interact with the atoms inside it. For backscatter imaging it is the reflected high energy backscatter electrons from just below the sample surface that is detected. They give information on the atomic numbers, which indicates the weight of each element. This is reflected as light (heavy atoms) and dark (light atoms) areas making up an image of the sample. When doing CL imaging the goal is to

examine the internal structures of the mineral, not just the surface. It is still electrons that are transferred into the sample, but it's the emitted photons with light in the visible spectre that is detected. These are analysed to give a spatial representation of the grains composition, which results in imaging where the zoning pattern and rim/core structure of zircons is easily detected. This is very useful when programming the paths of the LA-ICP-MS laser beam.

Theory of U-Pb radiometric dating

This method is based on the fact that radioactive uranium (U) isotopes break down to lead (Pb) isotopes at a constant rate of decay. By comparing the abundance of radioactive U-isotopes to its decay product of Pb-isotopes in minerals, absolute ages can be calculated. In this study zircons ($ZrSiO_4$) have been used, which is the most common mineral in radiometric dating. The decay chains from the two naturally existing uranium isotopes ^{238}U and ^{235}U to their daughter isotopes represent the two independent chronometers applied in this method:

$^{238}U \rightarrow {}^{206}Pb$, with half-life of 4.47Ga

$^{235}U \rightarrow {}^{207}Pb$, with half-life of 0.7Ga (Dickin, 2005)

The amounts of each isotope are found through analysis and the decay constants are known empirically, which leaves time as the only unknown factor. An age equation (Eq. 3.2; Dickin, 2005) can therefore be used to create an isotopic clock, here illustrated by the $^{206}Pb/^{238}U$ system where t = time and λ = decay constant of 238U (known empirically).

$$206Pb = 238U\,(e^{\lambda t} - 1) \qquad \text{(Eq. 3.2)}$$

This method is built on the preposition that the mineral originally only contained uranium and no lead, which to a large degree is true for zircons, due to its crystal lattice not easily allowing lead to build in. However, this is not always the situation, as the stable lead isotope ^{204}Pb, also referred to as common lead, can be present. This will contaminate the results, and therefore an intermediate step is used to normalize for this isotope (Eq. 3.3; Dickin, 2005), though this was as previously noted not done in this study.

$$\left(\frac{206Pb}{204Pb}\right)_t = \left(\frac{206Pb}{204Pb}\right)_0 + \left(\frac{238U}{204Pb}\right)\left(e^{\lambda t} - 1\right) \qquad \text{(Eq. 3.3)}$$

There are only ~20% ^{235}U isotopes found in uranium, and since the half-life are so short most of this isotope have already decayed to its daughter isotope (Dickin, 2005), and the system can only be used in younger rocks. The $^{206}Pb/^{238}U$ system has a much longer half-life and is therefore more reliable, and preferred when dating Caledonian aged rocks. However, if the rocks are older than ca. 900 Ma, the ratio of the $^{207}Pb/^{206}Pb$ system is best suited, as the uranium content is too low due to decay (Dickin, 2005).

Chapter 4 – Description of mapped units

4.1 – Topographic overview

The field area is situated around Dugurdsknappen, a small mountain top 1063 m.a.s.l in the Nerskogen area, Sør-Trøndelag County (Fig. 1.2; Fig. 4.1). The mapped area covers approximately 1.6km^2 and a vertical elevation difference of about 250 m from the topographic highest to the lowest point. To the east, the map area is bounded by a north-south trending fault, while to the south and west the map is restricted by the vegetated low lands of Leverdalen, and to the north the map is limited by a small topographic shoulder (Fig. 4.1). The mountain itself has most outcrops, with almost 100% rate of exposure. The lower surrounding areas are however characterized by marshes with scattered outcrops, as well as some larger more well-exposed hills (Map 6, appendix 1). This makes mapping more dependent on interpretations in the lower areas, while in the higher areas the lithologies and separating boundaries are much better defined.

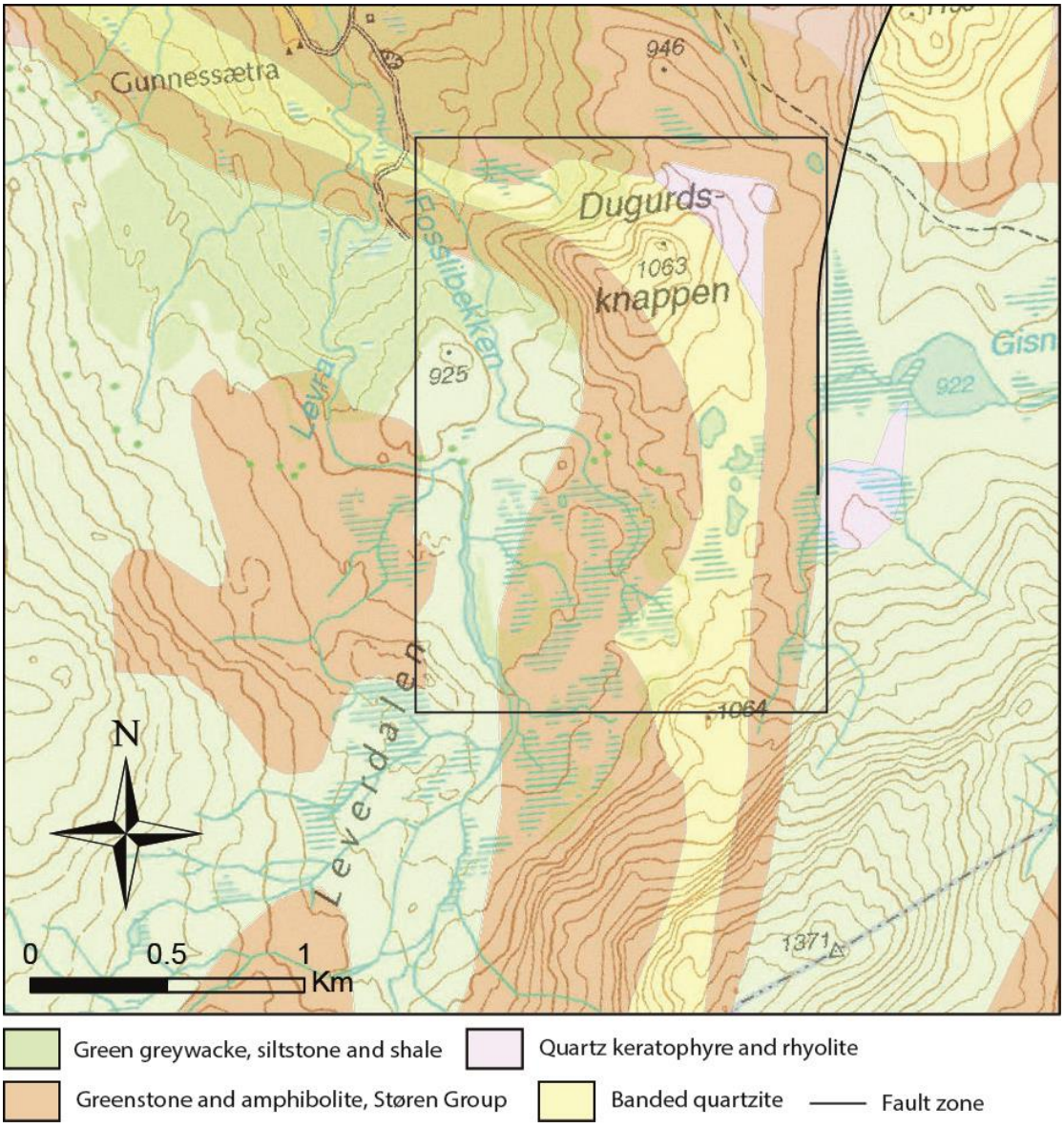

Figure 4.1: Topographic map of Dugurdsknappen and surrounding area. Note the many marshes in the southern flat area obscuring the geology, as well as the high surrounding mountains. Figure modified from Nilsen and Wolff, 1989.

4.2 – Description of the map

The map is based on exactly 1000 data points with observations collected during four weeks of fieldwork (Fig. 4.2). Due to the distribution of available outcrops, there are some areas with a higher density of observations, mainly in the higher areas and along lithological boundaries. To help with the interpretation in those areas where the exposure is low or too few observations have been made, observations made by Bjørgunn Dalslåen as well as the older map by Nilsen and Wolff (1989; Fig. 4.1) are used. The mapped rocks are divided into 14 different lithological units, making up 4 groups (Map, appendix 4). The three groups greenstone-related rocks, chert-related rocks and green siltstone dominate the map in the north, east and southeast, with greenstones as the most widespread lithology. The chert-related rocks lie inside the greenstone-related rocks, both in several smaller pockets and surrounding the central unit of green siltstone. The remaining group is limited to a smaller area in the western and southwestern parts of the map, separated from the underlying units by an unconformity, and comprise a basal conglomerate with the green sandstone on top with pockets of intermediate volcanics and intrusive inside.

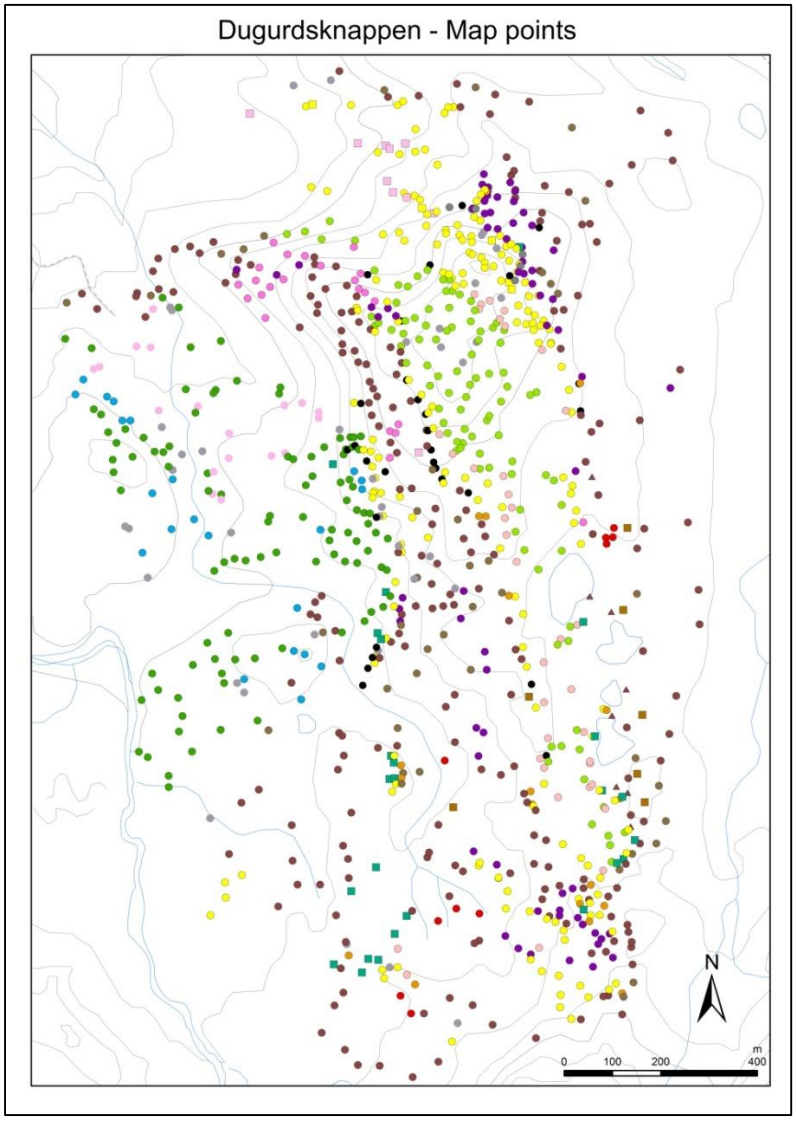

Figure 4.2: Map showing the distribution of GPS points with observations collected during fieldwork. Different colours indicate different lithologies based on field names. Note the accumulation of points in elevated areas and the more scattered pattern particularly in the western to southwestern lowlands.

4.3 – Mapped lithologies

4.3.1 – Greenstone-related rocks

Greenstone and pillow lava

This is the biggest unit containing mainly greenstones, with layers of pillows showing primary structures separated by massive lavas. There are also a few localities with pillow breccias, greenschist and greenstone dykes. The greenstones are generally massive and fine-grained with varying shades of green, with bigger biotite grains in a few areas.

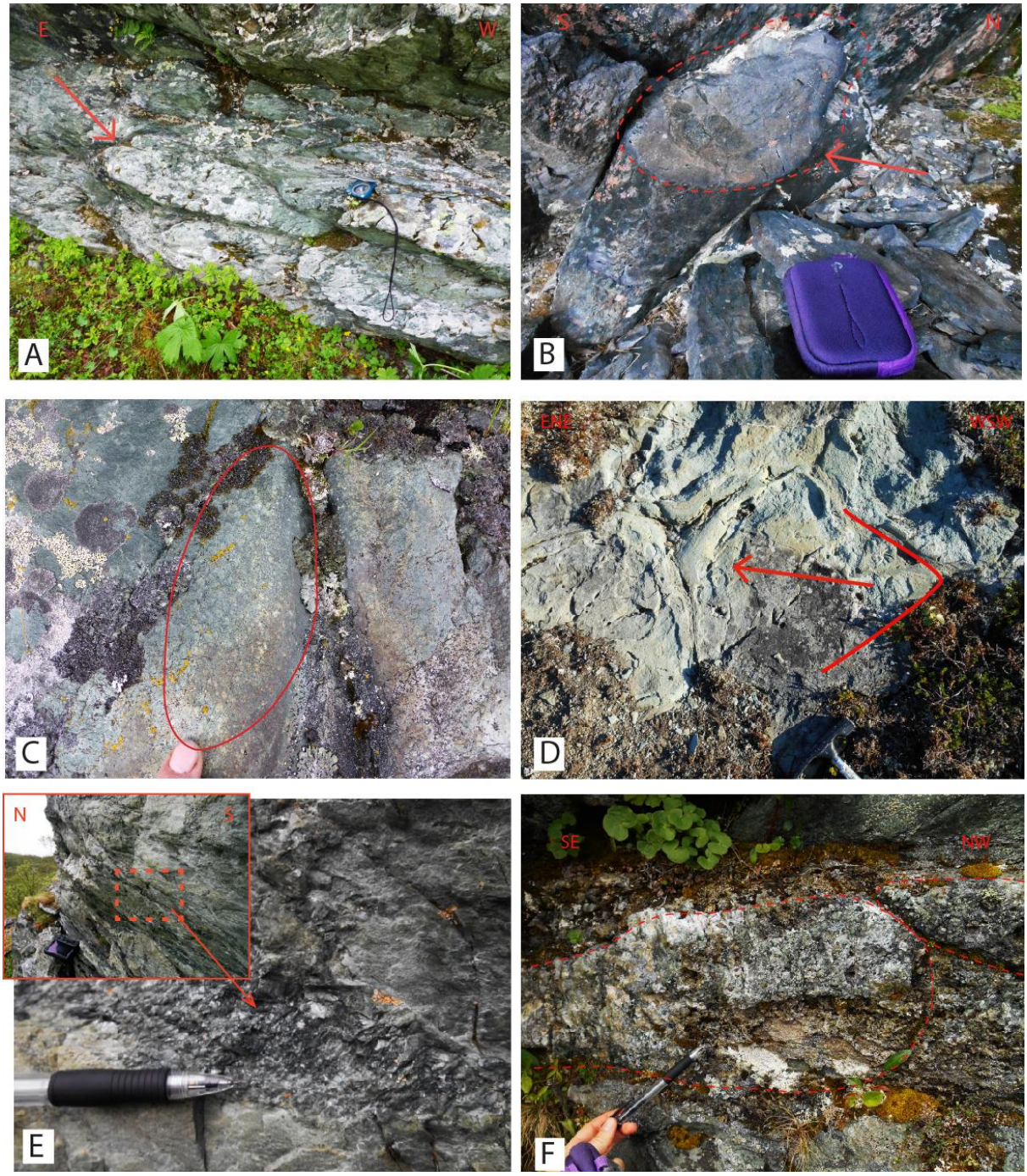

Figure 4.3: A) Elongated pillows. B) Cross section of elongated pillow show pillow rim. C) Filled gas vesicles in pillow. D) Pillow indicating way up due to the bottom sinking into the underlying pillows. Way up is towards east, indicated by the arrow. E) Green coarse crystals in the shaly layers between pillows. F) Recrystallized pillow, quartz crystals dominate

Pillow structures could be observed in about 50 localities (Map, appendix 4; 4.3-A). Many of these pillows display a clear pillow rim and gas vesicles (Fig. 4.3-B&C). The pillows are usually flattened and elongated with size varying between 5 and 50 cm in diameter, and separated by foliated, fine-grained, chlorite-rich material. Due to this deformation, there are only a few localities that give any indication on way up, of which only one can be used with any certainty (Fig. 4.3-D). At some localities, bigger dark green crystals, probably chlorite, occur in rose like structures in foliated parts between pillows (Fig. 4.3-E). In one locality, the entire pillow is recrystallized, with big quartz crystals and some long elongated green crystals, possibly epidote (Fig. 4.3-F). In addition, a few pillows contain scattered pyrite crystals and other sulphides.

Monomict pillow breccias, mainly consisting of greenstone clasts, occur in a few localities towards the ribbon-chert boundary (Fig. 4.4-A). Some areas are significantly more foliated, and interpreted as greenschist, which seems to be a phenomenon that is most common towards the boundary to ribbon-chert, a transition zone that is generally chaotic. This schisty greenstone is often coarser-grained than the usual greenstone and contains bigger oriented chlorite. At a few localities, greenstone dykes are observed cutting the greenstone (Fig. 4.4-B).

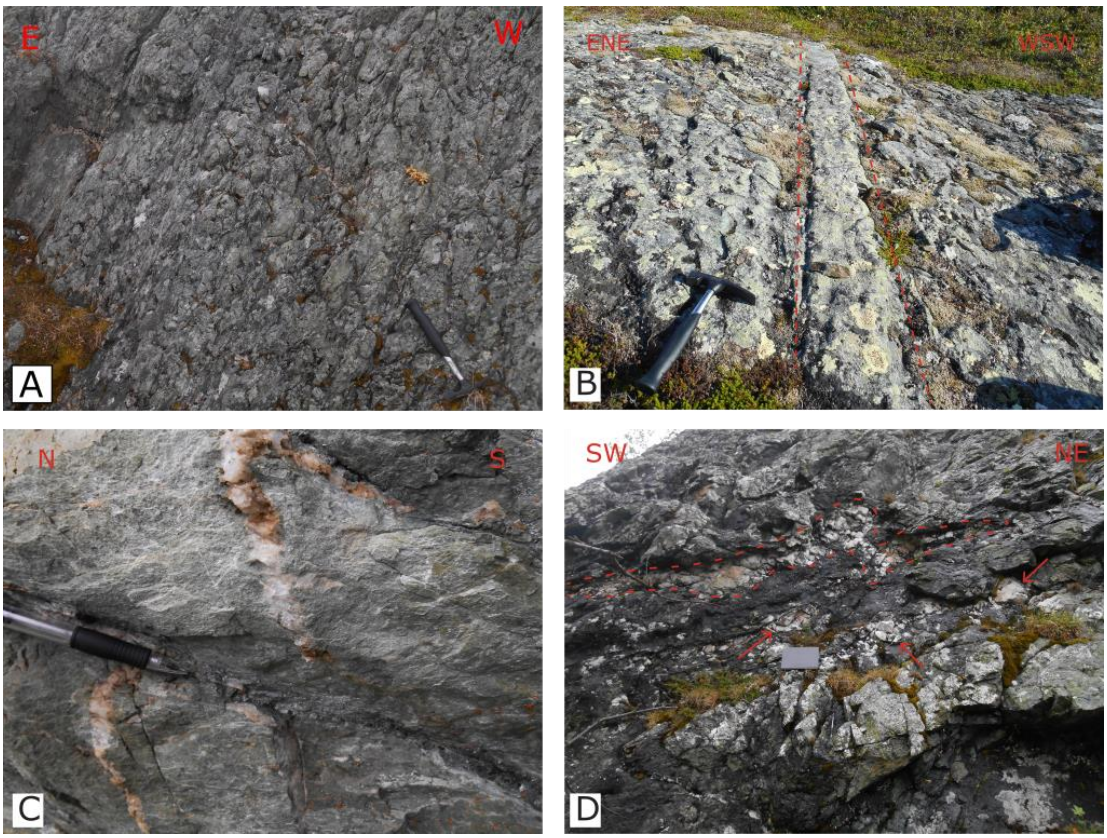

Figure 4.4: A) Possible pillow breccia from the southern end of the map. B) Basaltic dyke cutting the greenstone, from eastern part of the greenstone. C) Quartz veins and carbonate veins cutting pillows. D) Large folded quartz veins in greenstone.

A typical feature for this composite greenstone unit is abundant quartz and carbonate veins. The carbonate veins occur generally between pillows, sometimes as a layer around them, while the quartz veins follow any weaknesses in the rock, thus also occasionally cutting the

pillows. Some quartz veins are up to 30 cm in diameter, while the carbonate veins appear only in smaller local accumulations (Fig. 4.4-C&D).

Gabbroic intrusion

Within the greenstone four pockets of gabbroic-looking rocks are mapped (Map, appendix 4). These rocks have an almost white, coarse-grained crystalline groundmass with scattered dark green elongated amphibole grains (Fig. 4.5-A&B). The rocks look somewhat like the intermediate intrusion, but the texture is coarser and it does not contain biotite. The pockets lie within the greenstone, and represent probably a more intrusive version of this. They are only found in a few places and are thus not a dominating lithology in the area.

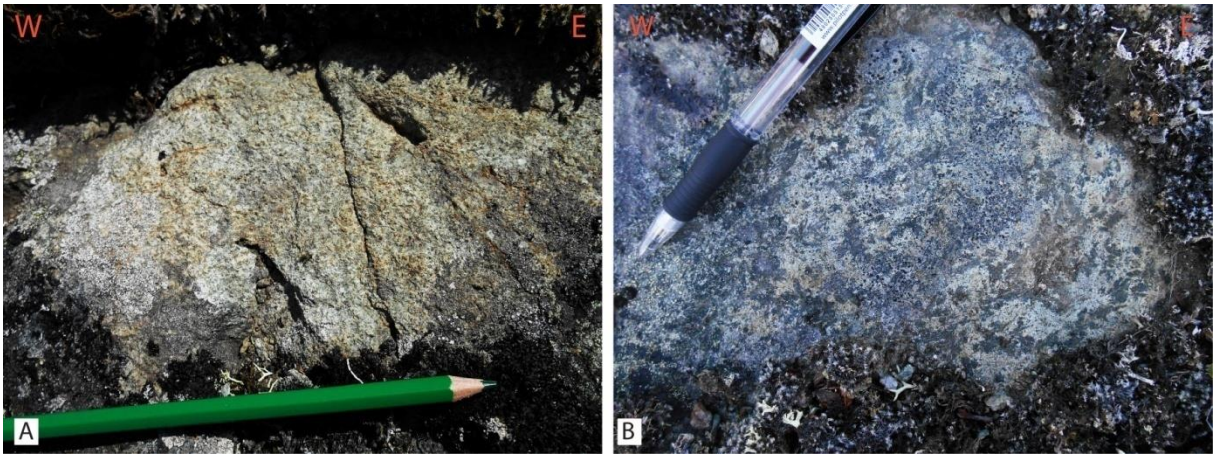

Figure 4.5: A) and B) Gabbroic texture.

Altered greenstone

This is a somewhat diffuse unit lying within the greenstone unit and is not always easy to define. In fact it might be a greenstone geochemically, but in the field the rocks have an altered appearance. Two versions were mapped in the field, based on a slight colour difference: felsic volcanic (Vuf) and intermediate greenstone (GrIn). Vuf is a very inhomogeneous rock, generally looking like greenstone with a mix of light and dark green, but with the addition of pink and purple areas, which result in a more felsic impression (Fig. 4.6-A). The GrIn, in contrast is more homogenous fine-grained with a grey to violet-blueish colour (Fig. 4.6-B&C). Vuf is mainly observed in the northwestern ridge up to Dugurdsknappen, while GrIn is dominant in all other areas. However, the field descriptions are so unclear that any clear boundary between Vuf and GrIn is yet to be defined, thus they are joined as altered greenstone in the final map (Map, appendix 4).

Figure 4.6: A) Felsic looking part of Vuf due to pink spots. B) Surface of pillow in GrIn, note the colour variations. C) Foliated surface of GrIn. D) Another conglomeratic part of GrIn, possibly pillow breccia.

The relation between greenstone and Vuf/GrIn is also hard to define properly. Vuf/GrIn have a surface similar to greenstone, with clear pillow structures in GrIn, and a generally fine-grained crystalline texture. Both Vuf and GrIn look a bit brecciated in some areas, though still very cohesive (Fig. 4.6-D), similar to the breccia seen in the greenstone. A more foliated version of the GrIn lies in the pass to the northeast of Dugurdsknappen, where the bounding greenstone unit is heavily foliated in the same fashion. Both carbonate and quartz veins are common, especially in Vuf, similar to the greenstone unit. These many similarities between the two have led to mapping Vuf/GrIn as an altered greenstone and not a completely separate unit.

Agglomerate

There are several diffuse zones with a polymict conglomeratic to agglomeratic look. They are generally found in the greenstone unit, mainly associated with the transition zone towards chert pockets as well as the large central ribbon-chert – siltstone unit (Map, appendix 4). They consist mainly of a mixture of greenstone and mafic clasts and lighter green to white leucocratic clasts (Fig. 4.7-A&B). There are also chunks of chert, sometimes complete layers (Fig 4.7-C&D), and occasional jasper clasts, but no granitic or quarzitic clasts. The clasts vary from angular to round and lie in a dark-green fine-grained matrix, possibly tuffitic. The unit has experienced deformation causing foliation in the matrix and elongated clasts following the orientation of the foliation (Fig 4.7).

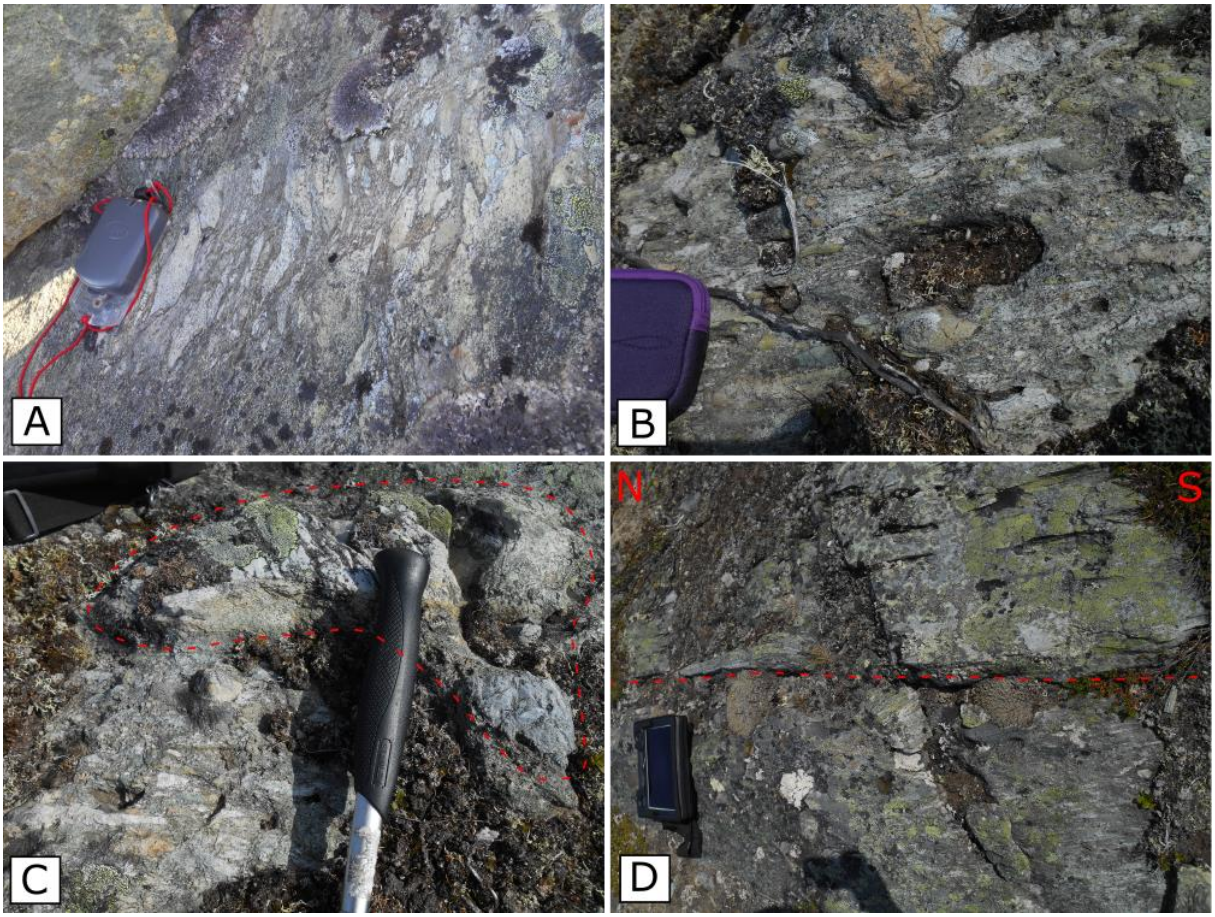

Figure 4.7: A) and B) Polymict agglomeratic texture with dark matrix and light to dark clasts. Note foliation of matrix and elongation of clasts. C) Big chert chunk and some other more rounded clast/bomb in otherwise similar agglomerate. D) Large area of chert in agglomerate.

4.3.2 – Chert-related rocks

Jasper

Several massive accumulations of jasper occur locally between the greenstone and ribbon-chert units (Map, appendix 4).The jasper appear as chunks up to 50 cm in diameter and as layers varying in size from tens of cm up to about 5 m long and 2 m wide on the most (Fig. 4.8-A). Jasper is a red coloured version of chert, due to haematite content, with similarly hard and dense microcrystalline texture (Fig. 4.8-B). Due to some magnetite content it is also magnetic, an important characteristic in the field. Several thin quartz veins are cutting the jasper occurrences, and it has several other inclusions and impurities as well (Fig. 4.8-B). There is no clear layering, nor any sedimentary or tectonic structures within these layers.

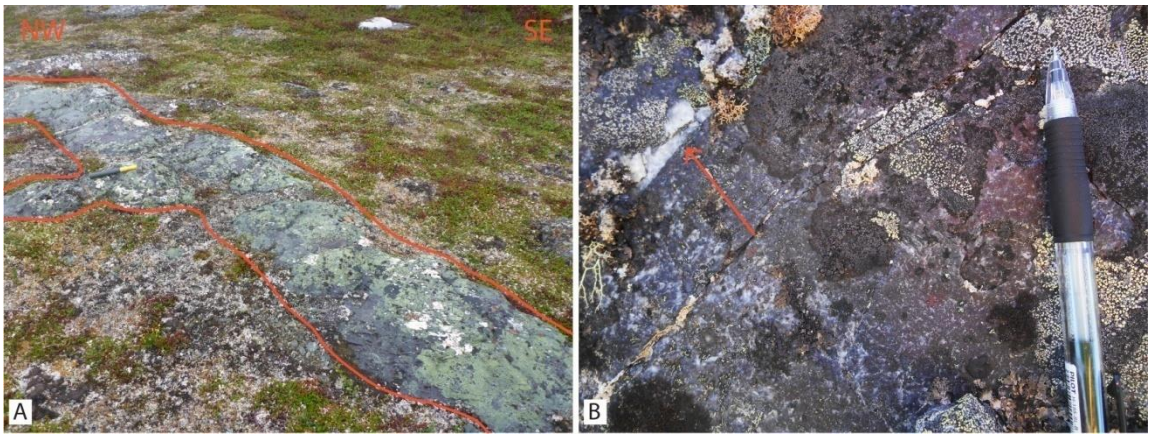

Figure 4.8: A) About 5 m long and ½ m wide layer of jasper between greenstone on the western side and ribbon-chert on the eastern. B) Jasper texture. Note the heterogeneous colour distribution and the quartz vein.

Ribbon-chert

The ribbon-chert unit in the area is dominated by a layered sequence of mainly ribbon-chert with minor intercalated sandstone and shale beds. The ribbon-chert itself consists of massive, cm- to m-thick chert layers separated by thin phyllosilicate-rich layers (Fig. 4.9-A). There are no sedimentary structures in the chert and the layers can sometimes be hard to follow, so there is some uncertainty as to whether the layering is a depositional bedding or caused by later deformation. Yet, the described sand and shale layers in between suggests that it is mainly a depositional layering. The chert layers are white and light- to dark-grey coloured, with variations towards green, and purple (Fig. 4.9-A&B). The texture of the chert layers is microcrystalline and the rock is very hard and dense, especially the white type. Due to the density and hardness, it breaks in a concoidal fashion (Fig. 4.9-C).

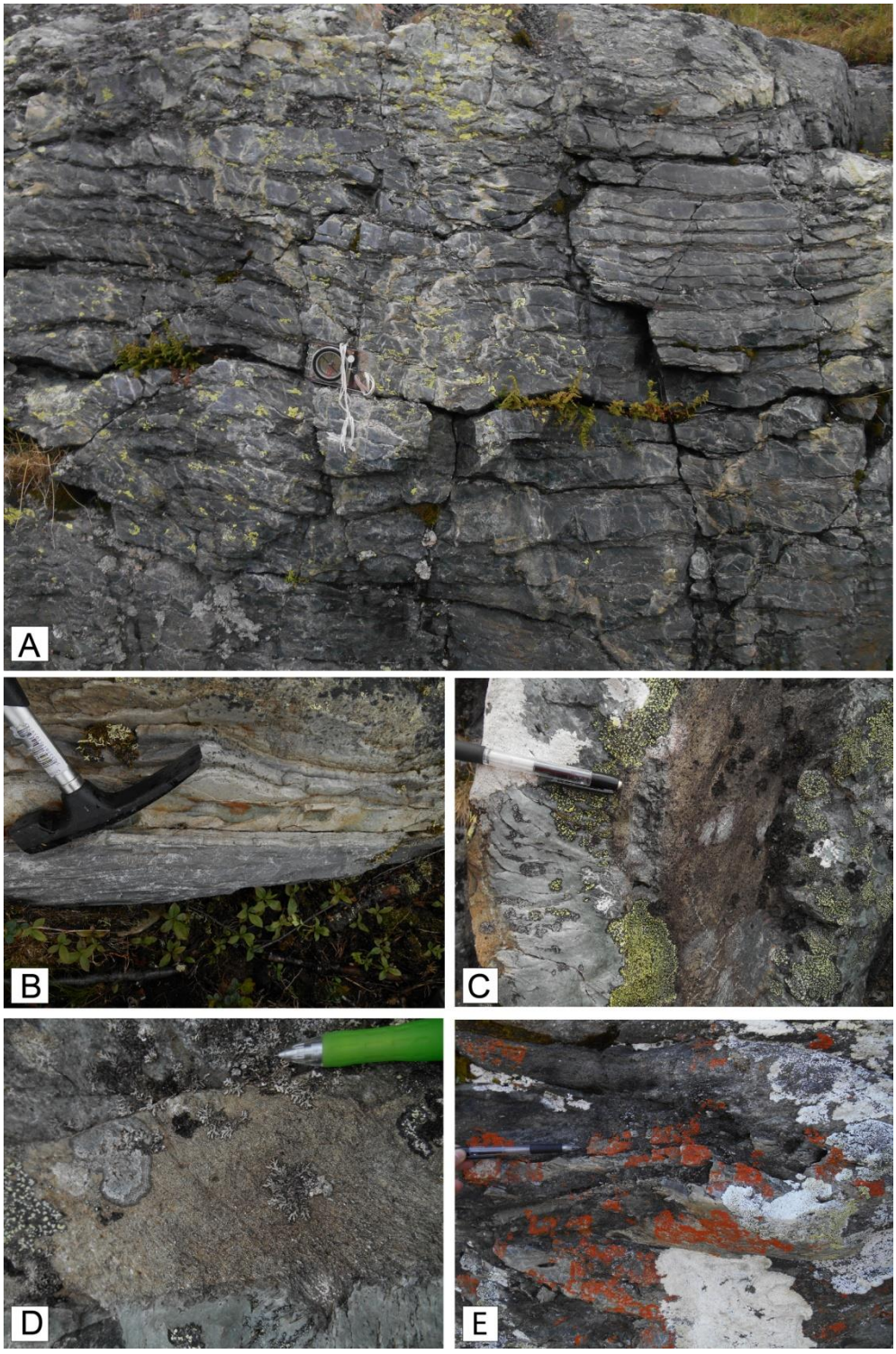

Figure 4.9: A) Typical layering of ribbon-chert. B) Texture and layering of ribbon-chert. C) Microcrystalline chert breaking in concoidal fashion. Note the shale layer between the two chert layers. D) Brown sandstone bed. E) Carbonate rich grey sandstone with chert lenses

The sandstone and shale beds appear in several locations, but they cannot be followed over larger areas. Two sandstone types were observed: 1) Brown medium-grained sandstone with angular grains slightly similar to shell fragments, but does not contain any carbonate indicating it is siliciclastic (Fig. 4.9-D); 2) Fine-grained, grey and carbonate-rich sandstones (Fig. 4.9-E), that appear as bigger separate beds closer to the eastern ribbon-chert/greenstone

boundary than the brown type. The shale is very fine-grained and greenish to brown in colour and appears in much thinner beds than the sandstones, often "flowing" between more competent chert. This shale, appearing in tightly alternating sequence with the chert, creates the typical ribbon-structure, as depicted in Fig. 4.10-A&B.

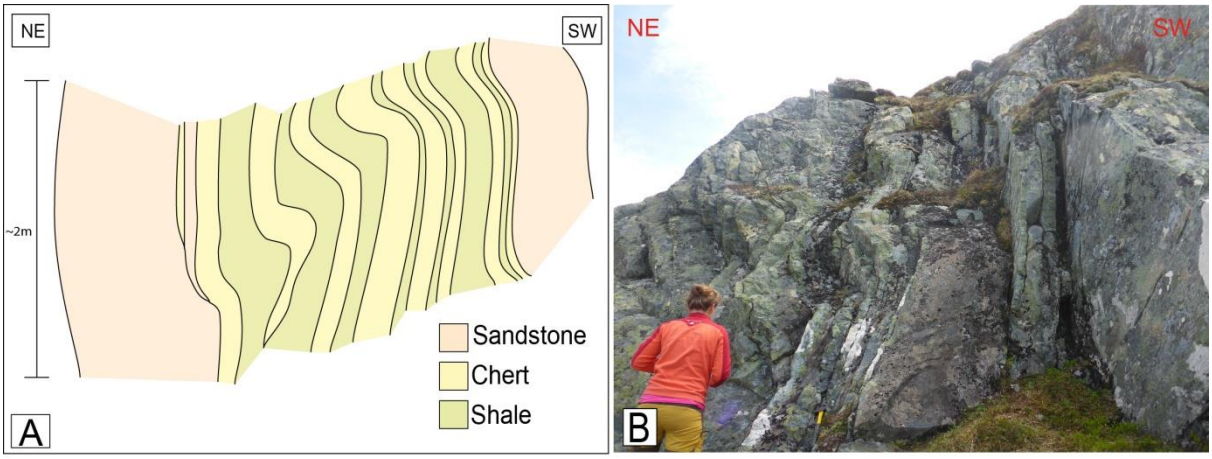

Figure 4.10: A) Sketch of section B) and extended area, shows how ribbon-chert (chert and shale) and sandstone beds alternate on a meter-scale. B) Ribbon-chert and sandstone beds interbedded. Photo: D. Gasser

Felsic conglomerate

At several localities in the northern parts of Dugurdsknappen, the ribbon-chert unit contains pockets of conglomerate (Map, appendix 4). It is dominated by light, almost white, felsic clasts in a light greenish to grey foliated matrix (Fig. 4.11). There are some darker sandstone clasts, but no clasts of chert or other lithologies. The clasts are normally rounded and of relatively small size, but some are big, up to 10-20 cm in diameter (Fig. 4.11-B). In some locations, the matrix is more foliated and darker, but it generally holds a very light colour. It is in some ways similar to the agglomerate described in chapter 4.3.1, but differs due to lighter colour and more clast variation.

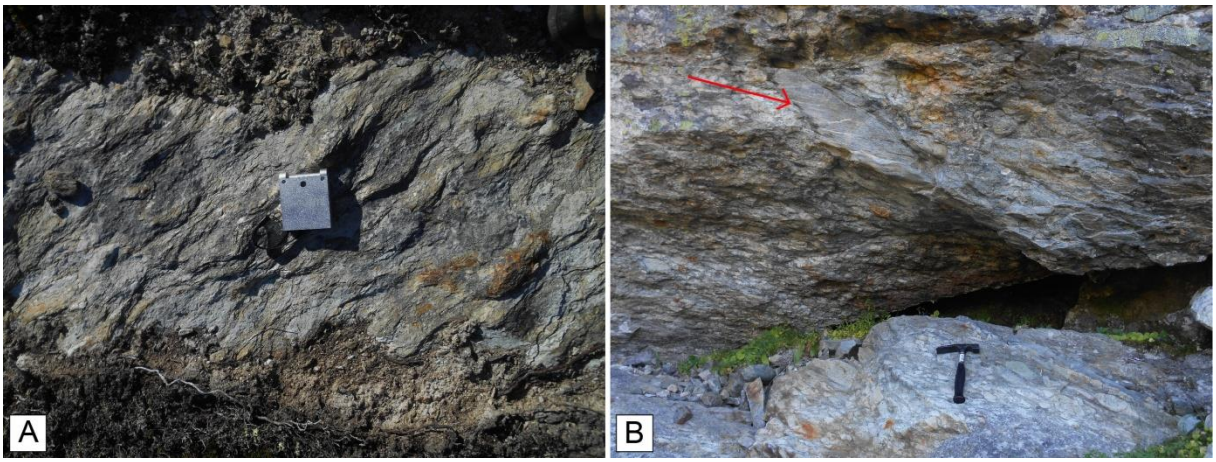

Figure 4.11: A) Light clasts in a grey/light green foliated matrix. B) Conglomeratic surface with light coloured clasts. Note the large sandstone boulder inside the otherwise fairy well sorted felsic clasts.

Silty chert

This unit lies between the ribbon-chert and the green siltstone in a discontinuous package around the main synform (Map, appendix 4). It is dark purple/grey and very fine-grained, with

a more clastic and softer texture than the ribbon-chert, almost like a siltstone (Fig. 4.12). It appears to become gradually more sedimentary further away from the ribbon-chert and closer to the siltstone, indicating that this unit represents a gradual transition from chert to siltstone.

Figure 4.12: Silty chert, or dark chert from a section closer to green siltstone than ribbon-chert. Note the silty texture compared to the previous microcrystalline texture of chert seen in figure 4.9.

4.3.3 – Green siltstone

This unit lies as one big package in the middle of the central synform, inside the ribbon-chert (Map, appendix 4). It is green and very fine-grained, consisting of silt-sized particles, with some slightly more sandy parts. Bedding can be observed in several areas, with continuous beds up to 10-20 cm thick, though more commonly 5-10 cm thick (Fig. 4.13-A). The siltstone typically contains golden flaky minerals, probably biotite flakes, as well as some pyrite/sulphide crystals. These grains are all medium-grained, in an otherwise very fine-grained and homogenous light green matrix. These medium-grained porphyroblasts are a typical distinguishing characteristic for this rock unit. The surface is also much smoother, thus very different from the lumpy surface of the volcanic units. No other sedimentary structures apart from bedding have been observed, thus there are no good indications of right way up. It is heavily foliated, which in many localities makes it look like a phyllite (Fig. 4.13-B).

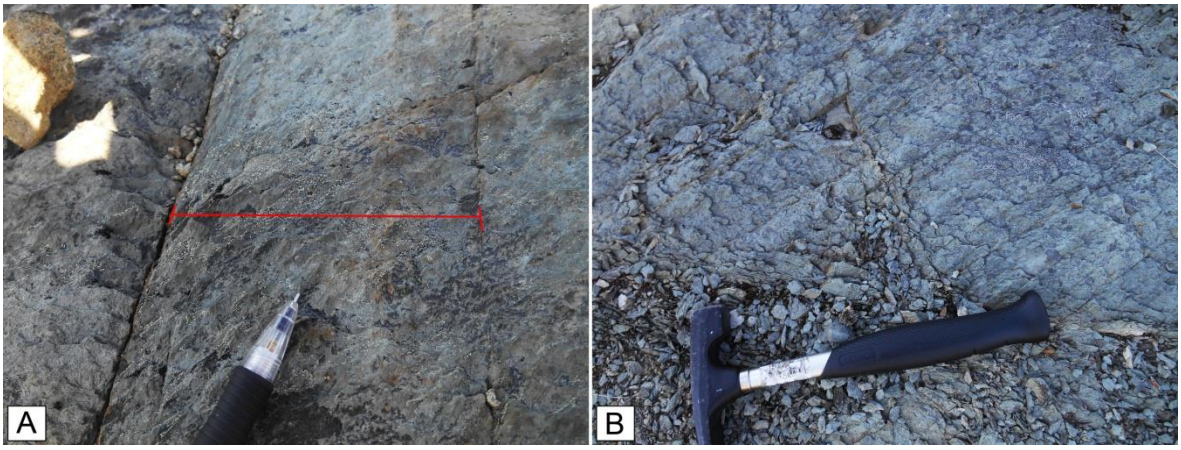

Figure 4.13: A) Foliated green siltstone. Red line indicates width of a bed. B) Foliated green siltstone, almost phyllitic looking.

4.3.4 – Rocks above the unconformity

Green sandstone

The green sandstone is the main unit above the unconformity (Map, appendix 4). It is a medium- to coarse-grained sandstone, with green to grey colour and visible quartz grains in the matrix (Fig. 4.14-A&B). It is characterized by clast-rich beds and occurrence of cross-lamination. It is clearly bedded in the well-preserved outcrops, with distinct lamination and occurrences of trough cross lamination in addition to the more common cross lamination (Fig. 4.14-C&D). The cross-lamination is fairly well preserved and indicates that the succession is laying the right way up.

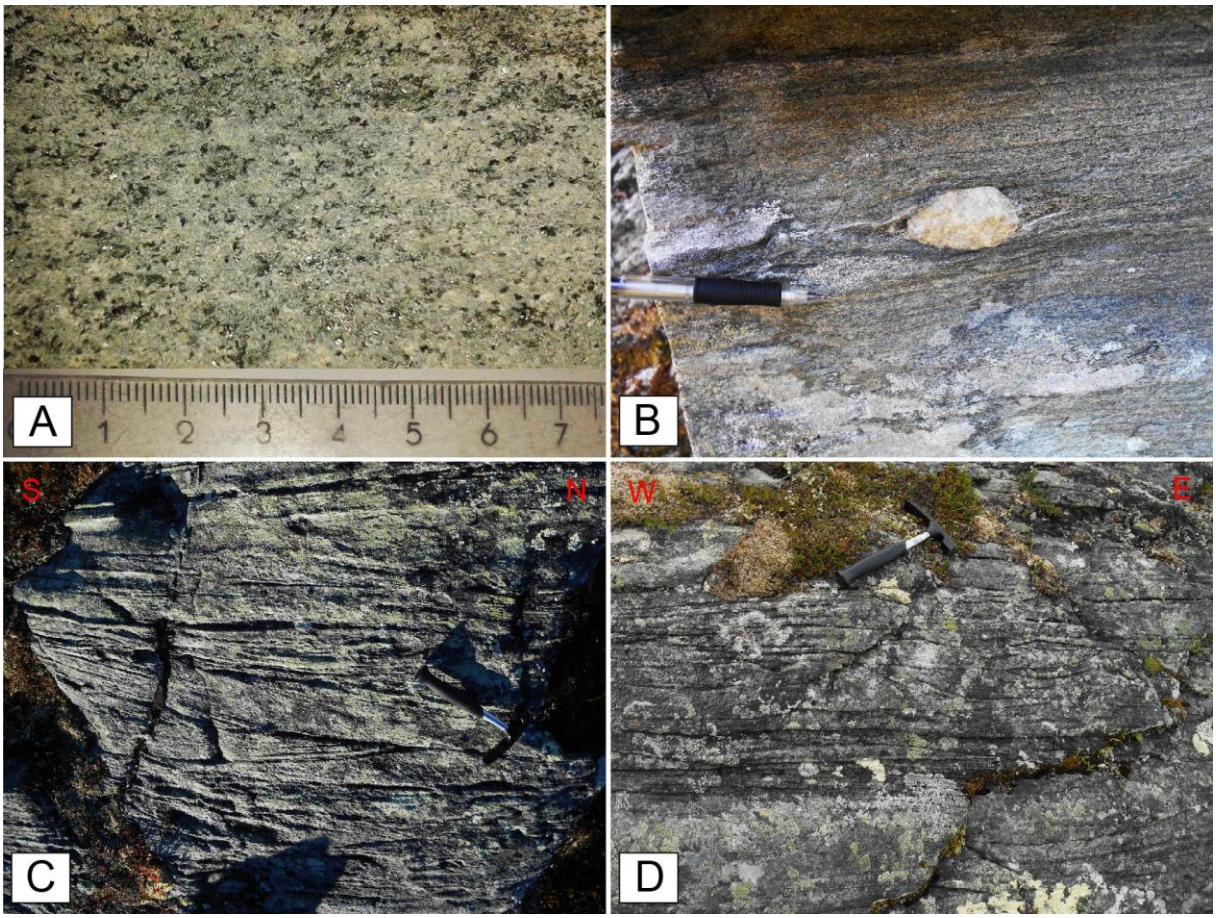

Figure 4.14: A) Close up of texture in hand sample shows clear biotite grains (dark) and quartz grains (white). Note the generally green colour. B) Distinct lamination and clast in sandstone. Note the green to grey colour and the visible white in the matrix, which is mainly quartz. C) Cross lamination. D) Trough cross lamination in the centre area shows it is lying the right way up.

There are quartzitic, granitic, felsic-volcanic and sandstone clasts scattered throughout the sandstone, both as single clasts and accumulated in more clast-rich layers (Fig. 4.14-B; Fig. 4.15-A-C). The clasts are generally rounded and of varying size from about 0.5-20 cm. The clast content increases towards the base of the sandstone, together with an increased input of angular to sub angular chert clasts (Fig. 4.15-B).

The sandstone is relatively inhomogeneous due to the clast content, and contains biotite grains in varying amount, with increasing size of biotite aggregates in more foliated and deformed outcrops. Upward in the succession the sandstone looks a bit “cherty” (Fig. 4.15-C&D),

possibly turning into a hornfels rock due to contact metamorphism by overlying lava. These factors make these outcrops difficult to distinguish from the more volcanic lithologies bounding the sandstone, such as the greenstone, the intermediate intrusion and especially the intermediate volcanic.

In addition to the big intermediate intrusion described below, there are some dykes of both intermediate and more mafic looking origin cutting the sandstone (Fig. 4.15-E).

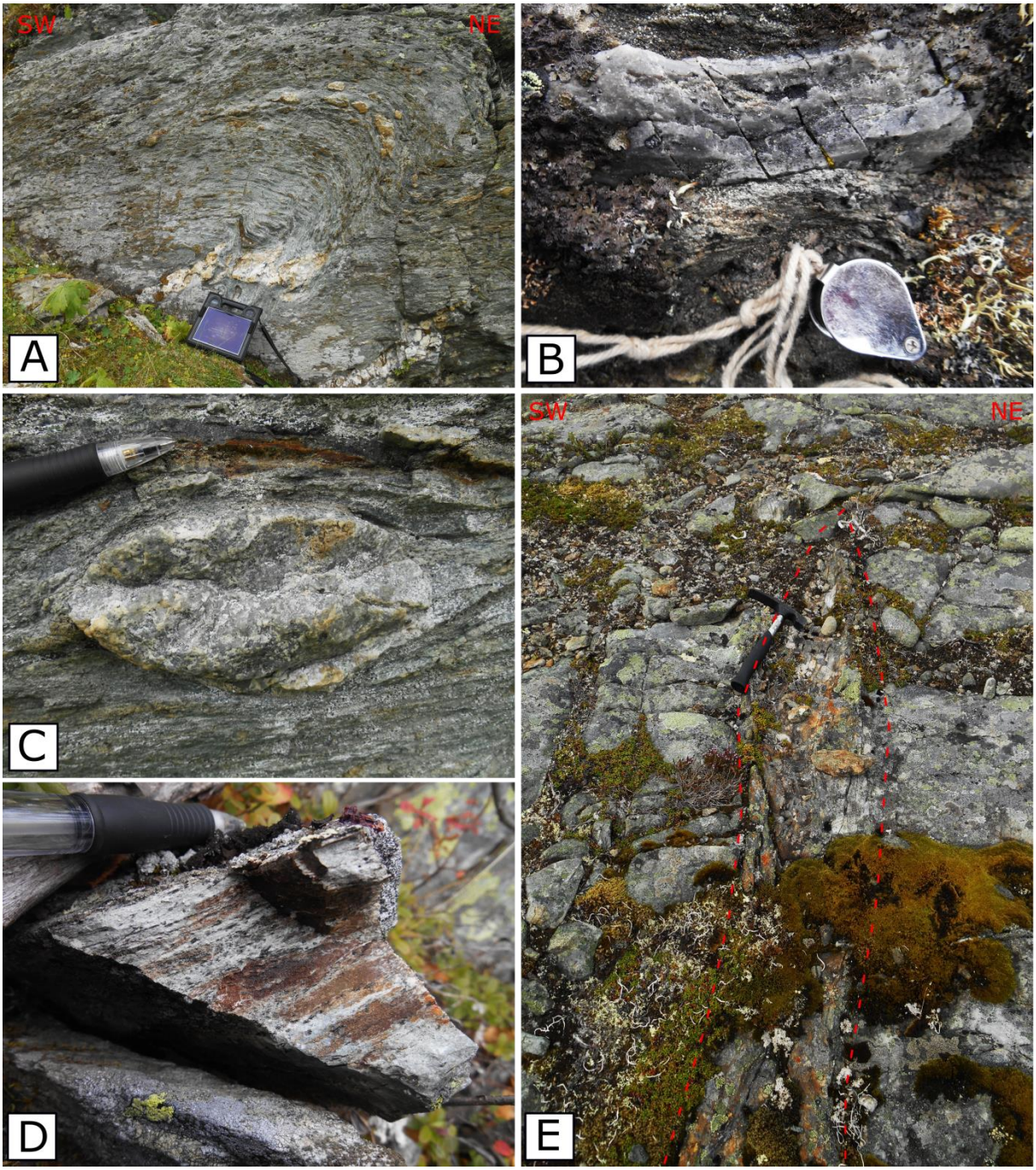

Figure 4.15: A) Folded clast-rich bed in the sandstone. Note the accumulation of clast in a bed, as well as some more scattered clasts. B) Angular chert clast close to the base of the sandstone. C) Quartzittic clast in the more "cherty" part of the sandstone. Note the lighter colour and more distinct biotite grains in the sandstone surrounding the clast. D) Texture of the more "cherty" sandstone close to the volcanic. Note the more prominent biotite grains relative to matrix than seen in the relatively undeformed texture in figure 4.14-A. E) Light coloured, possibly intermediate type dyke cutting the sandstone close to the intermediate volcanic.

Intermediate volcanic

This unit has been particularly difficult to define in the field, and it is still hard to define whether it is a volcanic, intrusive or actually metasedimentary rock. It lies as pockets or layers inside the green sandstone, but concentrated to two elevated hills, to some degree following the contours in the terrain (Map, appendix 4). It is possible it has had a larger extent, but has been eroded away in the lower areas between the hills. In the northern hill the intermediate volcanic is covered by another unit, probably some sort of sandstone. It is not properly correlated with the green sandstone, and might therefore be part of a younger sandstone unit, but this question requires further fieldwork and remains unanswered. The intermediate volcanic has a fine-grained green matrix with medium-grained biotite, and a texture somewhere between a volcanic and a shallow intrusion or sill. It also exhibit both carbonate and some quartz veins (Fig. 4.16-A). The biotite grains appear either as single grains or in aggregates, and are randomly distributed (Fig. 4.16-A&B), except for in more foliated versions where they are slightly more oriented (Fig. 4.16-C). In some locations, it shows vague layering, but this could also be deformed sandstone. This unit also appears in localities outside of the main polygons, especially close to the ribbon-chert boundary. It might correlate with the mafic dykes cutting the greenstone, as well as a few localities within the greenstone described as having larger biotite grains.

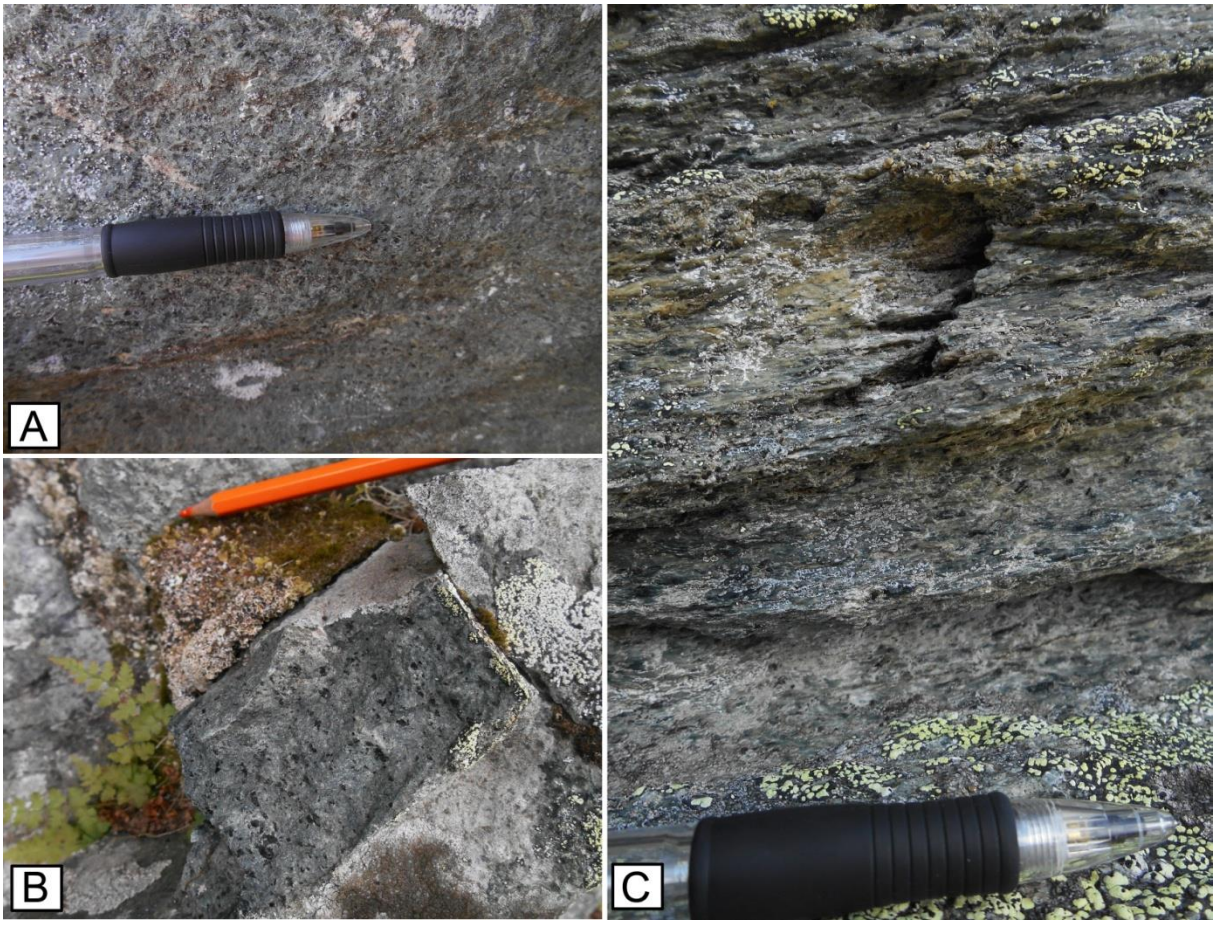

Figure 4.16: A) Texture of the intermediate volcanic. Note the thin carbonate veins. B) Texture including both clustered and separate biotite grains in an otherwise fine-grained matrix. C) More foliated version of Vul. Looks similar to the more deformed sandstone, thus very hard to distinguish in the field.

Intermediate intrusion

This is a medium-grained intrusive rock lying inside the green sandstone (Map, appendix 4). It has a light grey, almost white matrix and big dark crystals of biotite and possibly amphibole (Fig. 4.17). It has an intermediate looking composition, a bit like Trondhjemite or some other form of intermediate intrusion, differing from the other more mafic intrusions and lavas in the area.

Some outcrops have a greener colour, but the dark minerals are generally larger than the ones found in the intermediate volcanic, yet it is not always so easy to distinguish them. This intrusion does not have the coarse-grained texture of a deep intrusive crystalline rock, which indicates it could be fairly shallow. It is possibly more related to the intermediate volcanic than the field observations immediately indicate, as suggested in chapter 6.1.4; 6.2.1; 6.2.2, based on petrography and geochemistry.

Figure 4.17: Texture in the intermediate intrusion. Note the light colour and dark mineral grains. This is a weekly foliated version.

Chapter 5 – Structural description

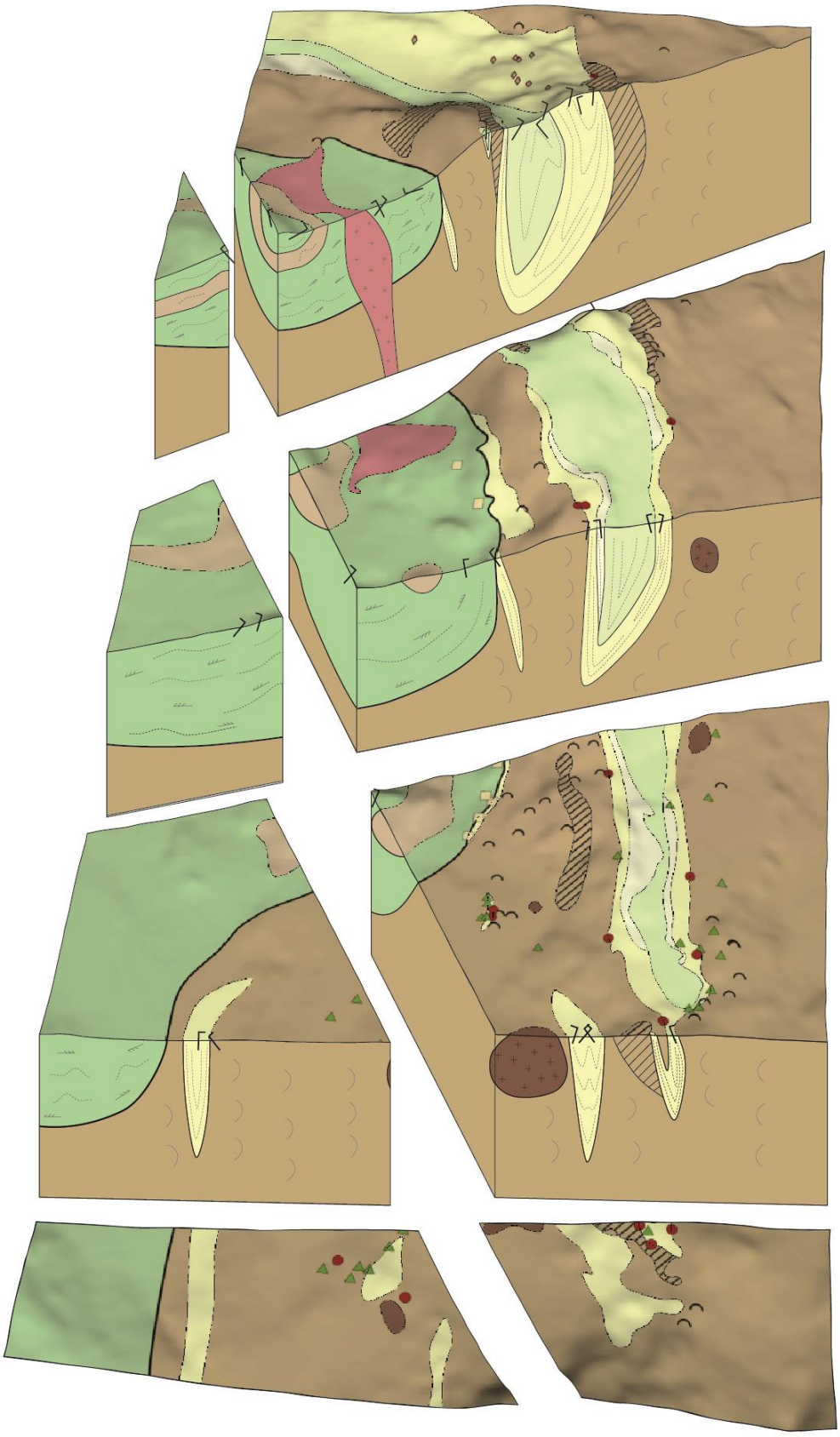

Figure 5.1: An interpretative 3D illustration of the geology of Dugurdsknappen. Legend is found in appendix 1 page I, surface map and interpolation of structures is made in Move (Midland Valley Exploration: Move Suite).

The rocks of the Dugurdsknappen area are characterized by a high degree of ductile deformation, which to a large degree defines the large-scale structures of the area as well. The ductile deformation can be seen especially well in the ribbon-chert unit, represented by numerous folds, which are a characteristic feature of this area. A few observations have been made on brittle structures, and though there might be plenty more, these have not been the focus for this study.

Three main structural elements are thought to control the Dugurdsknappen area (Fig. 5.1): 1) A southward closing synform incorporating the green siltstone, the chert-related units and the greenstone-related units, with related S-SE trending internal isoclinal folding; 2) A major unconformity separating the older highly deformed greenstone, ribbon-chert and siltstone units from the younger sandstone, where original depositional structures still can be seen; 3) Southwestward-trending second fold phase, folding the units both above and below the unconformity and particularly the contact zone, in open to closed folds. In this chapter the structural features of each unit within this structural framework will be described, with a chapter on two important boundary relations including the unconformity and a short characterization of the brittle structures towards the end.

5.1 – Mapped structures below the unconformity

5.1.1 – Greenstone-related rocks

Greenstone and altered greenstone

There are only a few strata measurements from the greenstone-related rocks, mainly from the greenstones with pillows. The pillows are often considerably elongated, showing possible direction of plastic deformation. The massive greenstones do not show any form of layering that can be measured, nor does the intrusive gabbro. However, the layering or orientation of the pillows can be measured, though it might not correspond to the previous horizontal since it is a lava. With this in mind, the few measurements of strata that have been taken in this unit seem to show two trends (Fig. 5.2-A). The main trend dips generally moderately S-SW, while the minor trend dips relatively steeply E. There have also been taken some measurements of the elongation of a few pillows, which seem to correlate with the dip of the layering, plunging moderately towards the SW (Fig. 5.2-A).

Foliation is more commonly seen in these units, mainly in the more heterogeneous pillow-structured parts. The foliation measurements show one main group dipping moderately towards the SE, and several measurements with NNW-SSE strike and variable dip (Fig. 5.2-B).

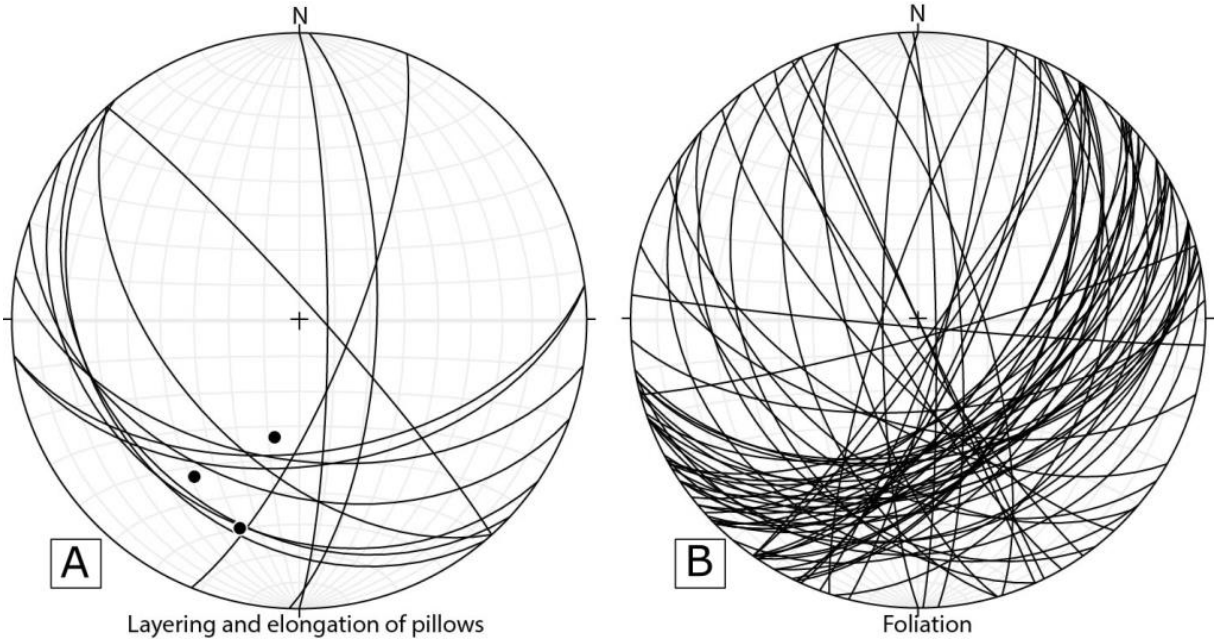

Figure 5.2: A) Steronet showing the relation between measured layering (lines) in the greenstone (including Vul/GrIn) and orientation of elongated pillows (points). Note the correlation between the two. B) Stereonet showing orientation of foliation in greenstone, gabbro and altered gtreenstone. Note the major trend dipping moderately to the SE.

The greenstone–related units show very little to no folding. There is some frequent small-scale folding or undulation in the foliation, but it is too minute to be properly measured. A few localities have visible large-scale folding, some visualized in quartz veins (Fig. 5.3-A), from which two fold axes have been recorded (Fig. 5.3-B). They plunge moderately S.

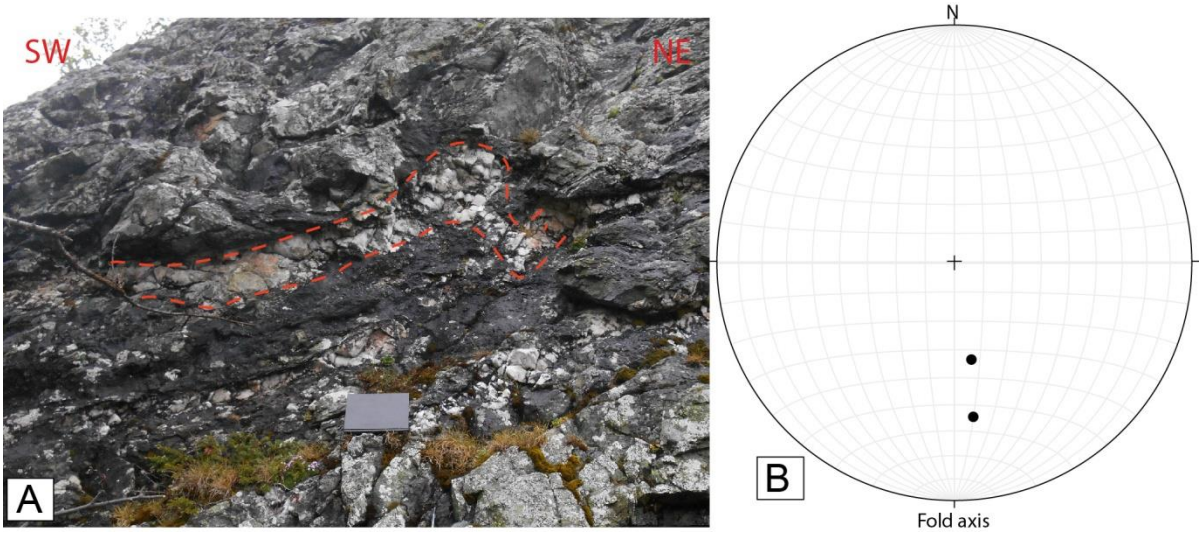

Figure 5.3: A) Folded quartz vein in pillow basalt greenstone. B) Stereonet showing the two measured fold axes in the greenstone-related rocks.

Agglomerate

This unit is characterized by a very strong foliation seen in the shaly matrix and oriented clasts (Fig. 4.7). There might have been an initial layering of the clasts, but this has been completely overprinted by the foliation. The main foliation in the western part dips almost vertically to the east and west, striking approximately N-S, while in the eastern area it dips more moderately towards the SE (Fig. 5.4).The foliation is generally parallel to the ribbon-chert/greenstone boundary both in the east and west, which in the eastern part incidentally coincide with the orientation of the main foliation (Map 2, appendix 1). It seems therefore that the foliation in the agglomerate is related to the main deformational phase, and not to any particular boundary processes.

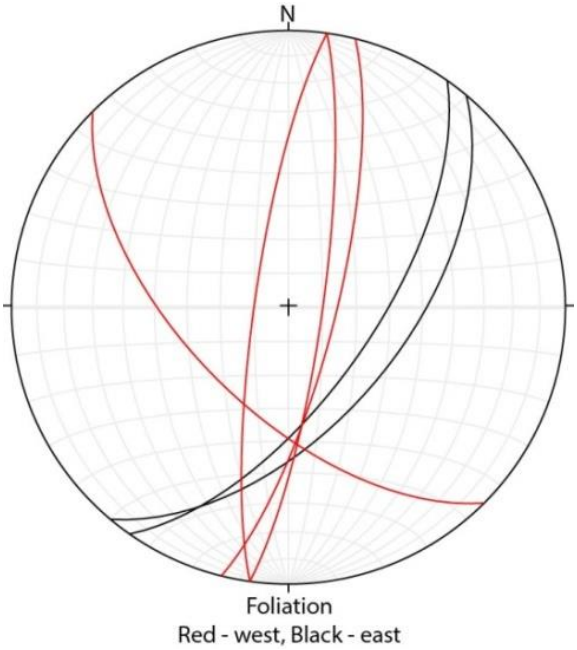

Figure 5.4: Stereonet showing the foliation in agglomerate. Red lines represent agglomerate in the west close to the green sandstone, while black lines represent eastern agglomerate bounding the central ribbon-chert unit

5.1.2 – Chert-related rocks

Ribbon-chert

The ribbon-chert shows clear layering which is easy to measure, and depicts a large amount of folding (Fig. 5.5-A). Layering is sometimes muddled by a crosscutting foliation, making it hard to determine which is which in some areas. Nonetheless, it is possible to point out two trends in the bedding measurements, though somewhat blurred by many outliers. The main trend dips moderately to steeply SW, though it is less steep in the northern area in front of Dugurdsknappen (Map 1, appendix 1). The minor trend dips steeply E and is most common southwards in the area (Fig. 5.5-B; Map 1, appendix 1).

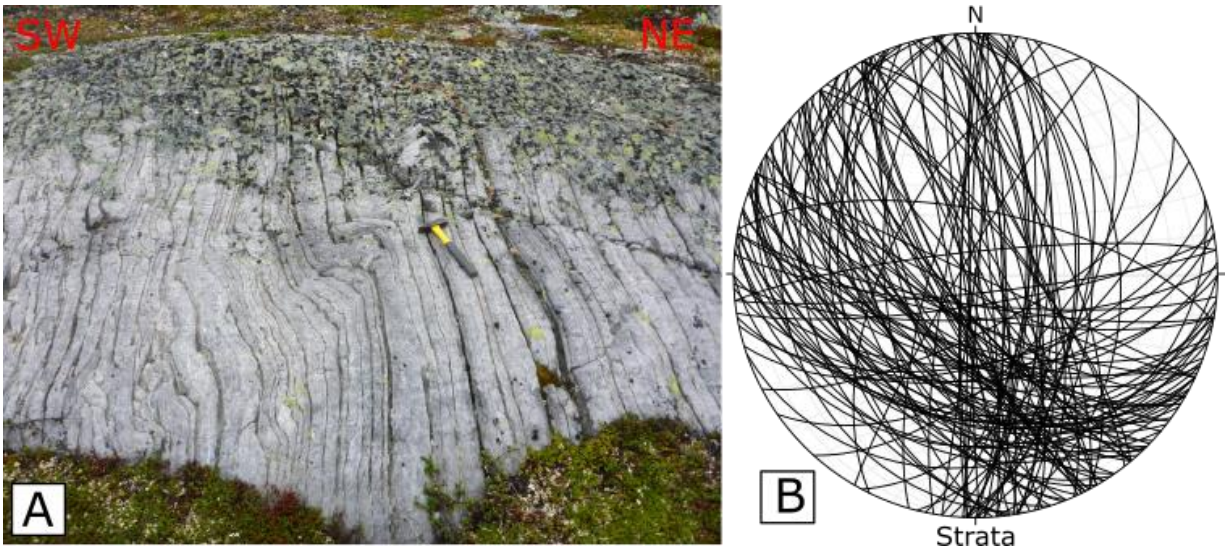

Figure 5.5: A) Typical layering of chert, with an example of fold development. B) Steronet showing bedding in ribbon-chert. Note the two clear trends, despite several outliers.

Chert is a very hard rock, and does not easily develop foliation. When it does, it often develops a spaced foliation or fracture cleavage, usually breaking up in a concoidal fashion, (Fig. 5.6-A&B). However, penetrative foliation is also not uncommon. The foliations measured in the ribbon-chert generally vary a great deal, especially around the top of Dugurdsknappen. However, two trends can be pointed out, related to a geographical pattern (Fig. 5.6-C). The major trend seems to have a moderate to gentle dip towards SE-SW, and is mainly dominant in the eastern ribbon-chert on both sides of the central green siltstone, while the minor trend dips more steeply to the ESE and is mainly found in the western ribbon-chert bordering the green sandstone. This geographical trend is concordant with that seen in the agglomerate. When looking at the stereonet depicting both penetrative and spaced foliation together with the one indicating geographical trend, it seems spaced foliation is dominantly SE-SW dipping concordant with the main eastern trend, while penetrative foliation dominates the E-SE dipping western trend (Fig. 5.6-C&D).

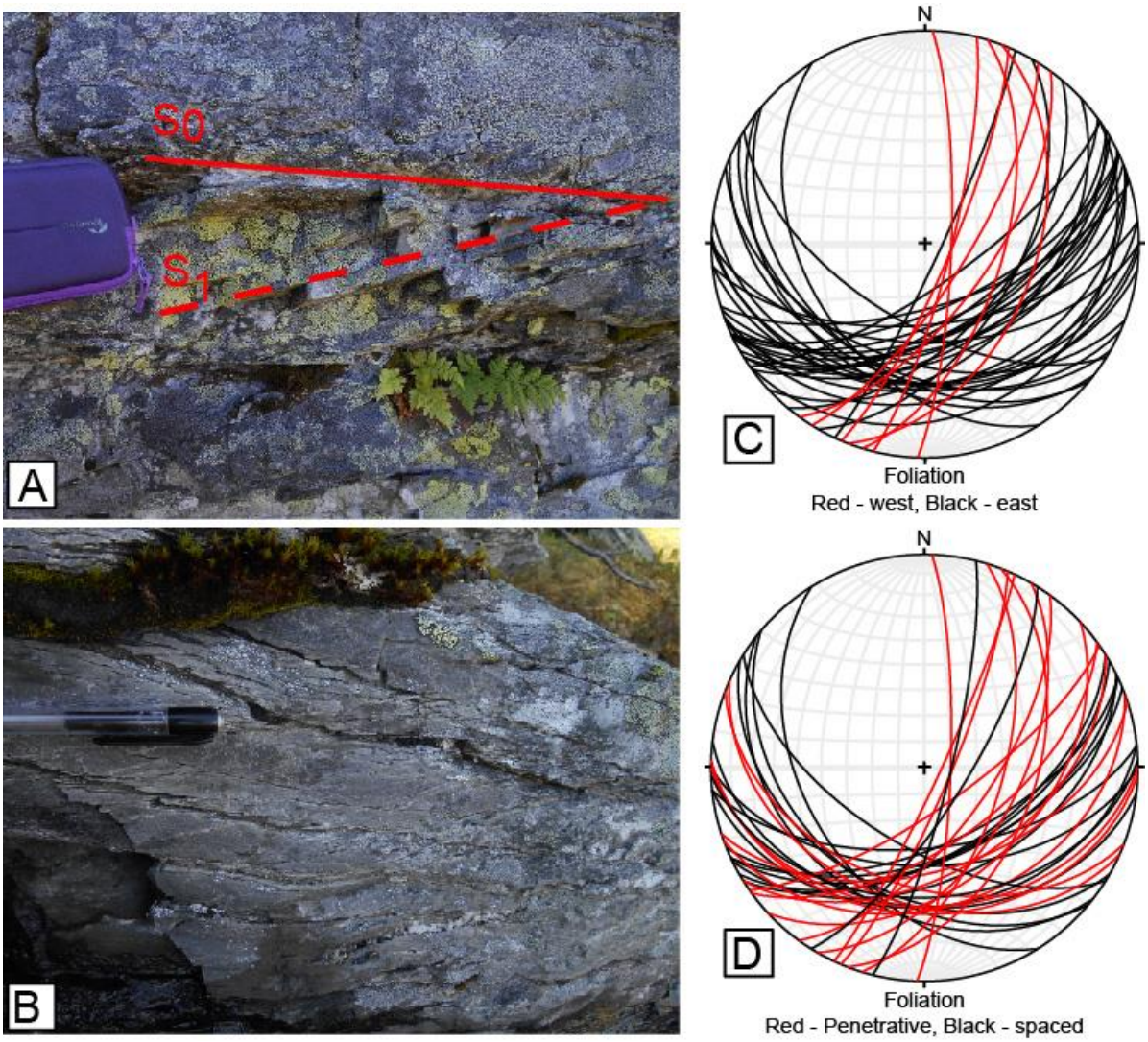

Figure 5.6: A) Spaced foliation cutting the chert layers at an angle. B) Typical foliation in chert, breaking it up in a concoidal fashion and disturbing the layering. This makes it difficult in some places to determine bedding and foliation. C) Stereonet showing spaced (black) and penetrative (red) foliation in ribbon-chert. No particular systematic are observed. D) Stereonet showing foliation in ribbon-chert sorted according to geographical location, where red are measurements from the western ribbon-chert close to the green sandstone, while black measurements are from the main ribbon-chert surrounding the central green siltstone unit.

Another interesting aspect of the foliation is found where shale is present between chert layers. In such cases there is a clear refraction of the foliation between the two layers, reflecting the difference in competence (Fig. 5.7). The chert is as mentioned hard and dense and develops a spaced foliation or tension fractures around fold hinges resulting in a systematic variation in foliation orientation (Fig. 5.7-stereonet). The interbedded shale develops a penetrative foliation with a different much more constant orientation. The stereonet (Fig. 5.7) shows that the refracting foliation has two main orientations. One is found only in chert and dipping moderately to the SE-SW, which incidentally is the same as the dominant foliation in the ribbon-chert unit. The other is mainly found in the phyllosilicate-rich layers, and is dipping moderately E-SE. Strata and fold axes follows the main trend of the ribbon-chert unit.

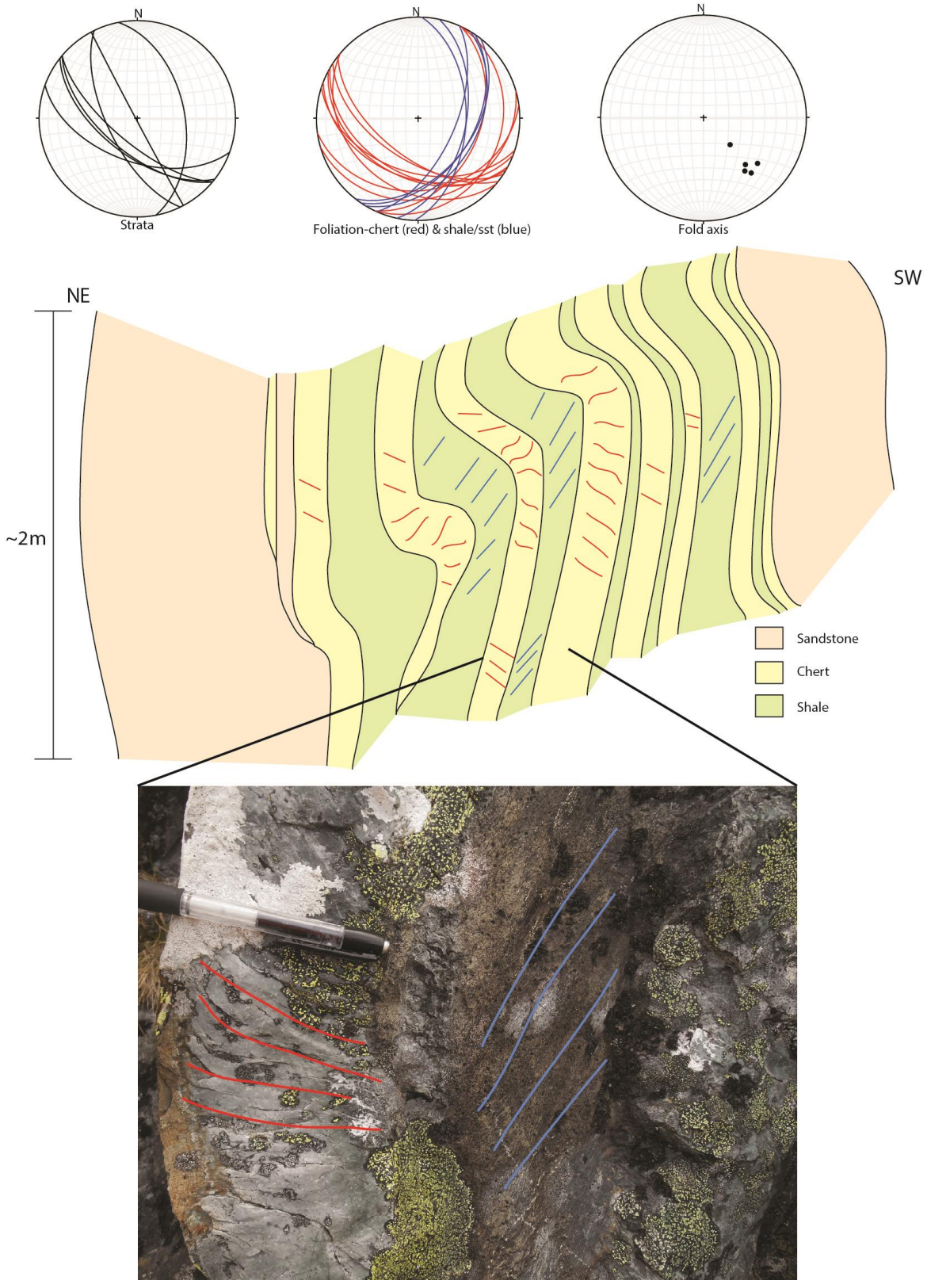

Figure 5.7: Illustration and photo from locality EST_30 in the northern front of the top of Dugurdsknappen. Photo shows the refracting foliation between the chert layer (red lines) and the interlayered phyllosilicate-rich layer (blue lines), which can also be seen in the log above it. This difference in foliation is also seen in the Stereonet on the top, together with bedding and fold axes. Note the different trends in the foliation between shale/sandstone (blue lines) and chert (red lines).

The ribbon-chert is generally heavily folded, displaying folds of all different types, varying from gentle to isoclinal folds, as well as occurrences of kink folds (Fig. 5.8-A to E). It was observed in the field that there seems to be some systematic in the orientation of folds based on the type. This is conformed in the stereonet, where it appears that the tighter folds tend to have fold axes plunging more directly to the south, while the gentler types are diverging more to the SE and SW, as seen in the stereonet (Fig. 5.8-F).

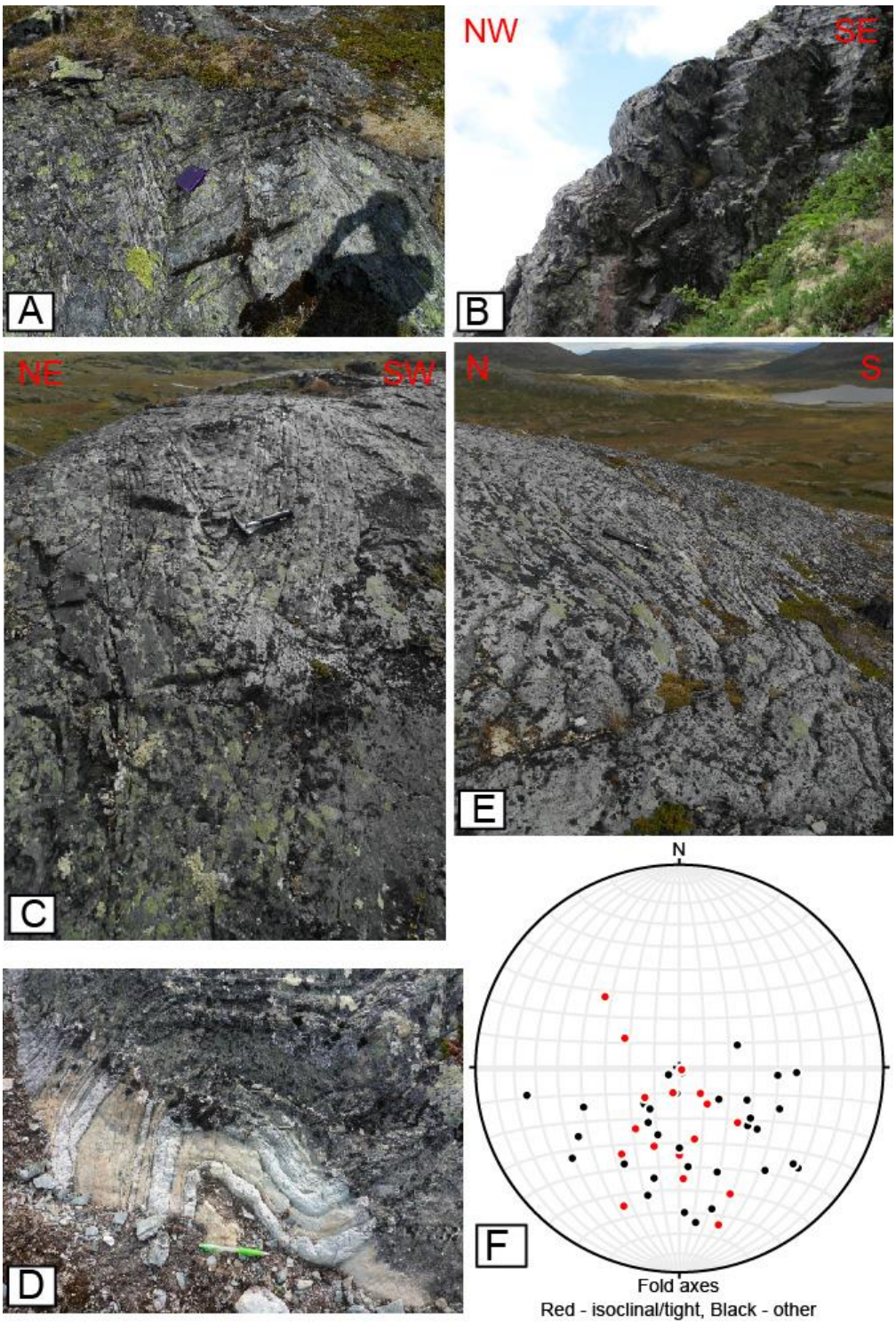

Figure 5.8: A) Kinkfolds in ribbon-chert. B) Semi-kinkfolds in ribbon-chert seen from below. Flower for scale. C) Large tight to isoclinal fold in ribbon-chert. D) Tight folding of chert and interlayered sandstone. E) Gentle folding of chert layers. F) Stereonet showing the fold axis distribution between tight and isoclinal folds (red) and closed, open and gentle folds (black). Note the general southerly trend of the red ones with variable plunge.

There are a large number of folds in the ribbon-chert unit, with somewhat diverging directions, yet there appear to be a couple of trends. The measured fold axes mainly plot in the southern hemisphere and are generally quite spread out, but with three indistinct clusters (Fig. 5.9-A). One trends a little to the S-SW and seems to be the dominant trend in the ribbon-chert bounding the green sandstone. The central ribbon-chert west of the green siltstone also trends to a degree SE, though generally steeply, but the main plunge is more moderate and trends dominantly south. The third trend plunges slightly more to the SE and is most common in the easternmost ribbon-chert bounding the east side of the green siltstone, especially in the northeastern parts (also seen in Map 3&4, appendix 1), though this area is generally characterized by more scattered fold axes. The axial planes are also diverging, but appear to have two indistinct trends as well (Fig. 5.9-B). One is dipping dominantly steeply between E and SE/NW and another dipping steep to moderately to the SW. It is however not possible to connect these trends properly to any geographical pattern, as is also seen in the diverging axial planes in Map 3 in appendix 1, so all axial planes are plotted together (Fig. 5.9-B). There seem to be one main trend dipping steeply SE and two minor dipping steeply to moderately SE and moderately to gently NE.

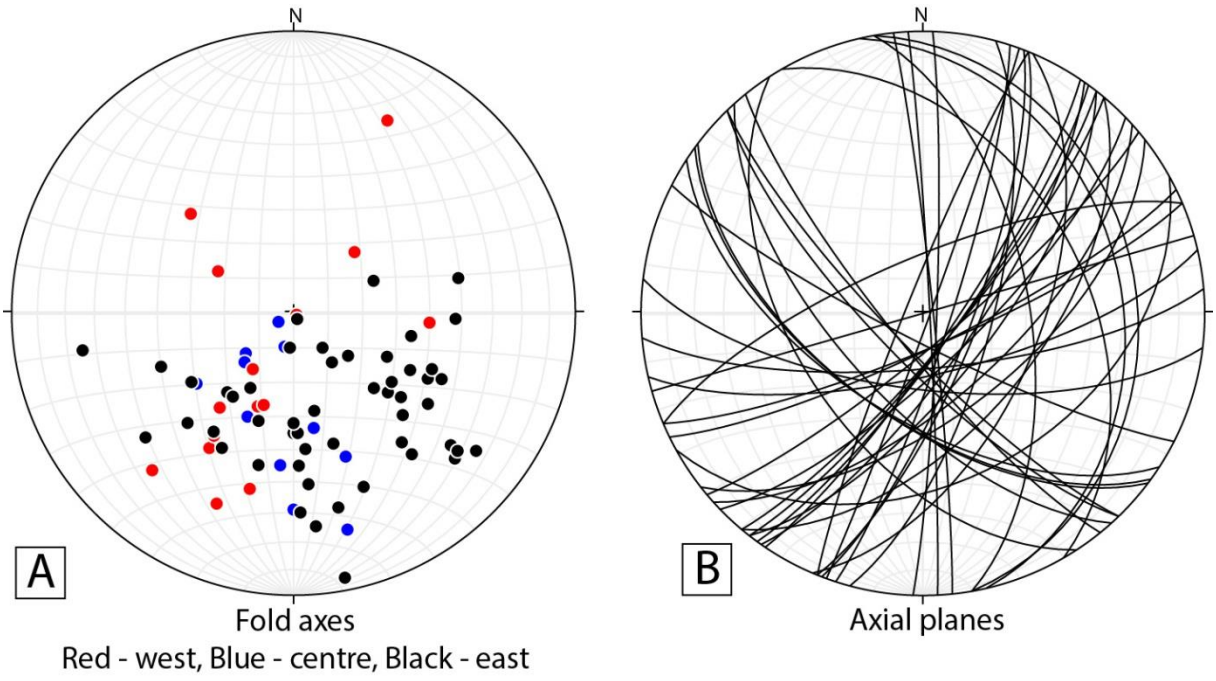

Figure 5.9: A) All fold axes collected in the ribbon-chert unit show some geographical pattern. Red represent fold axes from the western area close to the green sandstone, blue are fold axes bounding the western side of the green siltstone, and black bounds the eastern side of the green siltstone. B) All axial planes.

The top

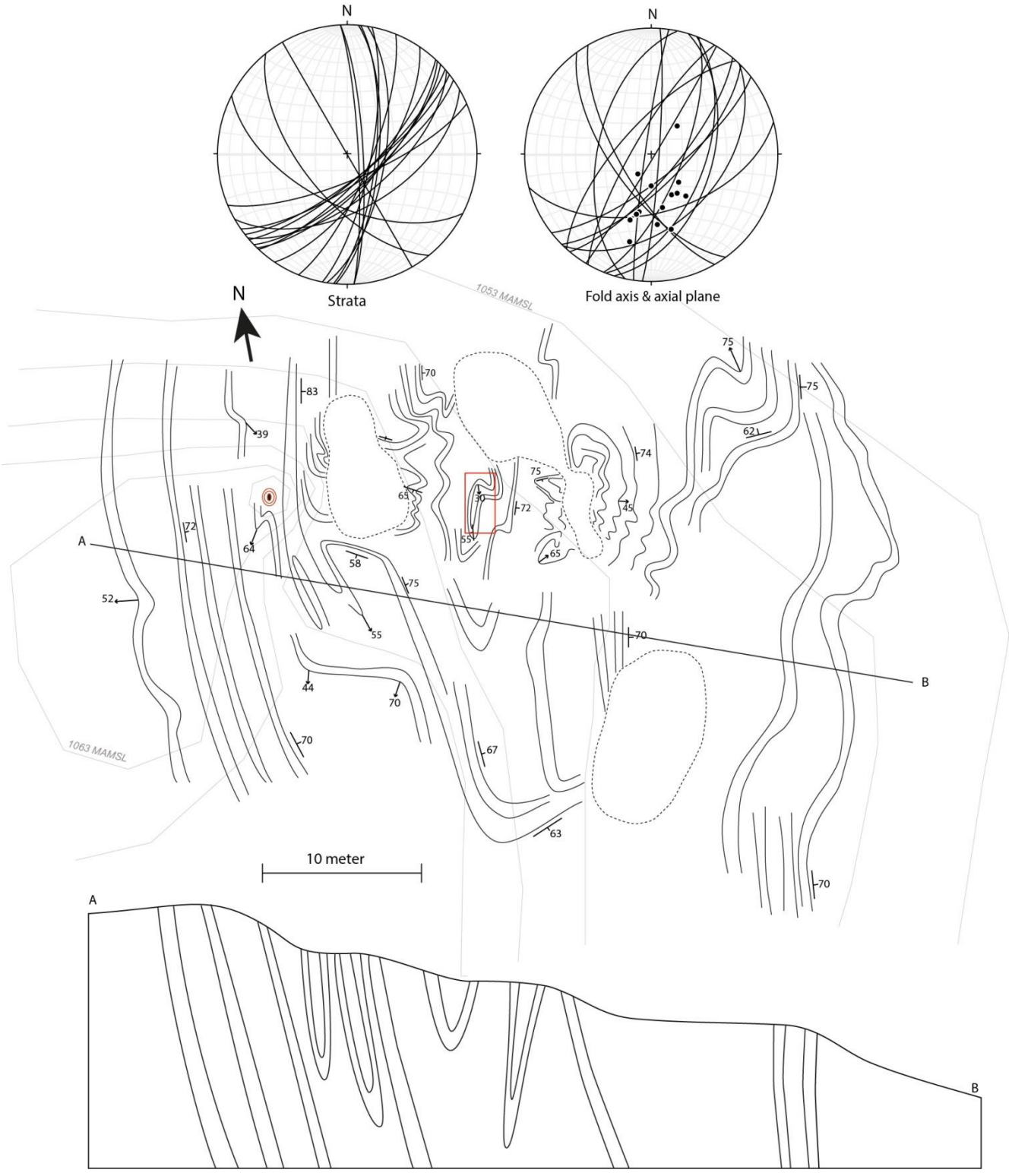

Figure 5.10: Assembled field sketches show the approximate pattern of bedding and folding in the Dugurdsknappen top area. Red point and contours indicate the top point and elevation. Note that this is a very simplified illustration, since the drawing is in 2D and the top of course 3D. Line A-B indicates position of the rough profile below. Above the sketch are stereonets showing the orientation of bedding, axial planes and fold axes. Red square indicates position of the photo in figure 5.11-A.

The Dugurdsknappen top area depicts particularly nice fold patterns, as seen in figure 5.10, enhanced by the high exposure of outcrops in 3D view. Stereonets from the top area show there are two distinct bedding directions, as well as one more indistinct trend striking NW-SE. Of the distinct trends, one dips steeply E and correlates with the minor trend found elsewhere in the ribbon-chert, and the other dips steeply to the SE. This last trend is not seen in the main ribbon-chert stereonets, and is more concordant with the main foliation in the ribbon-chert. It is important to note that the two trends have a very distinct crossing, and when looking at the fold data, the fold axes seem to lie in this crossing and the axial planes lies between the two trends. This indicates a general pattern in the strata of intense folding of the almost vertical layers causing the complexity, as seen in the cross section from the top as well.

There are also examples of refolded folds, seen in two or three locations at and around the top area, where isoclinal to tight folds are refolded by gentler folds (Fig. 5.11). This suggests that there are several folding phases, which further complicates the area. One fold is seen both in the sketch of the top (Fig. 5.10) and in the photo in figure 5.11-A, and has a south-dipping fold axis that is refolded by a gentler fold with fold axis plunging to the SW. Of the two other refolded folds, one has a fold axis plunging to the NW refolded by a SW plunging fold axis (Fig. 5.11-B), and the other has a fold axis plunging S refolded by a SE plunging fold axis (Fig. 5.11-C). Despite outliers, there seems there are one earlier fold phase trending S-SE refolded by a generally SW trending second fold phase.

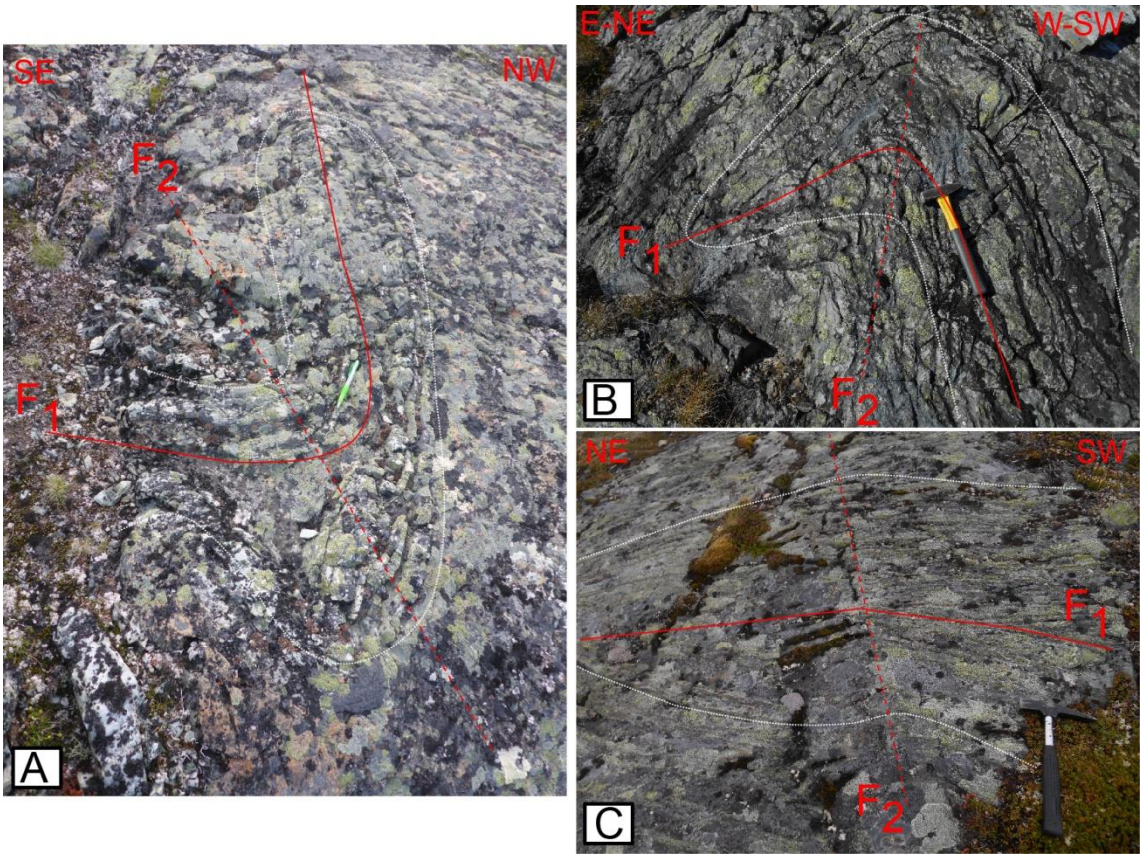

Figure 5.11: A) Refolded fold at the top, position indicated in the illustration in figure 5.11. B) Refolded fold just southeast of the top. C) Refolded fold a little further south than B.; Note that fold terminology is only applied locally.

Silty chert

This unit, as mentioned earlier, probably represent a transitional rock type between the hard and dense chert and the much softer silisiclastic green siltstone. The strata is generally parallel to the boundaries to the surrounding units (Map 1, appendix 1), dominantly dipping relatively steeply WSW (Fig. 5.12-A), with some variations dipping more WNW as the boundary curves. There are only five measurements of foliation (Fig. 5.12-A), which are concordant with the foliation in the ribbon-chert, dipping SE to S. Folds are also fairly scarce, but they seem to follow the pattern of the surrounding ribbon-chert unit with fold axes plunging southward (Fig. 5.12-B). The most noticeable structural feature in this unit is however the interference between bedding and foliation. Closest to the ribbon-chert the bedding is dominating and as mentioned dipping similarly to that of the ribbon-chert. Moving towards the green siltstone, foliation becomes gradually the dominant structure, giving a middle part with a vague crenulation where the two interfere (Fig. 4.12).

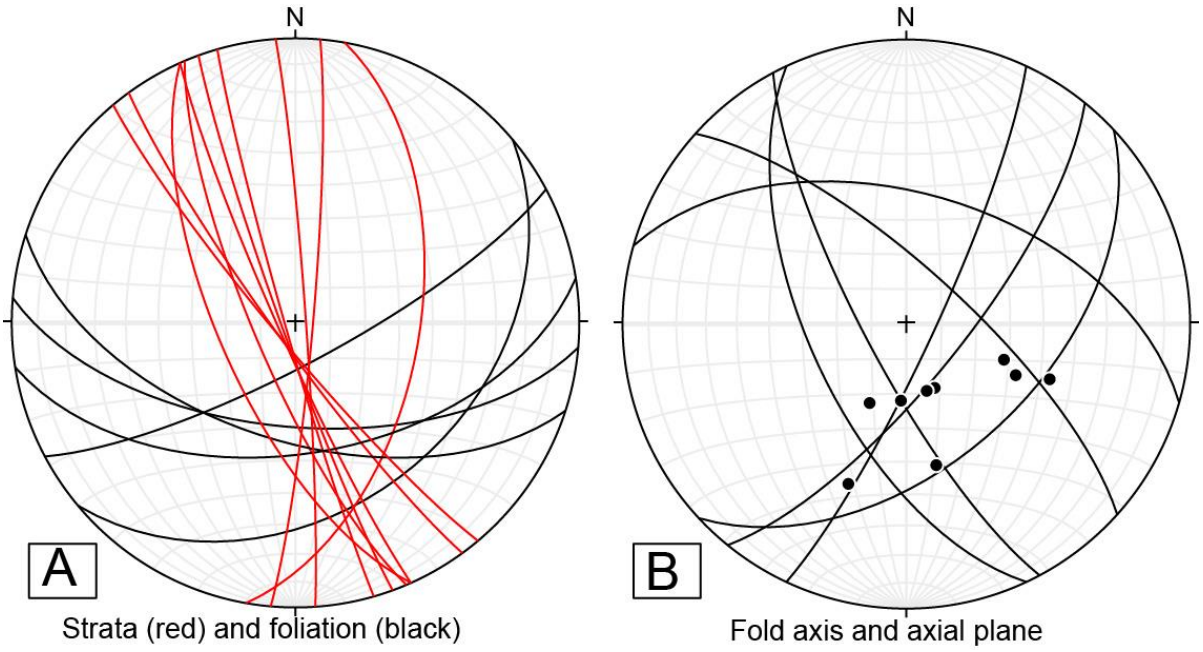

Figure 5.12: A) Stereonet showing strata (red) and foliation (black) from the silty chert. B) Stereonet showing axial planes and fold axis from the silty chert unit.

5.1.3 – Green siltstone

Bedding in this unit is relatively prominent with 10-20 cm thick beds, mainly lying parallel with the boundaries to the surrounding units (Map 1, appendix 1). This results in a transition from strata dipping steeply, almost vertical E and W in the south to gradually dipping more moderately SW in the northern part of the unit (Fig. 5.13-B; Map 1, appendix 1).

Foliation is the most common feature in this unit. It is cutting the bedding at an angle, which creates a sort of crenulation, or banding, analogous to that seen in the silty chert, though much more distinct in this unit (Fig. 5.13-A). Foliation is generally consistent throughout the unit, dipping moderately SE (Fig. 5.13-B). This is concordant with the main foliation in both the greenstone- and chert-related rocks as well.

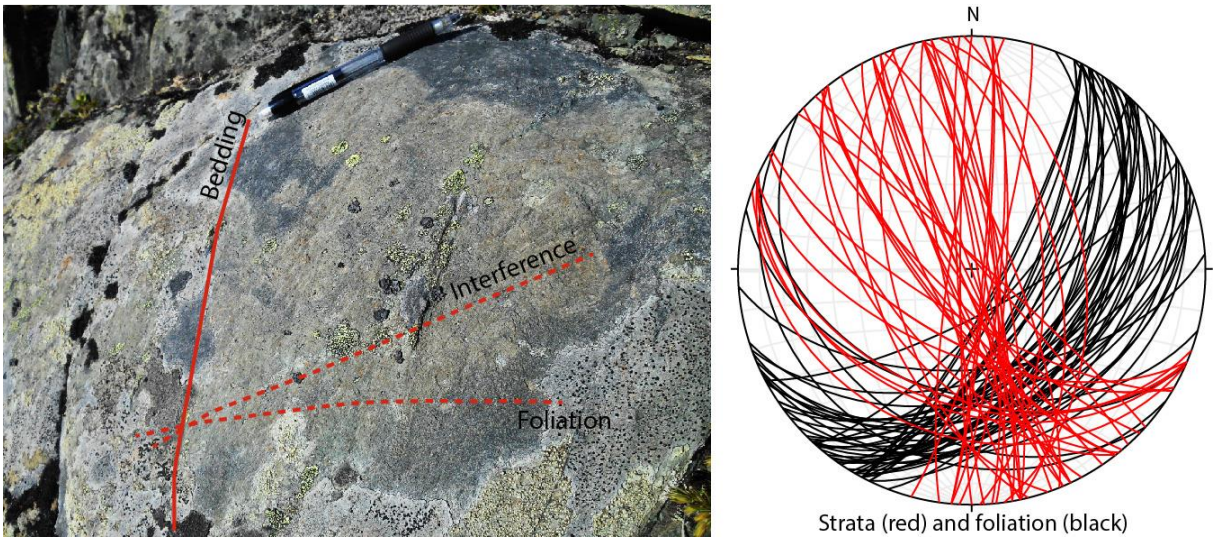

Figure 5.13: A) Relation between bedding and foliation causing interference seen as a sort of crenulation in the green siltstone. B) Stereonet showing bedding (red) and foliation (black) measured in the green siltstone.

This unit has not been folded much, and the few folds observed can be hard to interpret, as many are very tight kink folds (Fig. 5.14-A). Also gentle folds have been observed, though they are few and not measured. This scarceness of folds stands in contrast to the bounding ribbon-chert, which is so intensely folded. There are in total only five measurements of fold axes (Fig. 5.14-B), three plunging relatively gentle almost directly south and two plunging almost vertically, with a slight trend SE. Axial planes are all vertical and dipping E/W, parallel to bedding. These are all from isoclinal folds.

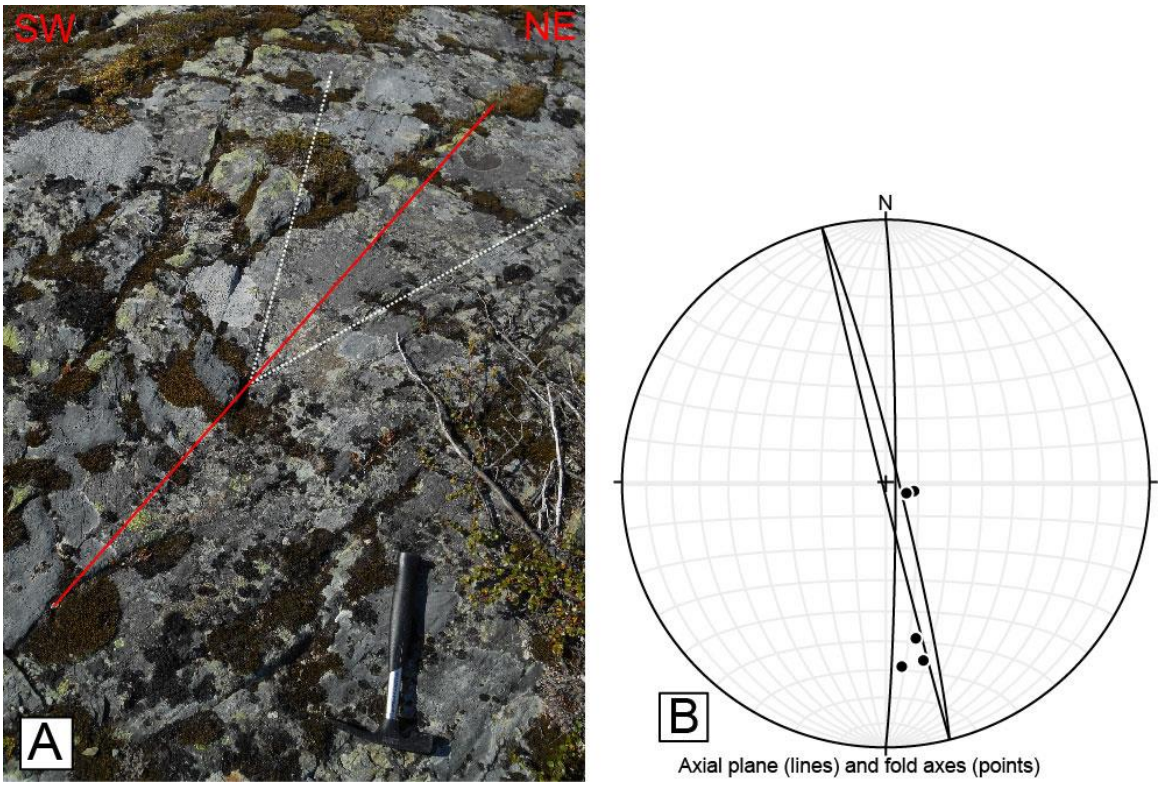

Figure 5.14: A) Steronet showing axial plane and fold axes measured in the green siltstone. Note the two almost vertical fold axes. B) Picture of a kink fold with vertical fold axis observed in the green siltstone.

5.2 – Mapped structures above the unconformity

5.2.1 – Green sandstone

Depositional bedding is clearly visible in this unit, as can be seen from the sedimentary structures described in chapter 4.3.4. There are two dominant directions of bedding (Fig. 5.15-A). One is almost vertically dipping E/W, and the other is dipping moderately to gently SW. Looking at the strata map in Map 1, appendix 1, it seems this is due to the bedding following the curve of the unconformity towards ribbon-chert and greenstone.

Foliation is not so common in this unit, and it generally shows a lower degree of deformation than the units below the unconformity. The foliations measured are more common towards the ribbon-chert boundary as well as towards the intermediate intrusion (Map 2, appendix 1), and have relatively systematic orientation dipping moderately to steeply between E and SW (Fig. 5.15-B). It is worth noting that the mean axial plane (described further below) lies within the foliation, indicating that the foliation could be partly an axial plane foliation (Fig. 5.15-B).

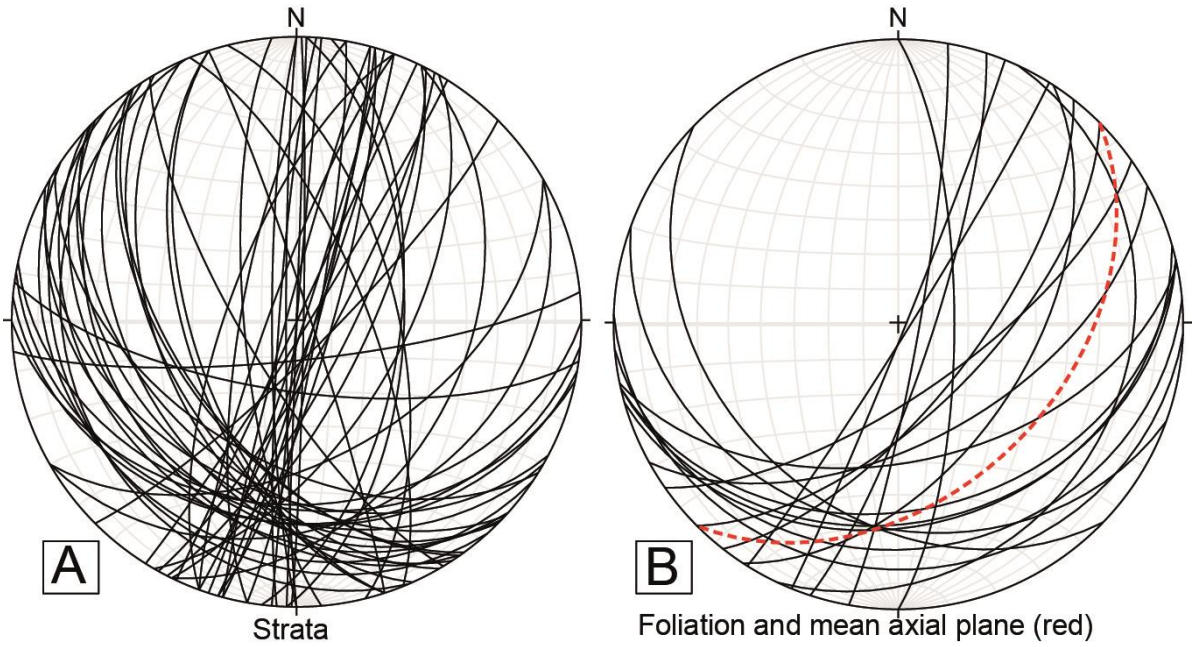

Figure 5.15: A) Stereonet showing orientation of bedding in the green sandstone. Note the two trends. B) Stereonet showing foliation (black) and the mean axial plane (dashed red line) measured in the green sandstone. Note the possible connection between the two.

Many of the localities with green sandstone are poorly exposed, due to erosion and vegetation, and thus folding is only possible to detect in a few outcrops. It is therefore likely there are more folds than it seems from the steronet (Fig. 5.16-A) and the map (Map 4, appendix 1). The folding observed comprises open to gentle folds (Fig. 5.16-B), as well as some tight to isoclinal types, especially among smaller folds and parasite folds (Fig. 5.16-C&D). Axial planes are mainly dipping moderately to the SE, and fold axes plunge moderately to the SW (Fig. 5.16-A).

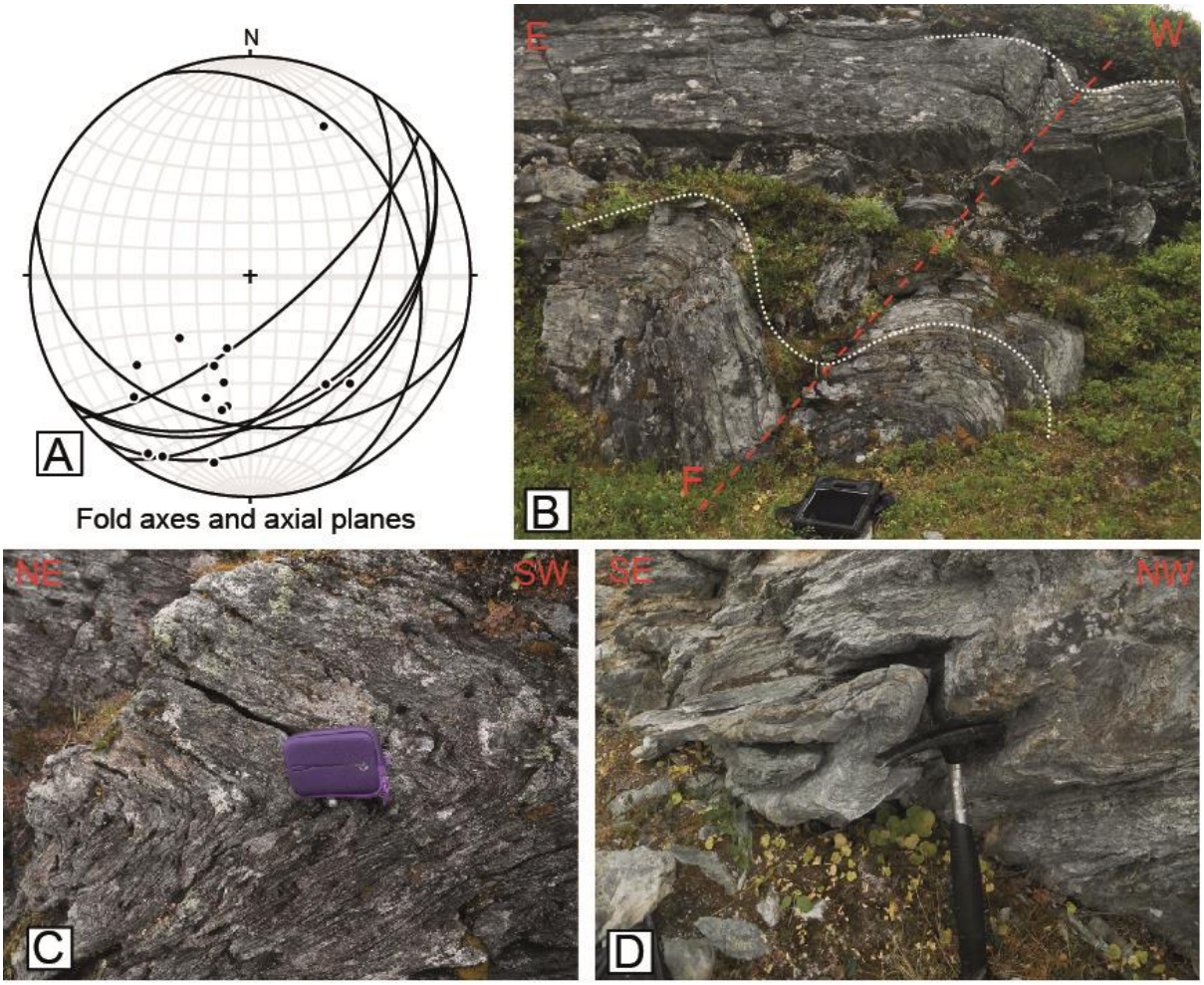

Figure 5.16: A) Large scale gentle folding in the green sandstone. Note that the fold decreases upwards. B) Stereonet showing fold axes (points) and axial planes (lines) measured in the green sandstone. C) Close up of folds in a more foliated part of the green sandstone. Note the small-scale folding within the larger closed fold. D) One example of tight folding in the green sandstone, found in the more "cherty" part of the unit and possible a parasite fold to the larger folding seen in 5.16-B.

5.2.2 – Intermediate volcanic and intrusion

Intermediate volcanic

This unit is interpreted to be a volcanic rock, appearing either as lavas or sills, and it is therefore relatively massive and does not exhibit many structures, similar to that of the greenstone. Two possible layering measurements have been made, but these might rather represent foliation, which they correlate with (Fig. 5.17-A). Foliation is the most common structural feature, and can be separated in two trends, one dipping steeply to moderately towards E/SE and another dipping moderately to gently S/SW (Fig. 5.17-A). It is interesting to note that this is concordant with the green sandstone (Fig. 5.15-A).

Only one possible fold is detected in the Intermediate volcanic, but it was unfortunately not photographed. It has a fold axis plunging gently to the S-SW and an axial plane dipping moderately to the SE (Fig. 5.17-B), both concordant with the folds observed in the green sandstone (Fig. 5.16-A). It seems likely the intermediate volcanic is folded together with the green sandstone.

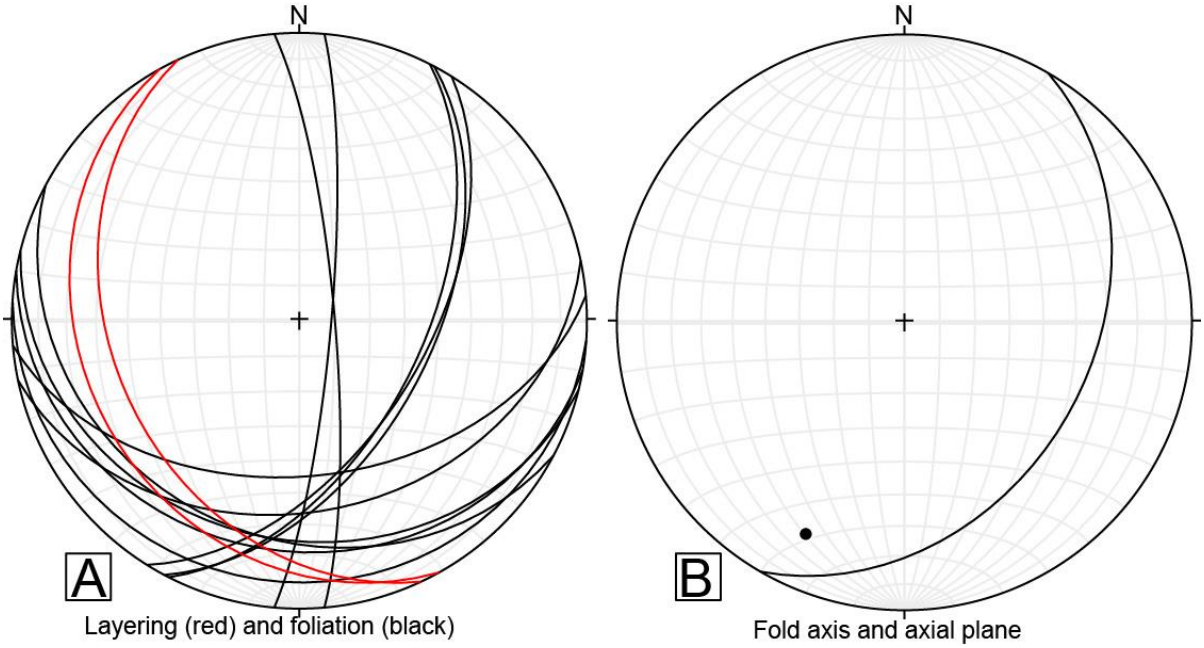

Figure 5.17: A) Stereonet showing foliation (black) and possible bedding/layering of the intermediate intrusion. Note the concordance between foliation and layering indicating the layering might be related to the foliation. B) Stereonet showing axial plane (line) and fold axis (point) for the one fold mapped in this unit.

Intermediate intrusion

There are few outcrops where this unit can be seen, and they are often heavily weathered and poorly exposed. The main structural feature of this unit is the foliation (as seen in Fig. 4.17 in chapter 4.3.4), which dips moderately to gently to the SW-SE (Fig. 5.18). This is more concordant with the green sandstone than the intermediate volcanic, yet they are not completely contradicting either. There is also one lineation plunging relatively gentle to the SW (Fig. 5.18), which represents the orientation of biotite in a foliated zone of the unit.

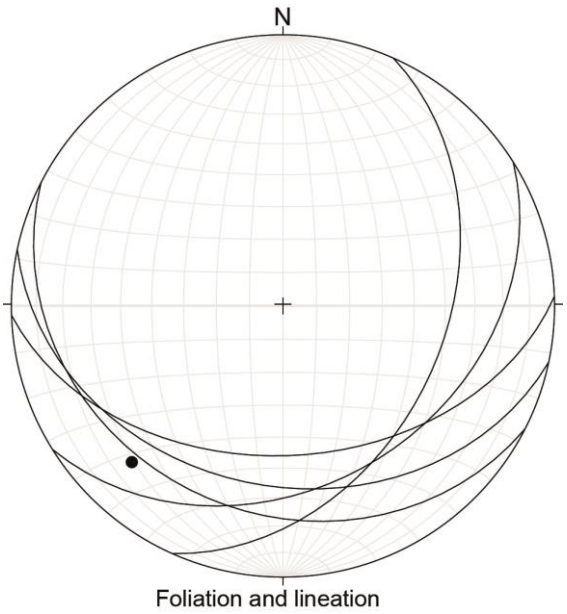

Figure 5.18: Stereonet showing foliation (lines) and lineation (point) in the intermediate intrusion.

5.3 – Main features

Summary of main features below the unconformity

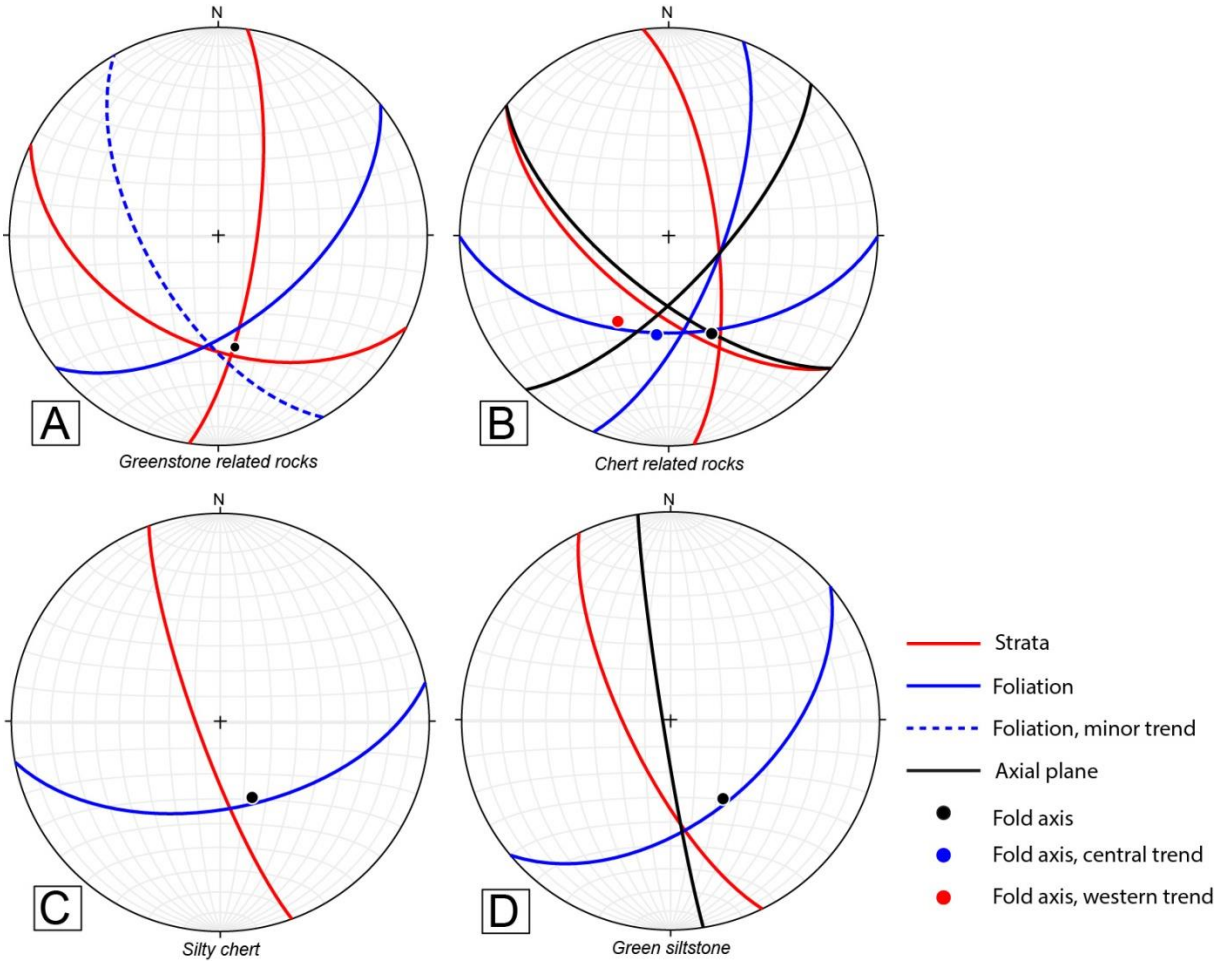

Figure 5.19: A) Stereonet showing the main structures in greenstone. Red lines represent the mean value of the two trends seen in the strata, with the main trend dipping SW and the minor trend dipping E. Blue lines are the mean values of the foliation, with dashed line indicating the minor trend. Black point indicate the mean fold axis. B) Stereonet showing the main structures in ribbon-chert. Red lines represent mean orientation of the two trends in strata, with main trend dipping SW and minor dipping E. The blue lines indicate two trends in foliation, western trend dipping E-SE and eastern trend dipping S. Black lines indicate two trends in the axial planes, and points indicate three trends in the fold axes (red is western trend, blue central and black eastern.) C) Stereonet showing the mean orientations of the main structures in silty chert. Red line indicates strata, blue line foliation and black point the mean fold axis. D) Stereonet showing the mean orientation of the main structural features in green siltstone. Red line represents the strata, blue line the foliation and black line and point indicates axial plane and fold axis respectively.

Four stereonets are presented in figure 5.19, one from each main unit below the unconformity, showing the mean orientations for the key structures in each. In both the greenstone-related rocks and the chert-related rocks there are two trends in the strata, with the main fold axis in the crossing between the two, indicating a relation. The main fold axis seems to plunge moderately to the S-SE in all units, with additional SW trending fold axis in the ribbon-chert unit. In the ribbon-chert the axial planes seem to lie close to the foliation, indicating a possible axial plane foliation, but the correlation is a bit imprecise. Note the highly correlating structures found in the silty chert and the green siltstone, reflecting the connection between the two. There also seems to be a regional trend in the foliation, it has roughly the same orientation in all four stereonets, dipping moderately S-SE.

Summary of the main features above the unconformity

The mean orientations from each of the three units above the unconformity are presented in figure 5.20. Only the green sandstone shows bedding, of which two trends are visible. One interesting aspect is the correlation with the layering measured in the greenstone below the unconformity. The axial plane and the foliation in the sandstone are almost parallel, as noted earlier in chapter 5.3.1. Foliation measured in the intermediate volcanic could be interpreted to have two trends, represented in the stereonet as dashed lines (Fig. 5.20-B). However, when calculating the mean value for all foliations in the unit (Fig. 5.20-B, blue solid line), it seems to be concordant with the foliation seen in both green sandstone and intermediate intrusion. Foliation generally seems to be correlating between all three units, dipping moderately SE. This is also concordant with the main trends of the foliation seen in the units below the unconformity. The mean fold axis in the green sandstone dips moderately SW, and is almost lying on the crossing of the two bedding trends, indicating they probably represent the fold hinges. The single fold axis mapped in the intermediate volcanic also trends SW, but with a slightly shallower plunge.

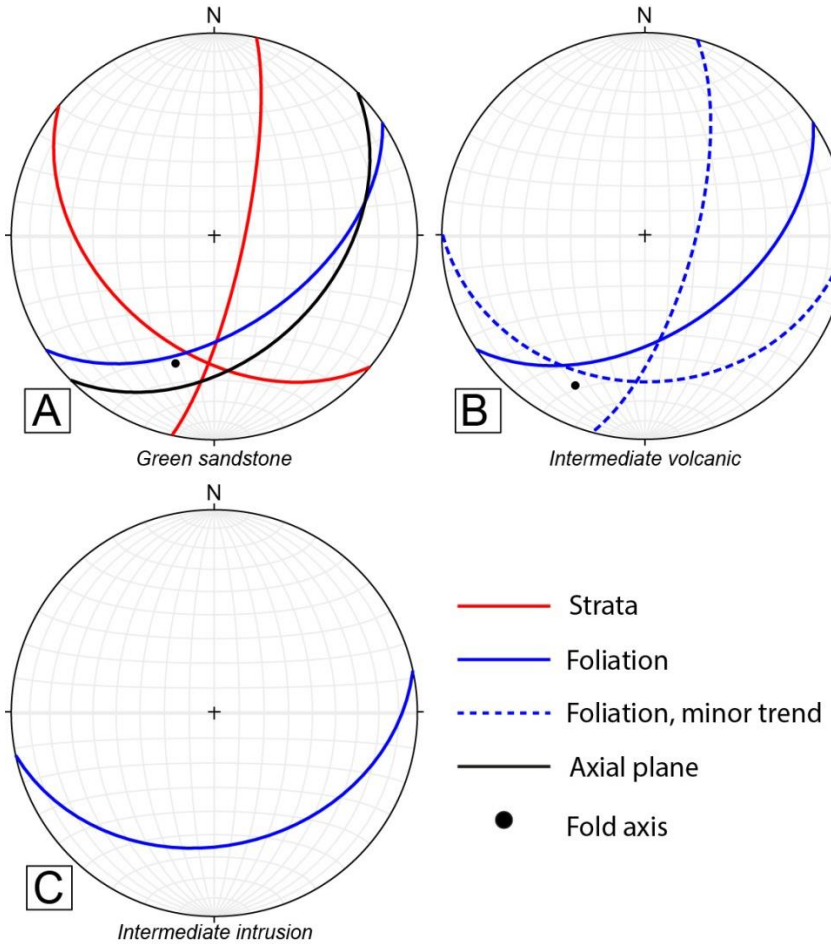

Figure 5.20: A) Stereonet showing the mean orientation of main structures in the green sandstone unit. Red line represents two trends in the bedding. B) Stereonet showing mean orientation of main structures in the intermediate volcanic. C) Stereonet showing mean orientation of foliation, which is the only structure mapped in the intermediate inrusion.

5.4 – Mapped boundaries

5.4.1 – Boundary between green sandstone and greenstone/ribbon-chert

The boundary is poorly exposed in the northern and southern part of the field area, with thick vegetation covering the slope into Leverdalen and large marshes in the south (Map 6, appendix 1). In the southwestern corner of the map no proper observations have been made (Fig. 4.2), and the boundary between green sandstone and greenstone is interpreted based on the previous geological map from Nilsen and Wolff (1989). In the central part of teh map where the boundary is best exposed, it is generally folded, and the sandstone cuts both the ribbon-chert and the greenstone (Map, appendix 4; Fig. 5.21), as well as possibly the agglomerate. Higher up in the sandstone there are abundant but scattered granitic and quartzittic clasts, while towards the contact, the sandstone gets even more clast-rich with pockets of conglomerate incorporating a larger input of more felsic-volcanic and angular chert clasts. This conglomeratic lower part of the sandstone is easily confused with the agglomerate.

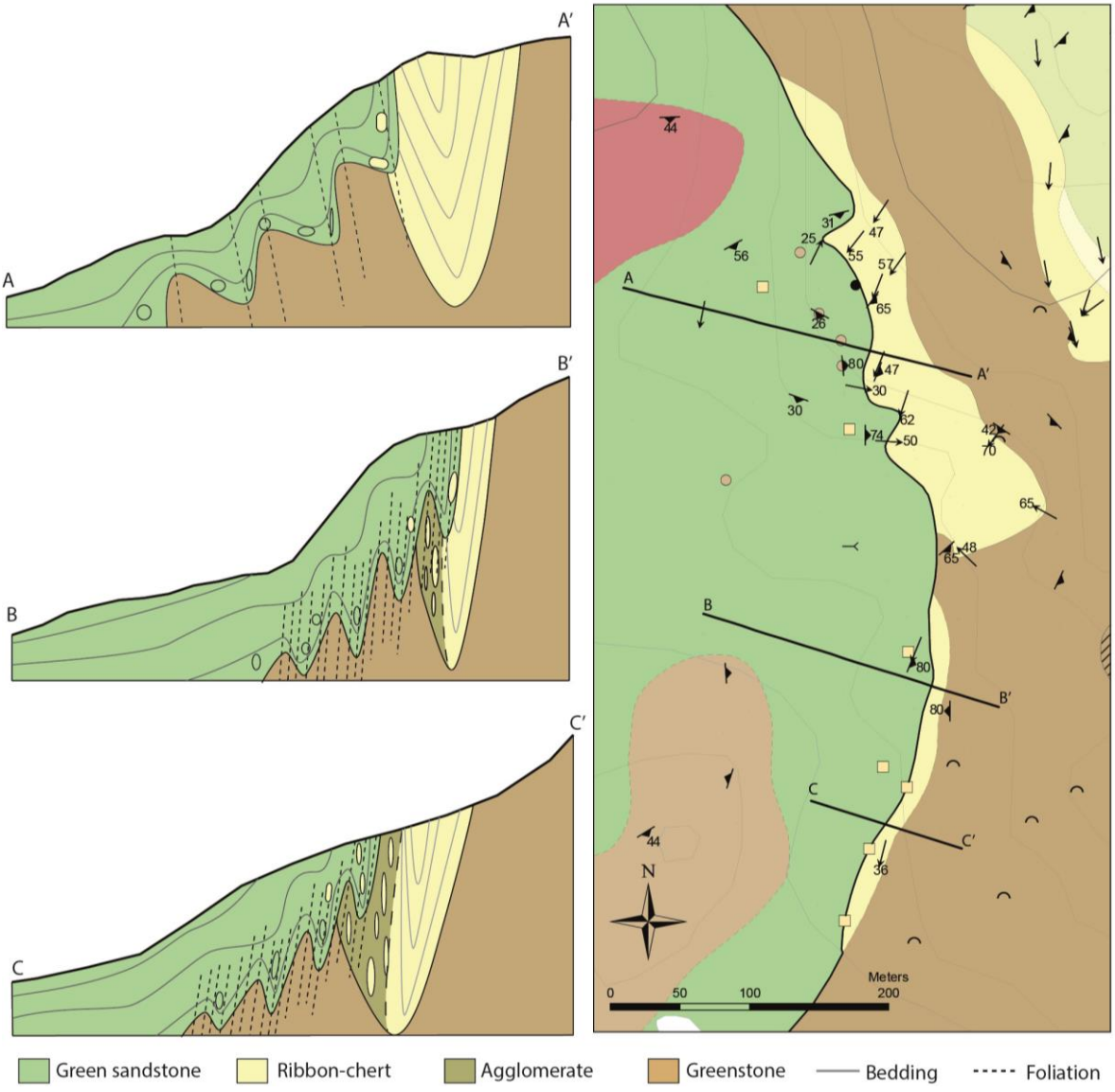

Figure 5.21: Three profiles through the contact between green sandstone and greenstone/ribbon-chert show a transition from a slightly folded and foliated boundary in the north towards an increasingly tight folding and penetrative foliation in the south. Note also how the bedding in the sandstone is affected by the folding making it almost vertical towards the contact.

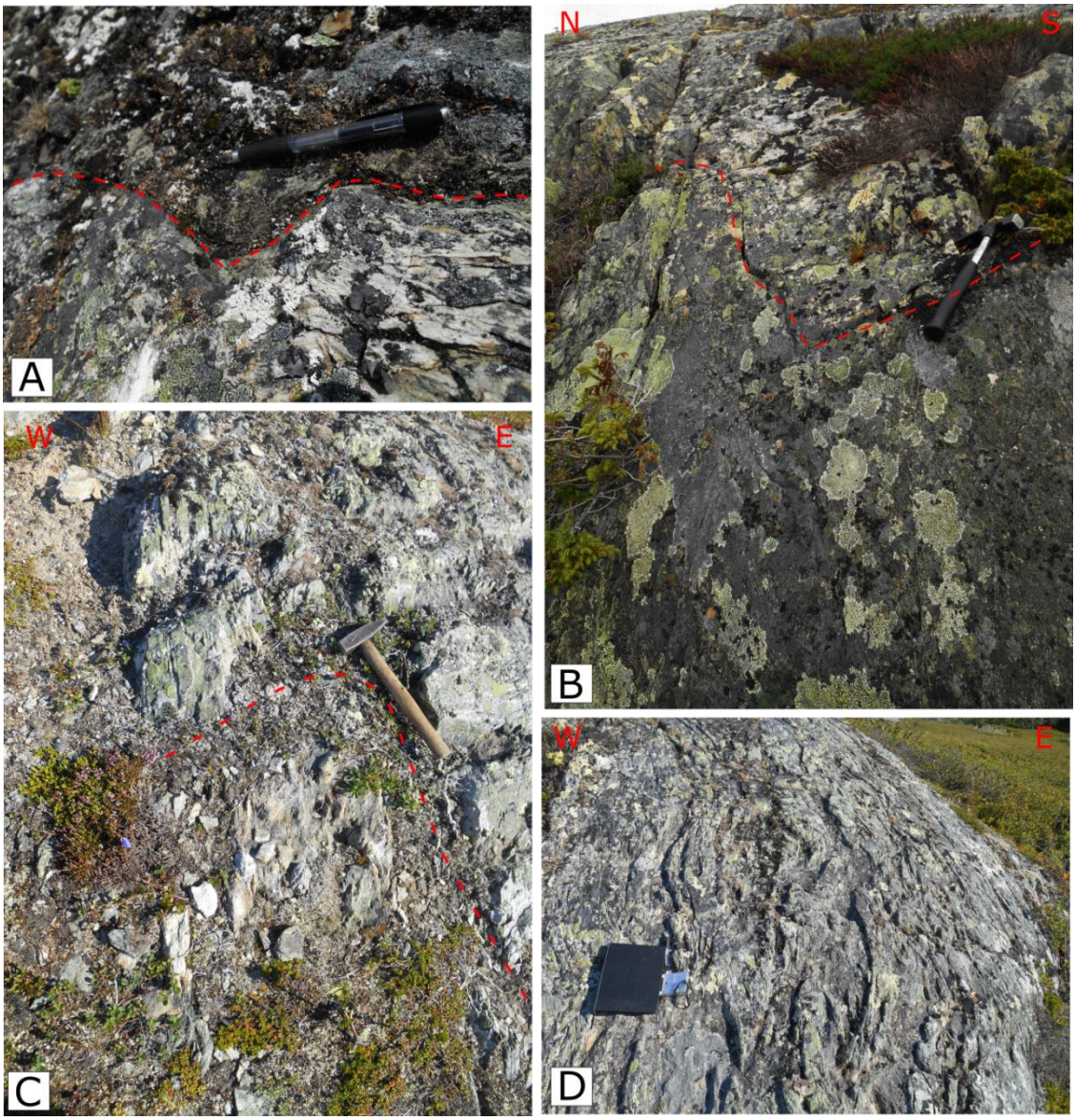

Figure 5.22: A) Sandstone above and ribbon-chert below in folded contact. Note the chert layer that looks like it has been cut off. B) Folded contact with sandstone bellow and ribbon-chert above. C) Folded contact between vertical ribbon-chert above and right, and vertical and foliated green sandstone/conglomerate below and left. D) Broken up chert layers folded into the sandstone/conglomerate or possibly the agglomerate.

The sandstone cuts the ribbon-chert in two areas (Fig. 5.21). The upper section is visibly folded in open to closed folds, which cuts the chert at an intermediate angle (Fig. 5.21; Fig. 5.22-A&B). An axial plane foliation is developed, but it is not as penetrative and steep as further south, and the orientation seems to be controlled both by the main foliation direction and by the contact (Fig. 5.21-profile A-A'). In the southern profiles the sandstone is penetratively and steeply foliated, possibly due to much tighter folding, making sandstone/conglomerate and ribbon-chert lying parallel to each other (Fig. 5.21-profiles B-B'&C-C'; Fig. 5.22-C). In this section, the conglomeratic lower part of the sandstone also cuts the agglomerate, which makes is hard to decide where the contact actually lies, especially as the agglomerate also contains large fragments of chert, further obscuring the boundary (Fig. 5.21-profile C-C'; Fig.5.22-D). The sandstone seems to experience a gradual transition from horizontal bedding only some ten meters away, to almost vertical at the boundary. This

could be caused by the folding, which is possibly tighter further south, making bedding in sandstone and ribbon-chert almost parallel (Fig. 5.21-all profiles). This causes additional confusion to the relation between foliation and strata, and contributes to increase the complexity of this contact.

5.4.2 – Boundary between greenstone and ribbon-chert

There are at least three long stretches where greenstone and ribbon-chert bounds each other, as well as several smaller pockets of chert inside the greenstone in the southern part (Map, appendix 4). The boundary is generally very sharp and often exposed over several meters, especially in the top area (Fig. 5.23). However, especially on the eastern side of the central ribbon-chert/siltstone unit the boundary zone is more diffuse, due to the presence of the agglomerate. Pillow breccias appear at the top of the greenstone, grading into the previously described agglomerate, making the boundary more transitional. The limits of the chert pockets in the southern areas are somewhat interpreted, as the exposure rate in this marsh area is low (Map 6, appendix 1). One important aspect of the ribbon-chert – greenstone boundary is the appearance of jasper in patches between the ribbon-chert and the greenstone. This could be a way up indicator, as it lies systematically in the boundary zone on each side of the central ribbon-chert unit, as well as around the smaller chert-pockets (Map, appendix 4).

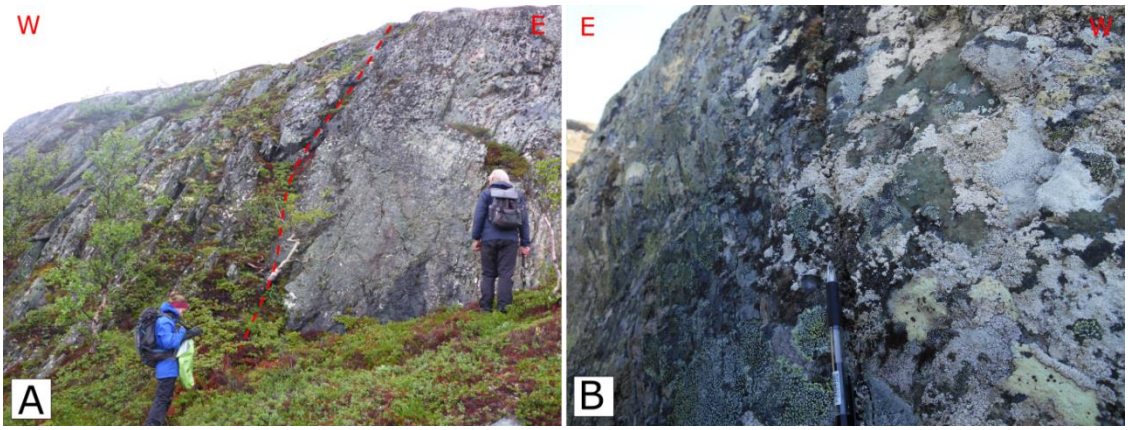

Figure 5.23: A) Well exposed relatively sharp boundary between greenstone to the west and ribbon-chert to the east. B) Sharp boundary between ribbon-chert to the east and greenstone to the west. Boundary indicated by the pen.

5.5 – Brittle deformation

The area is dominated by ductile deformation, like foliation and folding, while there is few observations of brittle deformation. However, there is some evidence of younger extensional faulting, creating parallel valleys cutting the southwestern ridge of Dugurdsknappen approximately NW-SE (Fig. 5.24-D). The fault planes are hard to measure properly, so four of them were measured only for direction and are therefore plotted as vertical in the stereonet (Fig. 5.24-A). It is more likely that they have a steep to moderate dip towards SW, similar to the two measured fault planes (Fig. 5.24-A). One locality shows stretching lineations plunging gently WNW, indicating transtensional dextral movement (Fig. 5.24-A&B), while another valley has a surface of fault breccia on one of the valley sides (Fig. 5.24-C).

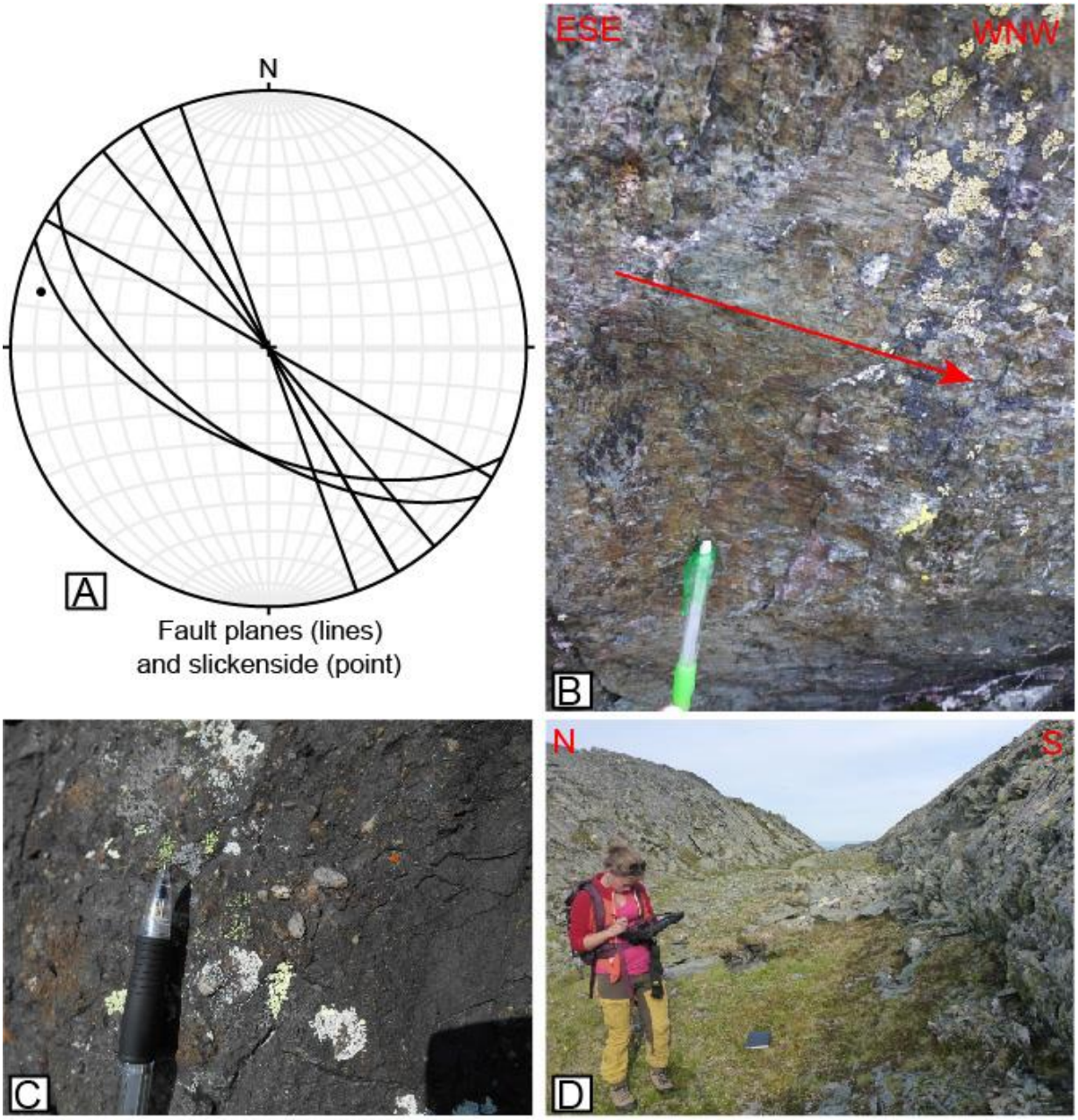

Figure 5.24: A) Stereonet showing orientation of fault planes indicated from valley direction. B) Slickensides from valley side. C) Consolidated fault breccia on one of the valley sides. D) One of the fault valleys. The faults have created a weakness leading to erosion of a valley. Last photo from D. Gasser.

There is little systematics to be found elsewhere among the brittle structures, as seen in the scattered measurements of joints in the sandstone and greenstone, which probably reflect more local or unsystematic processes (Fig. 5.25-A&B). However, in the ribbon-chert there have been observed many localized semi-brittle shear zones (Fig. 5.25-C) and a few joints, which seem to show an indistinct pattern. This pattern seem to consist of two trends, one dipping steep to moderately N-NE and another dipping moderately SE (Fig. 5.25-D).

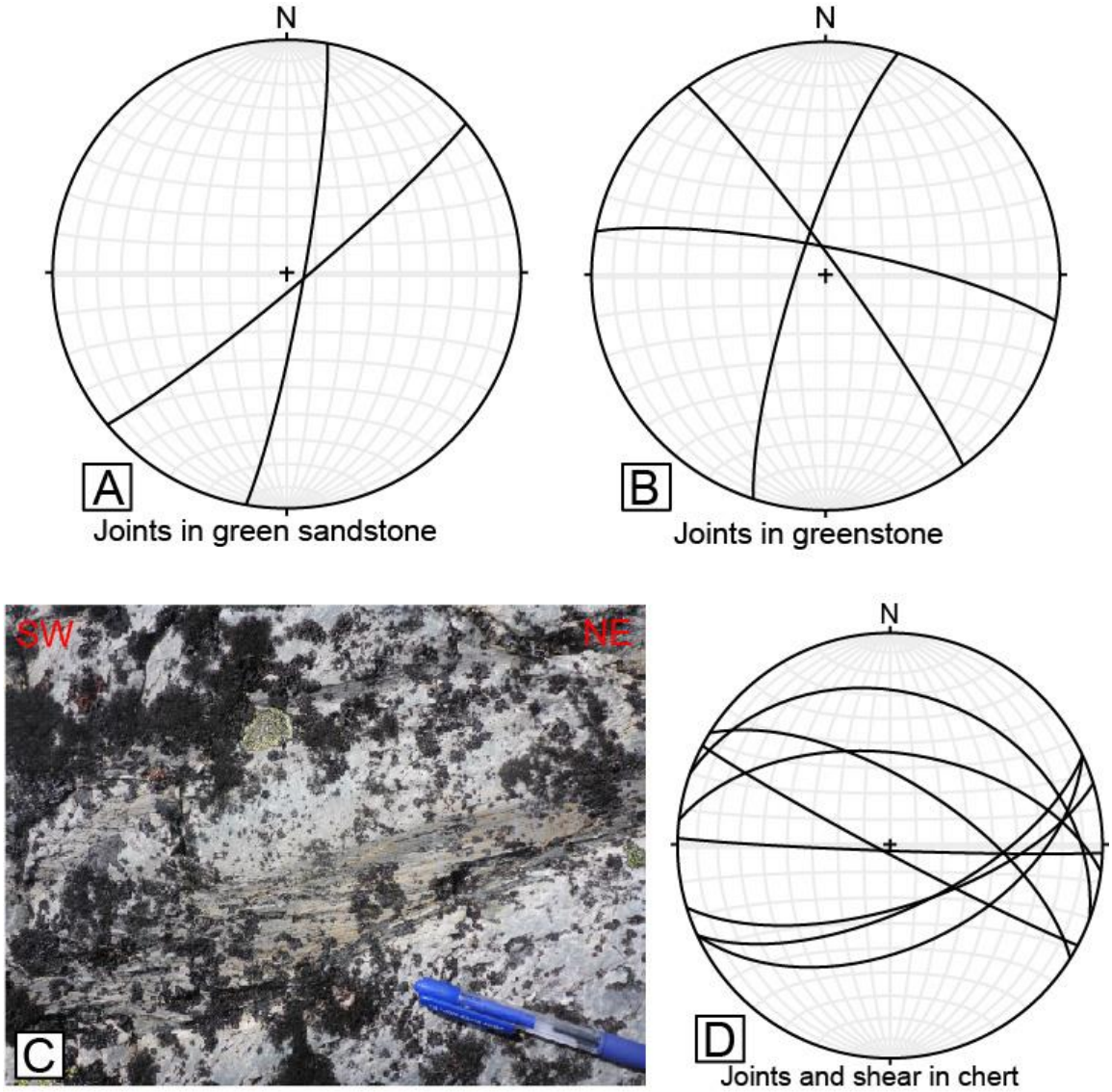

Figure 5.25 A) Stereonet showing two joints in green sandstone. B) Stereonet showing three joints in greenstone. **:** C) Small shear zone in chert, close to the top of Dugurdsknappen. D) Stereonet showing joints and shear zones in ribbon-chert, two indistinct trends can be observed.

Chapter 6 – Petrographic and geochemical description

Table 6.1: List over all samples used for petrography and geochemistry with overview of the methods applied.

Sample	Description	Thin section	XRF	LA-ICP-MS
A) Greenstone-related rocks				
EST_48A	Greenstone, with dark green mineral	X		
EST_48B	Greenstone	X	X	X
EST_64	Greenstone, with pillows	X	X	X
EST_79B	Greenstone		X	X
EST_160	Greenstone	X	X	X
EST_849	Greenstone, with pillows	X	X	X
EST_576	Schistose greenstone	X		
EST_445	Gabbro	X	X	X
EST_400	Dyke in Greenstone		X	X
EST_142	Altered greenstone, eastern side	X	X	X
EST_345	Altered greenstone, eastern side	X	X	X
EST_85	Altered greenstone, western side	X	X	X
EST_79A	Altered greenstone, western side	X	X	X
EST_96	Altered greenstone, western side	X		
EST_179	Altered greenstone, western side	X	X	X
EST_372	Altered greenstone, western side		X	X
EST_421	Altered greenstone, western side	X	X	X
EST_629	Altered greenstone, western side	X	X	X
B) Chert-related rocks				
EST_334	Jasper	X		
EST_392	Jasper	X	X	X
EST_390	Chert	X	X	X
EST_717	Chert	X	X	X
EST_843	Chert	X	X	X
EST_306	Chert, foliated	X		
EST_349	Chert, coarser type	X	X	X
EST_375	Silty chert	X	X	X
EST_30	Brown sandstone bed in ribbon-chert	X	X	
EST_19	Calcareous sandstone bed in ribbon-chert	X	X	
EST_317A	Felsic conglomerate	X	X	X
EST_317B	Felsic conglomerate	X	X	X
C) Green siltstone				
EST_170	Green siltstone	X	X	X
EST_191	Green siltstone, with possible pyrite	X		
EST_378	Green siltstone, oriented sample	X		
EST_632	Green siltstone	X	X	X
D) Rocks above the unconformity				
EST_2	Green sandstone	X	X	
EST_112	Green sandstone	X		
EST_702	Green sandstone, cherty looking	X		
EST_41	Intermediate volcanic, uncertain	X	X	X
EST_766	Intermediate volcanic, uncertain	X	X	
EST_700	Intermediate volcanic	X	X	X
EST_797	Intermediate volcanic	X		
EST_76	Intermediate intrusion	X	X	X
EST_696	Intermediate intrusion	X		

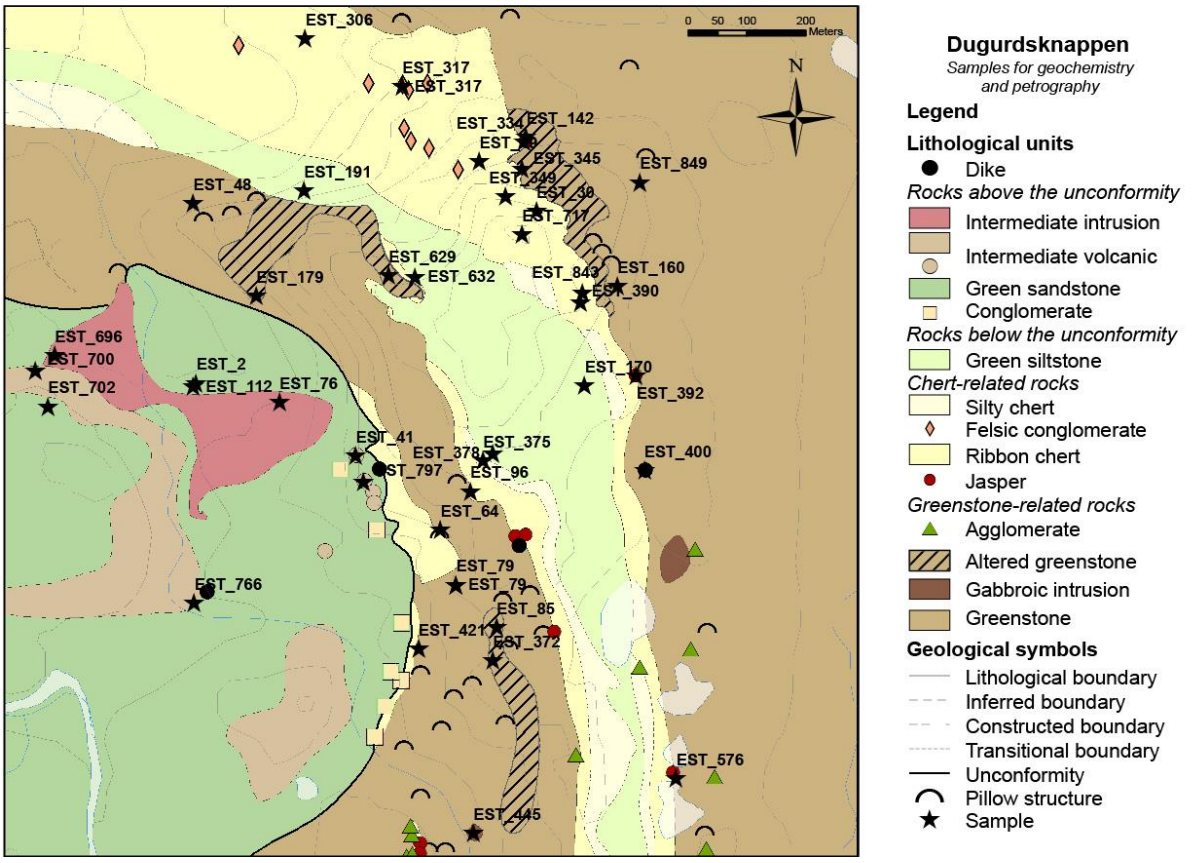

Figure 6.1: Map showing location of all samples analyzed petrographically and/or geochemically. Samples are listed in table 6.1.

6.1 – Petrography

6.1.1 – Greenstone-related rocks

18 samples were taken from different locations within this group (Fig. 6.1), all listed in table 6.1-A. Major and trace element analyses were acquired of fifteen samples, while three were only analyzed via thin section and three only by geochemical analysis, due to insufficient amount of material (Tab. 6.1-A). Seven samples are from proper greenstones/greenschists, one comes from a gabbro, one from a greenstone dyke, and the remaining nine samples are interpreted to represent variably altered greenstones. Sample EST_79B was sampled as an altered greenstone, but has geochemistry similar to the greenstones, and is therefore counted among them.

Greenstone

All seven greenstone thin sections share similar characteristics, though with some variations that does not seem to be directly related to the presence or absence of pillow structures in outcrop scale. The samples are generally dominated by a fine-grained dark matrix (Fig. 6.2-A), cut by several quartz veins and fractures. The matrix consists mainly of epidote, together with low relief gray (in XPL) minerals, comprising feldspars and possibly quartz (Fig. 6.2-B). In a few samples abundant carbonate is scattered in the matrix, as well as accumulated in a few bigger aggregates. Epidote also occurs as slightly bigger grains. All samples are chloritized, with fine-grained chlorite penetrating the thin section. The chlorite has in some

samples grown big enough to be seen as large green crystals in outcrop scale (Fig. 6.2-A), as described in chapter 4.3.1 (Fig. 4.3-F). Biotite, rutile, and titanite, as well as some amorphous opaque are present as accessory minerals. There is a planar fabric in most samples, which is evident in the oriented platy minerals, particularly the chlorite. One sample (EST_576) is described as greenschist due to the almost completely chloritized matrix showing a strong foliation. It also contains porphyroblasts, mainly of calcite and biotite, as well as occurrences of pyrite.

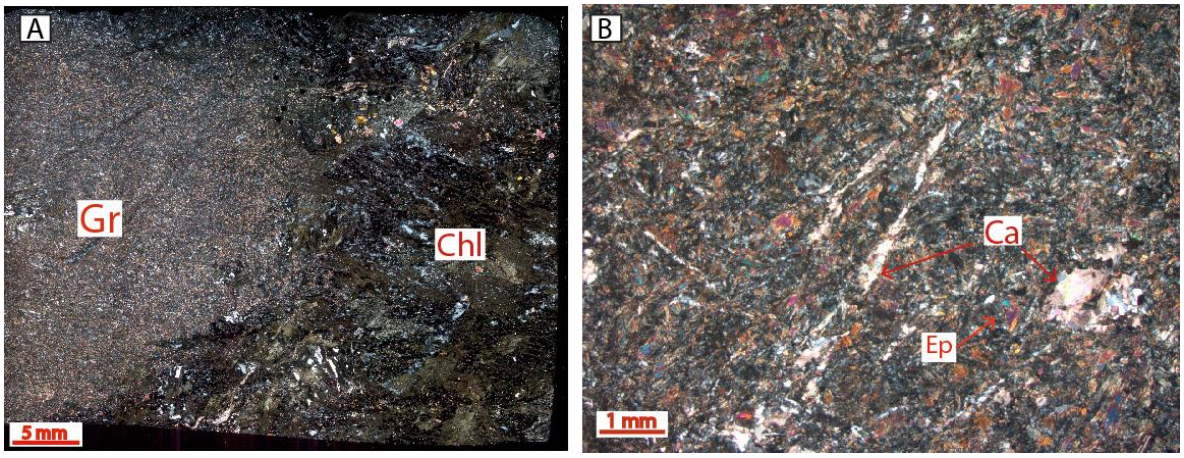

Figure 6.2: A) Thin section EST_48A in XPL. Typical greenstone groundmass (Gr) as seen in all other greenstone samples to the left in the thin section and large chlorite (Chl) crystals to the right, which can be seen in outcrop as well (Fig. 4.3-F). B) Thin section EST_849 in XPL. Close up of typical greenstone matrix. Note the dark colour with abundant epidote (Ep) and scattered calcium (Ca) crystals and veins.

The gabbro is dominated by large amphibole crystals surrounded by smaller, but still relatively coarse feldspar and epidote crystals (Fig. 6.3). There are also some large intergrown crystals of secondary muscovite and chlorite, as well as more fine-grained chlorite in the matrix. Rutile surrounded by fine-grained titanite is also observed, as well as separate aggregates of titanite. The gabbro sample has experienced deformation, breaking up and slightly reforming the crystals.

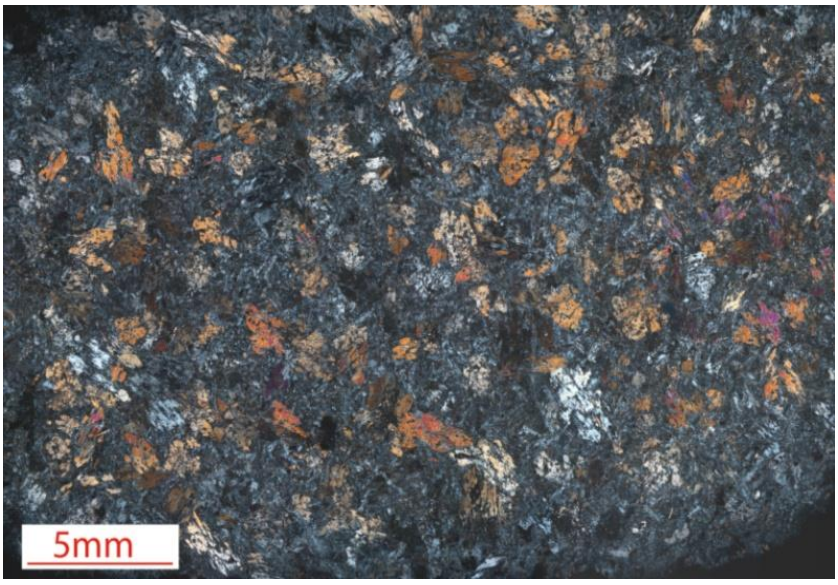

Figure 6.3: Thin section EST_445 showing gabbro. Note the much more coarse-grained texture than seen in the greenstones.

Altered greenstone

Eight thin sections were made from the nine samples, which were taken both inside defined polygons of altered greenstone, and from separate localities with an altered appearance (Fig. 6.1). There seem to be roughly two types. One (comprising thin sections EST_142 and EST_345) seems to have the same groundmass as the greenstone, but with an otherwise more heterogeneous texture and mineralogy. It is worth noting that these are the only ones sampled on the eastern side of the major synform (Fig. 6.1). Sample EST_345 has large porphyroblasts of zoisite, while in EST_142 they are much smaller (Fig. 6.4-A&B). Epidote is abundant, and there seem to be widespread amorphous opaques, e.g. hematite or leucoxite, both scattered and accumulated in veins and aggregates (Fig. 6.4-A).

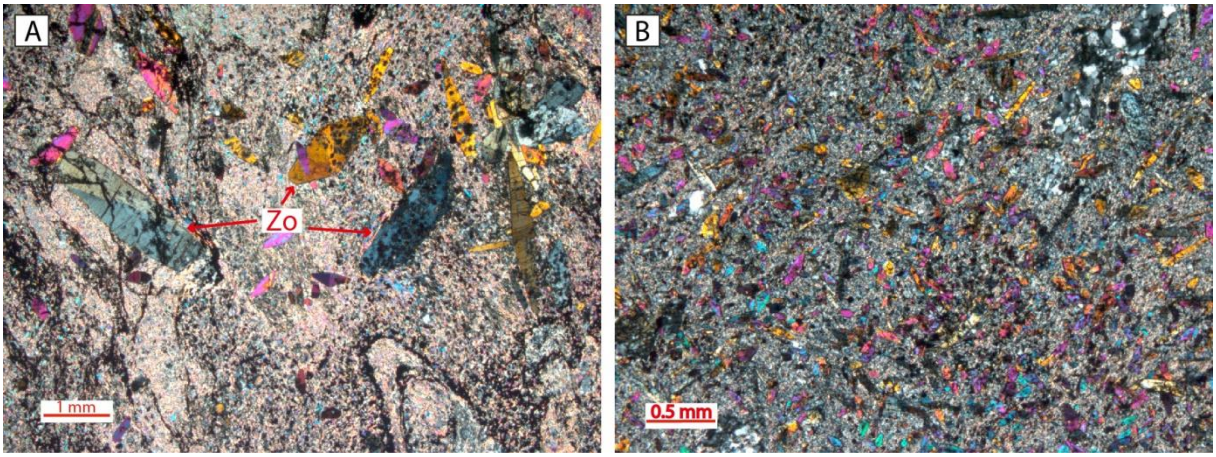

Figure 6.4: A) Thin section EST_345 in XPL. Note the more typical greenstone matrix with abundant amorphous opaque and the large zoisite (Zo) crystals. B) Thin section EST_142 shows similar mineralogy, but with smaller zoisite crystals, as well as abundant epidote crystals.

The other type has a porphyritic texture comprising a lighter, more intermediate matrix and large biotite grains, either as phenocrysts or porphyroblasts (Fig. 6.5-A). This is seen especially well in thin sections EST_85, EST_421 and EST_629, the latter containing abundant tabular albite (Fig. 6.5-B). The biotite grains have variable size and appearance in different samples, as in EST_96 where they are smaller and have anomalous purple interference colours (Fig. 6.5-C). There is generally a lot more carbonate within this unit, as well as abundant quartz veins. Sample EST_179 has layers of large carbonate crystals, together with veins of large recrystalized quartz (Fig. 6.5-D). Chlorite is common in most samples together with some fine-grained muscovite, and aggregates of amorphous opaques and fine-grained titanite occur as accessory minerals.

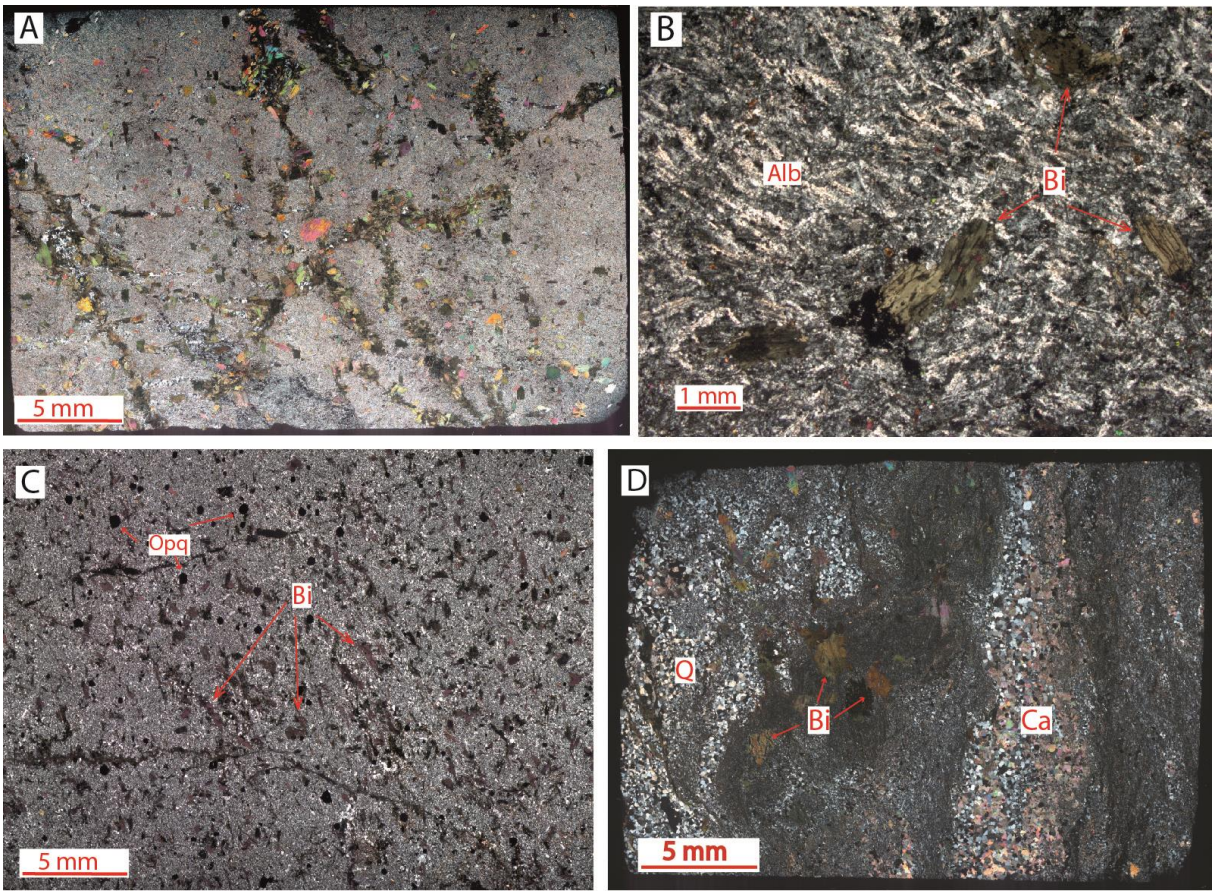

Figure 6.5: A) Thin section EST_421 in XPL. Note the lighter matrix and the large accumulations of biotite. B) Thin section EST_629. Note the tabular light albite (Alb) crystals making up the matrix in between the large biotites (Bi). C) Thin section EST_96 in XPL. Note the anomalous dark purple biotites (Bi) and the opaques (Opq) in a generally light matrix. D) Thin section EST_179 in XPL. Note the lighter matrix in between layers of calcite (Ca) and recrystalized quartz (Q), as well as some large biotite grains (Bi).

6.1.2 – Chert-related rocks

Twelve samples were taken in this group (Table 6.1-B; Fig. 6.1), which includes the ribbon-chert with interbedded sandstones, as well as jasper, silty chert and felsic conglomerate. Thin sections were made of all samples, while two samples, one of jasper and one of chert, were not geochemically analysed. Trace element analyses by ICP-MS were not made from the two interbedded sandstones.

Jasper, ribbon-chert and silty chert

These are all dominated by recrystallized quartz, either fine-grained, or in more coarse-grained layers/bands (Fig. 6.6-A). Fine-grained mica, chlorite and clay minerals are common in between the quartz grains in all samples, tough more abundant in the silty chert. The silty chert is generally distinguished from the typical chert on the dominantly very fine-grained quartz, with abundant fine-grained mica/sericite in between, creating a sort of cross-hatched texture. Muscovite is the most common mica, with only scarce amounts of biotite occurring in a few larger aggregates. Sample EST_349 represents an altered zone in the ribbon-chert, which in thin section reveals aggregates of larger biotite grains, some chloritized, in an otherwise fine-grained matrix of quartz and clay minerals. Jasper is distinguished from the

typical chert on the abundance of amorphous opaques, both scattered and in aggregates/bands in between the quartz (Fig. 6.6-B). Most samples have a planar fabric, emphasized by the oriented mica, chlorite and abundant clay minerals, which lies parallel to the bands of recrystallized quartz. Sample EST_306 is an example of a particularly developed cleavage in chert, with thick bands of abundant fine-grained mica and clay minerals, together with large amounts of anomalous blue (in XPL) chlorite and occurrences of titanite.

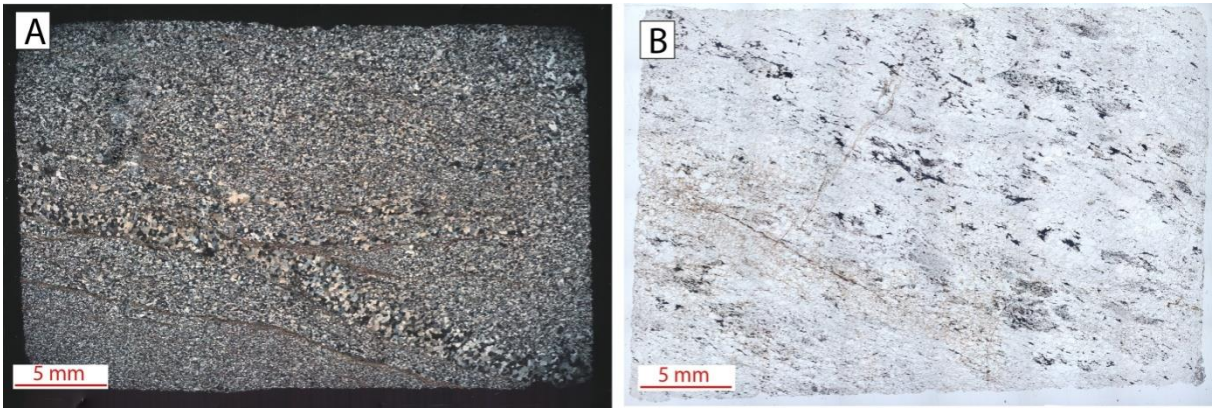

Figure 6.6: A) Thin section EST_717 in XPL. Note the recrystallized quartz of different grain-size in chert. B) EST_334 in PPL shows jasper thin section. Note the abundant amorphous opaque.

Interbedded sandstones

The brown sandstone reveals an abundance of relatively fine-grained quartz and feldspar with some larger grains of feldspar, including plagioclase, surrounded by brown clay minerals and very fine-grained mica/sericite (Fig. 6.7). These large grains are weathered and to a degree replaced by sericite, but still have a fairly euhedral shape indicating they are not metamorphic and also not transported very far. No zoning is found in the feldspars to indicate a magmatic origin, but there is plagioclase twinning. There are also some larger grains of biotite, and a planar fabric orienting the grains.

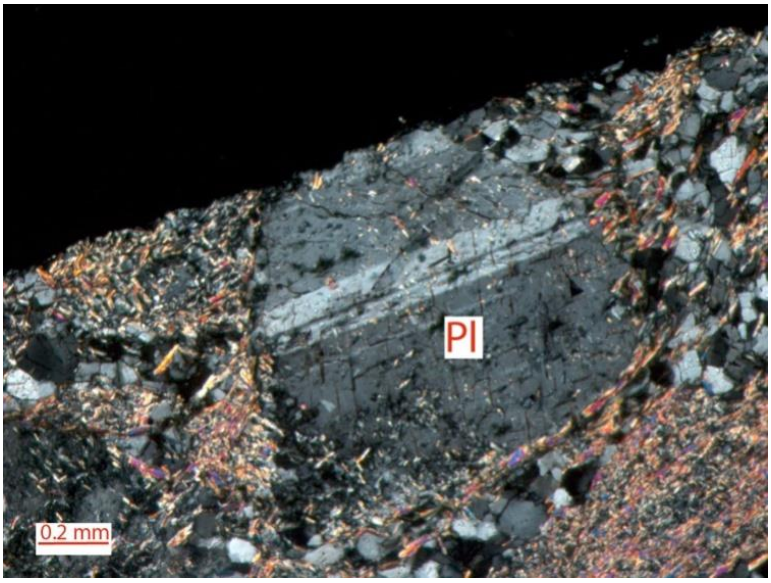

Figure 6.7: Large partially euhedral plagioclase crystal with visible twinning in a mica and quartz dominated matrix. From thin section EST_30 in XPL. Note the weathering, shown by the sericite crystallizing in the grain.

The calcareous sandstone is medium-grained with relatively equal amounts of similar sized quartz, calcite and biotite. The quartz is slightly more fine-grained, filling in between the other minerals. It has a random fabric where the biotite does not seem orientated.

Felsic conglomerate

These two samples both show a matrix dominated by quartz and abundant clay minerals from weathering, with biotite grains, both scattered and in aggregates, and rounded to sub-rounded clasts in varying sizes (Fig. 6.8-A). The rock fragments are mainly felsic looking, with quartz and feldspars and some plagioclase (Fig. 6.8-B), many severely chloritized or taken over by biotite or clay minerals. Chlorite is also seen in the matrix and in aggregates. Fractures and veins are fairly common, and the samples have a generally planar fabric, though somewhat vague, and often curving around rock fragments.

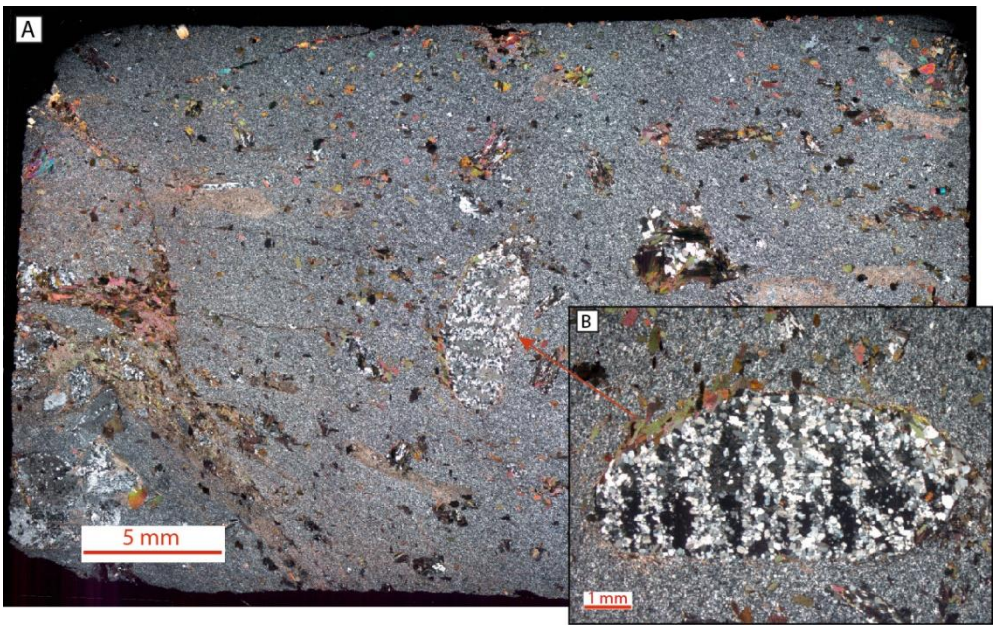

Figure 6.8: A) Thin section EST_317b in XPL. Note the light matrix and light clasts, as well as the biotite accumulations. B) Close up of one clast, revealing a quartz dominated mineralogy.

6.1.3 – Green siltstone

Four samples were taken from this unit, from four different localities (Fig. 6.1). Thin sections were made of all, while geochemical analyses were only done on two (Table 6.1-C). The thin sections show that the samples are dominated by a very fine-grained matrix, taking up about 80-90% of the thin section, with larger porphyroblasts in between (Fig. 6.9-A). The matrix consists of very fine-grained quartz with abundant fine-grained chlorite, as well as muscovite and sericite. The porphyroblasts comprise mainly biotites, though with a slightly altered appearance (Fig. 6.9-B), as well as some quartz/feldspar and opaques, possibly magnetite or ilmenite. The matrix is layered, possibly showing graded bedding (Fig. 6.9-A). There is also a vague planar fabric interfering with the bedding, creating crenulation folding (Fig. 6.9-C). The foliation in the matrix is bent around the porphyroblasts (Fig. 6.9-B), suggesting pre- to syn-kinematic growth.

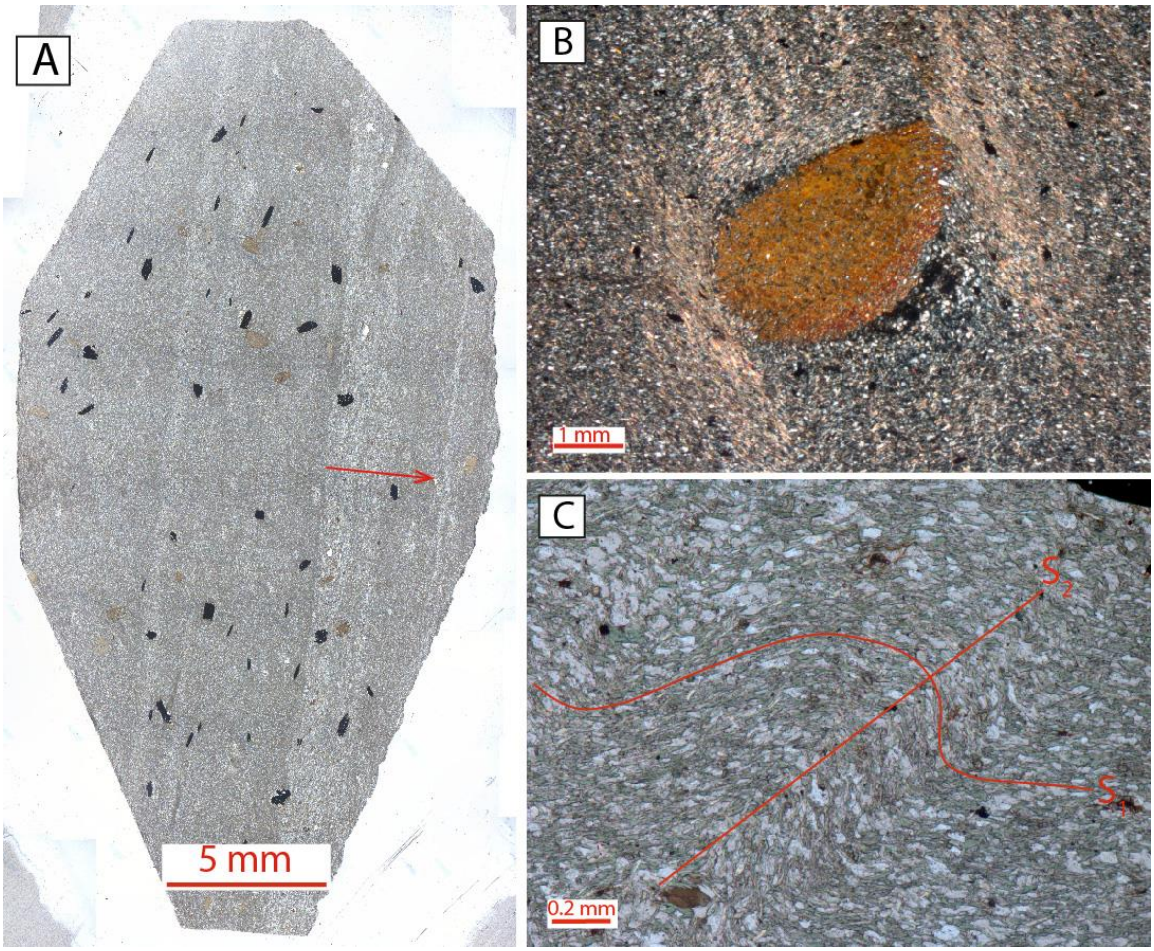

Figure 6.9: A) Thin section EST_191 in PPL. Note the very fine-grained matrix with a planar fabric and the scattered porphyroblasts of biotite and opaques. Arrow indicates direction of fining in the possible graded bedding. B) Biotite porphyroblast surrounded by fine-grained quartz/mica matrix that is bended around the blast. Note the possible tail on the blast. From EST_632 in XPL. C) Crenulation cleavage (S2) due to folding (F) of initial foliation (S1). This can also be seen in outcrop scale, as discussed in chapter 5.2.3. Note that the terminology is only local. From thin section EST_191 in PPL.

6.1.4 – Rocks above the unconformity

Nine samples from different localities above the unconformity have been analysed and thin sections are made from all (Fig. 6.1; Table 6.1-D). Two sandstone samples have been analysed with XRF, but no ICP-MS, while for the intermediate volcanic and intrusive both analyses have been done on one sample from each unit.

Green sandstone

The typical sandstones are medium-grained and relatively poorly sorted, but still with abundant quartz (both mono- and polycrystalline grains) as the main framework mineral, making up about 60% of the samples (Fig. 6.10-A), together with some feldspar. Abundant fine-grained silty matrix with mainly finer-grained quartz and other minerals are filling in between larger grains, together with fine-grained calcite and chlorite, both probably secondary as cement. Calcite also occurs relatively abundant as primary mineral in larger grains, together with abundant biotite. Epidote is observed in all samples as an accessory mineral. No clear lithic fragments are seen. EST_702 is taken from a more “cherty” part of the sandstone,

but seems to have the same mineralogy as the ordinary sandstone and is only differentiated on a stronger planar fabric reflecting a higher degree of deformation.

Two samples are a bit unclear as to which unit they belong to. EST_41 was sampled as either green sandstone or intermediate volcanic. This is a very deformed sample, making it hard to determine the mineralogy. It displays a tight folding of a very fine-grained matrix seemingly dominated by quartz or similar minerals, as well as abundant chlorite and calcite, with scattered larger biotite/chlorite grains that are following the folding (Fig. 6.10-B). The sample EST_766 was sampled as green sandstone based on field description, but in the thin section it is similar to the intermediate volcanic, as well as some of the altered greenstones from the western side (Ch. 6.1.1). It has a fine-grained matrix dominated by quartz/feldspar (plagioclase) together with chlorite and calcite, with large biotite phenocrysts scattered and in aggregates (Fig. 6.10-C).

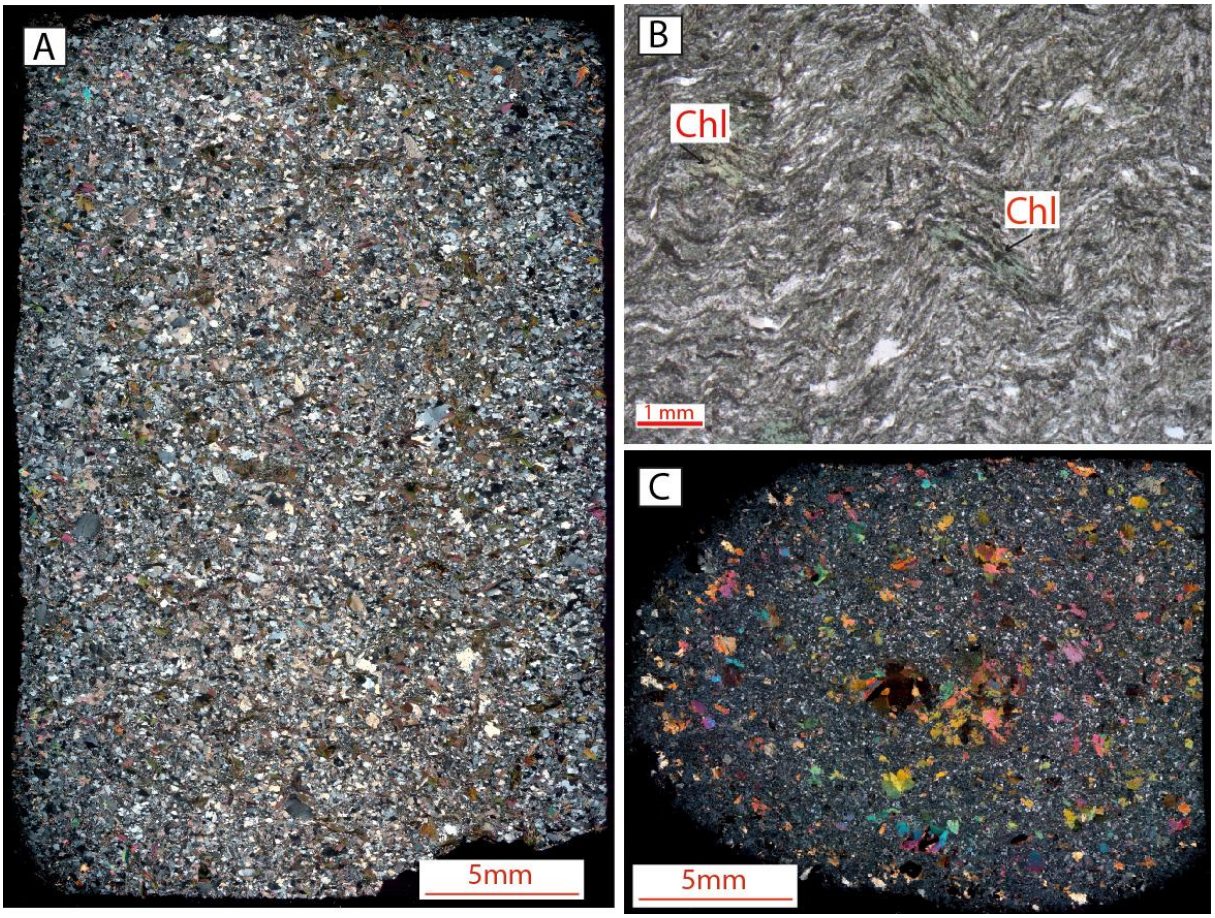

Figure 6.10: A) Thin section EST_2 in XPL. Shows the mineralogy and texture of the typical green sandstone. B) Severe folding of a fine-grained matrix. Note the large biotite/chlorite grains that are following the fold. From thin section EST_41 in PPL. C) Thin section EST_766 in XPL. Was sampled as a sandstone, but looks far more volcanic in thin section. Note the similarity to the intermediate volcanic seen in figure 6.11.

Intermediate volcanic

Two samples were taken from the intermediate volcanic. These show a porphyritic texture dominated by a fine-grained matrix of mainly quartz/ feldspar with scattered large biotite phenocrysts, as well as possibly a few hornblende phenocrysts (Fig. 6.11-A). The matrix is fairly evenly grained and comprises epidote and chlorite as well as some smaller amphibole

crystals and opaque phases that could be leucoxene or ordinary ilmenite (Fig. 6.11-B). Some fine-grained carbonate is scattered in the matrix, as well as larger grains and cross-cutting thin veins, all secondary. There is a distinct platy fabric seen in the matrix, which is made of oriented bands of recrystallized quartz and bands in the matrix of finer/coarser material (Fig. 6.11-A).

Intermediate intrusion

Both the mineralogy and texture are similar to that of the intermediate volcanic. The texture is porphyritic with about 70% fine-grained matrix and phenocrysts of biotite (Fig. 6.11-C). The matrix might be slightly more homogenous, with a bit more quartz-dominated mineralogy. It also displays a slightly larger difference between matrix and phenocrysts, with larger biotite grains/aggregates and a slightly more fine-grained matrix than that seen in the volcanic version (Fig. 6.11-B&C). This difference can indicate a more intrusive character of this unit, though the fine-grained matrix raises the question whether this really is an intrusion and not rather a more shallow intrusion or sill. The difference can also simply be the result of alteration, which suggests it was initially the same as the volcanic, but has experienced higher degree of alteration later. In thin section EST_696, there are also a few biotite grains in which a possible original amphibole crystal shape can be seen, but this is not certain.

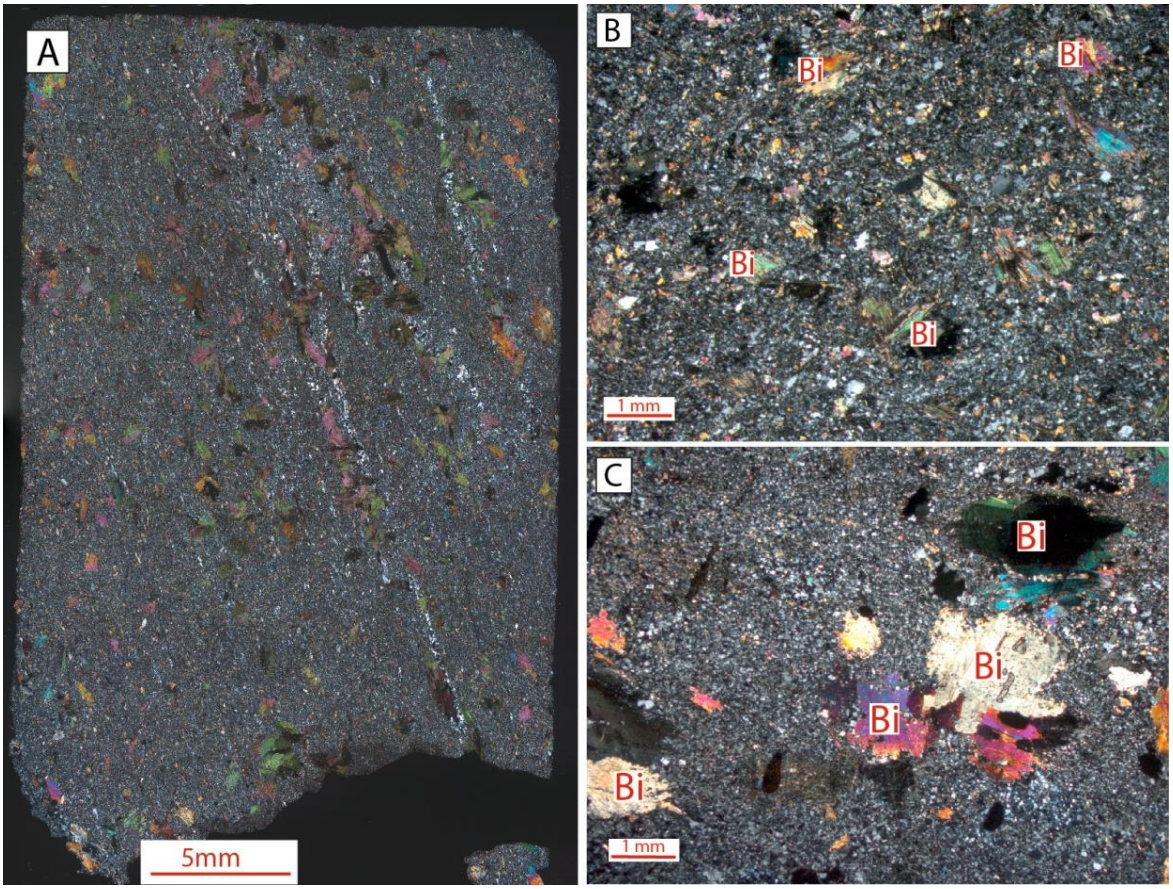

Figure 6.11: A) Thin section EST_700 in XPL: Shows the typical porphyritic texture of the intermediate volcanic. Note the platy fabric. B) Close up of matrix and biotites in the intermediate volcanic. Note the smaller size difference between matrix and fenocrysts than in figure 6.11-C. From thin section EST_797 in XPL. C) Close up of matrix and biotite in the intermediate intrusion. Note the somewhat larger size difference between matrix and fenocrysts, as well as the slightly more homogenous matrix than in the intermediate intrusion in figure 6.11-B. From thin section EST_696 in XPL.

6.2 – Geochemistry

6.2.1 – Igneous rocks - Major element geochemistry

Major element data is plotted in Harker diagrams (Fig. 6.12), with SiO_2 on the X-axis against other major element oxides on the Y-axis. The samples are described as basic or intermediate based on the classification by Winter (2010), where basic magma has a silica content ranging between 45-52 wt% and intermediate magma between 52-66 wt%.

Greenstones

The five greenstone samples are fairly clustered in most plots (Fig 6.12), though with a linear trend in the Fe_2O_3, TiO_2 and P_2O_5 plots. They all have silica contents ranging between 47.6-50.4 wt%, indicating a typical basic magma. It is also worth noting the very low amount of K_2O relative to CaO and Na_2O, and the abundance of Fe_2O_3 and TiO_2. The gabbro plots together with the greenstones in all plots, and is therefore considered to represent a coarser version of them and will be included in the greenstone descriptions and interpretations hence forward. The dyke, which is cutting the greenstone, has a slightly different geochemistry than the greenstones, with a silica concentration of 52.5 wt%, making it barely intermediate. It also shows slightly higher CaO and lower Fe_2O_3, TiO_2 and MgO concentrations than the greenstones, more concordant with the intermediate units.

Altered greenstones

The altered greenstones show a large variation in major element geochemistry, which might reflect the particularly varied appearance observed in the field. They have a generally higher K_2O and lower MgO and CaO concentrations than the greenstones, while in the remaining plots they plot too scattered to point out any particular trends (Fig. 6.12). Four have fairly basic silica content ranging between 46.9-51.6 wt%, while samples EST_79A, EST_142, EST_179 and EST_629 have intermediate silica levels between 52.6-61.7 wt%. The higher silica level in some (especially EST_179) could be due to the higher amount of quartz recrystallization and precipitation described in the thin sections (Ch. 6.1.1; Fig. 6.5-D).

Intermediate volcanics/intrusion

The intermediate volcanic rock and the intrusion all have intermediate silica levels ranging between 55-58 wt%. The two more uncertain samples EST_41 and EST_766 are plotted in figure 6.12, together with the green sandstone sample to see the difference. They both plot together with the intermediate volcanic in all plots, and very different from the proper green sandstone (Fig. 6.12). They will therefore be treated as igneous samples in the following chapters. In addition to the higher silica content, the intermediate volcanics have slightly lower Fe_2O_3, TiO_2, MgO and CaO and higher K_2O content than the greenstones, all indicating a more intermediate composition. The intermediate intrusion generally plots slightly away from the volcanic with higher silica and alkali content and slightly lower Fe_2O_3, TiO_2, MgO and MnO, indicating either a more intermediate composition or higher degree of alteration.

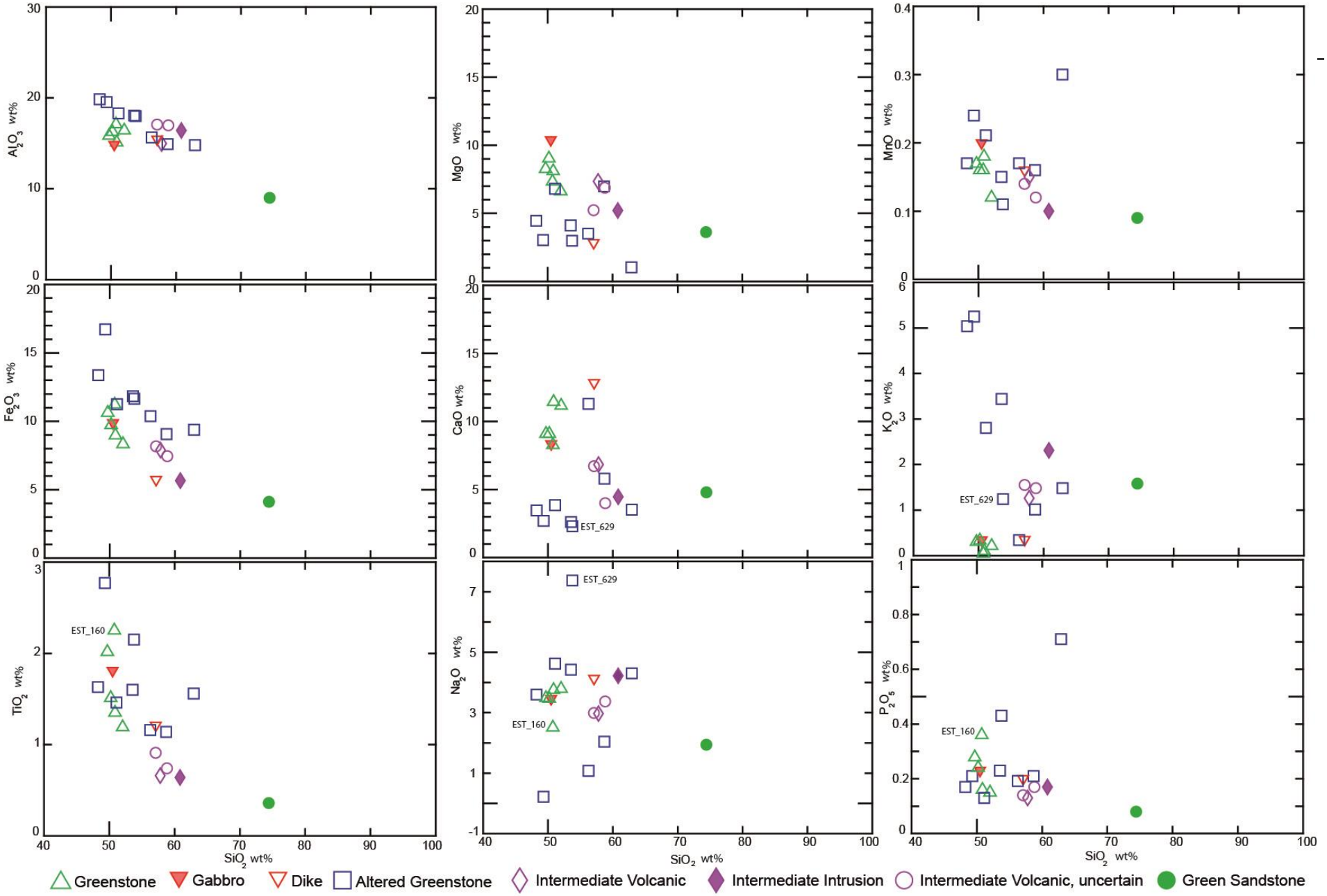

Figure 6.12: Harker diagrams with all igneous samples, showing the relationship between silica, the most abundant element in all samples, and other major elements analyzed. Note the general trend in all plots of decreasing values of the other oxide with increasing silica content. All values are listed in Table A, appendix 2

Discrimination diagrams based on major element geochemistry

The samples have been plotted in a TAS diagram, where SiO_2 is plotted on the X-axis against the alkalis (Na_2O+K_2O) on the Y-axis (LeBas etal., 1986). The alkalis are known to be highly mobile, which results in enrichment in the altered samples, placing them too high in the diagram (Rollinson, 2013). This is especially problematic in the TAS plot, where only one other parameter controls the distribution. Yet, it is still included, as it is one of the most useful plots to classify volcanic rocks (Rollinson, 2013), and because it indicates alteration in the altered greenstones, which most plots too high up (Fig. 6.13). It is also worth noting that the greenstones and the gabbro all plot in the basalt field, and the intermediate samples and the dyke all plot as andesites. The slightly higher plotting of the intermediate intrusion might indicate a higher level of alteration in this sample than in the volcanic, because it simply has a different geochemistry or because this diagram is not really meant for intrusive rocks.

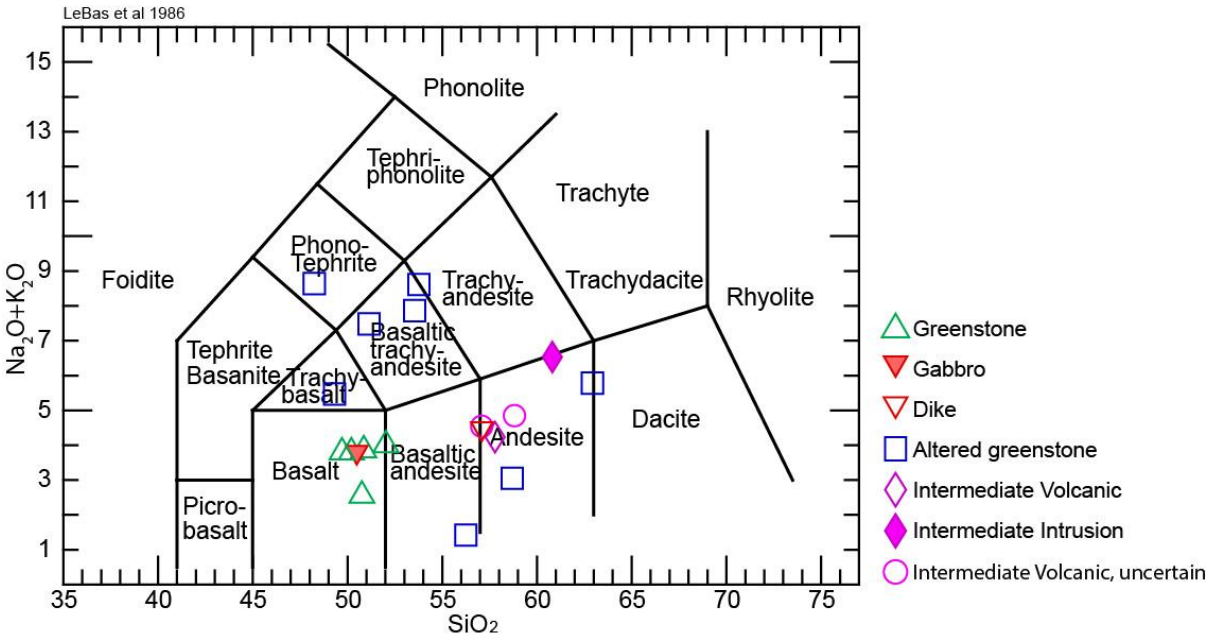

Figure 6.13: TAS diagram classifying volcanic rocks. Mainly note the greenstones and gabbro vs. the altered greenstones and the greenstones and gabbro vs. the intermediate volcanic (LeBas et al., 1986). All values are listed in Table A, appendix 2.

6.2.2 – Igneous rocks - Trace element and rare earth element (REE) geochemistry

Trace element analyses from all the igneous samples are plotted in the MORB-normalized spider diagram from Pearce (1983) (Fig. 6.14-A&B). The first four elements in this diagram, the incompatible large ion lithophile elements (LILE) Sr, K, Rb and Ba, are not shown due to their fluid mobility. When plotting the remaining elements, there are two clear trends. One incorporates all greenstones, the gabbro and the altered greenstones, which all follow the same trend (Fig. 6.14-A). From left to right, a negative slope from the high field strength element Th to Zr, followed by a small negative anomaly at the high field strength element Hf and a continued negative gentle slope from Sm to Yb. The other trend involves the intermediate volcanic and intrusion, the altered greenstone EST_179 and the dyke (Fig. 6.14-B). From left to right, enrichment of Th and Ce relative to Ta and Nb creating a characteristic U-shape, followed by a gentle negative anomaly at Hf or a plateau between Zr and Sm and a

negative slope from Sm to Yb. A typical calc-alkaline, volcanic-arc trace element assemblage from Pearce (1982) is shown in the same diagram for comparative purpose.

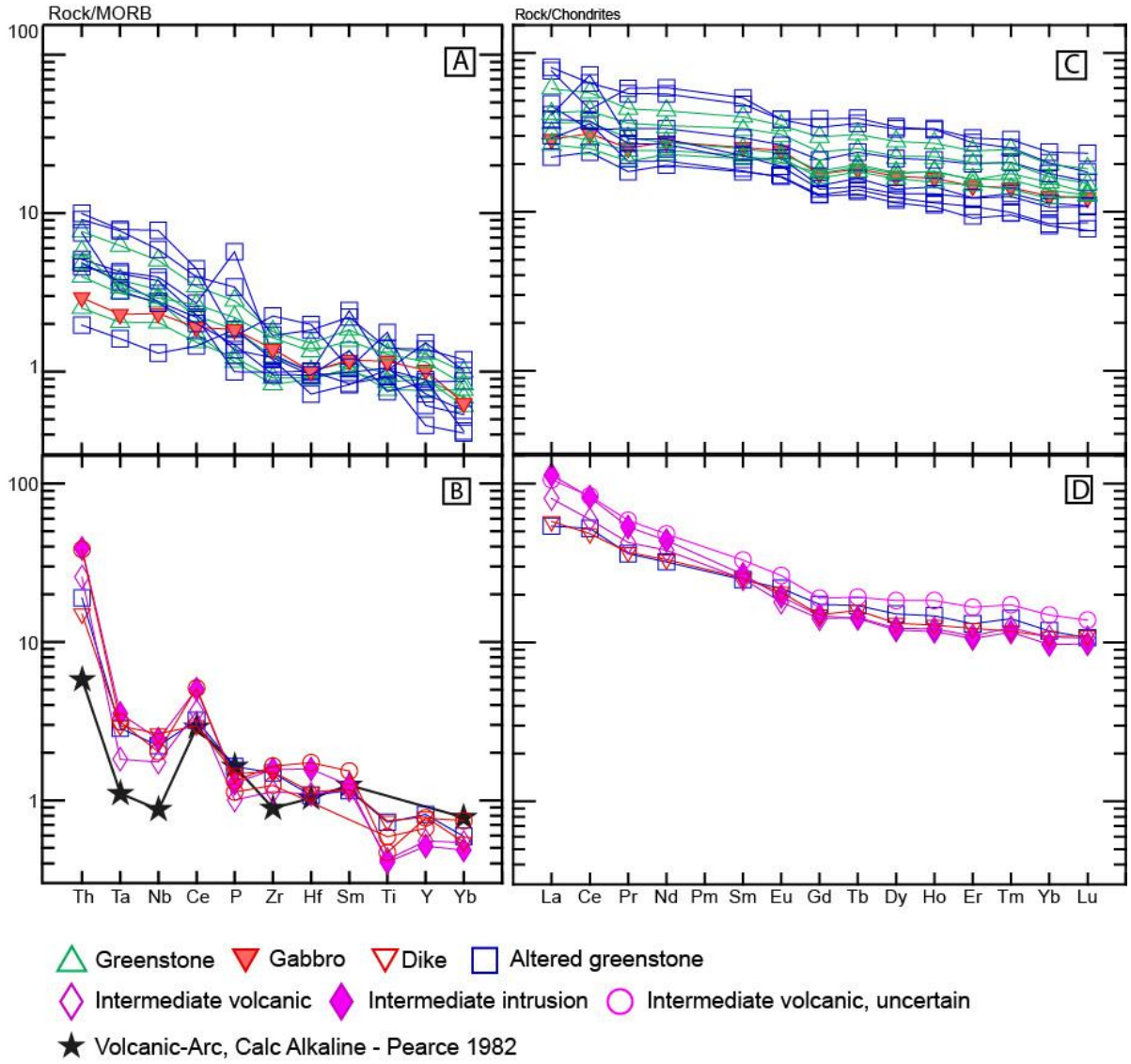

Figure 6.14: A & B) Spidergram with trace elements on the X-axis and their concentration normalized to MORB on the Y-axis. Note that the first four elements Sr, K, Rb and Ba in the original diagram are removed (Pearce, 1983). Typical calc-alkaline volcanic-arc trace element geochemistry is shown in B, values from Pearce (1982). C & D) Spidergram with REE on the X-axis and their concentration normalized to chondrites on the Y-axis (Sun and McDonough, 1989). The dyke and EST_179 is plotted together with the intermediate units in both figure 6.14-B&D. All values are listed in Tables B&C, appendix 2.

REE element analyses from the igneous samples are plotted in the chondrite normalized diagram from Sun and McDonough (1989) (Fig. 6.14-C&D). This diagram also has two trends including the same groups as in the trace elements. All greenstones, the gabbro and the altered greenstones (Fig. 6.14-C) appear to have a fairly even and gentle negative slope through all elements from La to Lu. There is some variation among the altered zones and greenstones at Ce, with both small positive and negative anomalies, resulting in a general enrichment of the light REE (LREE) relative to the heavy REE (HREE). The intermediate volcanic and intrusion, the dyke and the altered greenstone EST_179 (Fig. 6.14-D) have a much steeper negative slope from La to Gd, from where they follow the same gentle negative

slope down to Lu as the greenstones. This results in enrichment of LREE relative to the HREE, as well as an enrichment of LREE and depletion of HREE relative to the other units.

Discrimination diagrams based on trace element and REE geochemistry

Two discrimination diagrams from Pearce and Cann (1973) are used. These are mainly meant for tholeiitic basalts with CaO+MgO between 12-20%, and therefore most of the altered greenstones are not shown, as they have too low values. Only two of the intermediate volcanics have high enough CaO+MgO values, yet they are still included to indicate the difference from the greenstones.

Figure 6.15-A plots Ti, Zr and Y on a ternary plot, all elements which are relatively immobile throughout greenschist facies hydrothermal alteration (Slagstad, 2003). This diagram discriminates between island arc, ocean floor, calc-alkali and within-plate basalts, emphasizing the distinction between within-plate basalts and island-arc/sea-floor basalts. All greenstones together with gabbro and the altered greenstone EST_79A plot well within the ocean-floor basaltic field, while the intermediate volcanic and intrusion plots as calc-alcalic basalts. The dyke and the felsic type altered greenstone (EST_179) also plots as calc-alkali basalts.

Figure 6.15-B plots zirconium against titanium to discriminate between MORB/ocean-floor basalts, calc-alkali basalts and island arc tholeiites. The greenstones and the gabbro all plots fairly well within the MORB field, while the intermediate rocks plot as calc-alkali basalts together with the dyke and the two altered greenstones.

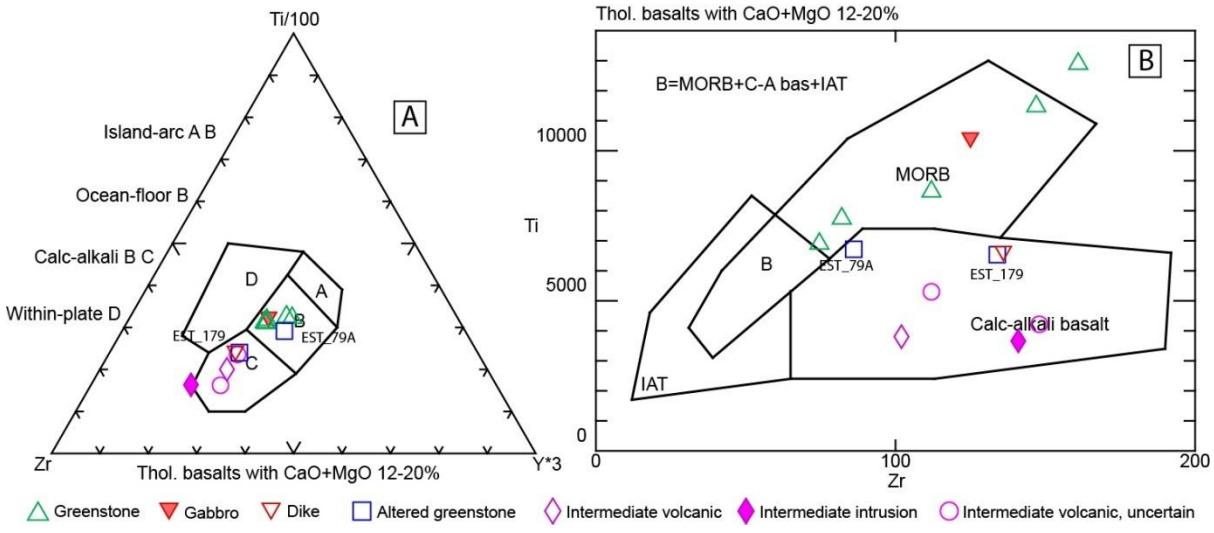

Figure 6.15: A) Ternary plot of Zr, Y and Ti discriminating between A=Island arc basalts, B=ocean-floor basalts, C=Calc-alkali basalts and D=Within plate basalts.(Pearce and Cann, 1973) B) Binary plot of Zr and Ti discriminating between mid-ocean ridge basalts (MORB), calc-alkali basalts, island-arc tholeiitic basalts (IAT) and B=all together (Pearce and Cann, 1973). All values are listed in Tables B&C, appendix 2.

The ternary discrimination diagram from Wood (1980) (Fig. 6.16) includes intermediate and silicic rocks with the mafic, and is therefore useful to present also the intermediate volcanic and intrusion. It is also especially good at recognizing volcanic-arc basalts (Rollinson, 2013). This diagram plots the immobile HFSE Hf, Ta and Th to discriminate between N-MORB (normal), E-MORB (enriched), ocean-island basalts and volcanic-arc basalts. All greenstones plot fairly clustered in the E-MORB field together with the gabbro and most altered greenstones, while the intermediate volcanic and intrusion plot clustered in the volcanic-arc field, together with the altered greenstone EST_179 and the dyke.

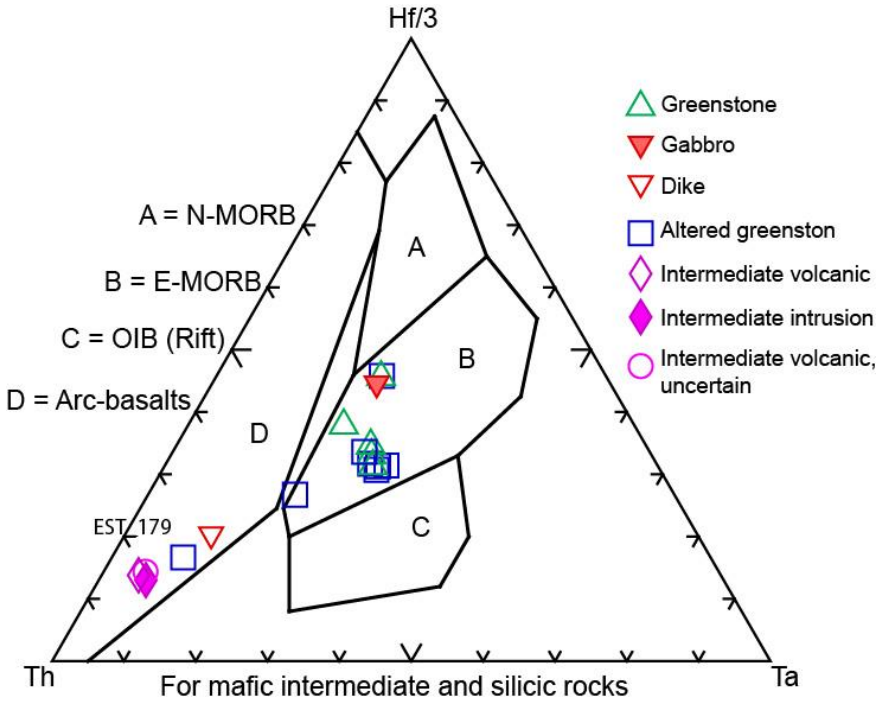

Figure 6.16: Ternary diagram plotting the HFSE Hf, Th and Ta. A=normalized mid-ocean basalt, (N-MORB) B=enriched mid-ocean basalts (E-MORB) C=ocean-island basalts (OIB) D=volcanic-arc basalts (Wood, 1980). All values are listed in Tables B&C, appendix 2.

6.2.3 – Sedimentary rocks

Major element geochemistry

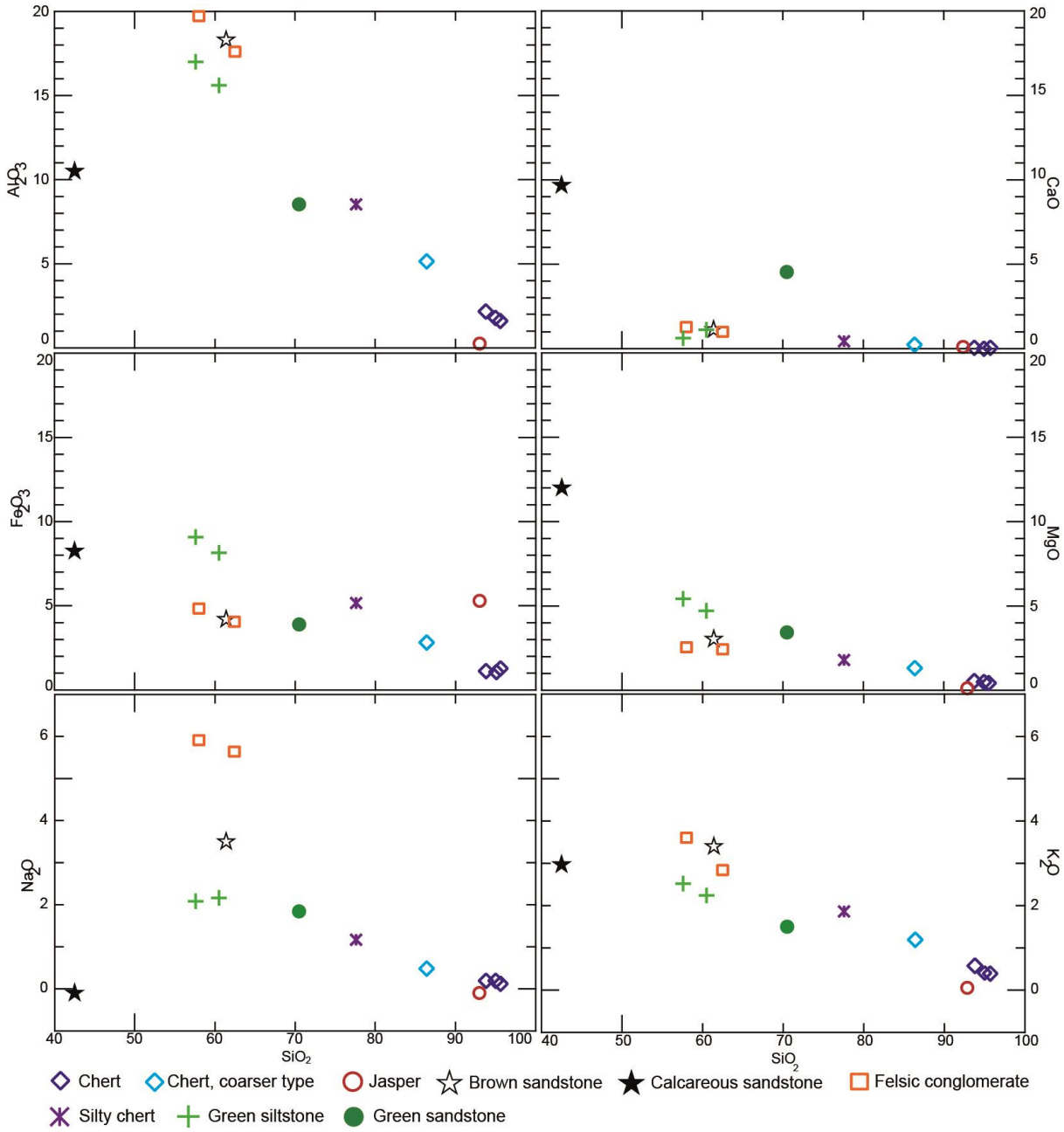

Figure 6.17: Major element oxides Al_2O, CaO, Fe_2O_3, MgO, Na_2O and K_2O plotted against SiO_2 to visualize certain trends in the sediments. All values are listed in Table A, appendix 2.

The sedimentary rocks have not been the main focus of this study, yet some plots are included to highlight a few interesting aspects. Six major element oxides have been plotted against silica to visualize the general geochemical patterns in the different units (Fig. 6.17). The chert consists almost entirely of silica, together with some aluminium and iron, due to the presence of sheet silicates described in chapter 6.1.2. The jasper analysis plots together with the chert in the lower right corner of the diagram. It is also dominated by silica, though with a relatively high concentration of iron-oxides, observed as opaque phases in thin sections (Fig. 6.6-B). The slightly coarser layer described in the chert has a slightly lower concentration of

silica and more aluminium and iron, which also reflects the higher amount of sheet silicates (Ch. 6.1.2). The two sandstone layers in the ribbon-chert both show very different chemistry than the surrounding ribbon-chert. The brown sandstone correlates with the felsic conglomerate in all plots, except the conglomerate has a higher Na_2O content. Note also the low calcium content, which is a feature of all samples except for the calcareous and the green sandstone. The calcareous sandstone is characterized by high calcium content, as well as iron and magnesium, and comparably low silica content. One very interesting aspect is the almost linear trend from chert through silty chert into green siltstone moving left and upwards in all plots, supporting the transitional development observed in the field (Ch. 4.3.2 & 4.3.3). The green sandstone has fairly high silica content and no significant variations in the other element concentrations, which correlates fairly well with the observed mineralogy (Ch. 6.1.4; Fig. 6.10-A).

REE geochemistry

The REE are insoluble and therefore present in very low concentrations in river- and seawater. Thus, they will mainly be detrital in sediments and are therefore a good indicator of provenance. Although they can be mobilized during weathering, studies show they are still most likely to precipitate in the same area (Nesbit, 1979; Rollinson, 2013). The REE concentrations for all samples except the sandstones have been normalized to North American Shale Composite (NASC) values from Gromet et al. (1984; Fig. 6.18), as studies show that REE are mostly contained in the clay fraction (Cullers et al., 1987; Rollinson, 2013). The felsic conglomerate data have also been plotted, but should not be given too much importance due to the heterogeneity of the unit. In the NASC-normalized diagram (Fig. 6.18) there is a general trend of upward increasing concentration in REE's from jasper, through chert and into silty chert and green siltstone, which plots mainly together. Jasper is below detection limit at Gd, Y, Tb, Dy, Ho, Tm, Yb and Lu, and the two lower chert samples are below detection at Lu. The upper chert sample is more enriched in REE, and was described in the field as slightly darker than the others. There is no clear trend in HREE versus LREE in any units except the conglomerate, which is enriched in the lighter fraction, with a negative anomaly at Eu contrasting all other samples. All samples above detection limit seem to increase from Yb to Lu.

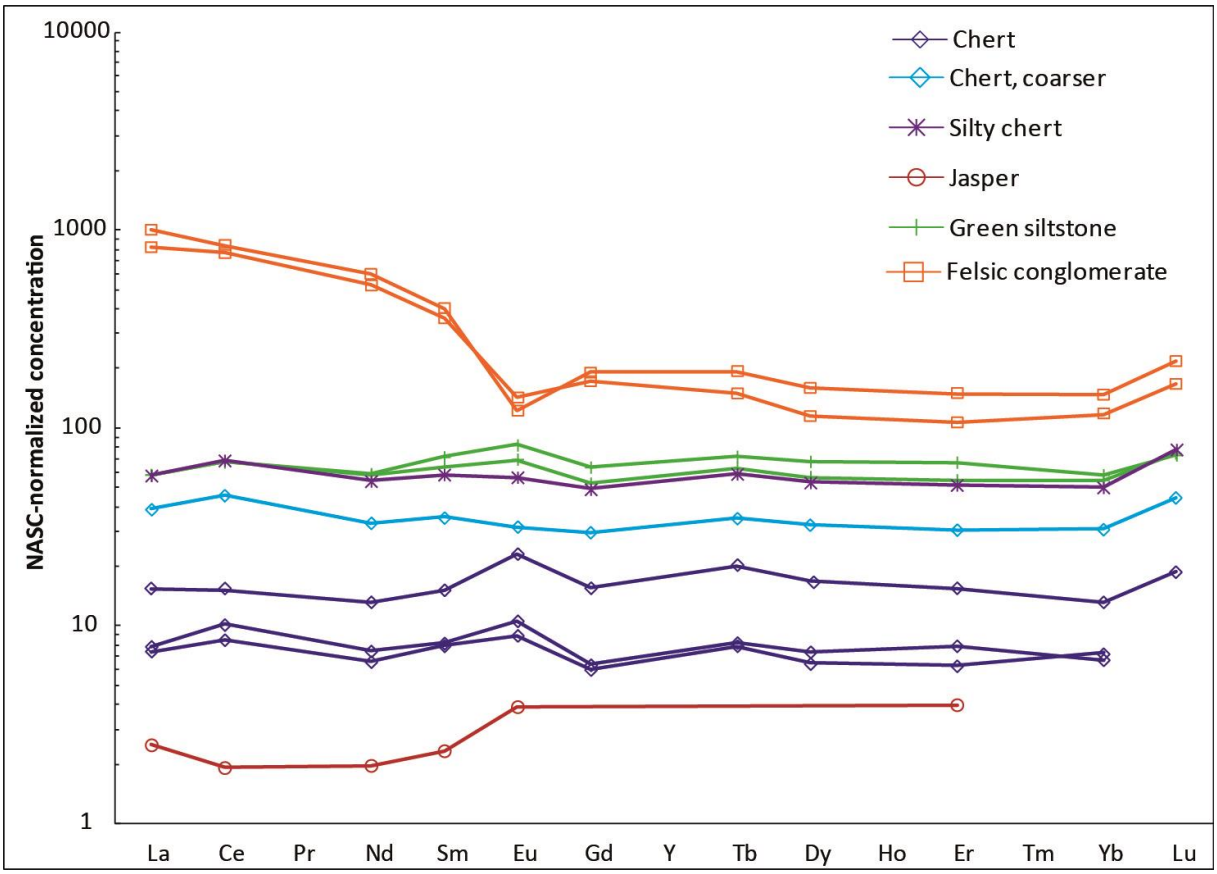

Figure 6.18: REE concentrations for all silty sized sediments and the conglomerate, normalized to NASC values from Gromet et al. (1984). All values are listed in Table C, appendix 2.

Discrimination diagrams for chert geochemistry

Chemistry of marine sediments is controlled by composition of the included particular material, components absorbed from the seawater and the diagenetic fractionation (Murray et al., 1992; Murray, 1994). The diagenetic factor is exceptionally strong in chert, where SiO_2 are strongly enhanced and acts as a dilutant during burial and diagenesis. Therefore one has to investigate the stable major elements aluminum, iron, titanium and the REEs, which remain immobile during diagenesis, to be able to characterize the depositional environment.

Major elements and REE concentrations in chert are plotted according to Murray (1994) (Fig. 6.19). The slightly coarser layer in the chert is plotted as well, as figures 6.17 and 6.18 indicate they have fairly similar chemistry to the chert. Three selected major element ratios are plotted in figure 6.19-A, B & C. In all plots the four samples are fairly clustered, with some variation in the coarser layer. They all plot inside the area typical for continental margin, though also inside the field of pelagic sedimentation in figure 6.19-C, though this diagram has poor environmental resolution (Murray, 1994).

Cerium tends to be non-depleted in terrigenous sources and depleted in seawater, and variations have been observed relative to the neighbouring REEs La, Pr and Nd, which have therefore been most commonly used to indicate depositional environment of chert. The La/Ce ratios are plotted against $Al_2O_3/Al_2O_3+Fe_2O_3$ in figure 6.19-D to improve the environmental

resolution according to Murray (1994). The samples plot just barely inside the field of continental margin, with one outside, but not significantly so (Fig. 6.19-D).

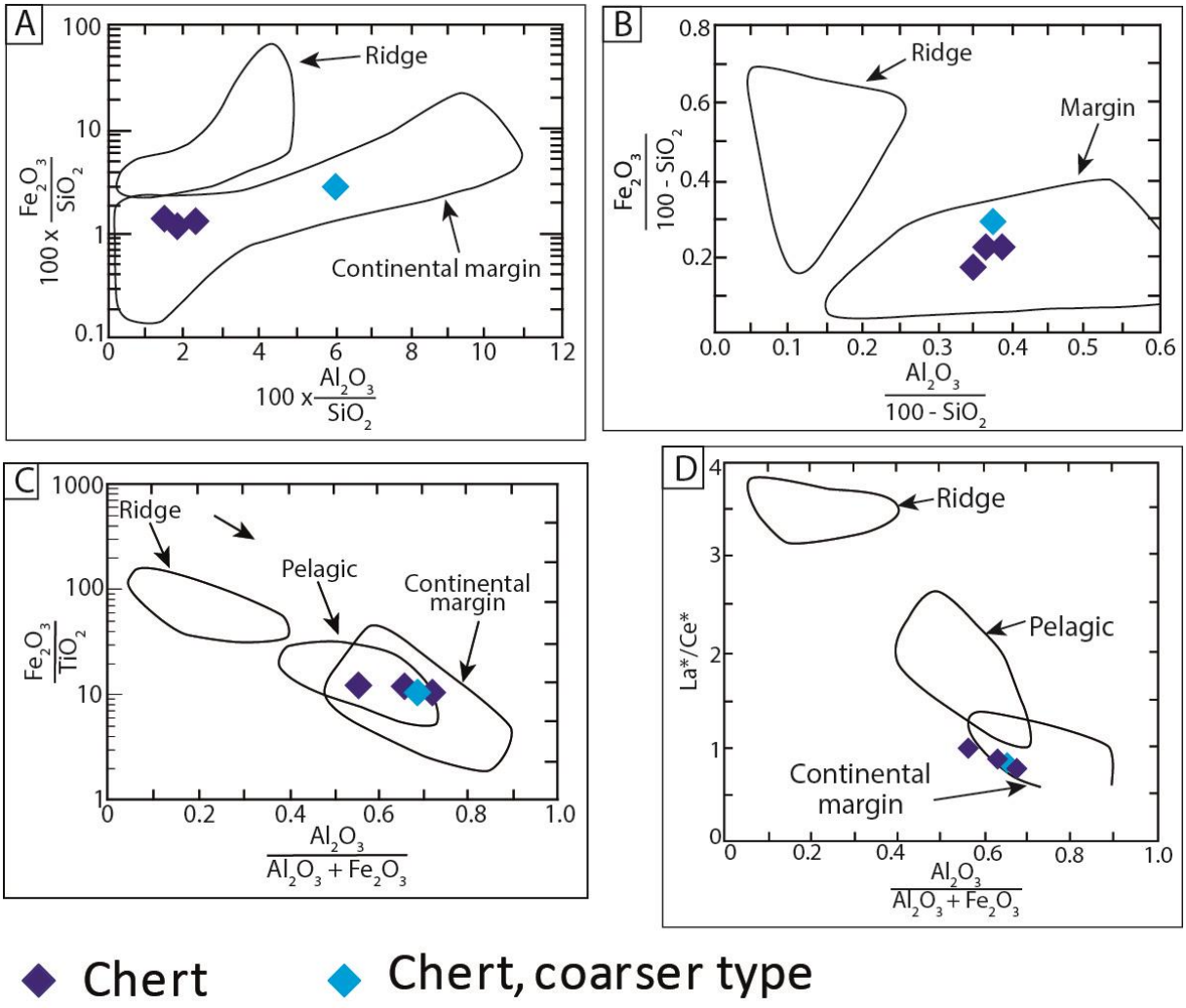

Figure 6.19 All plots are developed according to Murray (1994). A) Fe_2O_3 plotted against Al_2O_3, both normalized to SiO_2 to limit the effect of diagenetic dilution. All samples plot in the continental margin field. Note that the coarser layer in the chert plots further away from the chert in this plot than in any of the others, due to the higher silica concentration in the normal chert (Fig. 6.17) B) Fe_2O_3 plotted against Al_2O_3, both normalized to 100-SiO_2 to consider their contribution to the non-siliceous fraction of the chert. All samples plot in the continental margin field. C) Fe_2O_3/TiO_2 ratio plotted against Al_2O_3/ total Al_2O_3+ Fe_2O_3 ratio to indicate the influence of the terrigenous (Al_2O_3 and TiO_2) and metalliferous (Fe_2O_3) end-members. All samples plot within both the pelagic and the continental margin field. Note the poor environmental resolution in the division of the two fields. D) La/Ce ratio, normalized to NASC, to indicate the degree of terrigenous input. To improve the environmental resolution the ratio is plotted against the Al_2O_3/ total Al_2O_3+ Fe_2O_3 ratio. Three samples plot within the continental margin field, and one just outside. *=NASC-normalized All values are listed in Tables A&C, appendix 2.

Ce-anomalies can also be useful to discriminate between depositional environments, and are therefore calculated for the chert samples according to Murray et al. (1992), but with NASC normalizing values from Gromet et al. (1984). Results are presented in table 6.2.

Table 6.2: Ce-anomalies for the chert samples and the coarser chert. Ce-anomalies calculated according to Murray et al, 1992: Ce_{anom}=Ce*/(La*+Nd*/2) where *=NASC-normalized.

	Chert	Chert	Chert	Chert, coarser
Ce-anomaly	1.324109	1.06357	1.208371	1.275693

Chapter 7 – Geochronology

During fieldwork four samples were taken for geochronology, in an attempt to get a better age constraint on the area (Fig. 7.1). As most of the magmatic rocks in the area are greenstone-related, they were not considered to be suitable for dating. Two felsic looking magmatic rocks were sampled, as well as a magmatic clast from the younger sandstone and the sandstone itself. The zircons in the samples were analysed through U-Pb radiometric dating with LA-ICP-MS (Ch. 3.3; 3.4). In the following, the results are described for each sample separately.

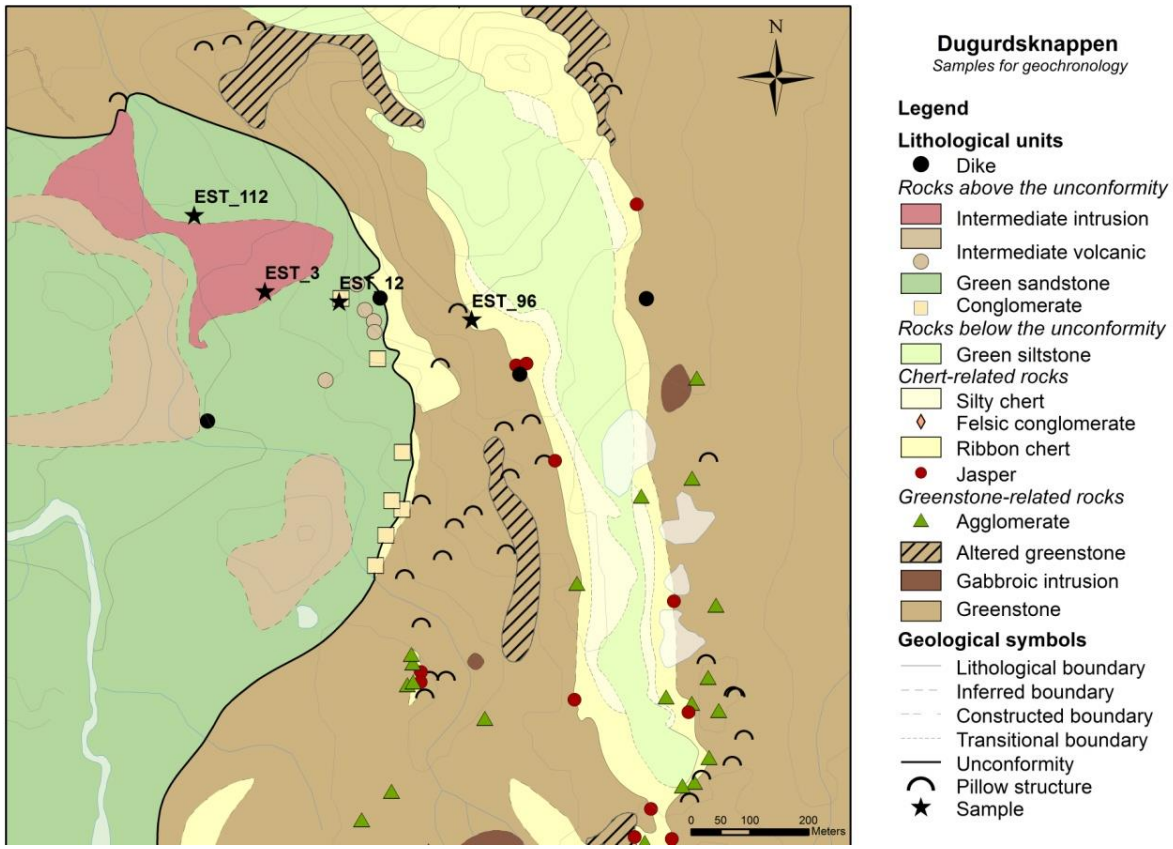

Figure 7.1: Section from the lithological map of Dugurdsknappen, indicating the position of the four different samples taken for geochronology.

7.1 – Samples EST_3 and EST_96

Sample EST_3 was taken from the intermediate intrusion (Fig. 7.1). In the field, this unit has a more felsic appearance than the more common greenstones and it was interpreted as a possibly intrusive rock (Fig. 7.2-A). However, geochemically the sample is not as felsic as first thought and the thin sections also suggests that it is more likely to represent an extrusive rock (Ch. 6.1.1; 6.2.1). After separating the sample it turned out not to hold any zircons, and is therefore not considered further.

Sample EST_96 comes from a layer in the border zone between greenstone and ribbon-chert. It appears in the field as a more felsic type volcanic rock (Fig. 7.2-B) and was sampled in an attempt to date the transition between basalt volcanism and sediment deposition. No geochemical analysis was done, but the thin sections confirm a different mineralogy than the

normal basalts, consisting mainly of quartz, feldspar and biotite. However, no zircons were found in the sample after mineral separation, and will therefore also not be considered any further in this study.

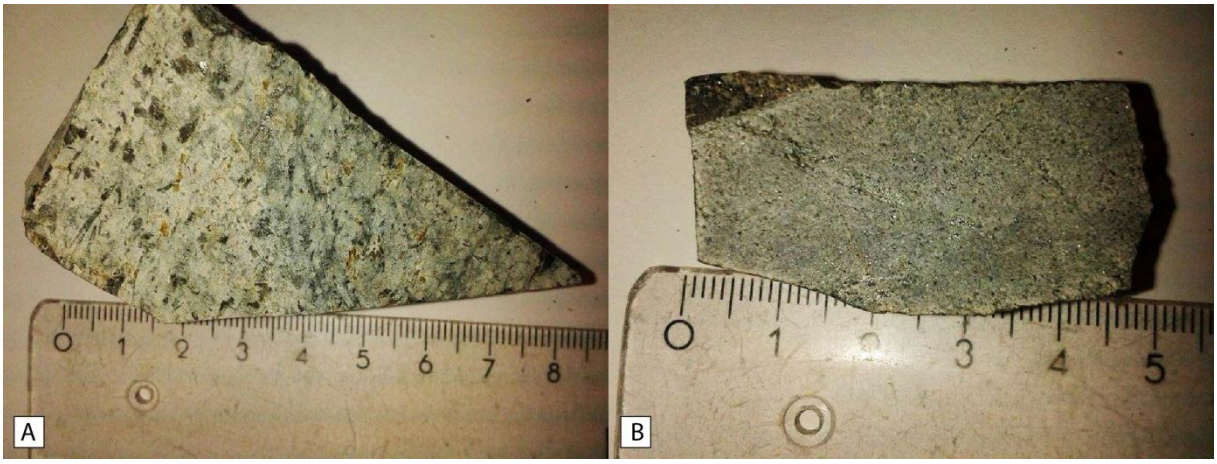

Figure 7.2: A) Hand sample of EST_3. Note the light felsic looking colour of the fine-grained matrix with large dark biotite grains. B) Hand sample of EST_96. Note the fine-grained texture and the light colour

7.2 – Sample EST_12

This sample is a light coloured coarse-grained tonalitic/trondhjemittic clast, rounded and about the size of a mandarin. It is taken from the lower conglomeratic part of the green sandstone (Fig. 7.1). Unfortunately, no picture was taken of this particular clast, and no geochemical analysis was done due to the heavy weathering of the clast. Figure 7.3-A shows a similar type of clast from the same part of the sandstone. The clast was heavily weathered and was crushed easily by hand.

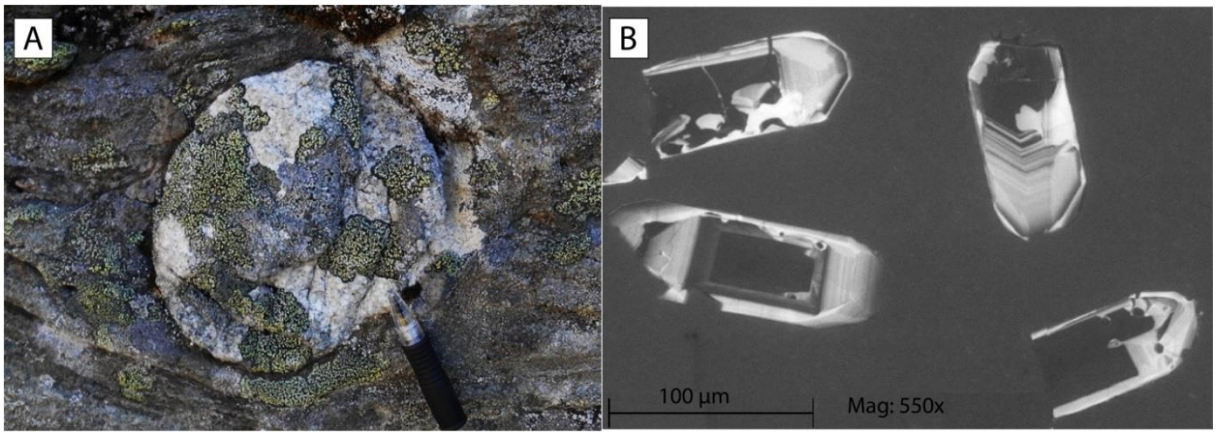

Figure 7.3: A) Granitic type clast taken from the green sandstone at a slightly different location than EST_12, but with the same characteristic as the one analysed. This clast type is fairly common in the green sandstone. B) CL-images of four examples of typical zircon grains from sample EST_12. Note the dark cores and light rims with zoning, as well as the continuation in shape from core to rim indicating magmatic growth and not metamorphic. Some fractures and inclusions can also be seen.

In this sample 136 zircons were found and sorted into three size fractions. The grains have a clear to light yellow colour and are relatively large, up to about 150µm, with 42 grains in the largest fraction. Unfortunately, the zircons have abundant fractures, possibly due to the heavy weathering of the clast, but the large size of the grains still makes analyses possible.

Catholdoluminescence imaging (Fig. 7.3-B) reveals that most of the zircons have a very dark core surrounded by a relatively broad and light coloured rim with varied zoning. They also show many inclusions in addition to the fractures.

Only zircons from the largest size fraction were analysed, with 25 analyses on 23 different grains. Both cores and rims were analysed, but on the same zircon only in two grains. In total 15 analyses were done in the cores and 10 in the rims. The black colour of the cores is due to very high uranium content, which makes it difficult to make good analyses. Of the 25 analyses, nine had too high $^{206}Pb/^{238}U$ and $^{207}Pb/^{235}U$ estimates due to the high uranium content causing a too strong signal. These were filtered out, together with three analyses that were more than 10% discordant. This results in total eight analyses from the rims of the zircons and four from the cores. The analyses showed that the ages from core and rim overlap, so they were plotted together in one concordia plot (Fig. 7.4), which yields an age for intrusion at 485 ± 4 Ma.

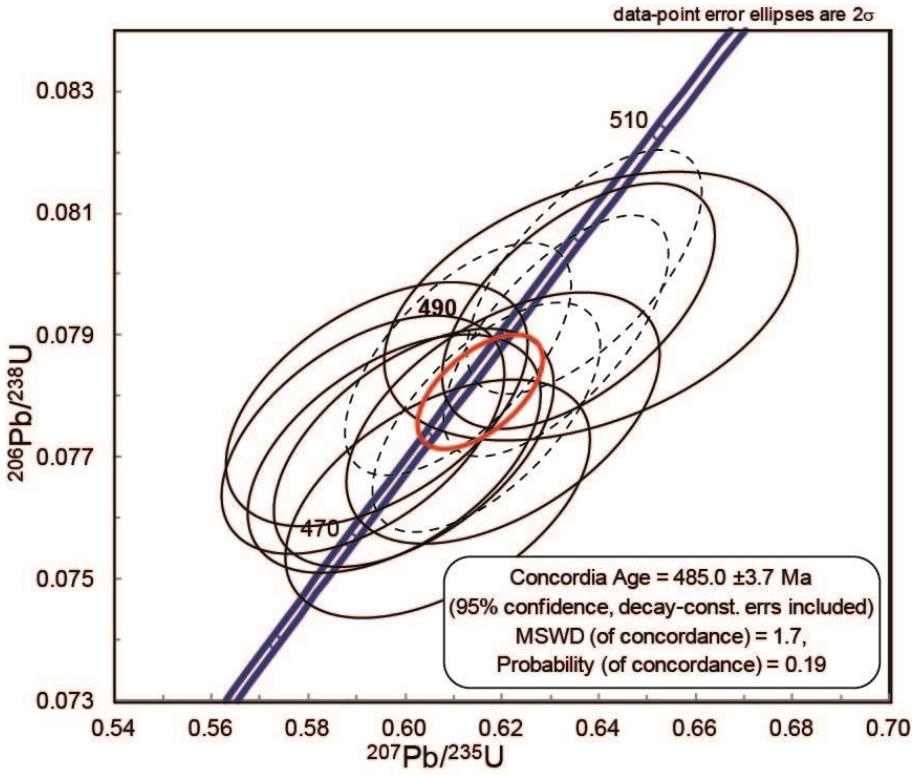

Figure 7.4: Concordia plot for all twelve analyses, dashed lines are from the cores and solid from the rims. Since they overlap as one population, they are plotted together, yielding one age for intrusion at 485 ± 4. The age is given with a 95% confidence, which was the closest possible to 2σ. All analyses are listed in Table D, appendix 3.

7.3 – Sample EST_112

This sample is taken from the green sandstone unit for detrital zircon analysis (Fig. 7.1). There is no geochemical analysis of this sample, although there is some of an equivalent sample, presented in chapter 6.2.3. The thin section shows a coarse-grained and slightly deformed sandstone, dominated by quartz and containing biotite, calcite and chlorite as well as some accessory epidote and plagioclase (Fig. 6.10-A). The sandstone is described in more detail in chapter 4.3.4.

In this sample 146 zircons were picked. They were sorted in two size fractions, medium and large, were the medium fraction was the largest with 120 grains. The zircons are clear, relatively well preserved and up to 200µm long, and were mainly euhedral suggesting a magmatic origin. The CL images (Fig. 7.5) reveal a mixture of zoned and unzoned grains, though mostly zoned, as well as some grains with a patchy appearance and a few grains with core/rim structure. Some inclusions and a few fractures are observed, mainly in the medium-size fraction.

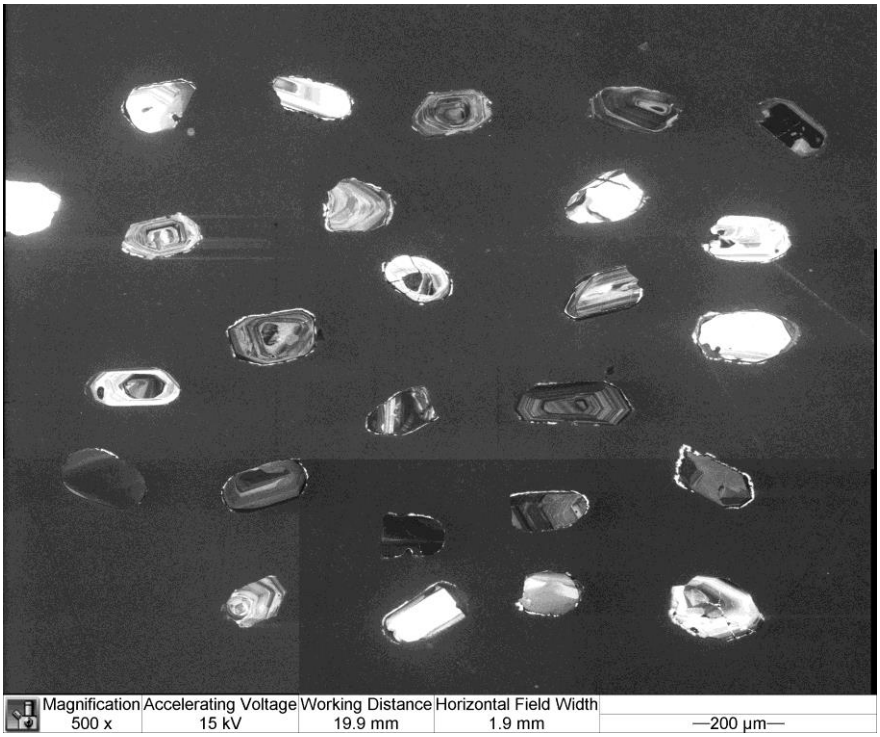

Figure 7.5: Cl-image of the entire largest size fraction of EST_112, where all 26 grains were analysed. Note the varying degree of zoning as well as the grains with no zoning or patchy appearance.

In total 100 analyses were performed on 100 grains, 26 grains in the large size fraction and 74 in the medium. Only ten analyses show >10% discordance, while the remaining 90 are less than 10% discordant. Of these, there seem to be three main age groups, with hiatuses in between (Fig. 7.6-A): 1) the smallest and oldest group provided three analyses of Proterozoic age, with peaks at ~2120 and ~2480 Ma, though no groups of significant number, as well as two Archean grains (Fig. 7.6-B); 2) the largest group includes ages between ~900-2000 Ma, with a big peak at 1100 Ma and smaller ones at ~900 and 1740 Ma, and a major hiatus at ~1300 Ma (Fig. 7.6-C); 3) the youngest group is ~420-500 Ma, with peaks of significant populations (minimum 3 grains) at around 430, 445, 460 and 490 Ma, and hiatuses between ~430-440, 465-470 and at 480 Ma (Fig. 7.6-D). The youngest population is estimated from the youngest significant peak comprising five overlapping concordant grains, according to recommendations of Dickinson and Gehrels (2009). This group has a concordia age of 427 ± 3 Ma (Fig. 7.6-E), which represents a conservative estimate of the maximum depositional age (Dickinson & Gehrels, 2009).

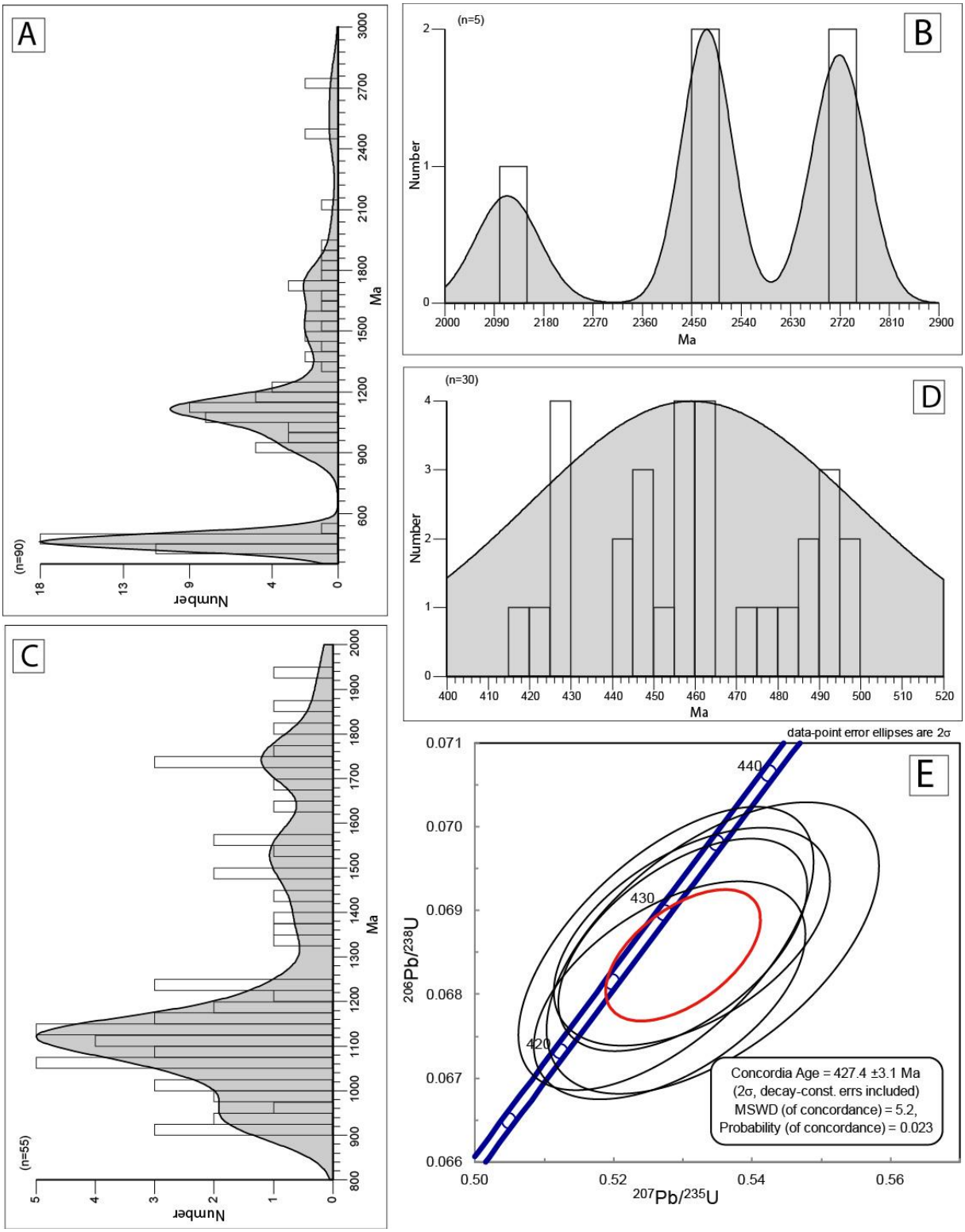

Figure 7.6: A) Histogram of all analyses from ~400-3000 Ma. Note the two major peaks in the Cambro-Silurian and in the Late Mesoproterozoic to Early Neoproterozoic. B) Histogram from the oldest age group, including the two Archean grains. Note that no peaks represent episodes with significant number of grains. C) Histogram from the middle age group with one particularly significant peak at 1100 Ma and a smaller peak at ~1700, both groups with significant number of grains. Also note the hiatus at 1300 Ma. D) Histogram from the youngest age group, incorporating three smaller sections with peaks at about 430, 445, 460 and 490Ma. Note the hiatuses between 430-440Ma and at 480Ma. E) Concordia plot for the youngest overlapping population in the youngest age group yields concordia age of 427 ± 3 Ma, which indicates the maximum depositional age for the sandstone. All analyses are listed in Table E, appendix 3.

Chapter 8 – Discussion

In the following, several aspects of the results will be discussed. Firstly, the tectonic setting and depositional environment of the different units will be elaborated on, followed by a discussion on the structural features and evolution of the area, all related to the previously described results. A short chapter summarizing the tectonic evolution for the study area based on the prior discussions will then be presented, with interpretive illustrations. This will be followed by a closing discussion attempting to see the Dugurdsknappen area in a larger perspective related to the Caledonian Evolution, including a discussion of the internal correlations within the Støren Nappe and related geology.

8.1 – Tectonic setting and depositional environment

8.1.1 – Magmatism and deposition in a rift-related basin

Basaltic volcanism

The silica levels and major element geochemistry in the greenstones and gabbro, as well as most of the altered greenstones, are that of tholeiitic basaltic magmas (Fig. 6.12; Fig. 6.13; Winter, 2010). According to discrimination diagrams from Pearce and Cann (1973) all greenstones and the gabbro plot as ocean-floor or MORB basalts (Fig. 6.15). This correlates with the observed mineralogy and texture in the greenstone thin sections, comprising a generally fine-grained texture without phenocrysts, as well as the field observations of pillow structures. The discrimination diagram from Wood (1980) defines them all as enriched MORB (E-MORB) basalts, including the altered versions (Fig. 6.16). The REE pattern of the greenstones, gabbro and most altered greenstones has a gentle negative slope showing enrichment in LREE relative to the HREE (Fig. 6.14-C). This is also indicative of E-type MORBs, and is suggestive of spreading ridge environment, though not exclusively (Winter, 2010). When comparing the trace elements from the Dugurdsknappen greenstones to diagrams of trace elements form modern examples of basalts from destructive plate margins, they seem to correlate closest with diagrams of ocean island basalt (OIB) (Pearce, 1982; Wilson, 1989, p.179), while the REE data are similar to the gentle and even negative curve described for marginal basin basalts according to Wilson (1989, p.236). Geochemistry, mineralogy and both micro- and macro-textures seem to be indicative of enriched tholeiitic magma from a spreading ridge origin, though tectonic setting is more uncertain.

The role of alteration and metamorphism

There has been some uncertainty to whether the altered greenstones are the result of a different magma source, or due to secondary alteration. Alteration and metamorphism leads to mobilization of soluble mobile elements like Na, K, Sr, Rb and Ba, often loss of Ca and Si and gain of Mg and Na, with enrichment of iron-titanium oxides and production of low-T hydrous minerals, particularly during hydrothermal alteration (Winter, 2010). This alteration is seen in the altered greenstones, which show general enrichment of alkalis and depletion of CaO (Fig. 6.12). This can be caused by spilitization (albitization of plagioclase; Gale and Pearce, 1982), which is seen particularly well in sample EST_629, both in thin section (Ch.

6.1.1; Fig. 6.5-B) and in the Harker diagrams (Fig. 6.12). Spilitization can also cause depletion of K (Gale and Pearce, 1982), and as the greenstones show almost no K_2O content, this might reflect higher albite levels in the plagioclase content than for completely unaltered basalts. However, many of the altered greenstones have fairly high K-concentration relative to the greenstones. This can be explained by the abundance of biotite porphyroblasts in most of the altered greenstones, which requires high K-concentrations to develop (Nesse, 2013). Both the altered and the normal greenstones show mineralogy typical for altered basalts, with low-T hydrous phases like chlorite, epidote and calcite substituting for the original pyroxenes, as well as abundance of iron-titanium-oxides like rutile, titanite, heamatite and leucoxene. Zoisite, which is abundant in the highly foliated altered greenstones from the eastern side, is commonly found in medium-grade metamorphic rocks (Nesse, 2013). This difference in samples from the eastern and the western sides is however only observed in the thin sections, and not in the geochemistry. The mineralogical association indicates peak deformation under greenschist-facies metamorphic conditions (Winter, 2010). Alteration is common in ancient greenstones and has been described from adjacent greenstone units in the Støren Nappe (Gale and Pearce, 1982; Walsh, 1983). Ocean floor metamorphism in general has been described in the Upper Allochthon (Bryhni and Andréasson, 1985) and the abundant effect of hydrothermal alteration in the Støren Nappe specifically in more recent studies (Slagstad, 2003). Slagstad (2003) also points out the correlation between abundant hydrothermal alteration and formation in the proximity of a spreading ridge. Hydrothermal alteration, devitrification and later low-grade metamorphism have probably played important parts in altering the greenstones. When considering the large variation in geochemistry, particularly in mobile elements, and the general mineral assemblage together with the relatively unsystematic geographical distribution of the secondary alteration, hydrothermal and later metamorphic processes are considered the most likely reason for the altered appearance, rather than formation from different magmatic sources.

Ribbon-chert and siltstone deposition succeeding rift-magmatism

Chert is a microcrystalline rock mainly composed of silica, usually recrystallized from opal-A (Pufahl, 2010), and originating from hydrothermal, detrital, biogenic or hydrogenous sources. The most common source is biogenic, which for Palaeozoic cherts implies either sponge spicules or radiolarians (Fig. 8.1), as diatoms did not evolve until late-Cretaceous. Radiolarians did not evolve until the Cambrian and are not commonly abundant until the Ordovician, when they pushed sponges into more shallow-water depositional environments (Pufahl, 2010). Signs of hydrothermal activity in proximity of the chert have already been mentioned, and could be a source for the chert, but it seems unlikely this would cause such thick deposits as seen at Dugurdsknappen. Some authors have pointed out, that the seawater in Palaeozoic time probably was much more silica-saturated than in present-day oceans, due to the absence of silica-absorbing diatoms (Grenne and Slack, 2003). However, the silica cannot precipitate on its own, but needs a site of nucleation. For the bedded jaspers of the Løkken ophiolite the Fe-oxides from hydrothermal plumes have been suggested as nucleation site (Grenne and Slack, 2003), which is very likely the case for the jasper accumulations found in the basalt-chert interface in the area. Yet, this is not a likely source for the ribbon-

chert itself, as the iron content is too low and the colour too light (Jones and Murchey, 1986), thus a biogenic (radiolarian) and/or detrital source or nucleation site is more probable. However, such large chert-deposits as at Dugurdsknappen would be dependent on a very rapid radiolarian production, as more than 98% of unstable opal will dissolve prior to burial (Jones and Murchay, 1986). Ordovician to lower-Cretaceous radiolarian cherts have therefore often been interpreted to have formed in nutritious waters with upwelling, conditions which can be linked to specific climatic conditions, but can also be caused by several tectonic environments, like with local upwelling in marginal basins in modern oceans (Jones and Murchay, 1986). Unfortunately, chert lithifies through silica diagenesis, which is a destructive process for radiolarians, and together with later metamorphic quartz-recrystallization commonly destroys all original radiolarian features (Jones and Murchey, 1986). Thus radiolarian might have been the source for the Dugurdsknappen cherts, even though none are observed in the present samples.

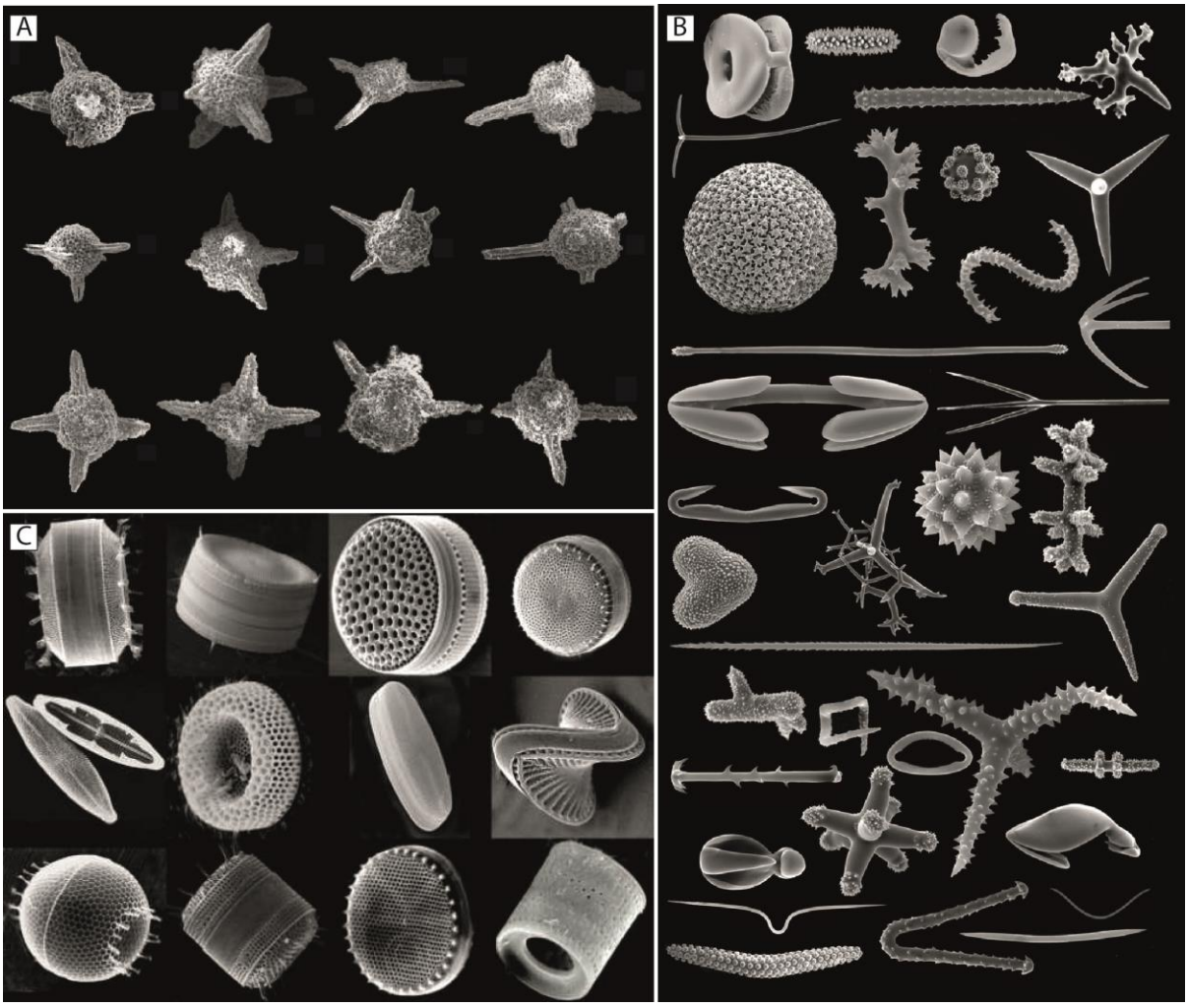

Figure 8.1: A) Assortment of Palaeozoic radiolarians. Image from Okay, Noble and Tekin (2011). B) Different types of sponge spicules. Image from Van Soest et al., 2012. C) Cenozoic diatoms. Image from: https://paleonerdish.wordpress.com/2013/06/10/an-introduction-to-diatoms/ (accessed 19.05.16)

According to the discrimination diagrams from Murray (1994, Fig. 6.19), the chert was most likely deposited in a continental margin environment, which includes back-arc basins, marginal seas, epicontinental seas and continental shelves. In a study from Armstrong et al.

(1999), they use REE geochemistry of chert from the Deap Sea Drilling Project (DSDP) and Ocean Drilling Program (ODP) compiled by Murray et al. (1992), and compares it with REE geochemistry of Ordovician chert from the Ballantrae Ophioite and Leadhills Imbricate Zone in the southern Scottish Caledonides. They conclude that the Ballantrae Ophiolite cherts were formed in a large marginal ocean basin close to the margin, while the Leadhills Imbricate Zone chert formed in the proximal part of a marginal basin closer to the continental margin than cherts of the Ballantrae Ophiolite (Armstrong et al., 1999). When comparing the NASC-normalize REE-geochemistry of the chert from Dugurdsknappen (Fig. 6.18) to their data, it correlates best to that of the Leadhills Imbricate Zone cherts, with similar relatively flat curve without enrichment in either LREE or HREE, and only a slight positive Ce-anomaly. This is supported by a study of chert from the Franciscan complex in California (Murray et al., 1991) and from the DSDP and ODP data compiled by Murray et al. (1992). They suggest that Ce-anomalies for spreading ridges are extremely large (Ce_{anom}=0.29 (Murray et al., 1991) or Ce<<1 (Murray et al., 1992)) due to Ce-scavenging by Mn and Fe from hydrothermal plumes, whereas open oceans have more mediocre anomalies (Ce_{anom}=0.55 (Murray et al., 1991) or Ce=0.19-0.61 (Murray et al., 1992)) and continental margin settings have almost no anomaly (Ce_{anom}=0.9-1.3 (Murray et al., 1991) or Ce=c. 1 (Murray et al., 1992)) as the ocean is more Ce-enriched. Ce-anomaly values from the chert at Dugurdsknappen range between 1.06 and 1.32, which correlates best with the continental margin setting. However, it is important to note that the sea-water chemistry has changed through times, and as the Ce-scavenging from the sea-water is dependent on available oxygen, some care should be shown when interpreting these values.

The presence of the sandstone layers and the felsic conglomerate within the ribbon-chert also supports an interpretation of relative closeness to a terrestrial source where sediments could be derived. Chert is commonly associated with ophiolites related to spreading ridge environments, both in the Caledonides and in other ancient successions (Moores, 1982; Jones and Murchey, 1986; Aitchison, 1998; Grenne and Slack, 2003). If one assumes the transition from basaltic volcanism to deposition of ribbon-chert was a continuous one, this would support the interpretation that the greenstones were initially formed at a spreading ridge in a marginal basin, rather than at a major mid-ocean spreading ridge. The mentioned connection between jaspers in the Løkken ophiolite and hydrothermal sources and the presence of jaspers at the boundary between ribbon-chert and the greenstones therefore supports the gradual transition, as well as suggests the ribbon-chert was deposited in closeness to a spreading ridge where hydrothermal processes were still active. The presence of chert also in smaller pockets westward in the greenstone suggests there were several episodes of quiescence during magmatism, where both chert and jasper deposition occurred, indicating a constant high silica-saturation in the overlying ocean.

The linear trend seen in both the major elements and in the REE from the sedimentary rocks suggests a gradual transition from ribbon-chert through silty chert into green siltstone, which was also suggested based on field observations. This is not an uncommon phenomenon, and is seen both in ophiolitic and continental margin associations (Jones and Murchay, 1986), and it gives a certain indication of the relative amounts of terrigenous input present, suggesting a

gradual increase of continental input to the basin. An increase in terrigenous detrital input would also dilute the silica and hinder chert deposition (Jones and Murray, 1986). This could have been caused by migration of the basin closer to a subduction zone itself and/or a general topographic increase in the surrounding potential source area for detrital material (e.g. an island arc or a continent). It could also be caused by a change to silica-depleted seawater, as an effect of changes in the basin geometry.

8.1.2 – Deposition in a shallow marine basin

A thorough study of the possible depositional environment for the green sandstone has not been a main topic of this study, but a few observations are made. The green sandstone has mineralogy and texture indicating it's moderately immature and fairly poorly sorted, especially due to the abundant clast-content, which both indicate a relatively proximal position (Tucker, 2001; Boggs, 2011). The sandstone seems to be part of what Rohr-Torp (1972; 1974) categorized as a greywacke. Greywackes typically show a fine-grained matrix of abundant chlorite, sericite and silt-sized quartz and feldspar, either of primary or secondary origin, and a generally immature nature similar to the green sandstone (Tucker, 2001). There is also abundant cross-bedding and occurrences of trough-cross bedding, which both suggests deposition above wave-base (Boggs, 2011). Based on the level of maturity and presence of laterally extensive parallel bedding, lamination, abundant cross-bedding and occasional trough cross-bedding, a marine shelf setting is suggested, probably upper shoreface (Boggs, 2011). The abundant cross-bedding could also suggest a tidal-influenced shelf setting, as ancient tidal-dominated shelves are thought to be characterized by abundant cross-bedding with a dominantly unidirectional paleocurrent (Boggs, 2011), which seems to be the dominant trend in the topical sandstone as well, though this is fairly speculative. However, many greywackes are deposited by turbidity currents, often off continental margins in association with volcanic, in fore- or back-arc basins (Tucker, 2001). Turbidity deposits often have cross lamination in the upper part, and could easily transport the large clasts found scattered in the sandstone (Boggs, 2011). Yet no full Bouma sequences, intercalated finer layers or other indications of turbiditic deposition are observed in the sandstone, thus this is highly suggestive at this stage and is only stated as a possible alternative. The main interpretation is therefore deposition in a shallow-marine upper shoreface environment, as this is the best suggestion based on the present evidence. The sandstone contains abundant biotite and chlorite, suggesting post-depositional metamorphism did not exceed greenschist facies grade.

The intermediate volcanic unit separates the typical green cross-bedded sandstone from an overlying sandstone found on the top of the small hill west of Dugurdsknappen (Map, appendix 4). In adjacent areas mapped by B. H. Dalslåen (work in progress), a sandstone is found to overlie similar volcanic units, different from the sandstone below the volcanics. Definitively, further studies are required to properly define the regional-scale stratigraphy of the sandstones above the unconformity and to understand their relationship with the intermediate volcanic unit.

8.1.3 – Extent and setting of the younger intermediate volcanic/intrusion: subduction-related shallow magmatism

There are many questions related to the younger intermediate volcanic and intrusive rocks. First of all, it is difficult to decide whether they represent proper extrusive or intrusive rocks. The biotites are phenocrysts in a fine-grained, but not glassy matrix, which could either be a primary feature or be the result of later devitrification (Winter, 2010). Though the biotites are larger in the intermediate intrusion, this is not a typically coarse-grained intrusive unit, thus it might be more correct to interpret this as a shallow intrusion or sill. It still seems appropriate to differentiate the two, as the volcanic unit is consistently more fine-grained and it seems to follow the bedding in the sandstone to a larger degree.

The dyke sampled from inside the greenstone, as well as the altered greenstone sample EST_179 both have strikingly similar geochemistry to the intermediate intrusion and volcanic (Fig.6.14-B&D; Fig. 6.15-A&B; Fig. 6.16). Though this altered greenstone is described to have high amounts of secondary quartz and calcite (Ch. 6.1.1; Fig. 6.5-D), which might affect the geochemical analyses despite that both the HFS elements and the LREE are thought immobile, it might still suggest a correlation to the intermediate volcanic rather than the greenstone. No thin section has been made of the dyke, but hand samples show a green fine-grained matrix with slightly larger biotite grains, not unlike the intermediate volcanic. One other dyke is mapped inside the greenstone (Map, appendix 4), though it is not sampled nor described properly. Still, it is suggested that the sampled dyke is part of the same young intrusive complex as the intermediate volcanic unit and the intermediate intrusion, and that there might be several other similar dykes cutting the greenstone. Based on these observations it is suggested that the intermediate intrusion is part of a shallow intrusion feeding sills, dykes, and possibly extrusives, and penetrating both the green sandstone and the greenstone.

The geochemistry indicates an intermediate composition of all these rocks, and they plot as andesitic in the TAS diagram (Fig. 6.13) and as calc-alkali basalts based on stable trace elements in discrimination diagrams from Pearce and Cann (1973; Fig. 6.15). They also have the steeper negative REE curve indicating stronger LREE-enrichment more typical for calc-alkaline relative to the tholeiitic magma series (Wilson, 1989, p.178; Fig. 6.14-D). This is supported by the observed mineralogy comprising a light quartz- and feldspar-dominated matrix and biotite phenocrysts (Fig. 6.11). Biotite phenocrysts are commonly seen in more evolved silicic and alkali rocks of the medium to high K-series, typically basaltic andesites, andesites, dacites and rhyolites (Winter, 2010; Nesse, 2013). While tholeiitic rocks occur at all plate boundaries, the calc-alkaline series is mainly restricted to, and dominates, destructive plate boundaries and subduction zones (Winter, 2010). Suitably, both the intermediate volcanic and the intrusion plot as arc-basalts in the discrimination diagram from Wood (1980; Fig. 6.16). When looking at the trace elements they form the very characteristic Th-Ta-Nb-Ce U-shape typical for subduction-related rocks (Wilson, 1989, p. 179; Winter, 2013), similar to the data of typical calc-alkaline subduction related volcanics from Pearce (1982) shown together with the Dugurdsknappen data in figure 6.14-B. So there is a clear difference between the intermediate volcanic/intrusion and the older greenstones, indicating a change in tectonic environment.

8.2 – Structural evolution

8.2.1 – First folding phase

Large-scale tight to isoclinal synform

The greenstone, ribbon-chert, green siltstone sequence is interpreted to be folded into a large southward-closing synform, as depicted in figure 5.1. This interpretation is based on the systematic repetition of the strata, with green siltstone in the centre surrounded by silty chert, ribbon-chert and greenstone outward east and west, as well as the presence of jasper on the top of the greenstone towards the ribbon-chert in both flanks. Both jasper and chert can be deposited within a greenstone sequence, but it does indicate some sort of quiescence and possibly an indication of way up, at least when it is as systematic as in this case. The agglomerate also lies towards the ribbon-chert succession, often together with jasper and incorporating chert. This could as well be an indication of way up, as described from the Scottish Caledonides (Bluck, 2010), but this is very speculative. The synform seems to open northward and close southward, with a possibly boudinaged end in the south. This is suggested based on the separate pockets of chert in the southern end, possible torn off from the main ribbon-chert unit either during internal deformation related to diagenesis prior to the major folding, or due to ductile stretching related to the event folding the synform. Interestingly, there doesn't seem to be a penetrative axial planar foliation developed related to this large-scale folding, the main foliation seen in the rocks is rather related to the younger second folding phase described below (Ch. 8.2.3).

The profiles (Fig. 5.1) give an indication of the synform, with greenstone at the base. It is possible this is part of a bigger system of syn- and antiforms throughout the area. The western separate chert pockets could thus be part of the next synform, though they could also be depositional intercalations. Major upright isoclinal folding is not uncommon in the Trondheim region and has been described by several authors as one of the earlier deformational events in the Upper Allochthon during the Caledonian Orogeny (Rohr-Torp, 1972; Roberts and Wolff, 1981; Gee et al., 1985; Roberts and Stephens, 2000). A study from the Oppdal-Innset area (Rohr-Torp, 1972) presents a profile going NE-SW through the area just north of Dugurdsknappen (Fig. 2.6; Fig. 8.2-above), depicting severe upright isoclinal folding of a lava-green sediments-banded quartzite sequence; similar to what is observed in the Dugurdsknappen area. In this interpretation the whole folded sequence is thought to be inverted before folding, based on a few observations of way-up structures, something which is also suggested by B. H. Dalslåen (work in progress). Based on this interpretation, the described synform might in fact be an antiformal syncline, as a result of antiformal folding of the already inverted section, as depicted in figure 8.2-below. However, it is important to note that Rohr-Torp (1972) suggests that the sandstone lying unconformably on the greenstone, correlative to the green sandstone at Dugurdsknappen, is folded and inverted together with the underlying units (Fig. 8.2-above). This is contradicting with observations made in the Dugurdsknappen area, where the sandstone is clearly deposited post-isoclinal folding and not a part of the big synform, which is supported by observations from B. H. Dalslåen (personal communication) in the adjacent areas. Considering these contradicting observations, as well as the small extent of the Dugurdsknappen area without repetition of syn- and antiforms, no

certainty can be said about either an inverted or non-inverted interpretation, and must conclude only that the area is folded in a synform with way up towards the centre.

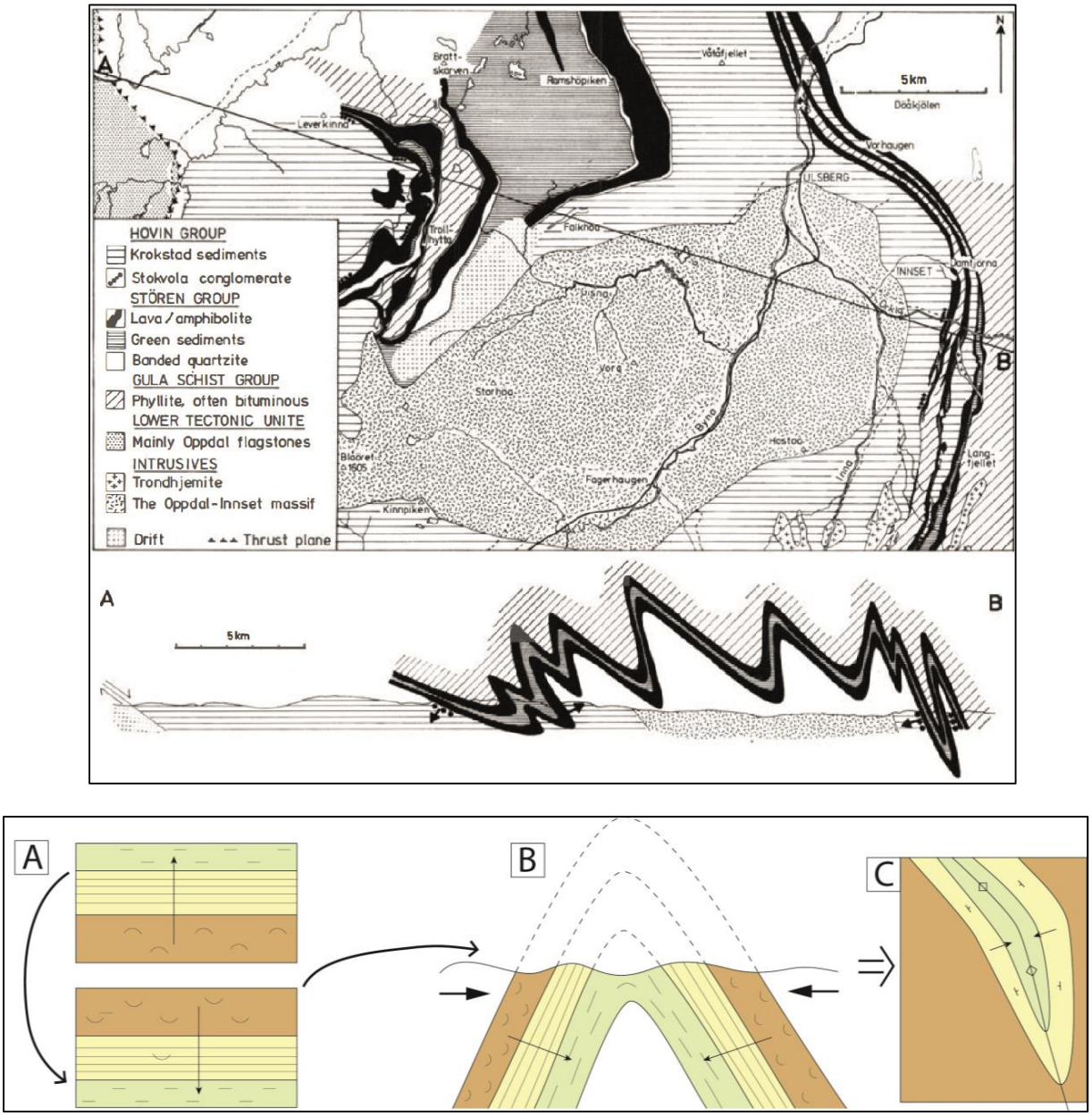

Figure 8.2: Above: Map and profile from Rohr-Torp (1972). Note how the sandstone (termed the Krokstad sediments by Rohr Torp) is folded together with the Støren and Gula units. The profile is drawn into the more recent map by Nilsen and Wolff (1989) in figure 2.6 to give a better presentation of the relation to the Dugurdsknappen area. Below: Illustration of a possible antiformal synform interpretation in the Dugurdsknappen area, based on observations from Rohr-Torp (1972) and B. H. Dalslåen (work in progress): A) The original greenstone – Ribbon-Chert – Green siltstone sequence got inverted, possibly through large-scale recumbent isoclinal folding of a larger part of the Trondheim Nappe Complex. B) The inverted sequence mapped at Dugurdsknappen is folded in an antifom and the top eroded, resulting in the map view expression illustrated in C).

Small-scale folding in chert

The ribbon-chert is described in chapter 5.1.2 as strongly folded, with most fold axes plunging southward between SE and SW, while the greenstone, silty chert and green siltstone all have mean fold axes trending S-SE (Fig. 5.3; Fig. 5.9; Fig. 5.12-B; Fig. 5.14; Fig. 5.19). The folds

in the ribbon-chert are divided into three trends, where one trends S-SE and another incorporating most of the isoclinal folds trend almost directly south (Fig. 5.8-F; Fig. 5.19). These two trends are generally concordant with the direction of the synform and are interpreted to represent folds belonging to this first large-scale folding phase, prior to deposition of the green sandstone. One interesting aspect of this first folding phase is the difference in deformation style within the ribbon-chert and the overlying and underlying units. While the ribbon-chert is severely folded with abundant isoclinal folds (e.g. Fig. 5.1; Fig. 5.8), only a handful folds can be found in the greenstone and green siltstone, though it's worth noting that they all trend concordantly southward. It is also seen internally in the ribbon-chert itself, as shown in figure 5.7, where the regional foliation is recorded in the phyllosilisiclastic layers in between chert in the ribbon-chert sequence, while the chert layers rather depict refracting concoidal tension fractures varying dependent on stresses around the fold hinges. This difference in deformation style is not an uncommon phenomenon in areas of chert interbedded with other lithologies, and has been explained by the difference in rheology (Fink and Reches, 1983). Before transforming into quartz-chert, the chert consists of biogenic opal-A which gradually transforms to Opal-CT and then into quartz. When chert is in these two primary stages it is very soft and behaves viscous under very small stresses (Boggs, 2011), and can therefore also develop density differences and slumping which will later affect the response to deformation. While the dominant orientation would reflect the regional tectonic stresses, the amount and amplitude of the folds within the chert maybe the effect of density differences within the chert caused by diagenesis and a viscous reaction to slow regional compression (Fink and Reches, 1983), or simply because it is much softer at this stage. This would also explain the frequent lateral and vertical inconsistency in the layering and flow like patterns in folds, often with finer material flowing into fold hinges, and possibly also the boudinage of the southern end of the large-scale synform. This might also partly be causation for the complex patterns mapped on the top of Dugurdsknappen (Fig. 5.10), where despite good exposure it is still very difficult to follow layers for a longer distance. However, no proper studies have been done regarding palaeostress-levels, amount of shortening or rheology of the chert, thus further studies would be required to properly understand the ribbon-chert deformation style.

8.2.2 – Genesis of the unconformity

One of the main goals of this study was to investigate the apparent unconformity between the isoclinally folded greenstone, ribbon-chert, green siltstone succession and the overlying less deformed green sandstone. Through field work no indications of a tectonic contact were found, and the contact is interpreted to be that of an erosional unconformity. This is largely based on the absence of tectonic indicators and the presence of a basal conglomerate incorporating angular clasts of chert, interpreted to be derived from the underlying ribbon-chert. The well preserved sedimentary structures and the low degree of deformation in the sandstones are thought to support this, as they are so close to the contact. There is however some deformation in the zone adjacent to the contact, as the contact itself is folded, which is reflected in the units below and above the unconformity. This is thought to be mainly due to folding succeeding deposition, and not related to tectonic thrusting.

8.2.3 – Second folding phase and related foliation

The third mean fold axis trend described in the ribbon-chert unit is most common in the western part close to the sandstone and plunges moderately SW, concordantly with the mean fold axis in the green sandstone and the intermediate volcanic unit (Fig. 5.19-B; Fig. 5.20). This is interpreted to represent the second fold phase F2 folding the F1 synform and the unconformity in a large scale fairly gentle fold, with locally tighter folds, as for example along the green sandstone/ribbon-chert contact (Fig. 8.3-A) and within the different units (e.g. 5.16-D). The SW plunging fold axes indicate NW-SE compressional deformation with a NW vergence based on the dominantly SE dipping axial planes (Fig. 8.3-B).

Most axial planes related to this fold event, mainly those in the green sandstone, but also some seen in the ribbon-chert, are parallel to that of the main foliation direction, which strikes approximately NE-SW (Fig. 8.3-B; Map 2&3, appendix 1). This foliation is interpreted to be related to the second fold phase, probably developed as an axial plane cleavage, based on the relation to the F2 axial planes and that it penetrates all units both below and above the unconformity as the main foliation (Fig. 8.3-B; Map 2, appendix 1). No systematic foliation has been observed prior to this, and it has therefore been termed the S2 foliation due to the relation to the F2 folding, while the primary bedding is termed S0 (Fig. 8.3-A).

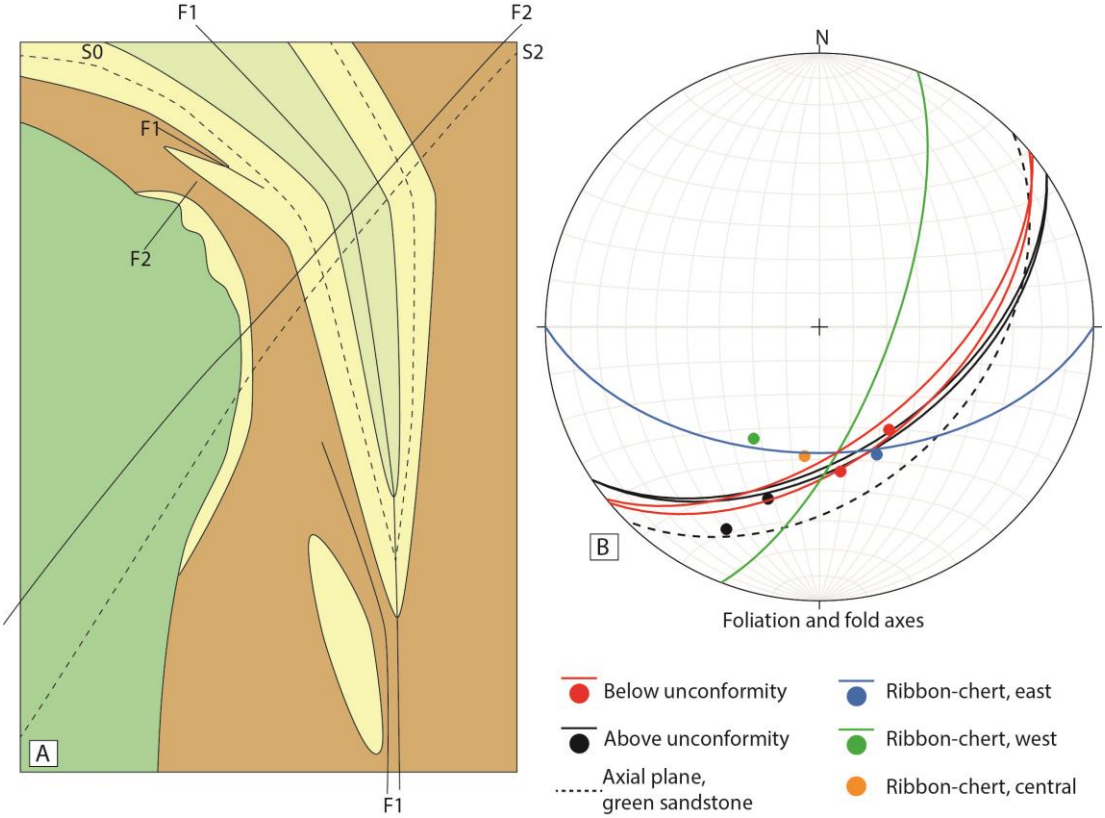

Figure 8.3: A) Map sketch with indication of the main deformation events. S_0 is primary bedding and F_1 the first fold phase, while the main foliation S_2 is related to the second fold phase F_2. The first fold phase also folds the boudinaged end and the sides of the synform. B) Stereonet depicting the mean foliation and fold axes, same as was seen in figures 5.19 and 5.20. Red lines represent the greenstone and the green siltstone, which are parallel to the black lines representing the green sandstone and the intermediate volcanic, indicating a regional foliation. Dotted line shows orientation of the axial planes in the green sandstone, which are parallel to the regional foliation, indicating an axial plane cleavage. Red dot represent fold axes from below the unconformity, which both trend to the SE following the first fold phase, while the black dots of the rocks above the unconformity trend SW concordant with the second fold phase. Both fold phases are recorded in the ribbon-chert, with the second one most common in the western part close to the contact. Foliation in ribbon-chert is generally more inconsistent.

8.3 – Palaeotectonic interpretation

The greenstone is interpreted to represent the oldest unit, together with the small genetically related gabbroic intrusions. They seem to have originated along a spreading ridge, with an enriched tholeiitic source and abundant hydrothermal activity, though it is not properly understood whether this spreading ridge was part of a major basin spreading centre, or a minor back-arc rifting system. It does seem there is a larger probability for back-arc basin ophiolites to be obducted, than it is for those from major rift zones which are older and heavier and therefore rather subducted. Together with the evidence from the sedimentary rocks overlying the greenstones it seems most likely that the basalts formed in an environment related to a destructive plate boundary, possibly in the proximity of a subduction zone, either close as a back-arc basin, or in a major basin further away (Fig. 8.4-A).

The overlying ribbon-cherts are thought to be formed relatively continuous following basalt formation, and interpreted to most likely have been deposited in a proximal marine environment, close to a continental source, based on the REE-geochemistry. The gradual continuation into more silt-rich sediments upward in the succession is suggestive of a gradually more proximal environment. This could be explained by the migration of a subduction zone, or increased compression lifting up adjacent areas causing a closer source of terrigenous input. The whole sequence must have been accreted onto a continent or an island-arc at some point succeeding deposition of the green siltstone. A migration of a subduction zone is therefore not an unlikely theory, as suggested in figures 8.4-A&B.

Possible E-W compressional stresses caused the first folding phase, folding the greenstone – ribbon-chert – green siltstone succession prior to deposition of the green sandstone. Folding shortly after deposition before transformation from opal-A or opal-CT to quartz-chert has been suggested as explanation for the higher degree of folding inside the ribbon-chert unit relative to the over- and underlying units (Ch. 8.2.1; Fink and Reches, 1983), which would indicate folding prior to accretion, though folding could also be an effect of the compressional stresses leading to accretion. Figure 8.4-C shows accretion onto an island arc, but this is only suggestive and further studies are required to properly understand the process and timing of this step.

The green sandstone above the unconformity is interpreted to have been deposited in a shallow marine environment or by turbidity currents. Deposition of the green sandstone occurred after or concurrently with erosion of the underlying units, suggested by the angular chert clasts found in the basal part of the sandstone, in a period of subsidence creating a basin (Fig. 8.4-D). Whether this deposition occurred on a shallow shelf of a continent or related to a subduction zone volcanic arc is not properly understood. The presence of intruding volcanites with typical subduction zone signature in the geochemistry suggests the sandstone overlay a subduction zone at some point following deposition, as illustrated in figure 8.4-E. But as the age of the intrusion is unknown, the period and amount of movement of the sandstones between deposition and volcanism is not known and could be almost continuous or millions of years, giving room for large tectonic changes in the meantime. The second fold phase as well as the development of the regional foliation occurred subsequent to the volcanic activity (Fig. 8.4-F).

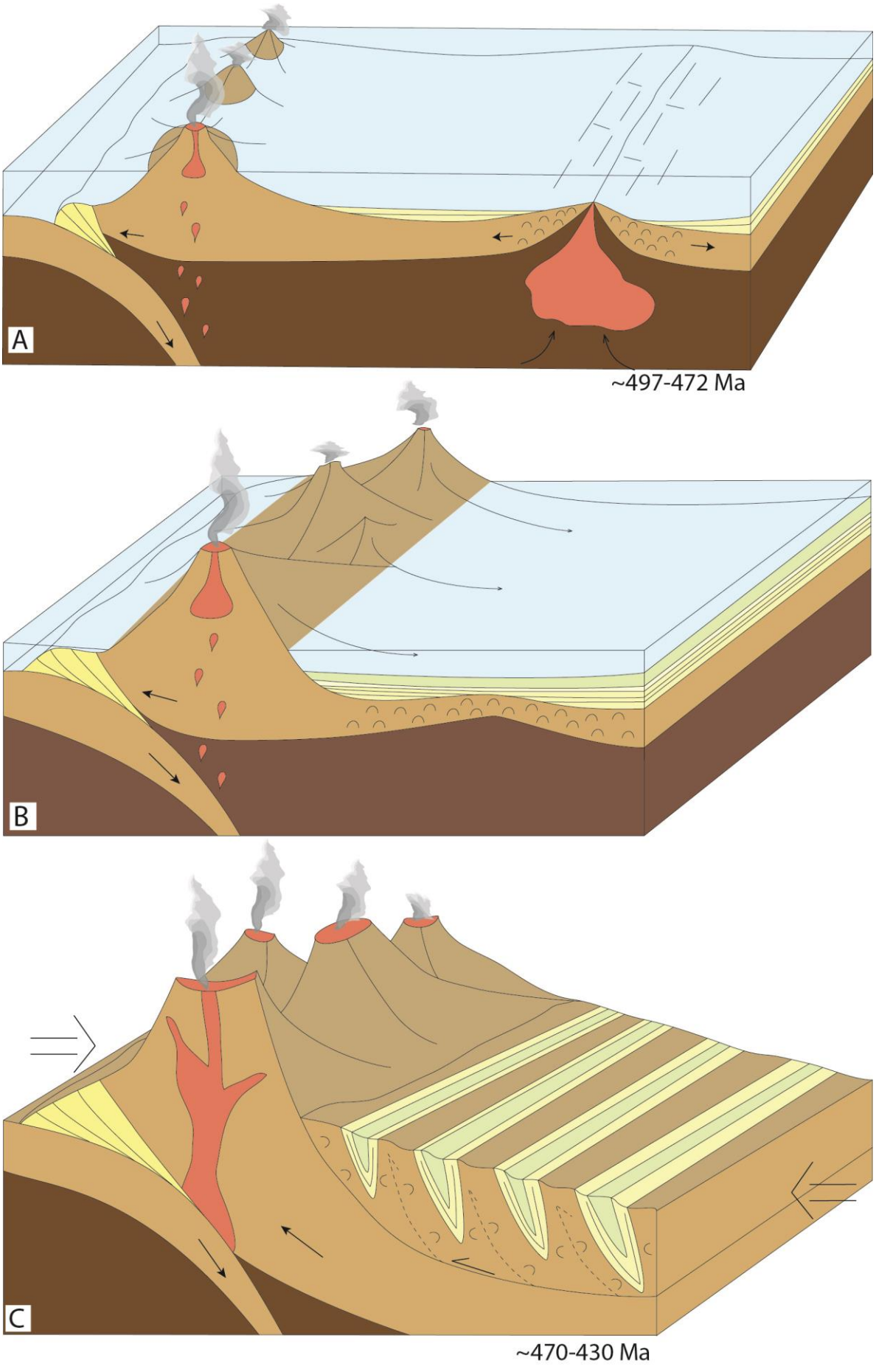
A
~497-472 Ma
B
C
~470-430 Ma

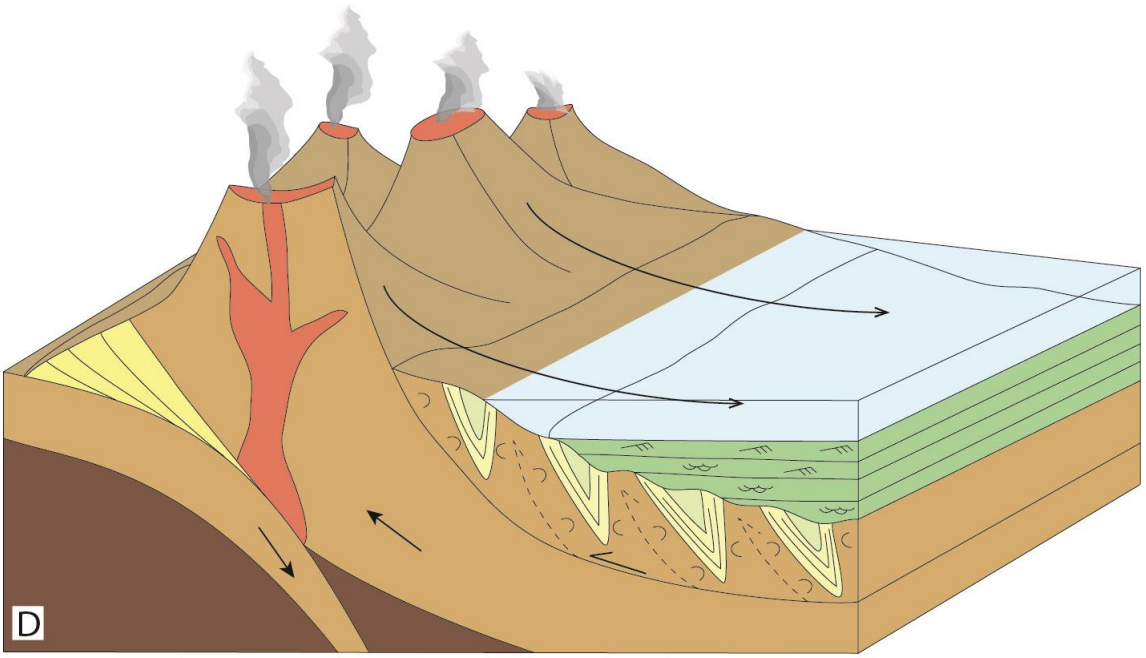

< 430 Ma

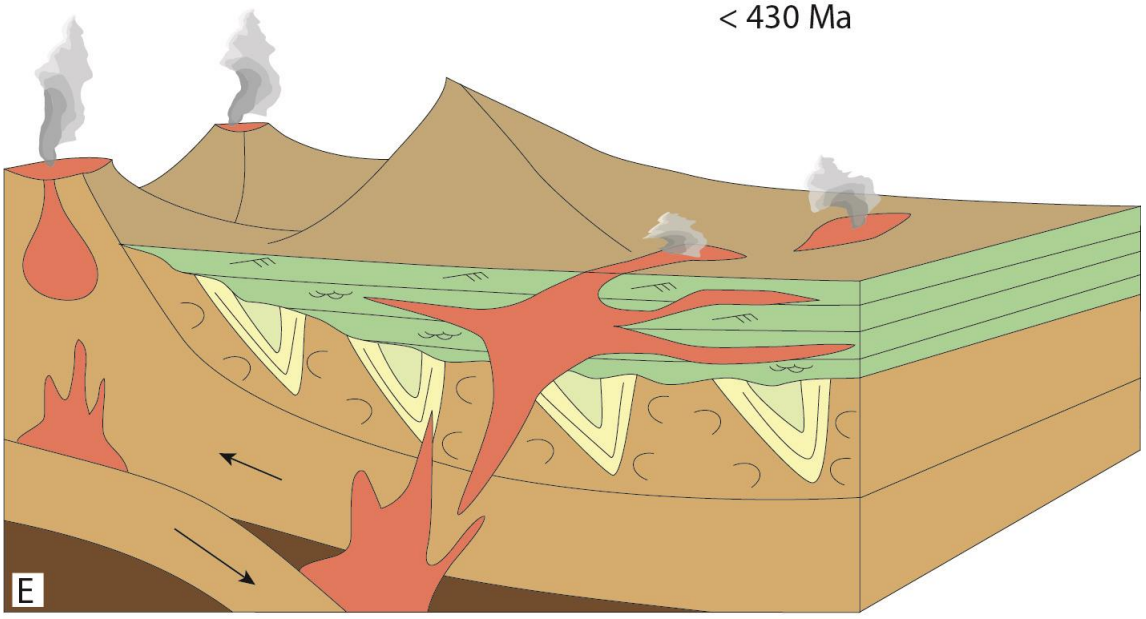

< 430 Ma

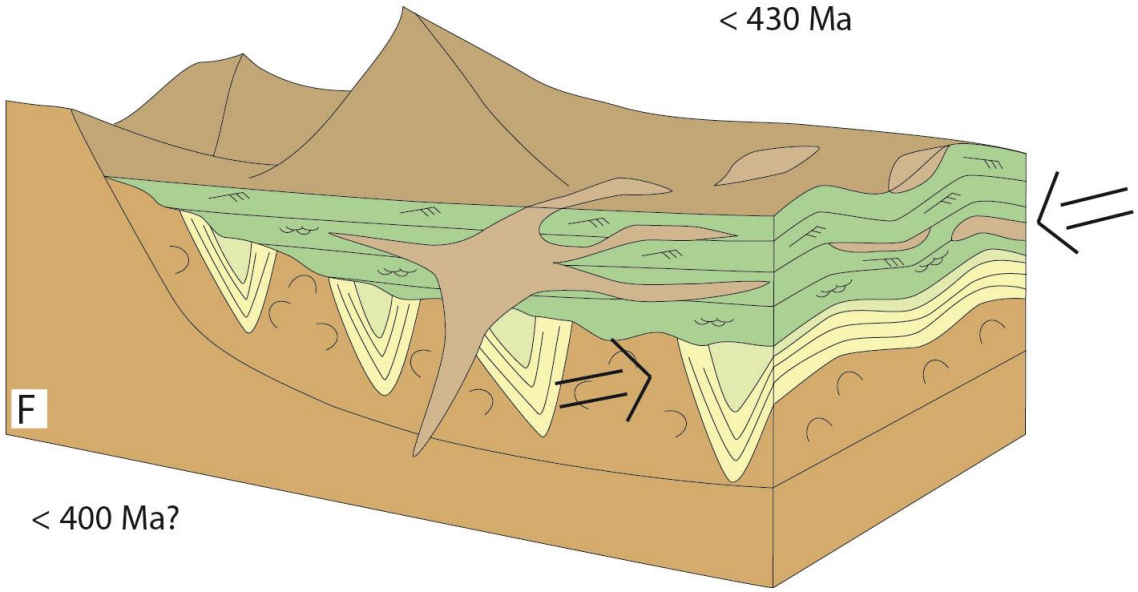

< 400 Ma?

Figure 8.4: Suggested tectonic interpretation of the Dugurdsknappen area. A) Formation of greenstones along a spreading ridge in a marginal basin or at a major spreading ridge in proximity to a destructive plate boundary. B) Compression leads to migration or uplift causing deposition of chert and silty units in a more proximal environment giving higher influx of terrigenous input than seen at a deep marine spreading ridge. C) Further compression leads to folding, accretion and uplift, followed by a period of exposure to erosion. Proximity to a volcanic arc is suggested, but not certain. Period lasting from ended formation of the green siltstone until deposition of the green sandstone. D) Deposition of the green sandstone onto the eroded greenstone, ribbon-chert and siltstone succession. Simultaneous erosion leads to incorporation of the underlying chert in the lower parts of the sandstone. E) Volcanic intrusions with typical subduction zone geochemistry penetrate the green sandstone and probably the underlying units as well, suggesting position of the area above a subduction zone. F) Changing compressional stresses succeeding the volcanism folds all units in a second folding phase, concurrently with development of the main foliation. Note: Few interpretations of direction of these processes have been done; thus the orientation of each illustration is not indicated. Timing and ages of the units indicated in the illustrations will be discussed in chapter 8.4.

8.4 – Relation to the Scandinavian Caledonides

8.4.1 – Early Cambrian to Ordovician greenstone units

The greenstone is part of an area that has been termed the Tronget unit (Ch. 2.4.2), which has traditionally been correlated with the Støren Group greenstones (Nilsen and Wolff, 1989). Most studies of the Støren Group greenstones have been conducted in the northwestern part of the Støren Nappe, in the Løkken, Vassfjellet and Bymarka ophiolites (Heim, Grenne and Prestvik, 1987; Slagstad, 2003), and the temporal and genetic relationships between these and the Støren greenstones senso stricto (Fig. 2.5) are unclear (Furnes et al., 1980; T. Grenne, work in progress). Further work is needed to declare the division between the northwestern greenstones, the Støren greenstones senso stricto and the Dugurdsknappen and Tronget unit greenstones. Mainly sheets of pillow lavas and no full ophiolites are observed in the Støren greenstones senso stricto, and studies yet unpublished suggest a different composition and possibly genesis, than for the northwestern Løkken-Bymarka greenstone units (T. Grenne, personal communication; B. H. Dalslåen, work in progress). The northwestern units have been described as tholeiitic ocean floor basalts from a spreading ridge in a major or marginal basin (Furnes et al., 1980; Gale and Pearce, 1982), and more recent studies done on the Løkken and Bymarka greenstones suggest formation in a marginal basin in a suprasubduction-zone setting, probably along the Laurentian margin related to the closing of the Iapetus Ocean (Heim, Grenne and Prestvik, 1987; Slagstad et al., 2013). In the Dugurdsknappen greenstones, there is however enrichment in LREE and the high field strength trace elements Th-Zr, which does not correlate with the diagrams from the northwestern units (Slagstad et al., 2013), suggesting a different origin. Such an enrichment is also seen in greenstones sampled from the Støren greenstones senso stricto in an area just east of Dugurdsknappen (T. Grenne, personal communication), suggesting a difference from the northwestern ophiolites and a connection between the Dugurdsknappen greenstones and the Støren greenstones senso stricto. Further southwest within the Scandinavian Caledonides, in the Solund-Stavfjord ophiolite complex, pillow basalts found in the Smelvær unit show similar enriched geochemistry as the Dugurdsknappen greenstones, and are interpreted to represent ocean island basalts which formed off-axis in a back-arc basin (Furnes, Dilek and Pedersen, 2012). Though these units have not been time-correlated and any relation is uncertain, it still suggests a not unlikely tectonic interpretation for the Dugurdsknappen greenstones.

The Støren Nappe greenstones were previously thought to range in age from Early Cambrian to Early Ordovician (Arenig) (Roberts and Wolff, 1981). More recent U-Pb zircon dating of greenstone-related felsic rocks place the formation of the Leka and Ytterøya magmatic rocks at about 495-497 Ma in the Late Cambrian (Dunning and Pedersen, 1988; Roberts and Tucker, 1998), and the formation of the Trondheim Region Løkken, Bymarka and Vassfjellet ophiolites between 487-480 Ma in the Early Ordovician, followed by intrusion of intermediate volcanic rocks at about 468-467 Ma, thought to relate to the establishment of a volcanic arc subsequent to accretion (Slagstad et al., 2013). However, the Støren greenstones senso stricto, as well as the Dugurdsknappen greenstones, are so far of unknown age, but a possible younger age of about 472 Ma has recently been suggested for greenstones just east of Dugurdsknappen (B. H. Dalslåen, work in progress; T. Grenne, personal communication). Age variations within ophiolite-arc assemblages are not uncommon, and can be explained both by the time-aspect of ophiolite generation, which can take 10-15 million years (Roberts et al., 2002) and the polyphase nature of arc-processes in general. The available data including the so far unpublished 472 Ma age from Dugurdsknappen greenstone rocks indicate at least 20 m.y. of marginal-basin and subduction-zone magmatism in the wider Trondheim region.

It is worth noting that the old map from Nilsen and Wolff (1989) differs somewhat from the map presented in this study, the most striking feature being the quartz keratophyre which is mapped by Nilsen and Wolff (1989), but not by the present author. It is likely that this is in fact the same as the altered greenstone mapped in this study, seeing that the geometrical extent is somewhat similar and that the altered greenstone can have a fairly felsic appearance in the field, even though the geochemistry indicates basaltic origin.

8.4.2 – Mid-Silurian sandstone basins

The green sandstone above the unconformity overlies the Dugurdsknappen greenstone above what is interpreted an erosional and not a tectonic contact. A similar contact is described further north between the Hovin-Horg Group sediments and the underlying Støren greenstones (Vogt, 1945). However, the Hovin-Horg sediments of the northwestern Trondheim Region are thought to have been deposited on the newly obducted and eroded ophiolite at about 475-465 Ma (Grenne, 1989), while the green sandstone has a maximum depositional age of 427 ±3 Ma. It is evident that this unit was deposited at a much later stage in the Caledonian orogeny and is thus not related to the Ordovician sediments which are otherwise common in the Trondheim region of the Scandinavian Caledonides (Roberts, Grenne and Ryan, 1984; Pedersen, Bruton and Furnes, 1992; Roberts et al., 2002). Llandovery or perhaps younger Silurian-aged turbidites and conglomerates are described from the Lower Köli Nappe (UA) in central Västerbotten (Gee et al., 2014), but no further correlations are made at this point. The green sandstone can be correlated with the sediments shown as a c. 8 km wide, restricted circular unit in the 1:250 000 map by Nilsen and Wolff (1989; Fig. 2.6), as discussed in chapter 8.1.2, were Rohr-Torp (1972; Fig. 2.6; Fig. 8.2) observed a basal conglomerate along an erosive contact towards the greenstones similar to what is described at Dugurdsknappen. Recent studies also map sandstones of comparable appearance with concordant maximum depositional ages of 430 Ma in several places within the Oppdal-Innset area (B. H. Dalslåen, work in progress). Simultaneously, conglomerates,

sandstones and shales of the Lyngenstein and Sandå units of the Hovin-Horg area show similar young maximum depositional ages of ca. 430 Ma (Gasser et al., 2016), suggesting an originally larger extent of Middle Silurian basins prior to erosion. If the Dugurdsknappen greenstones were accreted coevally with the northwestern ophiolites, this would indicate a larger time-gap between accretion and renewed covering by sediments. This suggests placement of the greenstones comprising the Dugurdsknappen greenstone at a high topographic level exposed to erosion for a longer period, before subsidence and basin development. The tectonic regime during deposition of the green sandstone is not completely understood; as such young Silurian basins are not commonly described. It could have been deposited in a piggy-back basin on a fold and thrust belt comprising the Laurentian-derived allochthons, placed on the continental margin of Baltica just prior to Scandian thrusting over the Baltic continent. This could explain the initial uplift, causing the succeeding erosion and subsequent deposition of the green sandstone, and does not exclude either shallow marine or turbiditic deposition which could both occur depending on the position in the fold and thrust belt, though this is all highly speculative.

There are several potential sources for the provenance of the green sandstone. No attempt has been made to use the geochemistry of the sandstone for provenance study, as this is a complex field with many pitfalls (Rollinson, 2013). The mineral assemblage neither gives any clear indication of provenance. The green colour which was initially interpreted as a sign of volcanic derivation, is strongly influenced by the subsequent greenschist-facies metamorphism causing abundant secondary growth of chlorite, and the high silica content suggests a rather felsic source (Boggs, 2011). Towards the base of the sandstone, angular chert clasts occur, together with some greenstone-like clasts, suggesting a local provenance for at least parts of the lower sandstone. Throughout the mapped section there are also rounded granitic, tonalitic and quartzitic clasts, indicating a more distal source. The rounded tonalitic/trondhjemitic clast EST_12 sampled from the lower part of the sandstone is dated to 485 ± 4 Ma (Ch. 7.2). This age correlates with ages of plagiogranites from Løkken and Bymarka ophiolites (Slagstad et al., 2013) and of trondhjemite and rhyodacite from the Bymarka ophiolite (Roberts et al., 2002). Considering the rounded nature of the clast, such a distal derivation is not impossible, yet there might be more proximal sources of similar ages that are not yet known.

The detrital ages are dominated by Sweconorwegian ages, with a distribution of 34% Caledonian and 66% Precambrian and Archean grains (Fig. 7.6-A), which indicates a bimodal source with larger continental input (Sweconorwegian) than volcanic (Caledonian), though some can also be recycled (Gee et al., 2014). The youngest detrital zircon ages indicate a source with ages of about 430-420 Ma (Fig. 7.6-D). The adjacent Gula and Meråker nappes contain abundant intrusions of c. 430 Ma (Dunning and Grenne, 2000; Nilsen, Corfu and Roberts, 2007) and also the Støren Nappe contains smaller plutons of c. 430 Ma (F. Corfu, personal communication). It is interesting to note that the sandstone does not contain detrital zircon ages corresponding to the large proximal Innset massif, which has an age of about 435 Ma (Nilsen et al., 2003; Nilsen, Corfu and Roberts, 2007). The older Caledonian ages represent several phases of volcanic activity, with Middle to Late Ordovician ages about 440-

460 Ma correlating with intrusive ages described among others at Smøla and Hitra (Tucker et al., 2004) and older Early Ordovician and Late Cambrian ages between c. 470-500 Ma, correlating with igneous ages in the northwestern Trondheim Region (Dunning and Pedersen, 1988; Slagstad et al., 2013; Fig. 7.6-D). Most of the data has typical Sveconorwegian signature with ages between 900 and 1900 Ma, where a smaller peak has typical Transcandinavian Igneous Belt ages between c. 1650-1800 Ma, while the dominant peak has Sveconorwegian sensu stricto ages between c. 900-1200 Ma. The presence of Archean grains has often been used as an indication of Laurentian provenance, but can also be inherited ages from Neoproterozoic sediments from elsewhere (Bingen and Solli, 2009). This age distribution is highly undiagnostic considering that Sweconorwegian and Caledonian ages can be found on both the Laurentian and Baltic side (Bingen and Solli, 2009) and that the deposition probably occurred at a time where most of the Iapetus Ocean was gone and Laurentia and Baltica were so close a discussion on origin does not make sense.

8.4.3 – Post-mid-Silurian volcanics

The intermediate younger volcanic and intrusuon have been interpreted to be younger than 430 Ma, as they intrude the green sandstone with a maximum age of about 427 ± 3 Ma. Subduction-related intermediate volcanism has been described several places in the Trondheim Nappe Complex (Slagstad, 2003; Nilsen, Corfu and Roberts, 2007), though all related to older magmatic phases, the youngest ending at about 435-430 Ma including the proximal Innset and Toset trondhjemites. A possible Permian biotite-bearing Lamprophyre was described on Ytterøya (Carstens, 1961), however the reliability of this data is low, and the geochemistry of the Dugurdsknappen volcanite is much too silica-rich to resemble a lamprophyre. Walsh (1986) describes the Fanabekken biotite-bearing tuff from the Meldal area of the Hovin Group sediments, however it has already been shown that the Hovin and Horg Group sediments do not correlate to the green sandstone from this study, and the volcanics from this study cannot be described as tuffs. A 418±9 Ma trondhjemitic dyke described from the Lindås Nappe of the Bergen Arc is more similar, and interpreted as a result of decompression melting caused by the exhumation of the nappe (Kühn et al., 2000). There is also Middle to late Silurian magmatism described from the Ofoten and Troms areas, comprising felsic dykes and small plutons, the youngest dated to about 425 ± 1 Ma (Augland et al., 2014). No such young magmatic episodes have previously been described from the Trondheim Nappe Complex. However, volcanites with biotite phenocrysts and a geochemistry comparable to that of the intermediate intrusion and volcanite have been described recently in the adjacent area (B. H. Dalslåen, work in progress), which very likely correlate with the volcanites described here. It is possible that these young intrusions and volcanites represent a young subduction-related volcanic episode so far not described in the Trondheim Region.

8.4.4 – Structural evolution in a wider context

An E-W oriented compressional stress regime has been suggested for the first folding phase (Ch. 8.2.1), but without kinematic indication. It is thought that the initial deformation of the Støren ophiolite senso lato was in the Early Ordovician, coevally with obduction and prior to erosion and deposition of the younger Hovin and Horg Groups (Gee et al., 1985; Roberts et

al., 2002), which according to some authors occurred about 475-465 Ma (Grenne, 1989). Strong isoclinal deformation in the nearby area was also described by Rohr-Torp (1972; 1974), who depicts similar NE-trending isoclinal folds and relate them to a corresponding F1 deformation phase, while his F2 deformation is related to later E-W trending minor folds and crenulations affecting the earlier structures. Development of a regional schistosity is thought to postdate the earliest isoclinal folding (Gee et al., 1985); similar to what is seen at Dugurdsknappen, though Rohr-Torp (1974) describes a regional schistosity related to the F1 deformation phase, rather than F2. It is possible this first folding phase is closer related to ophiolite obduction and arc accretion, than to allochthonous thrusting during the main Scandian phase. A top-to-the ESE directed movement has been described as the prevailing direction throughout the Scandian part of the Caledonian orogeny (Roberts and Stephens, 2000), which was initiated at about 430 Ma and lasted into the Early Devonian (Tucker et al., 2004, Corfu, Andersen and Gasser, 2014), yet no structures clearly related to this top-to-the east movement and nappe thrusting have been recorded in the Dugurdsknappen area. The second fold phase of Dugurdsknappen has a marked NW-verging sense of movement, which is concordant with Late- and Post-Caledonian extensional tectonics dominated by overprinting ductile top-to–the west deformation (Fossen, 1992; Roberts and Stephens, 2000). The crenulations seen in the green siltstone and silty chert, as well as vaguely in the intermediate volcanic (e.g. Fig. 6.9-C; Fig. 6.10-B), might also be related to this second fold phase, similar to that described by Rohr-Torp (1974), or it indicates the regional foliation overprinting an earlier foliation. This indicates that the area experienced most deformation in the first fold phase during accretion or possibly later during east directed nappe translation, while the second episode of less tight folding occurred during westward post-orogenic reactivation, possibly also related to development of a regional foliation. It is also worth noting that some authors describe major late and post-orogenic NW-SE striking fractures transecting the Caledonides, which correlates with the direction of the younger brittle faults cutting the higher area of Dugurdsknappen (Roberts and Stephens, 2000; Ch. 5.5; Fig. 5.24; Map, appendix 4). Further studies are required to better constrain the process and timing of the structural events observed at Dugurdsknappen.

Chapter 9 – Conclusion

At least 70 m.y. of geologic evolution have been constrained in the previous chapters, considering many different aspects of the geology of the Dugurdsknappen and its relation to the Scandinavian Caledonides. Based on these results and discussions a short summary concerning the most important aspects will now be presented. The oldest group mapped in the Dugurdsknappen area comprises greenstone, gabbro, altered greenstones and agglomerates. The greenstone comprise ocean floor or MORB type tholeiitic enriched basalts interpreted to have been deposited along a major spreading ridge, or along an off axis spreading centre, in a major or marginal basin. A marginal basin formation is suggested by overlying sedimentary sequences. The altered greenstones are mainly caused by hydrothermal alteration, supporting formation along a spreading axis. The geochemistry of the Dugurdsknappen greenstones suggests stronger correlation with the senso stricto Støren greenstones (Fig. 2.5) than with the northwestern Løkken and Støren ophiolites.

The overlying ribbon-chert is interpreted to have formed close to a terrestrial source based on the Ce-enrichment and the intercalated coarser sedimentary layers of sandstone and conglomerate, probably in a marginal basin and possibly related to a volcanic arc. Upward increasing silt-content from ribbon-chert through silty chert and into the green siltstone is seen in linear trends in both major element and REE diagrams, as well as from field observations, suggesting migration toward a terrestrial source or another change in basin geometry causing suffocating SiO_2-rich chert-sedimentation.

The greenstone – ribbon-chert – green siltstone sequence is isoclinally folded in a large S-SE trending synform (Fig. 5.1). This is possibly part of a larger sequence of syn-and antiforms folding the whole area. This could be related to deformation during accretion of the units or to later east-directed nappe translation during the Scandian phase. Higher fold-amplitude within the ribbon-chert is explained by difference in rheology, particularly shortly after deposition before diagenetic transition from Opal-A or Opal-CT to quartz, when the chert is much softer and reacts easily to deformation. Since the ribbon-chert is folded following the same trend as the surrounding units, it suggests that folding occurred shortly after deposition and most likely related to accretion rather than later nappe-translation.

An erosive unconformity parts the underlying isoclinally folded sequence from the less deformed overlying green sandstone. The unconformity cuts both greenstones and ribbon-chert and is marked by a basal conglomerate comprising angular chert clasts, though it is obscured in the southern part where it also cuts the very similar agglomerate (Fig. 5.21). Folding and steep penetrative foliation related to the second fold phase also obscures the contact.

The green sandstone is interpreted to be a greywacke or similar lithology, most likely deposited in a shallow marine upper shoreface environment, possibly on a fold and thrust belt along a continental margin. A 485 ± 4 Ma tonalitic clast possibly derived from the northwestern part of the Støren Nappe is found in the sandstone, together with detrital zircons suggesting 2/3 continental derivation and 1/3 volcanic (Fig. 7.6). The sandstone has a

maximum age of 427 ± 3 Ma, possibly correlating with other Mid-Silurian sedimentary units recently described in the Oppdal-Støren area.

The intermediate intrusion and volcanic unit intrudes the sandstone and probably the underlying units as volcanics, sills, dykes and/or shallow intrusions sometime after 430 Ma. Calc-alkaline geochemistry with strong subduction signature and abundant biotite phenocrysts suggest subduction-zone-related volcanism. Such young subduction-related volcanism has not been previously described in the Trondheim Region.

A second deformational phase folds all units in open to close SW-trending folds (Fig. 8.5). The main foliation found in all units in the area correlates with the axial plane of the second fold phase and is interpreted as the axial-plane foliation to this phase. The folds are generally NW-verging which is correlated with the post-orogenic extensional phase of the Caledonian Orogeny. NW-SE trending transtensional younger faults cutting the top of Dugurdsknappen are also correlated to this late extensional phase.

References

Aitchison, J. C. 1998. A lower Ordovician (Arenig) radiolarian fauna from the Ballantrae Complex, Scotland. *Scottish Journal of Geology*, 34(1), 73-81.

Allmendinger, R. W., Cardozo, N. C. and Fisher, D., 2013, *Structural Geology Algorithms: Vectors & Tensors*. Cambridge: Cambridge University Press, 289 pp.

Armstrong, H. A., Owen, A. W. and Floyd, J. D. 1999. Rare earth geochemistry of Arenig cherts from the Ballantrae Ophiolite and Leadhills Imbricate Zone, southern Scotland: implications for origin and significance to the Caledonian Orogeny. *Journal of the Geological Society*, 156(3), 549-560.

Augland, L. E., Andresen, A., Gasser, D. and Steltenpohl, M. G. 2014. Early Ordovician to Silurian evolution of exotic terranes in the Scandinavian Caledonides of the Ofoten–Troms area–terrane characterization and correlation based on new U–Pb zircon ages and Lu–Hf isotopic data. *Geological Society, London, Special Publications*, 390(1), 655-678.

Bingen, B. and Solli, A. 2009. Geochronology of magmatism in the Caledonian and Sveconorwegian belts of Baltica: synopsis for detrital zircon provenance studies. *Norwegian Journal of Geology*, 89(4), 267-290.

Black, L. P., Kamo, S. L., Allen, C. M., Davis, D. W., Aleinikoff, J. N., Valley, J. W., ... and Foudoulis, C. 2004. Improved 206 Pb/238 U microprobe geochronology by the monitoring of a trace-element-related matrix effect; SHRIMP, ID–TIMS, ELA–ICP–MS and oxygen isotope documentation for a series of zircon standards. *Chemical Geology*, *205*(1), 115-140.

Bluck, B. J. 2010. The Highland Boundary Fault and the Highland Border Complex. *Scottish Journal of Geology*, 46(2), 113-124.

Boggs, S. J. 2011. *Principles of Sedimentology and Stratigraphy*. 5th ed. New Jersey: Pearson Education, Inc. 585 pp.

Bryhni, I. and Andréasson, P. G. 1985. Metamorphism in the Scandinavian Caledonides. In: Gee, DG, Sturt, BA,(Eds.), *The Caledonide Orogen-Scandinavia and Related Areas*. Chichester: Wiley & Sons Ltd, 763-782.

Buiter, S.J. and Torsvik, T.H. 2014. A review of Wilson Cycle plate margins: A role for mantle plumes in continental break-up along sutures? *Gondwana Research*, 26, 627-653.

Burke, K. 2011. Plate tectonics, the Wilson Cycle, and mantle plumes: geodynamics from the top. *Annual Review of Earth and Planetary Sciences*, 39, 1-29.

Cardozo, N. and Allmendinger, R. W., 2013, Spherical projections with OSXStereonet: Computers & Geosciences, v. 51, no. 0, p. 193 - 205, doi: 10.1016/j.cageo.2012.07.021

Carstens, H. 1961. A post-Caledonian ultrabasic biotite lamprophyre dyke of the Island Ytterøy in the Trondheimsfjord, Norway. *Norwegian Geological Survey Bulletin*, 215, 10-21.

Cocks, L.R.M. and Torsvik, T.H. 2005. Baltica from the late Precambrian to mid-Palaeozoic times: the gain and loss of a terrane's identity. *Earth-Science Reviews,* 72**,** 39-66.

Corfu, F., Andersen, T. and Gasser, D. 2014. The Scandinavian Caledonides: main features, conceptual advances and critical questions. *Geological Society, London, Special Publications,* 390**,** 9-43.

Cullers, R. L., Barrett, T., Carlson, R. and Robinson, B. 1987. Rare-earth element and mineralogic changes in Holocene soil and stream sediment: a case study in the Wet Mountains, Colorado, USA. *Chemical geology*, 63(3), 275-297.

Dewey, J.F. and Burke, K. 1974. Hot spots and continental break-up: implications for collisional orogeny. *Geology,* 2**,** 57-60.

Dickin, A.P. 2005. *Radiogenic Isotope Geology*. 2nd ed. Cambridge: Cambridge University Press, 101-135.

Dickinson, W. R. and Gehrels, G. E. 2009. Use of U–Pb ages of detrital zircons to infer maximum depositional ages of strata: a test against a Colorado Plateau Mesozoic database. *Earth and Planetary Science Letters*, 288(1), 115-125.

Dunning, G. and Grenne, T. 2000. U-Pb age dating and paleotectonic significance of trondhjemite from the type locality in the Central Norwegian Caledonides. *Norwegian Geological Survey Bulletin,* 437**,** 57-66.

Dunning, G. R. and Pedersen, R. B. 1988. U/Pb ages of ophiolites and arc-related plutons of the Norwegian Caledonides: implications for the development of Iapetus. *Contributions to Mineralogy and Petrology*, 98(1), 13-23.

Fink, J. H. and Reches, Z. E. 1983. Diagenetic density inversions and the deformation of shallow marine chert beds in Israel. *Sedimentology*, 30(2), 261-271.

Fossen, H. 1992. The role of extensional tectonics in the Caledonides of south Norway. *Journal of structural geology*, 14(8), 1033-1046.

Furnes, H., Roberts, D., Sturt, B. A., Thon, A. and Gale, G. H. 1980. Ophiolite fragments in the Scandinavian Caledonides. In: Panayiotou, A.,(Ed.), *Ophiolites,* Cyprus: Proceedings of the International Ophiolite Symposium, pp. 582-600.

Furnes, H., Dilek, Y. and Pedersen, R. B. 2012. Structure, geochemistry, and tectonic evolution of trench-distal backarc oceanic crust in the western Norwegian Caledonides, Solund-Stavfjord ophiolite (Norway). *Geological Society of America Bulletin*, 124(7-8), 1027-1047.

Gale, G. H., and Pearce, J. A. 1982. Geochemical patterns in Norwegian greenstones. *Canadian Journal of Earth Sciences*, 19(3), 385-397.

Gasser, D., Grenne, T., Corfu, F. and Augland, L., E., 2016. Characterization of depositional age and structure of sedimentary successions by U-Pb TIMS and LA-ICP-MS dating of volcanic horizons and detrital zircons: an example from the western Trondheim Nappe Complex, Scandinavian Caledonides. *Geophysical Research Abstracts*, 18, EGU2016-12961, 2016

Gee, D.G., Guezou, J.C., Roberts, D. and Wolff, F.C. 1985. The central-southern part of the Scandinavian Caledonides. ln: Gee,D.G.& Sturt , BA (ed.): *The Caledonide Orogen - Scandinavia and Rel ted Areas.* Chichester: John Wiley & Sons, 109-133.

Gee, D. G., Ladenberger, A., Dahlqvist, P., Majka, J., Be'eri-Shlevin, Y., Frei, D. and Thomsen, T. 2014. The Baltoscandian margin detrital zircon signatures of the central Scandes. *Geological Society, London, Special Publications*, 390(1), 131-155.

Grenne, T. 1987. Marginal basin type metavolcanites of the Hersjø Formation, eastern Trondheim District, Central Norwegian Caledonides. *Norwegian Geological Survey Bulletin*, 412, 29-42.

Grenne, T. 1989. Magmatic evolution of the Løkken SSZ Ophiolite, Norwegian Caledonides: Relationships between anomalous lavas and high-level intrusions. *Geological Journal*, *24*(4), 251-274.

Grenne, T. and Lagerblad, B. 1985. The Fundsjø group, central Norway–a Lower Palaeozoic island arc sequence: geochemistry and regional implications. . ln: Gee,D.G.& Sturt , BA (ed.): *The Caledonide Orogen - Scandinavia and Related Areas.* Chichester: John Wiley & Sons, 745-762.

Grenne, T. and Slack, J. F. 2003. Bedded jaspers of the Ordovician Løkken ophiolite, Norway: seafloor deposition and diagenetic maturation of hydrothermal plume-derived silica-iron gels. *Mineralium Deposita*, *38*(5), 625-639.

Grenne, T., Ihlen, P. and Vokes, F. 1999. Scandinavian Caledonide metallogeny in a plate tectonic perspective. *Mineralium Deposita,* 34**,** 422-471.

Gromet, L. P., Haskin, L. A., Korotev, R. L. and Dymek, R. F. 1984. The "North American shale composite": its compilation, major and trace element characteristics. *Geochimica et Cosmochimica Acta*, 48(12), 2469-2482.

Heim, M., Grenne, T. and Prestvik, T. 1987. The Resfjell ophiolite fragment, Southwest Trondheim Region, Central Norwegian Caledonides. *Norwegian Geological Survey Bulletin*, 409, 49-71

Jackson, S. E., Pearson, N. J., Griffin, W. L. and Belousova, E. A. 2004. The application of laser ablation-inductively coupled plasma-mass spectrometry to in situ U–Pb zircon geochronology. *Chemical Geology*, *211*(1), 47-69.

Jones, D. L. and Murchey, B. 1986. Geologic significance of Paleozoic and Mesozoic radiolarian chert. *Annual Review of Earth and Planetary Sciences*, 14, 455.

Kartverket, Norgeskart. Available at: http://www.norgeskart.no (accessed May 2016)

Krill, A. G. 1980. Tectonics of the Oppdal area, central Norway. *GFF,* 102**,** 523-530.

Kühn, A., Glodny, J., Austrheim, H. and Raheim, A. 2000. The Caledonian tectono-metamorphic evolution of the Lindas Nappe: constraints from U-Pb, Sm-Nd and Rb-Sr ages of granitoid dykes. *Norsk Geologisk Tidsskrift*, 82(1), 45-58.

Le Bas, M. J., Le Maitre, R. W., Streckeisen, A. and Zanettin, B. 1986. A chemical classification of volcanic rocks based on the total alkali-silica diagram. *Journal of petrology*, 27(3), 745-750.

Letters from Godwana, an introduction to diatoms. Available at: https://paleonerdish.wordpress.com/2013/06/10/an-introduction-to-diatoms/ (Accessed 19.05.16)

Ludwig, K. R. 2001. Isoplot/Ex 2.49, a Geochronological Toolkit for Microsoft Excel. *Berkeley Geochronology Center, Berkeley, CA. Special Publication 1a*.

McClellan, E.A. 1994. Contact relationships in the southeastern Trondheim Nappe Complex, central-southern Norway: implications for early Paleozoic tectonism in the Scandinavian Caledonides. *Tectonophysics*, 231**,** 85-111.

Moores, E. M. 1982. Origin and emplacement of ophiolites. *Reviews of Geophysics*, 20(4), 735-760.

Murray, R. W. 1994. Chemical criteria to identify the depositional environment of chert: general principles and applications. *Sedimentary Geology*, *90*(3), 213-232.

Murray, R. W., ten Brink, M. R. B., Jones, D. L., Gerlach, D. C. and Russ, G. P. 1990. Rare earth elements as indicators of different marine depositional environments in chert and shale. *Geology*, 18(3), 268-271.

Murray, R. W., Ten Brink, M. R. B., Gerlach, D. C., Russ, G. P. and Jones, D. L. 1991. Rare earth, major, and trace elements in chert from the Franciscan Complex and

Monterey Group, California: Assessing REE sources to fine-grained marine sediments. *Geochimica et Cosmochimica Acta*, 55(7), 1875-1895.

Murray, R. W., Brink, M. R. B., Gerlach, D. C., Russ, G. P. and Jones, D. L. 1992. Interoceanic variation in the rare earth, major, and trace element depositional chemistry of chert: perspectives gained from the DSDP and ODP record. *Geochimica et Cosmochimica Acta*, 56(5), 1897-1913.

Nesbitt, H. W. 1979. Mobility and fractionation of rare earth elements during weathering of a granodiorite. *Nature* 279, 206 – 210.

Nesse, W. D. 2013. *Introduction to Optical Mineralogy*.4th ed. Oxford: Oxford University Press. 361 pp.

Nilsen, O., Sundvoll, B., Roberts, D. and Corfu, F. 2003. U-Pb geochronology and geochemistry of trondhjemites and a norite pluton from the SW Trondheim Region, Central Norwegian Caledonides. *Norwegian Geological Survey Bulletin*, 441, 5-16.

Nilsen, O., Corfu, F. and Roberts, D. 2007. Silurian gabbro-diorite-trondhjemite plutons in the Trondheim Nappe Complex, Caledonides, Norway: petrology and U-Pb geochronology. *Norwegian Geological Journal*, 87(3), 329.

Nilsen, O. and Wolff, F.C. 1989. Geological map of Norway, bedrock map Røros & Sveg, 1:250 000, Trondheim: Norwegian Geological Survey.

Okay, A. I., Noble, P. J. and Tekin, U. K. 2011. Devonian radiolarian ribbon cherts from the Karakaya Complex, Northwest Turkey: implications for the Paleo-Tethyan evolution. *Comptes Rendus Palevol*, 10(1), 1-10.

Pearce, J. A. 1982. Trace element characteristics of lavas from destructive plate boundaries. *Andesites*, 8, 525-548.

Pearce, J. A. 1983. The role of sub-continental lithosphere in magma genesis at destructive plate margins. In: C. J. Hawkesworth & M. J. Norry (eds). *Continental basalts and mantle xenoliths.*, 230-49. Nantwich: Shiva

Pearce, J. A. and Cann, J. R. 1973. Tectonic setting of basic volcanic rocks determined using trace element analyses. *Earth and planetary science letters*, 19(2), 290-300.

Pedersen, R. B., Bruton, D. L. and Furnes, H. 1992. Ordovician faunas, island arcs and ophiolites in the Scandinavian Caledonides. *Terra Nova*, 4(2), 217-222.

Pufahl, P.K., 2010, Bioelemental Sediments, In: James, N.P. and Dalrymple, R.W. (Eds.), *Facies Models 4*, GEOtext 6 Geological Association of Canada, Newfoundland and Labrador, Canada, p. 477-503

Ramberg, I.B., Bryhni, I., Nøttvedt, A. and Rangnes, K. (ed.) 2008. *The Making of a Land - Geology of Norway*, Trondheim: Norwegian Geological Association.

Roberts, D. 2003. The Scandinavian Caledonides: event chronology, palaeogeographic settings and likely modern analogues. *Tectonophysics,* 365**,** 283-299.

Roberts, D. and Gee, D. G. 1985. An introduction to the structure of the Scandinavian Caledonides. ln: Gee,D.G.& Sturt , BA (ed.): *The Caledonide Orogen - Scandinavia and Related Areas.* Chichester: John Wiley & Sons, 55-68.

Roberts, D. and Stephens, M. 2000. Caledonian orogenic belt. *Description to the bedrock map of central Fennoscandia (Mid-Norden). Geological Survey of Finland Special Paper,* 28**,** 78-104.

Roberts, D. and Tucker, R. D. 1998. Late Cambrian U-Pb zircon age of a metatrondhjemite from Ytterøya, Trondheimsfjorden, central Norwegian Caledonides. *Norsk Geologisk Tidsskrift*, *78*, 253-258.

Roberts, D. and Wolff, F. 1981. Tectonostratigraphic development of the Trondheim region Caledonides, central Norway. *Journal of Structural Geology*, 3**,** 487-494.

Roberts, D., Grenne, T. and Ryan, P. 1984. Ordovician marginal basin development in the central Norwegian Caledonides. *Geological Society, London, Special Publications*, 16(1), pp.233-244.

Roberts, D., Nordgulen, Ø. and Melezhik, V. 2007. The Uppermost Allochthon in the Scandinavian Caledonides: From a Laurentian ancestry through Taconian orogeny to Scandian crustal growth on Baltica. *Geological Society of America Memoirs*, 200, 357-377.

Roberts, D., Walker, N., Slagstad, T., Solli, A. and Krill, A. 2002. U-Pb zircon ages from the Bymarka ophiolite, near Trondheim, central Norwegian Caledonides, and regional implications. *Norwegian Geological Journal*, *82*(1), 19-30.

Rohr-Torp, E. 1972. A major inversion of the western part of the Trondheim Nappe. *Norwegian Geological Journal*, 52, 453-458.

Rohr-Torp, E. 1974. Contact metamorphism around the Innset massif. *Norwegian Geological Journal*, 54, 13-33.

Rollinson, H. 2013. *Using geochemical data*. London: Routledge. 352 pp.

Root, D. and Corfu, F. 2012. U–Pb geochronology of two discrete Ordovician high-pressure metamorphic events in the Seve Nappe Complex, Scandinavian Caledonides. *Contributions to Mineralogy and Petrology*, 163(5), pp.769-788.

Skår, Ø. (2002). U–Pb geochronology and geochemistry of early Proterozoic rocks of the tectonic basement windows in central Nordland, Caledonides of north-central Norway. *Precambrian Research*, *116*(3), 265-283.

Slagstad, T. 2003. Geochemistry of trondhjemites and mafic rocks in the Bymarka ophiolite fragment, Trondheim, Norway: petrogenesis and tectonic implications. *Norwegian Geological Journal*, *83*(3), 167-185.

Slagstad, T., Pin, C., Roberts, D., Kirkland, C., Grenne, T., Dunning, G., Sauer, S. and Andersen, T. 2013. Tectonomagmatic evolution of the Early Ordovician suprasubduction-zone ophiolites of the Trondheim Region, Mid-Norwegian Caledonides. *Geological Society, London, Special Publications*, 390(1), pp.541-561.

Steiger, R. and Jäger, E. 1977. Subcommission on geochronology: convention on the use of decay constants in geo-and cosmochronology. *Earth and planetary science letters*, *36*(3), 359-362.

Sturt, B. A., Pringle, I. R. and Ramsay, D. M. 1978. The Finnmarkian phase of the Caledonian orogeny. *Journal of the Geological Society*, *135*(6), 597-610.

Sun, S. and McDonough, W. (1989). Chemical and isotopic systematics of oceanic basalts: implications for mantle composition and processes. *Geological Society, London, Special Publications*, 42(1), pp.313-345.

Torsvik, T.H. and Cocks, L.R.M. 2005. Norway in space and time: a centennial cavalcade. *Norwegian Journal of Geology*, 85**,** 73-86.

Torsvik, T.H., Smethurst, M., Meert, J.G., Van der Voo, R., McKerrow, W., Brasier, M., Sturt, B. and Walderhaug, H. 1996. Continental break-up and collision in the Neoproterozoic and Palaeozoic—a tale of Baltica and Laurentia. *Earth-Science Reviews*, 40**,** 229-258.

Tucker, M. R. 2001. *Sedimentary Petrology.* 3rd ed. United Kingdom: Blackwell Science. 262 pp.

Tucker, R. D., Robinson, P., Solli, A., Gee, D. G., Thorsnes, T., Krogh, T. E., Nordgulen, Ø. and Bickford, M. 2004. Thrusting and extension in the Scandian hinterland, Norway: New U-Pb ages and tectonostratigraphic evidence. *American Journal of Science*, 304**,** 477-532.

Yoshinobu, A. S., Barnes, C. G., Nordgulen, Ø., Prestvik, T., Fanning, M. and Pedersen, R. B. 2002. Ordovician magmatism, deformation, and exhumation in the Caledonides of central Norway: An orphan of the Taconic orogeny? *Geology*, *30*(10), 883-886.

Van Achterbergh, E., Ryan, C. G., Jackson, S. E. and Griffin, W. L. 2001. Data reduction software for LA-ICP-MS. *Laser-Ablation-ICPMS in the earth sciences—principles and applications. Miner Assoc Can (short course series)*, *29*, 239-243.

Van Soest, R. W., Boury-Esnault, N., Vacelet, J., Dohrmann, M., Erpenbeck, D., De Voogd, N. J., ... and Hooper, J. N. 2012. Global diversity of sponges (Porifera). *PLoS one*, 7(4), e35105.

Van Staal, C. R., Whalen, J. B., Valverde-Vaquero, P., Zagorevski, A. and Rogers, N. 2009. Pre-Carboniferous, episodic accretion-related, orogenesis along the Laurentian margin of the northern Appalachians. *Geological Society, London, Special Publications*, *327*(1), 271-316.

Vermeesch, P. 2012. On the visualisation of detrital age distributions. *Chemical Geology*, *312*,190-194.

Vogt, T. 1945. The geology of part of the Hølonda-Horg district, a type area in the Trondheim region. *Norsk Geologisk Tidsskrift*, *25*, 449-528.

Walsh, J. J. 1983. Secondary elemental mobility within the Støren greenstones, Norway. *Norwegian Geological Journal*, *63*, 27-37.

Walsh, J. J. 1986. *The geology of the Caledonian rocks of SE Meldal, Sør Trøndelag, Norway*. PhD. University College Gallway.

Wiedenbeck, M. A. P. C., Alle, P., Corfu, F., Griffin, W. L., Meier, M., Oberli, F., ... and Spiegel, W. 1995. Three natural zircon standards for U-Th-Pb, Lu-Hf, trace element and REE analyses. *Geostandards newsletter*, *19*(1), 1-23.

Wilson, J. T. 1966. Did the Atlantic close and then re-open?, *Nature*, 211, 676-681.

Wilson, M. 1989. *Igneous Petrology: A global tectonic approach*. 1st ed. London:Chapman & Hall. 466 pp.

Winter, J.D. 2010. *Principles of Igneous and Metamorphic Petrology.* 2nd ed. New Jersey: Pearson Education. 702 pp.

Wolff, F., 1976. Geological map of Norway, bedrock map Trondheim, 1:250 000, Trondheim: Norwegian Geological Survey.

Wood, D. A. 1980. The application of a Th Hf Ta diagram to problems of tectonomagmatic classification and to establishing the nature of crustal contamination of basaltic lavas of the British Tertiary Volcanic Province. *Earth and planetary science letters*, *50*(1), 11-30.

Appendix 1 – Maps of Dugurdsknappen

Five maps with structural measurements collected during fieldwork are presented, as well as one map indicating the amount of areas covered by vegetation, marshes and water. The last map is not entirely accurate, but represents a minimum estimate. The legend below applies for all maps in appendix and in the thesis itself.

Structure maps:

- Map 1 – Strata
- Map 2 – Foliation, penetrative and inclined
- Map 3 – Fold axes and axial planes
- Map 4 – Fold axes
- Map 5 – Faults, joints, shear and lineation

Cover map:

- Map 6 – Cover map, vegetation, marshes and water

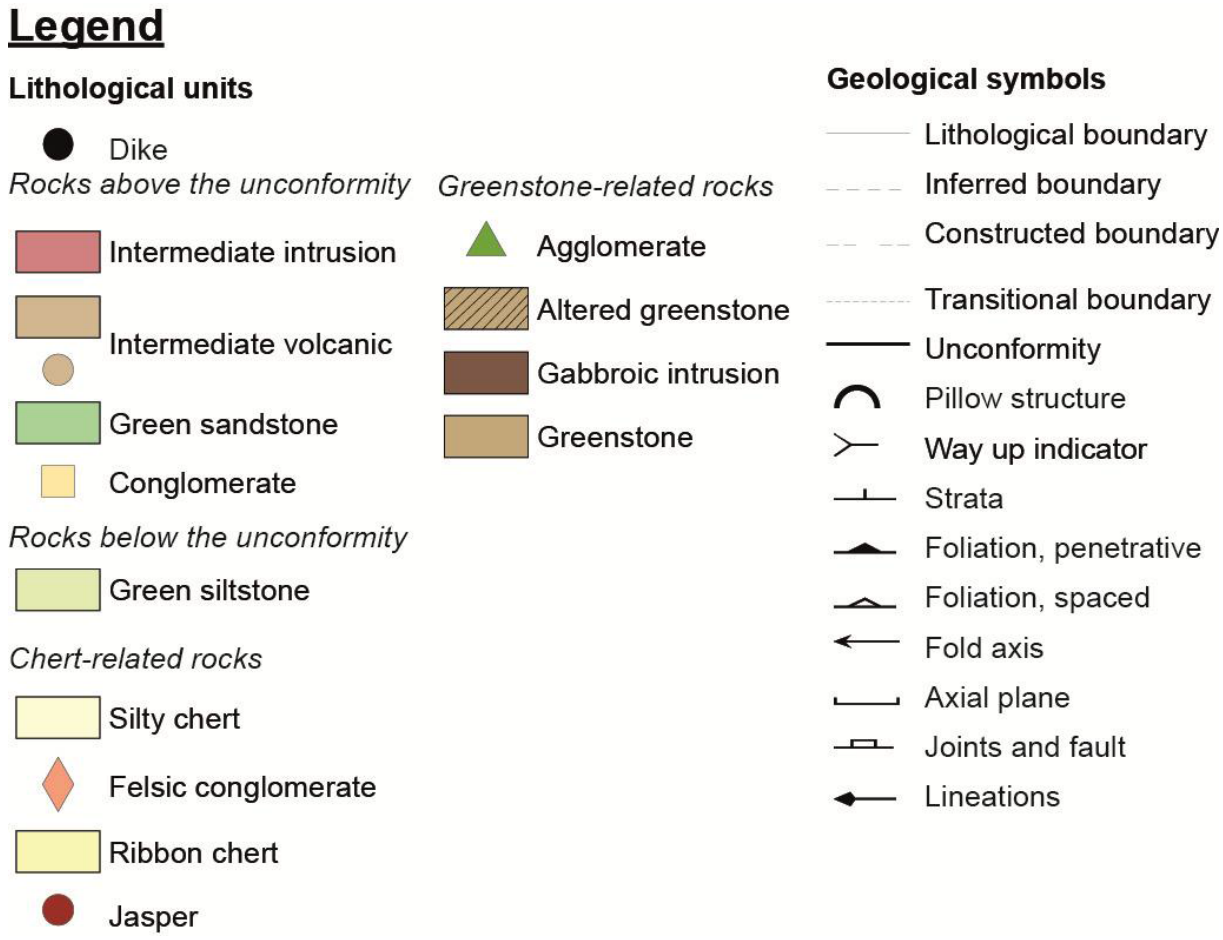

Map 1 - Strata

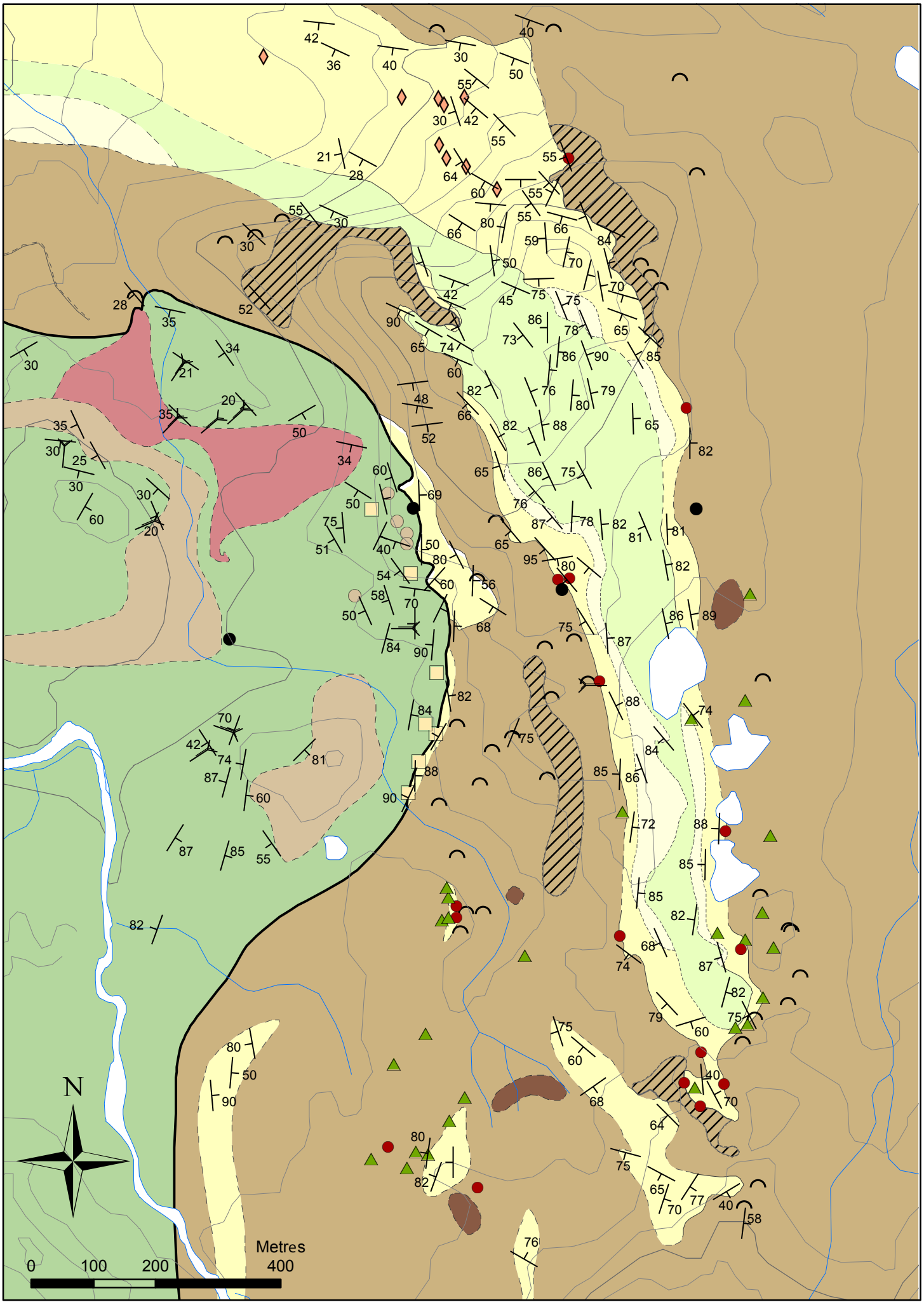

Map 2 - Foliation, penetrative and spaced

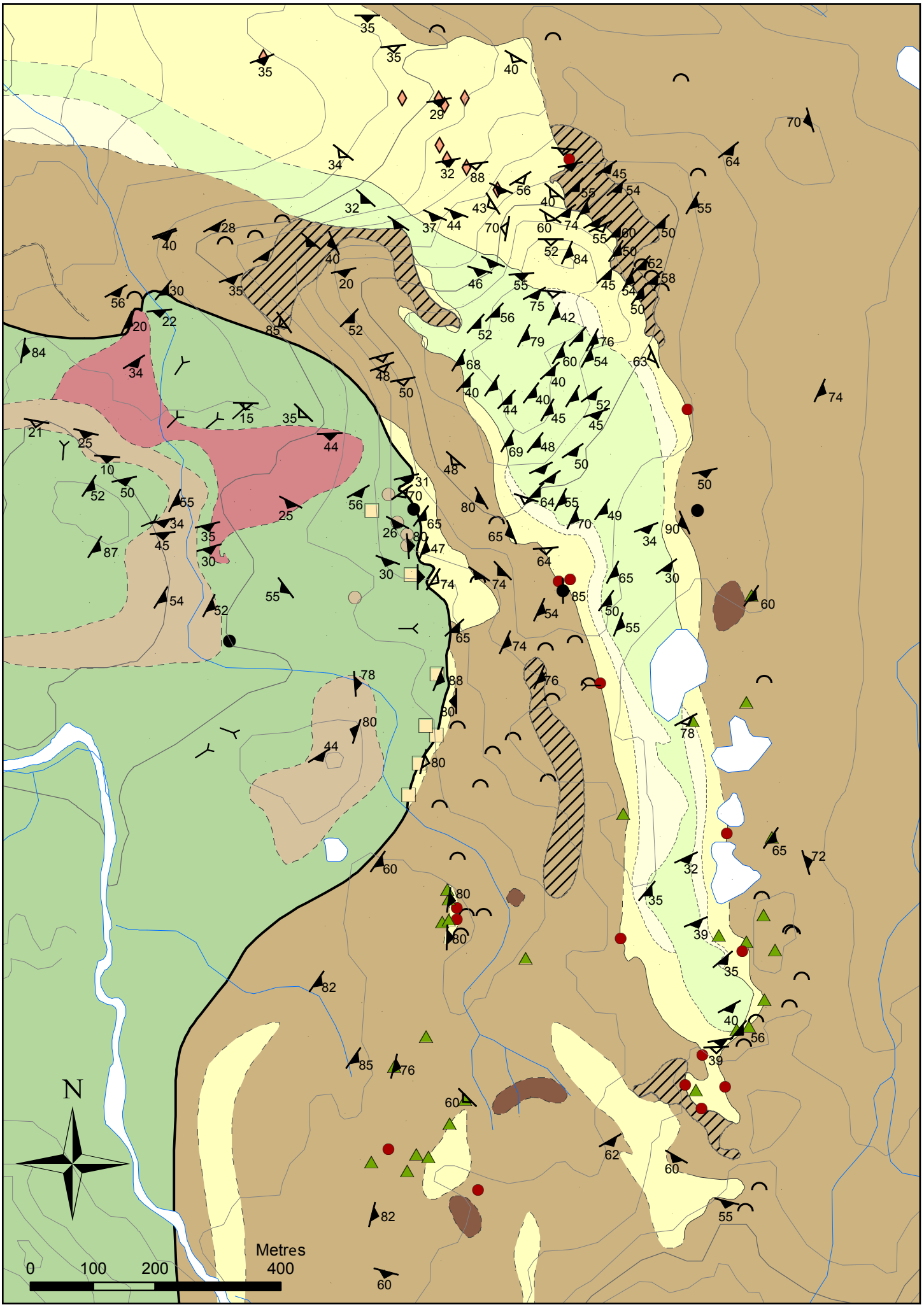

Map 3 - Fold axes and axial planes

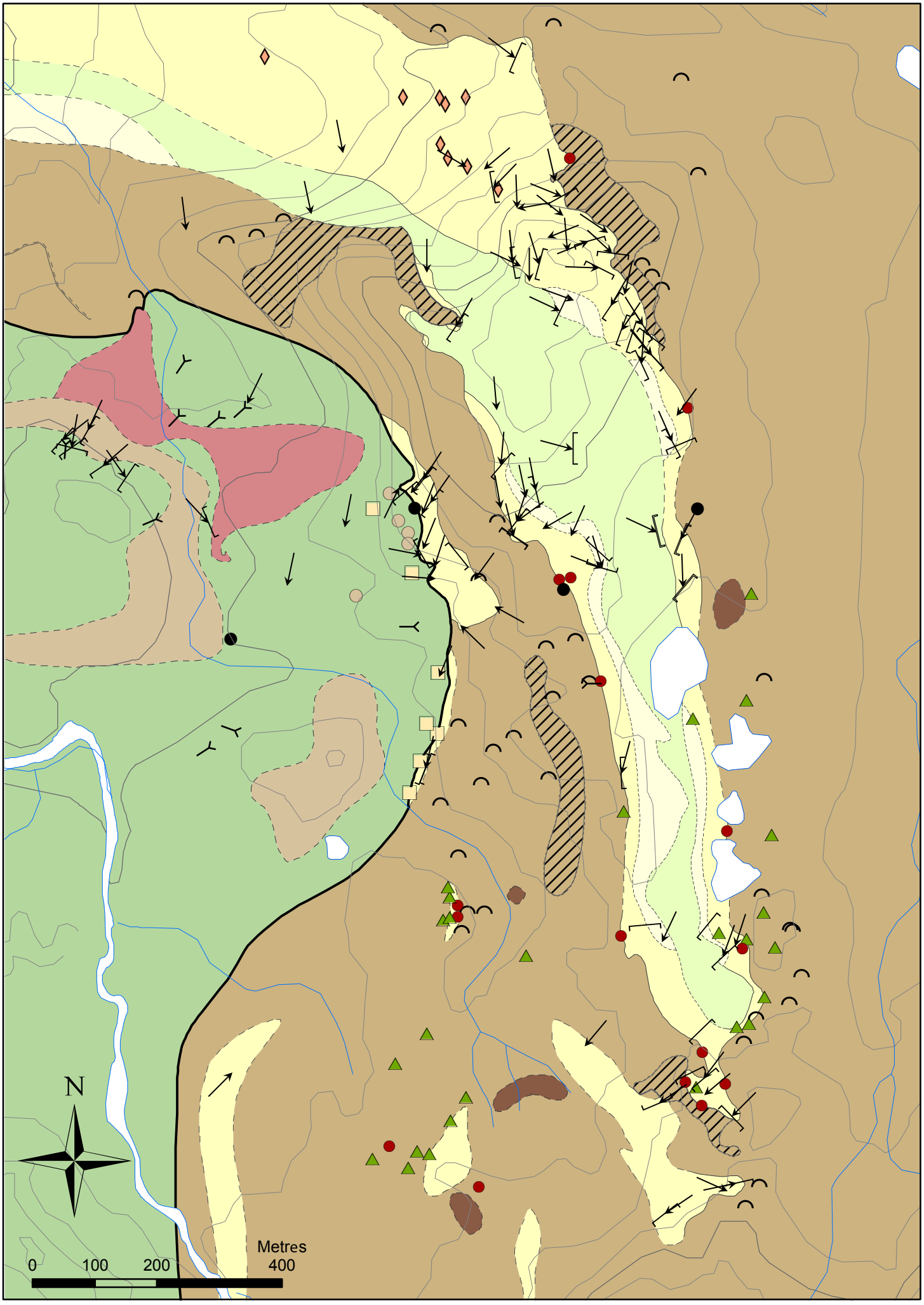

Map 4 - Fold axes

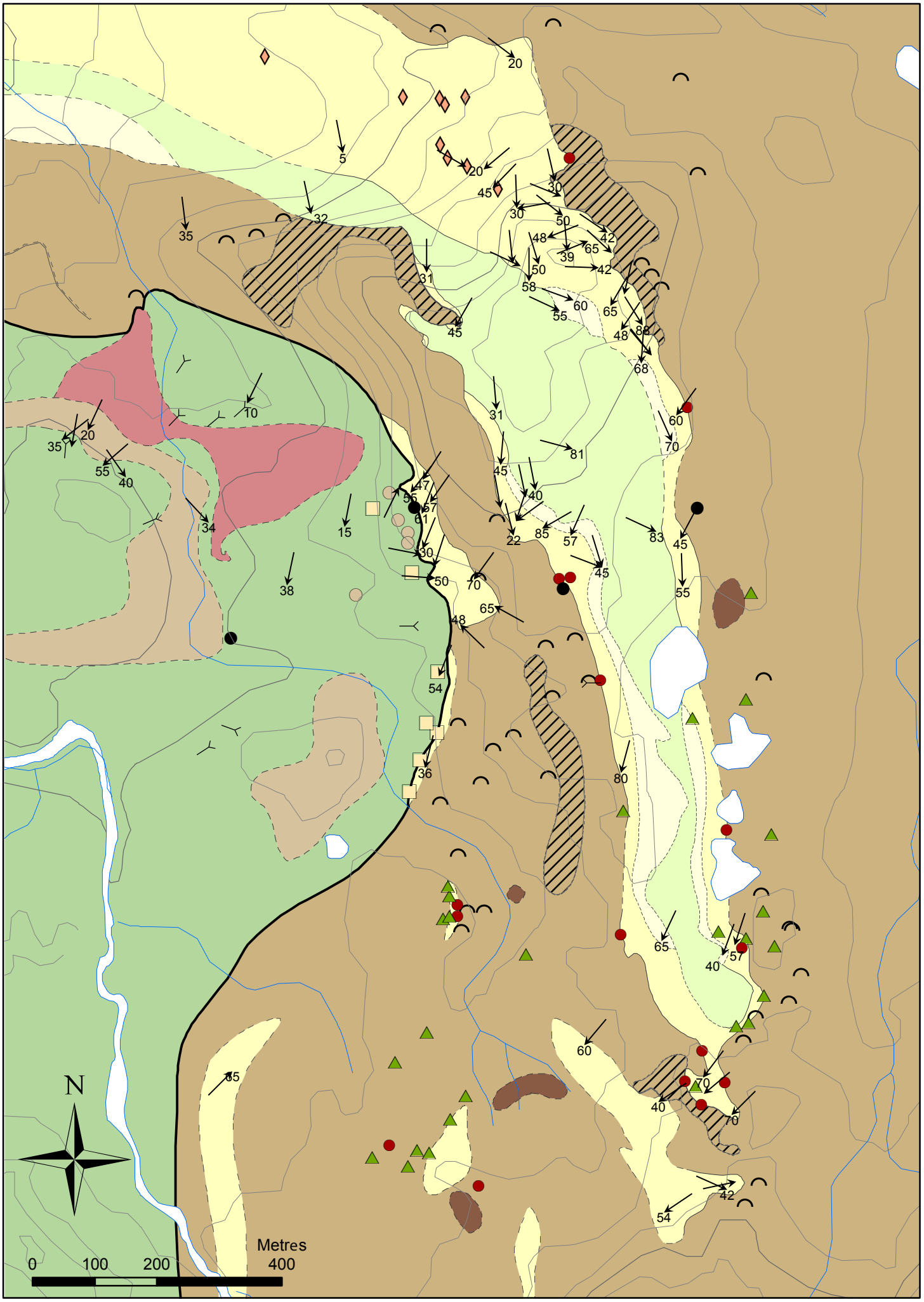

Map 5 - Faults, joints, shear and lineations

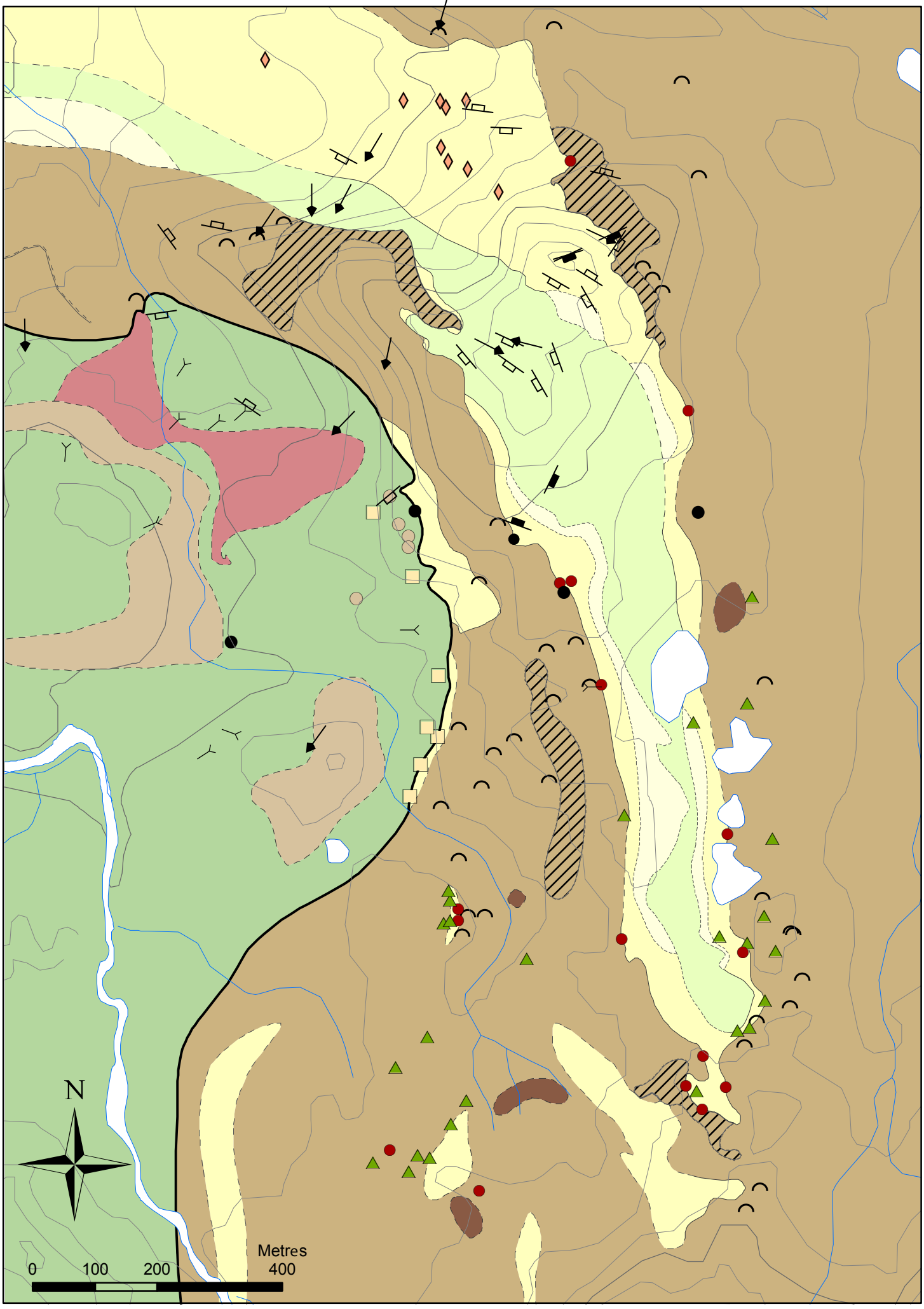

Map 6 - Cover map, vegetation, marshes and water

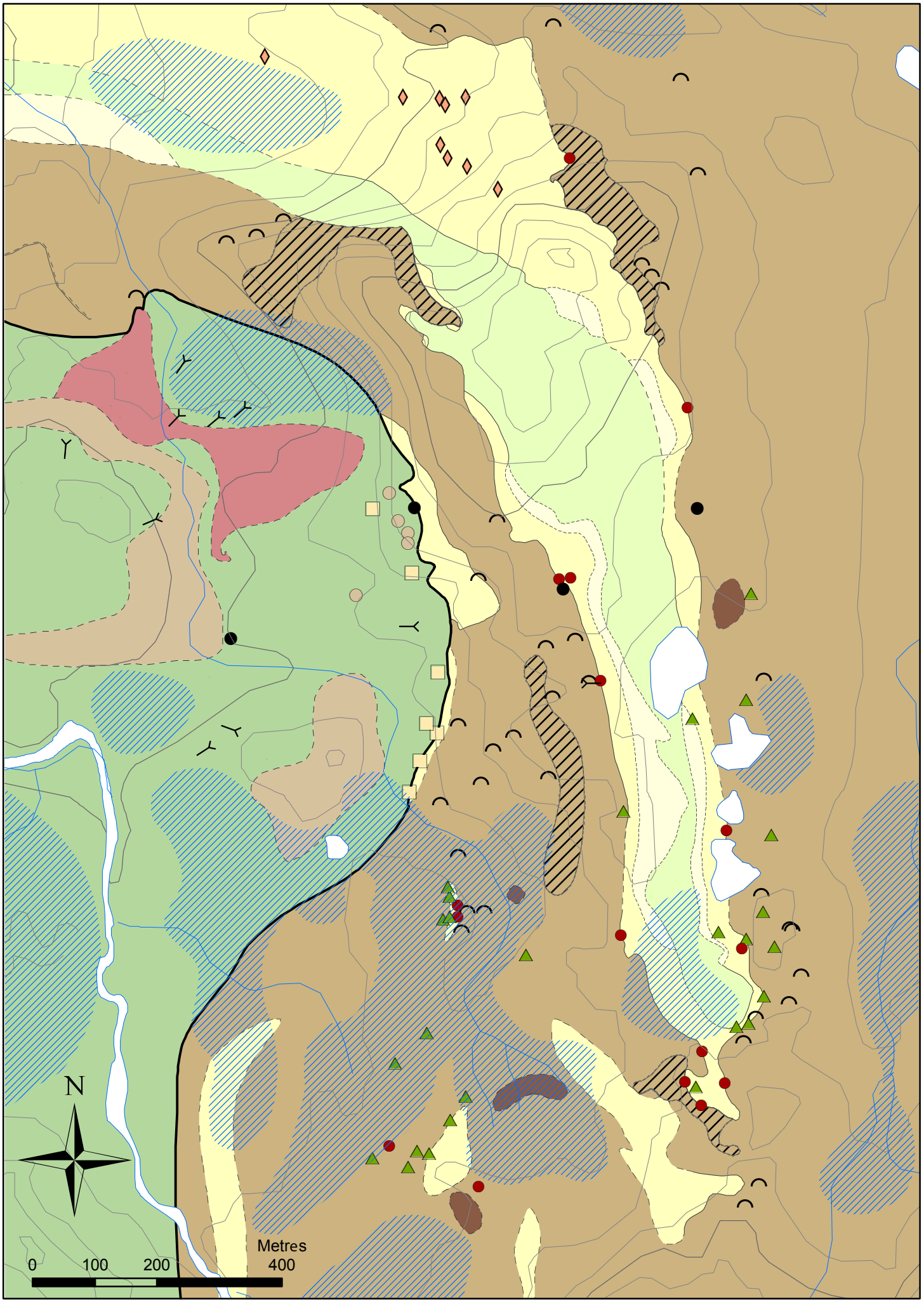

Appendix 2 – Geochemical analyses

Table A: XRF-analysis of major elements (wt%)

Sample	SiO2	Al2O3	FeO	Fe2O3	TiO2	MgO	CaO	Na2O	K2O	MnO	P2O5	LOI	BaO	Cr2O3	CuO	NiO	PbO	SrO	ZnO	V2O5	ZrO2	SO3
Greenstone-related rocks																						
EST_48B	50.4	15.9	7.3	8.07	1.15	6.41	10.8	3.67	0.201	0.121	0.141	2.66	<0.025	0.049	0.015	0.016	<0.01	<0.04	<0.01	0.052	<0.02	<0.1
EST_64	47.9	15.5	8.4	9.28	1.44	8.62	8.67	3.30	0.316	0.157	0.225	3.16	<0.025	0.093	<0.01	0.033	<0.01	<0.04	<0.01	0.049	<0.02	<0.1
EST_79B	47.6	15.2	9.3	10.3	1.93	7.95	8.69	3.35	0.309	0.163	0.269	3.06	<0.025	0.039	<0.01	0.014	<0.01	<0.04	<0.01	0.060	0.021	<0.1
EST_160	48.4	16.3	9.6	10.7	2.15	6.99	7.89	2.39	0.040	0.148	0.343	3.89	<0.025	0.036	0.011	0.013	<0.01	<0.04	0.011	0.054	0.023	<0.1
EST_849	48.5	14.4	7.7	8.55	1.29	7.72	10.9	3.58	0.091	0.174	0.150	3.92	<0.025	0.046	<0.01	0.015	<0.01	<0.04	<0.01	0.052	<0.02	<0.1
EST_445	48.6	14.3	8.6	9.51	1.74	10.0	8.03	3.33	0.328	0.195	0.225	3.15	<0.025	0.080	<0.01	0.018	<0.01	<0.04	<0.01	0.045	<0.02	<0.1
EST_400	52.5	14.2	4.7	5.27	1.11	2.61	11.8	3.80	0.325	0.151	0.181	6.97	<0.025	<0.02	<0.01	<0.01	<0.01	<0.04	<0.01	0.034	<0.02	<0.1
EST_142	61.7	14.5	8.3	9.20	1.53	1.02	3.44	4.22	1.45	0.290	0.698	1.33	<0.025	0.063	<0.01	<0.01	<0.01	<0.04	<0.01	<0.02	<0.02	<0.1
EST_345	47.2	18.7	14.4	16.0	2.65	2.91	2.57	0.21	5.02	0.228	0.205	3.32	0.052	0.102	<0.01	0.014	<0.01	<0.04	0.015	<0.02	0.031	<0.1
EST_79A	54.3	15.1	9.0	10.0	1.12	3.39	10.9	1.04	0.333	0.163	0.181	2.69	<0.025	0.105	<0.01	0.019	<0.01	0.090	<0.01	0.035	<0.02	<0.1
EST_85	49.2	17.4	9.6	10.7	1.39	6.53	3.57	4.39	2.70	0.198	0.122	2.65	<0.025	0.096	<0.01	0.024	<0.01	<0.04	0.012	0.035	<0.02	<0.1
EST_179	55.9	14.2	7.8	8.63	1.09	6.65	5.51	1.94	0.959	0.151	0.200	3.35	<0.025	0.062	<0.01	0.019	<0.01	0.078	<0.01	0.026	<0.02	<0.1
EST_372	46.9	19.3	11.7	13.0	1.58	4.33	3.36	3.50	4.90	0.168	0.168	2.08	0.068	0.138	<0.01	0.027	<0.01	<0.04	0.012	0.035	<0.02	<0.1
EST_421	51.6	17.4	10.3	11.4	1.54	3.96	2.51	4.26	3.31	0.145	0.226	2.39	0.054	0.044	<0.01	0.015	<0.01	<0.04	0.010	<0.02	<0.02	<0.1
EST_629	52.6	17.6	10.3	11.4	2.10	2.92	2.25	7.21	1.21	0.107	0.418	1.62	<0.025	0.037	<0.01	0.018	<0.01	<0.04	0.012	0.025	0.023	<0.1
Chert-related rocks																						
EST_392	93.0	0.183	4.8	5.29	0.011	0.161	0.105	<0.1	0.040	0.041	0.044	0.020	<0.025	<0.02	<0.01	<0.01	<0.01	<0.04	<0.01	<0.02	<0.02	<0.1
EST_390	93.8	2.17	1.0	1.12	0.093	0.585	0.082	0.19	0.576	0.027	0.026	0.473	<0.025	<0.02	<0.01	<0.01	<0.01	<0.04	<0.01	<0.02	<0.02	<0.1
EST_717	95.0	1.78	0.9	1.04	0.071	0.549	0.054	0.17	0.408	0.043	0.029	0.569	<0.025	<0.02	<0.01	<0.01	<0.01	<0.04	<0.01	<0.02	<0.02	<0.1
EST_843	95.6	1.60	1.1	1.27	0.079	0.431	0.085	0.12	0.390	0.103	0.028	0.385	<0.025	<0.02	<0.01	<0.01	<0.01	<0.04	<0.01	<0.02	<0.02	<0.1
EST_349	86.4	5.14	2.5	2.83	0.244	1.32	0.240	0.48	1.19	0.181	0.052	1.11	<0.025	<0.02	<0.01	<0.01	<0.01	<0.04	<0.01	<0.02	<0.02	<0.1
EST_375	77.6	8.56	4.6	5.11	0.429	1.80	0.436	1.18	1.86	0.371	0.071	1.56	<0.025	<0.02	<0.01	<0.01	<0.01	<0.04	<0.01	<0.02	<0.02	<0.1
EST_30	61.4	18.3	3.8	4.19	0.251	3.04	1.13	3.50	3.40	0.117	0.117	3.19	<0.025	<0.02	<0.01	<0.01	<0.01	<0.04	<0.01	<0.02	0.151	<0.1
EST_19	42.5	10.5	7.4	8.25	0.922	12.0	9.68	<0.1	2.97	0.333	0.844	10.2	0.043	0.162	0.013	0.057	<0.01	0.055	<0.01	0.026	0.049	<0.1
EST_317A	62.5	17.6	3.6	4.05	0.290	2.43	1.04	5.64	2.84	0.048	0.138	1.90	<0.025	<0.02	<0.01	<0.01	<0.01	<0.04	<0.01	<0.02	0.139	<0.1
EST_317B	58.0	19.7	4.3	4.83	0.501	2.55	1.27	5.91	3.60	0.059	0.208	1.82	0.029	<0.02	<0.01	<0.01	<0.01	<0.04	0.011	<0.02	0.195	<0.1
Green siltstone																						
EST_170	60.5	15.6	7.3	8.14	0.775	4.71	1.12	2.16	2.24	0.149	0.144	3.46	0.033	0.027	<0.01	0.012	<0.01	<0.04	0.012	0.029	<0.02	<0.1
EST_632	57.6	17.0	8.2	9.08	0.825	5.42	0.622	2.08	2.52	0.108	0.184	3.86	0.033	0.029	<0.01	0.015	<0.01	<0.04	0.016	0.027	<0.02	0.13
Rocks above the unconformity																						
EST_2	70.5	8.53	3.5	3.89	0.340	3.43	4.54	1.84	1.50	0.089	0.073	3.96	0.029	0.050	<0.01	0.018	<0.01	<0.04	<0.01	<0.02	<0.02	<0.1
EST_41	56.1	16.2	6.4	7.11	0.703	6.56	3.81	3.21	1.41	0.118	0.162	4.01	0.053	0.029	<0.01	<0.01	<0.01	0.053	<0.01	0.023	<0.02	<0.1
EST_766	55.2	16.5	7.1	7.90	0.884	5.06	6.49	2.89	1.50	0.134	0.138	2.56	0.028	<0.02	<0.01	<0.01	<0.01	0.042	<0.01	0.036	<0.02	<0.1
EST_700	55.2	14.3	6.8	7.54	0.634	7.02	6.52	2.84	1.20	0.141	0.123	2.54	0.043	0.033	<0.01	<0.01	<0.01	0.077	<0.01	0.030	<0.02	<0.1
EST_76	57.8	15.6	4.8	5.38	0.610	4.95	4.24	4.01	2.20	0.092	0.157	3.62	0.048	0.035	<0.01	<0.01	<0.01	0.057	<0.01	0.023	<0.02	<0.1

Table B: XRF-analysis of trace elements (ppm)

		EST_48B	EST_64	EST_79B	EST_160	EST_849	EST_445	EST_400	EST_142	EST_345	EST_79A	EST_85	EST_179	EST_372	EST_421	EST_629
As	**Greenstone-related rocks**	<10	<10	<10	<10	<10	<10	<10	<10	<10	<10	<10	<10	<10	<10	<10
Ba		29	57	52	12	15	85	75	224	436	46	167	140	578	450	181
Cd		<10	<10	<10	<10	<10	<10	<10	<10	<10	<10	<10	<10	<10	<10	<10
Ce		18	21	19	28	15	19	35	27	35	23	21	35	20	18	28
Co		32.9	55.3	40.8	47.5	34.3	33.7	15.1	28.9	56.4	37.4	61.3	40.4	63.0	47.5	55.2
Cr		341	620	264	325	313	516	74.5	398	662	632	584	416	845	290	237
Cu		106	16.4	43.3	90.5	57.2	31.6	<5	12.6	<5	50.2	<5	75.5	14.4	21.5	24.8
Ga		15.1	14.7	16.2	17.5	13.4	14.1	15.1	14.6	22.9	15.9	14.8	15.7	18.1	16.5	14.4
La		<15	<15	<15	<15	<15	<15	16	20	<15	<15	<15	16	<15	<15	<15
Mo		<3	<3	<3	<3	<3	<3	<3	<3	<3	<3	<3	<3	<3	<3	<3
Nb		10.0	13.2	12.9	21.2	7.6	10.0	11.4	16.4	26.4	10.7	11.8	10.9	13.9	6.5	18.8
Nd		<10	17	16	16	<10	14	12	33	12	16	13	19	10	14	17
Ni		131	268	119	126	122	152	19.7	67.8	132	163	205	163	216	134	153
Pb		<5	<5	<5	<5	<5	<5	<5	<5	7.2	<5	<5	14.1	<5	<5	<5
Rb		<5	6.6	5.8	<5	<5	<5	<5	29.8	147	7.7	51.0	24.9	90.5	74.1	22.1
Sb		<15	<15	<15	<15	<15	<15	<15	<15	<15	<15	<15	<15	<15	<15	<15
Sc		27.5	27.4	26.3	22.2	26.8	28.1	16.1	19.8	45.1	23.1	26.5	21.3	37.6	33.3	21.4
Sn		<5	<5	<5	<5	<5	<5	<5	<5	<5	<5	<5	<5	<5	<5	<5
Sr		244	197	219	272	209	268	310	271	241	650	122	628	270	108	126
Th		<3	<3	<3	<3	<3	<3	<3	<3	<3	<3	<3	4.6	<3	<3	<3
U		<5	<5	<5	<5	<5	<5	<5	<5	<5	<5	<5	<5	<5	<5	<5
V		257	250	298	279	236	256	179	45.4	139	177	221	174	204	132	145
W		<5	<5	<5	<5	<5	<5	<5	<5	n.a.	<5	<5	<5	<5	<5	<5
Y		22.8	26.8	34.5	38.7	26.9	30.6	23.5	45.5	18.3	25.8	13.7	24.4	21.7	26.7	41.5
Yb		<5	<5	<5	<5	<5	<5	<5	<5	<5	<5	<5	<5	<5	<5	<5
Zn		45.7	73.5	74.0	87.2	53.8	65.3	33.5	47.0	124	47.8	94.4	73.3	87.0	82.7	94.2
Zr		74.6	112	147	161	82.1	125	136	115	202	86.1	89.0	134	110	107	152
Cl		<0.02	<0.02	<0.02	<0.02	<0.02	<0.02	<0.02	<0.02	<0.02	<0.02	<0.02	<0.02	<0.02	<0.02	<0.02
F		<0.2	<0.2	<0.2	<0.2	<0.2	<0.2	<0.2	<0.2	<0.2	<0.2	<0.2	<0.2	<0.2	<0.2	<0.2
S		<0.1	<0.1	<0.1	<0.1	<0.1	<0.1	<0.1	<0.1	<0.1	<0.1	<0.1	<0.1	<0.1	<0.1	<0.1
Cs		<10	<10	<10	<10	<10	<10	<10	<10	<10	<10	<10	<10	<10	<10	<10
Hf		<5	<5	<5	6.0	<5	<5	<5	<5	5.3	<5	<5	<5	<5	<5	<5
Sm		<10	<10	<10	<10	<10	<10	<10	<10	<10	<10	<10	<10	<10	<10	<10
Ta		<5	<5	<5	<5	<5	<5	<5	<5	<5	<5	<5	<5	<5	<5	<5

		EST_392	EST_390	EST_717	EST_843	EST_349	EST_19	EST_375	EST_30	EST_317A	EST_317B		EST_170	EST_632		EST_2	EST_41	EST_766	EST_700	EST_76
As		<10	<10	<10	<10	<10	21	<10	<10	<10	<10		<10	<10		<10	<10	<10	<10	<10
Ba		<10	91	52	59	217	389	230	363	238	299		338	345		254	448	216	269	420
Cd		<10	<10	<10	<10	<10	<10	<10	<10	<10	<10		<10	<10		<10	<10	<10	<10	<10
Ce		<15	<15	<15	<15	28	118	42	559	552	517		46	46		35	47	22	25	41
Co		<4	<4	5.6	4.2	15.0	60.9	32.2	4.5	<4	7.0		27.1	29.0		14.4	23.6	23.4	24.2	19.2
Cr		103	83.1	11.0	61.9	67.6	1130	229	<5	41.1	38.8		287	209		380	243	89.1	254	224
Cu		<5	<5	<5	<5	11.2	111	<5	56.7	<5	23.8		5.3	33.2		<5	<5	65.7	10.5	18.6
Ga		<3	3.0	<3	<3	6.8	15.6	10.9	20.7	20.9	24.9		19.6	21.0		9.0	16.8	17.6	15.4	15.4
La		<15	<15	<15	<15	<15	46	<15	327	299	267		20	28		19	20	<15	<15	21
Mo		<3	<3	<3	<3	<3	<3	<3	<3	<3	<3		<3	<3		<3	<3	<3	<3	<3
Nb		2.5	3.3	3.5	2.5	9.3	21.7	8.0	40.2	34.1	68.0		11.6	12.3		5.3	8.5	7.0	7.1	9.6
Nd		<10	<10	<10	<10	<10	98	<10	198	188	187		16	18		16	20	<10	19	18
Ni		10.0	7.2	7.1	6.4	25.2	483	50.7	9.2	10.9	11.2		108	129		128	77.6	32.1	50.8	64.4
Pb		<5	<5	<5	<5	8.3	36.4	13.1	21.5	18.5	33.7		15.1	16.5		12.7	8.5	7.9	15.3	15.7
Rb		<5	25.6	17.5	14.3	52.1	246	79.2	141	111	168		86.0	94.1		57.4	45.8	46.0	32.8	77.7
Sb		<15	<15	<15	<15	<15	<15	<15	<15	<15	<15		<15	<15		<15	<15	<15	<15	<15
Sc		<5	<5	<5	<5	6.1	35.1	10.5	6.1	5.1	5.9		21.2	24.0		9.2	20.4	23.6	16.6	12.1
Sn		<5	<5	<5	<5	<5	7.9	<5	10.5	12.0	13.6		<5	<5		<5	<5	<5	<5	<5
Sr		<5	10.9	9.9	10.1	35.7	473	86.2	249	311	282		157	75.1		301	432	328	600	480
Th		<3	<3	<3	<3	<3	65.2	4.5	98.9	116	103		7.6	9.9		4.6	6.4	3.3	4.2	6.8
U		<5	<5	<5	<5	<5	10.9	<5	7.9	13.0	6.1		<5	<5		<5	<5	<5	<5	<5
V		79.9	19.2	16.9	16.8	38.9	178	70.1	<5	6.5	18.7		166	180		86.3	147	196	150	107
W		<5	<5	<5	<5	<5	n.a.	6.2	7.4	6.3	n.a.		5.7	<5		<5	<5	<5	<5	<5
Y		<3	3.2	<3	7.1	8.0	17.6	12.8	59.9	48.2	39.9		23.2	22.3		14.6	23.2	20.0	16.6	15.4
Yb		<5	<5	<5	<5	<5	<5	<5	5.9	<5	<5		<5	<5		<5	<5	<5	<5	<5
Zn		<5	13.1	11.6	7.5	35.2	72.7	53.5	62.4	73.9	83.3		105	122		37.5	79.1	63.1	75.1	51.9
Zr		<5	17.5	13.8	13.3	52.3	401	76.6	1210	1110	1430		133	141		93.5	148	112	102	141
Cl		<0.02	<0.02	<0.02	<0.02	<0.02	<0.02	<0.02	<0.02	<0.02	<0.02		<0.02	<0.02		<0.02	<0.02	<0.02	<0.02	<0.02
F		<0.2	<0.2	<0.2	<0.2	<0.2	0.20	<0.2	<0.2	<0.2	<0.2		<0.2	<0.2		<0.2	<0.2	<0.2	<0.2	<0.2
S		<0.1	<0.1	<0.1	<0.1	<0.1	<0.1	<0.1	<0.1	<0.1	<0.1		<0.1	<0.1		<0.1	<0.1	<0.1	<0.1	<0.1
Cs		<10	<10	<10	<10	<10	27	<10	17	18	24		<10	<10		<10	<10	<10	<10	<10
Hf		<5	<5	<5	<5	<5	10.9	<5	33.9	33.2	41.1		<5	<5		<5	5.4	<5	<5	<5
Sm		<10	<10	<10	<10	<10	22	<10	31	28	30		<10	<10		<10	<10	<10	<10	<10
Ta		<5	<5	<5	<5	<5	<5	<5	<5	<5	<5		<5	<5		<5	<5	<5	<5	<5

Chert-related rocks | **Green siltstone** | **Rocks above the unconformity**

Table C: LA-ICP-MS analysis of trace elements (ppm)

		EST_48b	EST_64	EST_160	EST_849	EST_79B	EST_445	EST_400	EST_142	EST_345	EST_79A	EST_85	EST_179	EST_372	EST_421	EST_629
LOI	**Greenstone-related rocks**	2.66	3.16	3.89	3.92	3.06	3.15	6.97	1.33	3.32	2.69	2.65	3.35	2.08	2.39	1.62
Be		<1	<1	<1	<1	1.0	<1	<1	<1	1.5	<1	<1	<1	1.1	<1	1.1
Y		22.7	19.4	30.0	24.1	26.1	22.2	18.0	32.3	18.6	26.3	12.7	16.2	18.4	17.1	42.9
Zr		83.5	92.9	142	88.0	124	105	119	90.7	221	85.7	88.5	91.9	101	79.4	184
Nb		9.68	11.5	17.6	7.13	10.2	8.14	9.21	13.8	27.2	9.42	9.68	7.74	13.1	4.57	20.6
Cs		<0.4	<0.4	<0.4	<0.4	<0.4	<0.4	<0.4	1.65	7.02	<0.4	3.28	1.54	6.73	3.33	0.79
Ba		31.5	61.3	12.1	16.9	57.5	73.2	77.0	176	399	55.3	168	136	537	370	182
La		7.38	8.58	14.1	6.26	9.98	6.78	13.7	18.3	9.68	11.0	6.88	12.8	9.04	5.24	19.2
Ce		17.3	22.5	34.4	15.3	26.4	19.0	29.6	27.0	44.5	20.1	22.0	32.0	22.8	14.5	39.6
Pr		2.30	2.76	4.23	1.98	3.43	2.39	3.51	5.69	2.74	3.18	1.97	3.44	2.56	1.70	5.27
Nd		11.4	12.8	20.2	10.7	16.3	12.9	15.5	28.2	13.4	15.6	9.76	15.0	12.4	9.18	25.8
Sm		3.46	3.82	6.06	3.31	5.14	3.89	3.88	7.99	3.45	4.47	2.77	3.80	3.26	2.73	7.27
Eu		1.19	1.35	2.03	1.27	1.78	1.41	1.20	2.22	1.12	1.53	0.957	1.27	1.26	0.969	2.21
Gd		3.59	3.71	6.08	3.35	4.90	3.55	3.07	7.91	2.86	4.35	2.58	3.57	3.00	2.63	6.98
Tb		0.715	0.741	1.15	0.669	0.934	0.695	0.596	1.45	0.538	0.886	0.483	0.638	0.608	0.515	1.35
Dy		4.41	4.48	7.04	4.11	5.68	4.25	3.36	8.70	3.30	5.52	2.89	3.84	3.53	3.11	8.44
Ho		1.02	1.01	1.53	0.868	1.26	0.921	0.727	1.86	0.735	1.20	0.608	0.832	0.814	0.644	1.89
Er		2.63	2.65	4.00	2.43	3.38	2.40	2.03	4.51	2.02	3.31	1.51	2.17	2.03	1.79	4.82
Tm		0.444	0.407	0.629	0.354	0.518	0.362	0.301	0.644	0.318	0.523	0.243	0.360	0.333	0.253	0.726
Yb		2.60	2.33	3.39	2.06	2.82	2.14	1.85	3.46	1.82	2.96	1.39	2.01	1.93	1.43	4.04
Lu		0.335	0.324	0.474	0.320	0.384	0.310	0.280	0.452	0.274	0.395	0.194	0.272	0.277	0.217	0.594
Hf		2.15	2.41	3.62	2.19	3.22	2.41	2.71	2.38	4.75	2.28	2.42	2.58	2.28	1.73	4.39
Ta		0.561	0.681	1.12	0.369	0.610	0.413	0.531	0.769	1.42	0.582	0.661	0.514	0.746	0.290	1.39
W		0.24	0.33	<0.2	0.31	0.29	0.29	0.27	0.87	6.44	0.27	<0.2	0.23	0.60	0.56	0.46
Bi		<0.5	<0.5	<0.5	<0.5	<0.5	<0.5	<0.5	<0.5	<0.5	<0.5	<0.5	<0.5	<0.5	<0.5	<0.5
Th		0.794	0.950	1.53	0.503	1.14	0.586	3.00	1.02	1.99	1.50	0.971	3.79	0.913	0.393	1.82
U		0.232	0.329	0.539	0.169	0.419	0.262	1.19	0.357	0.511	0.330	0.244	1.57	0.245	0.143	0.403

		EST_392	EST_390	EST_717	EST_843	EST_349	EST_375	EST_317A	EST_317B		EST_170	EST_632		EST_41	EST_700	EST_76
LOI	**Chert-related rocks**	-0.02	0.473	0.569	0.385	1.11	1.56	1.90	1.82	**Green siltstone**	3.46	3.86	**Rocks above the unconformity**	4.01	2.54	3.62
Be		<1	<1	<1	<1	1.2	1.3	11.1	8.1		1.9	1.8		1.7	1.2	2.2
Y		1.32	2.20	1.95	4.97	9.19	16.7	49.6	35.6		17.2	16.4		22.2	18.5	15.8
Zr		3.8	15.7	14.5	12.1	65.5	107	1370	1590		108	114		149	110	148
Nb		1.09	1.71	2.47	1.85	9.15	8.38	41.6	77.7		9.94	10.6		7.08	6.10	8.51
Cs		<0.4	1.12	0.81	<0.4	2.38	3.42	5.93	12.9		3.34	3.26		0.64	2.58	3.46
Ba		11.9	73.9	49.8	48.3	201	232	185	229		272	282		473	329	446
La		0.78	2.45	2.29	4.74	12.1	17.9	313	254		18.1	18.1		25.1	19.1	26.9
Ce		1.29	6.81	5.66	10.1	30.7	46.0	555	517		45.2	45.3		51.1	36.4	50.3
Pr		0.151	0.517	0.510	0.958	2.54	3.49	52.8	45.4		4.52	4.25		5.58	4.05	5.07
Nd		0.60	2.27	2.01	3.98	10.0	16.4	183	160		17.9	17.6		22.5	17.8	20.5
Sm		0.14	0.49	0.48	0.91	2.13	3.48	24.0	21.3		4.28	3.82		5.05	3.84	4.10
Eu		0.049	0.133	0.112	0.287	0.396	0.707	1.52	1.80		1.03	0.859		1.53	1.04	1.13
Gd		<0.3	0.35	0.33	0.86	1.63	2.70	10.5	9.40		3.49	2.89		3.90	2.90	3.03
Tb		<0.04	0.070	0.067	0.170	0.298	0.499	1.64	1.27		0.612	0.529		0.722	0.537	0.529
Dy		<0.16	0.41	0.36	0.94	1.79	2.94	8.85	6.40		3.76	3.09		4.66	3.12	3.04
Ho		<0.04	0.093	0.074	0.199	0.398	0.643	1.77	1.27		0.801	0.669		1.04	0.691	0.664
Er		0.131	0.260	0.213	0.508	0.992	1.69	4.87	3.57		2.20	1.79		2.76	1.82	1.75
Tm		<0.04	0.044	<0.04	0.071	0.172	0.273	0.766	0.595		0.333	0.296		0.440	0.316	0.296
Yb		<0.2	0.21	0.23	0.41	0.96	1.56	4.60	3.64		1.81	1.69		2.53	1.84	1.65
Lu		<0.04	<0.04	<0.04	0.065	0.154	0.269	0.751	0.573		0.252	0.256		0.351	0.271	0.249
Hf		<0.13	0.46	0.39	0.34	1.68	2.63	31.7	34.9		2.93	2.92		4.15	2.62	3.78
Ta		<0.04	0.104	0.099	0.088	0.733	0.527	2.29	4.83		0.613	0.615		0.563	0.327	0.636
W		0.21	0.36	0.31	0.29	0.98	1.33	1.01	1.48		0.91	0.87		0.73	<0.2	1.05
Bi		<0.5	<0.5	<0.5	<0.5	<0.5	<0.5	<0.5	0.62		<0.5	<0.5		<0.5	<0.5	<0.5
Th		0.217	0.988	1.09	0.863	4.35	6.38	126	98.2		7.21	7.55		7.68	5.13	7.78
U		0.068	0.173	0.197	0.300	0.656	1.10	23.5	18.0		2.31	1.84		2.55	1.69	2.93

Appendix 3 – Geochronological analyses

Table D: Sample EST_12

	Concordia output					Age estimates (ma)							Concentrations			
Analysis_#	Pb207/U235	1s%	Pb206/U238	1s%	roh	Pb207/Pb206	1s	Pb207/U235	1s	Pb206/U238	1s	conc	Th/U	U	Th	Pbtot
EST12_001	0.6789	1.49	0.08465	1.03	0.69	536	24	526	6.1	524	5.2	98	0.40	1286	512	128
EST12_002	0.6495	1.98	0.07999	1.08	0.54	564	36	508	7.9	496	5.1	88	0.19	84	16	8
EST12_003	0.6215	2.84	0.07626	1.18	0.42	572	55	491	11.0	474	5.4	83	0.19	62	12	5
EST12_004	0.6311	1.51	0.07899	1.03	0.68	529	25	497	5.9	490	4.8	93	0.45	842	379	79
EST12_005	0.6491	1.49	0.08197	1.02	0.69	509	23	508	5.9	508	5.0	100	0.49	1428	702	141
EST12_006	0.6371	1.56	0.08004	1.02	0.66	520	26	501	6.1	496	4.9	95	0.33	952	313	89
EST12_007	0.6202	2.12	0.07764	1.08	0.51	528	40	490	8.2	482	5.0	91	0.18	69	12	6
EST12_008	0.6856	1.50	0.08670	1.03	0.68	506	24	530	6.2	536	5.3	106	0.37	1261	469	127
EST12_009	0.6441	1.53	0.07940	0.99	0.65	561	25	505	6.0	493	4.7	88	0.41	1068	434	101
EST12_010	0.6358	1.81	0.07947	1.03	0.57	530	33	500	7.1	493	4.9	93	0.51	280	143	27
EST12_011	0.6017	1.96	0.07715	1.04	0.53	474	37	478	7.4	479	4.8	101	0.19	93	18	8
EST12_012	0.6662	1.54	0.08420	1.00	0.65	506	26	518	6.2	521	5.0	103	0.39	1548	610	154
EST12_013	0.6616	1.54	0.08326	1.00	0.65	515	25	516	6.2	516	5.0	100	0.44	1006	440	100
EST12_014	0.6560	1.53	0.08225	1.00	0.65	523	25	512	6.1	510	4.9	97	0.49	1558	766	156
EST12_015	0.6388	1.55	0.08112	1.00	0.64	495	26	502	6.1	503	4.8	102	0.39	1116	432	106
EST12_016	0.6111	1.56	0.07860	0.99	0.64	466	27	484	6.0	488	4.7	105	0.34	676	229	62
EST12_017	0.5941	2.14	0.07786	1.05	0.49	425	40	474	8.1	483	4.9	114	0.21	80	17	7
EST12_018	0.5913	2.02	0.07736	1.03	0.51	429	38	472	7.6	480	4.8	112	0.31	148	46	13
EST12_019	0.6167	1.56	0.07764	0.99	0.64	514	26	488	6.0	482	4.6	94	0.43	836	363	77
EST12_020	0.6068	2.12	0.07632	1.05	0.50	516	40	482	8.1	474	4.8	92	0.18	116	21	10
EST12_021	0.5978	2.07	0.07706	1.04	0.50	462	40	476	7.8	479	4.8	104	0.24	109	26	9
EST12_022	0.6247	1.57	0.07984	0.99	0.63	480	27	493	6.1	495	4.7	103	0.36	1076	391	100
EST12_023	0.6598	1.55	0.08212	0.99	0.63	539	27	515	6.3	509	4.8	94	0.40	1355	542	132
EST12_024	0.6384	2.74	0.07948	1.13	0.41	538	55	501	10.8	493	5.4	92	0.23	90	21	8
EST12_025	0.6409	1.56	0.08010	0.99	0.63	530	27	503	6.2	497	4.7	94	0.57	2057	1168	203

Table E: Sample EST_112

	Concordia output					Age estimates (ma)							Concentrations			
Analysis_#	Pb207/U235	1s%	Pb206/U238	1s%	roh	Pb207/Pb206	1s	Pb207/U235	1s	Pb206/U238	1s	conc	Th/U	U	Th	Pbtot
EST112_001	5.2780	1.50	0.32078	0.81	0.54	1946	23	1865	12.8	1794	12.7	92	0.85	39	33	19
EST112_002	1.6844	1.46	0.16419	0.77	0.53	1052	25	1003	9.3	980	7.1	93	0.31	142	44	28
EST112_003	0.5313	1.53	0.06869	0.77	0.50	456	29	433	5.4	428	3.2	94	0.67	388	258	36
EST112_004	0.5300	1.39	0.06859	0.76	0.55	454	25	432	4.9	428	3.2	94	0.67	771	519	70
EST112_005	2.0170	1.34	0.18611	0.76	0.56	1162	22	1121	9.1	1100	7.7	95	0.18	571	102	123
EST112_006	1.9584	1.32	0.18334	0.76	0.57	1133	22	1101	8.9	1085	7.6	96	0.58	467	269	114
EST112_007	0.5199	1.74	0.06706	0.81	0.46	461	34	425	6.0	418	3.2	91	0.57	274	157	24
EST112_008	4.9705	1.33	0.30594	0.76	0.57	1924	19	1814	11.2	1721	11.5	89	0.18	225	41	82
EST112_009	1.9650	1.38	0.18395	0.77	0.56	1134	22	1104	9.3	1089	7.7	96	0.43	201	86	46
EST112_010	1.8172	1.40	0.17341	0.77	0.55	1095	23	1052	9.1	1031	7.3	94	1.26	166	210	46
EST112_011	12.1936	1.36	0.45982	0.78	0.57	2762	18	2619	12.7	2439	15.9	88	0.58	194	111	125
EST112_012	0.5281	1.51	0.06805	0.78	0.51	463	29	431	5.3	424	3.2	92	0.91	829	750	80
EST112_013	2.2729	1.33	0.20318	0.76	0.57	1225	21	1204	9.4	1192	8.3	97	0.66	584	386	160
EST112_014	1.8784	1.33	0.18136	0.76	0.57	1072	22	1074	8.8	1074	7.5	100	0.66	727	478	175
EST112_015	1.4613	2.00	0.15346	0.85	0.43	900	37	915	12.0	920	7.3	102	1.06	26	28	6
EST112_016	0.5823	1.41	0.07439	0.77	0.54	482	26	466	5.2	463	3.4	96	0.73	535	392	54
EST112_017	3.6111	2.05	0.25282	0.94	0.46	1689	33	1552	16.2	1453	12.2	86	1.74	16	28	7
EST112_018	1.9999	1.38	0.18553	0.77	0.55	1151	23	1116	9.3	1097	7.8	95	0.54	282	153	67
EST112_019	0.5551	1.43	0.07176	0.77	0.53	456	26	448	5.2	447	3.3	98	0.75	609	456	59
EST112_020	1.6310	1.42	0.16177	0.77	0.54	1017	24	982	8.9	967	6.9	95	0.22	526	116	99
EST112_021	2.1040	1.44	0.19273	0.78	0.54	1176	24	1150	9.9	1136	8.1	97	0.34	145	50	34
EST112_022	0.5656	1.62	0.07374	0.79	0.48	437	31	455	5.9	459	3.5	105	0.28	411	116	35
EST112_023	0.5774	1.57	0.07369	0.79	0.50	484	30	463	5.8	458	3.5	95	0.23	297	67	25
EST112_024	2.6141	1.78	0.21875	0.85	0.47	1353	30	1305	13.0	1275	9.8	94	0.88	18	16	6
EST112_025	1.4292	1.53	0.14748	0.79	0.52	937	27	901	9.1	887	6.5	95	0.39	124	48	22
EST112_026	0.6263	1.42	0.08071	0.77	0.54	463	26	494	5.5	500	3.7	108	0.67	1737	1165	184
EST112_027	4.0979	1.50	0.28869	1.03	0.68	1679	20	1654	12.2	1635	14.8	97	0.50	279	139	100
EST112_028	0.5874	1.51	0.07462	1.02	0.67	496	25	469	5.7	464	4.6	94	1.06	778	823	80
EST112_029	0.5921	1.65	0.07585	1.03	0.62	477	29	472	6.2	471	4.7	99	0.51	460	233	42
EST112_030	1.9805	1.57	0.18849	1.03	0.66	1101	24	1109	10.5	1113	10.5	101	0.38	114	43	25
EST112_031	1.5848	1.85	0.16030	1.06	0.57	979	31	964	11.5	959	9.5	98	0.35	29	10	5
EST112_032	0.5586	1.64	0.07132	1.02	0.62	484	29	451	6.0	444	4.4	92	0.60	414	249	37
EST112_033	3.1829	1.55	0.25448	1.03	0.66	1441	22	1453	11.9	1462	13.4	101	0.41	174	71	53
EST112_034	0.5718	1.85	0.07196	1.04	0.56	516	34	459	6.8	448	4.5	87	0.70	142	100	13
EST112_035	2.1256	1.52	0.19592	1.02	0.67	1166	22	1157	10.5	1153	10.8	99	0.42	167	70	40
EST112_036	11.9432	1.44	0.45184	1.02	0.70	2758	17	2600	13.4	2403	20.4	87	0.58	314	181	193
EST112_037	3.5989	1.48	0.27387	1.02	0.69	1535	20	1549	11.7	1560	14.1	102	0.50	190	96	65
EST112_038	0.5517	1.60	0.07193	1.03	0.64	439	27	446	5.7	448	4.4	102	0.65	429	281	39
EST112_039	1.9375	1.47	0.18569	1.02	0.69	1088	21	1094	9.8	1098	10.3	101	0.32	480	153	104
EST112_040	2.0626	1.51	0.19265	1.02	0.68	1139	22	1137	10.3	1136	10.6	100	0.64	253	163	62
EST112_041	10.3284	1.61	0.46564	1.07	0.66	2466	20	2465	14.8	2464	21.8	100	0.52	35	18	21
EST112_042	0.5835	1.58	0.07427	1.02	0.65	492	27	467	5.9	462	4.6	94	0.75	505	376	48

EST112_043	1.8127	1.49	0.18006	1.02	0.68	1016	22	1050	9.7	1067	10.0	105	0.30	272	83	57
EST112_044	0.6088	1.93	0.07862	1.06	0.55	459	36	483	7.4	488	5.0	106	0.15	178	26	15
EST112_045	4.9392	1.46	0.31384	1.01	0.69	1867	19	1809	12.3	1760	15.6	94	0.52	314	162	124
EST112_046	3.3001	1.47	0.25634	1.01	0.69	1497	20	1481	11.4	1471	13.4	98	0.41	266	108	83
EST112_047	1.7881	1.52	0.17361	1.02	0.67	1062	22	1041	9.8	1032	9.7	97	0.55	208	114	45
EST112_048	2.3129	1.53	0.20911	1.02	0.67	1204	22	1216	10.8	1224	11.4	102	1.60	145	232	47
EST112_049	3.4456	1.48	0.26793	1.02	0.68	1495	20	1515	11.6	1530	13.9	102	0.74	241	179	84
EST112_050	1.9819	1.52	0.18675	1.02	0.67	1122	22	1109	10.2	1104	10.3	98	0.53	230	122	53
EST112_051	0.5474	2.12	0.07127	1.07	0.50	442	40	443	7.6	444	4.6	100	0.66	140	93	13
EST112_052	4.5373	1.52	0.30951	1.02	0.67	1738	20	1738	12.6	1738	15.6	100	0.47	164	76	64
EST112_053	4.1367	1.55	0.29938	1.03	0.66	1629	21	1662	12.6	1688	15.3	104	1.00	62	62	25
EST112_054	0.5336	1.79	0.07122	1.04	0.58	386	32	434	6.3	444	4.4	115	0.43	162	70	14
EST112_055	0.5740	1.90	0.07433	1.05	0.55	454	35	461	7.0	462	4.7	102	0.51	226	116	20
EST112_056	2.3590	1.49	0.21077	1.02	0.68	1227	21	1230	10.6	1233	11.4	100	0.33	253	83	63
EST112_057	4.5270	1.48	0.30966	1.01	0.69	1733	20	1736	12.2	1739	15.5	100	0.37	171	63	64
EST112_058	2.6553	1.49	0.22285	1.01	0.68	1349	21	1316	10.9	1297	11.9	96	0.63	241	151	68
EST112_059	2.2220	1.49	0.20329	1.01	0.68	1180	21	1188	10.4	1193	11.0	101	0.35	268	95	64
EST112_060	0.5642	1.72	0.07151	1.02	0.59	501	30	454	6.3	445	4.4	89	0.77	175	135	16
EST112_061	0.5590	1.56	0.07286	1.02	0.65	440	26	451	5.7	453	4.4	103	0.90	770	693	75
EST112_062	0.6375	1.94	0.07924	1.05	0.54	544	35	501	7.6	492	5.0	90	0.36	148	54	14
EST112_063	1.5461	1.63	0.15832	1.02	0.63	954	26	949	10.0	947	9.0	99	0.79	98	78	20
EST112_064	2.3571	1.48	0.20940	1.01	0.68	1238	21	1230	10.5	1226	11.3	99	0.18	377	70	90
EST112_065	0.6008	1.58	0.07674	1.02	0.64	484	27	478	6.0	477	4.7	99	0.18	372	67	32
EST112_066	0.6109	2.06	0.07809	1.06	0.52	482	39	484	7.9	485	5.0	101	0.64	148	95	14
EST112_067	4.8495	1.45	0.33080	1.00	0.69	1738	19	1794	12.1	1842	16.1	106	0.43	901	384	365
EST112_068	0.5661	1.51	0.07354	1.01	0.67	447	25	456	5.5	457	4.4	102	1.02	791	809	79
EST112_069	0.6312	1.51	0.08044	1.01	0.67	489	25	497	5.9	499	4.8	102	0.17	934	161	83
EST112_071	1.4216	1.36	0.14863	0.81	0.60	910	22	898	8.1	893	6.8	98	0.40	345	137	160
EST112_072	1.5713	1.60	0.16414	0.85	0.53	912	28	959	9.9	980	7.8	107	0.26	342	91	63
EST112_073	0.5149	1.42	0.06603	0.82	0.57	474	26	422	4.9	412	3.3	87	0.01	1468	10	90
EST112_074	13.2738	1.34	0.50859	0.82	0.61	2736	17	2699	12.6	2651	17.8	97	0.30	222	66	68
EST112_075	4.0398	1.41	0.27022	0.83	0.59	1773	21	1642	11.4	1542	11.4	87	1.68	185	311	6
EST112_076	12.5928	1.35	0.49248	0.82	0.61	2702	18	2650	12.6	2581	17.5	96	2.21	139	308	37
EST112_077	3.4175	1.41	0.25646	0.83	0.59	1561	21	1508	11.0	1472	11.0	94	0.50	116	59	53
EST112_078	1.3872	1.52	0.14319	0.85	0.56	936	26	884	8.9	863	6.8	92	0.36	155	57	84
EST112_070	1.9069	1.59	0.18595	1.02	0.64	1053	25	1084	10.6	1099	10.3	104	0.98	135	133	34
EST112_079	1.8254	1.52	0.17312	1.01	0.66	1109	22	1055	9.9	1029	9.6	93	0.47	203	94	43
EST112_080	2.9423	1.53	0.24057	1.01	0.66	1399	22	1393	11.5	1390	12.7	99	0.59	121	72	37
EST112_081	0.6096	1.56	0.07803	1.01	0.65	479	26	483	6.0	484	4.7	101	0.33	399	130	36
EST112_082	0.6263	1.64	0.07912	1.01	0.62	509	28	494	6.4	491	4.8	97	0.69	431	298	43
EST112_083	3.4799	1.64	0.26070	1.03	0.63	1565	24	1523	12.8	1493	13.8	95	0.86	43	37	15
EST112_084	1.9345	1.53	0.18452	1.01	0.66	1097	23	1093	10.2	1092	10.1	99	0.27	347	95	74
EST112_085	1.8347	1.56	0.18199	1.01	0.65	1019	24	1058	10.2	1078	10.0	106	0.53	146	77	33
EST112_086	6.9993	1.55	0.38709	1.02	0.66	2114	20	2111	13.6	2109	18.4	100	0.45	44	20	22
EST112_087	0.5727	1.70	0.07367	1.02	0.60	468	30	460	6.3	458	4.5	98	0.50	298	149	27
EST112_088	1.9034	1.56	0.18109	1.01	0.65	1102	24	1082	10.4	1073	10.0	97	0.39	228	89	49
EST112_089	11.0050	1.52	0.48947	1.03	0.67	2489	19	2524	14.1	2568	21.7	103	0.51	55	28	35

EST112_090	2.0954	1.54	0.19661	1.01	0.65	1130	23	1147	10.5	1157	10.7	102	0.40	243	97	57
EST112_091	4.5150	1.50	0.30370	1.01	0.67	1764	20	1734	12.4	1710	15.1	97	0.54	292	156	112
EST112_092	2.1562	1.49	0.20139	1.00	0.67	1139	22	1167	10.3	1183	10.8	104	0.32	271	86	64
EST112_093	0.5343	1.84	0.06855	1.04	0.56	474	34	435	6.5	427	4.3	90	0.91	308	280	28
EST112_094	9.7325	1.51	0.40003	1.02	0.68	2621	18	2410	13.8	2169	18.7	83	0.39	150	58	78
EST112_095	0.5276	1.65	0.06855	1.01	0.61	446	29	430	5.8	427	4.2	96	0.91	354	322	33
EST112_096	1.6546	1.82	0.16770	1.04	0.57	975	30	991	11.5	999	9.7	103	0.65	70	45	15
EST112_097	0.5499	1.57	0.07153	1.01	0.64	444	26	445	5.6	445	4.3	100	0.51	412	209	36
EST112_098	4.6878	1.49	0.30785	1.00	0.68	1808	20	1765	12.4	1730	15.2	96	0.94	168	158	71
EST112_099	0.6199	1.65	0.07932	1.01	0.61	480	29	490	6.4	492	4.8	103	0.91	687	627	73
EST112_100	1.8104	1.61	0.17627	1.02	0.63	1056	25	1049	10.5	1047	9.8	99	0.91	116	106	28

Appendix 4

Dugurdsknappen - Geological map

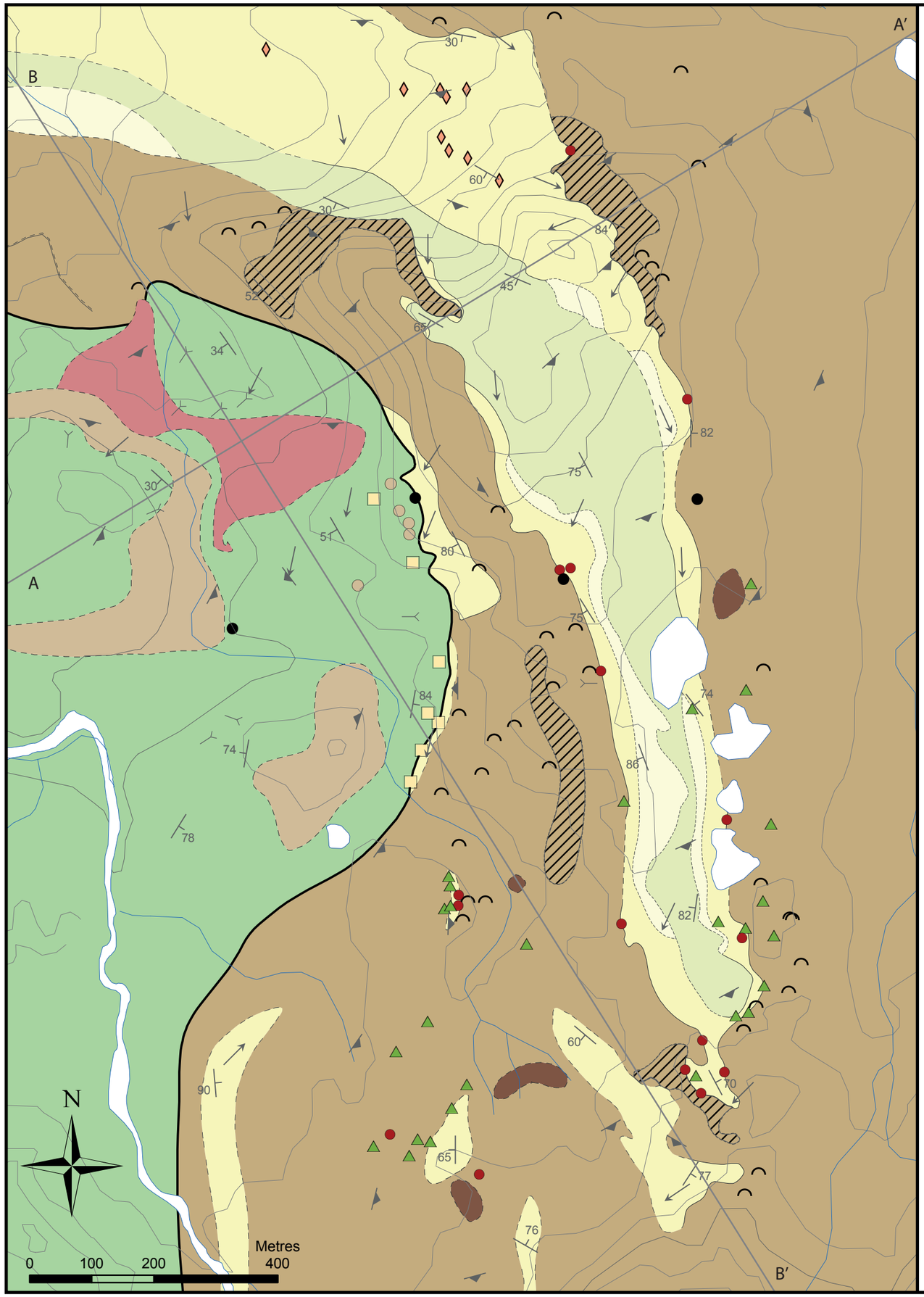

Legend

Lithological units

Dike

Rocks above the unconformity

Intermediate intrusion

Intermediate volcanic

Green sandstone

Conglomerate

Rocks below the unconformity

Green siltstone

Chert-related rocks

Silty chert

Felsic conglomerate

Ribbon chert

Jasper

Greenstone-related rocks

Agglomerate

Altered greenstone

Gabbroic intrusion

Greenstone

Geological symbols

Lithological boundary

Inferred boundary

Constructed boundary

Transitional boundary

Unconformity

Pillow structure

Way up indicator

Strata

Foliation, penetrative

Fold axis

Measured strata